APOPTOSIS-INDUCING FACTOR MEDIATES METABOLISM AND OXIDATIVE STRESS SIGNALING THROUGH FUNCTIONALLY UNCOUPLED MECHANISMS TO THE BENEFIT OF TUMORIGENESIS

A Dissertation
Submitted to the Graduate Faculty
of the
North Dakota State University
of Agriculture and Applied Science

By

Andrew Joseph Scott

In Partial Fulfillment of the Requirements
for the Degree of
DOCTOR OF PHILOSOPHY

Major Program:
Biochemistry

April 2019

Fargo, North Dakota

North Dakota State University
Graduate School

Title

APOPTOSIS-INDUCING FACTOR MEDIATES METABOLISM AND OXIDATIVE STRESS SIGNALING THROUGH FUNCTIONALLY UNCOUPLED MECHANISMS TO THE BENEFIT OF TUMORIGENESIS

By

Andrew Joseph Scott

The Supervisory Committee certifies that this ***disquisition*** complies with North Dakota State University's regulations and meets the accepted standards for the degree of

DOCTOR OF PHILOSOPHY

SUPERVISORY COMMITTEE:

John C. Wilkinson, Ph.D.
Chair

D.K. Srivastava, Ph.D.

Stuart J. Haring, Ph.D.

Katie M. Reindl, Ph.D.

Approved:

April 10, 2019
Date

Gregory R. Cook, Ph.D.
Department Chair

ABSTRACT

Cancer is one of the leading causes of death in the world, arising when cells accumulate genomic mutations that render them incapable of controlling their own proliferation and survival. While substantial improvements in patient outcome have been achieved over the years, completely eliminating tumorigenic cells remains a significant challenge, and some cancer types (such as pancreatic cancer) have not shown meaningfully improved patient survival rates despite our advancements in understanding cancer cell biology and treatment.

Genetic targeting approaches to the treatment of cancer have yielded some success, but have shown rather disappointing results overall. In contrast to the diversity of genetic aberrations within tumor cells (making treatment difficult), cancers share common phenotypes that are more universally targetable. As cancers evolve within their biological environment to become aggressive, the net effects of their genetic alterations lead to 1) decreased sensitivity to cell death cues, 2) altered oxidative state and redox-dependent signaling, and 3) dramatically increased demand for energy production and biosynthesis (altered metabolism).

The work of this study shows that in pancreatic cancer cells reversible metabolic adaptation alters oxidative stress sensitivity and triggers persistent drug resistance, demonstrating the interplay of the above three cellular activities. Further experimentation identifies the mitochondrial protein apoptosis-inducing factor (AIF) as an essential signaling node functioning at the convergence of all three of these processes. In response to cellular metabolic cues, AIF controls the ability of the mitochondria to produce energy required for tumorigenic growth, invasion, and survival while functioning as mitochondrial translation factor. Distinct from this pivotal metabolic role, AIF serves as a transmitter of extra-mitochondrial redox signaling cues regulating pro-tumor gene expression programs that are lethal without AIF. Finally, AIF exhibits

involvement in atypical death pathways associated with the cell death regulators PGAM5 and XIAP. Remarkably, these AIF activities are functionally dissociable and demonstrate the multifunctional nature of AIF in control of tumorigenesis.

Overall this study defines a variety of diverse AIF activities at the intersection of multiple tumorigenic phenotypes, furthering our understanding of how cancer cells converge upon different aggressive characteristics and revealing potential vulnerabilities for therapeutic intervention.

ACKNOWLEDGEMENTS

I wouldn't have it made it here without the support of family, friends, and mentors.

My deepest gratitude goes to my advisor, Dr. John Wilkinson, for the years of mentoring and commitment to my growth as a scientist, and who has always motivated me to become the best scientist and best person I can be. Your guidance, teaching, and friendship have all been instrumental to my success as a graduate student. I also thank my advisory committee, Dr. Stuart Haring, Dr. D.K. Srivastava, and Dr. Katie Reindl, for their guidance and feedback over the years.

I'm incredibly thankful to my colleagues in the lab, both past and present, who have made me look forward to coming to work every day—Amanda Wilkinson, Sierra Walker, Kaitlyn Johnson, Joshua Krank, Sierra Giebel, Sujata Birua, Kaitlin Dailey, and Shahzeb Khan. I thank each of you for the laughs, friendship, support, and comradery.

I'm grateful to my undergraduate mentor, Dr. Marina Cetkovic-Cvrlje, for introducing me to the world of scientific research, fostering my growth as a young scientist, and being a source of encouragement to this day.

Finally, I want to thank my family and friends for their unwavering support and encouragement throughout my time as a PhD student, especially my parents, my brothers, my girlfriend, and my nephew. You all have my sincerest gratitude and appreciation. I couldn't have done it without you.

DEDICATION

To the memory of my grandpa, Charlie.

TABLE OF CONTENTS

LIST OF TABLES

LIST OF FIGURES

LIST OF ABBREVIATIONS

1,3-BGP 1,3-Bisphosphoglycerate

2DG.....2-Deoxyglucose

2-PG 2-Phosphoglycerate

3-PG 3-Phosphoglycerate

aa-tRNA .....Aminoacyl tRNA

ABL1.....Abel murine leukemia viral oncogene homolog 1

ActD .....Actinomycin D

ADP.....Adenosine diphosphate

AIF .....Apoptosis-inducing factor

ALDOA.....Aldolase A

AMP .....Adenosine monophosphate

AMPK .....AMP-activated protein kinase

Apaf-1 .....Apoptotic protease activating factor 1

ASK1.....Apoptosis signal-regulating kinase 1

ATO .....Arsenic trioxide

ATP .....Adenosine triphosphate

AVPI .....Alanyl-valyl-prolyl-isoleucine

Bak .....Bcl-2 homologous antagonist/killer

Bax .....Bcl-2-like protein 4

Bcl-2.....B cell lymphoma 2

Bcl-X_L .....B cell lymphoma extra large

Bid.....BH3 interacting-domain death agonist

BIR.....Baculoviral IAP repeat

BIRC .....Baculoviral IAP repeat-containing protein

BRUCE	BIRC ubiquitin-conjugating enzyme
bVAD-fmk	Biotinyl-carbobenzoxy-valyl-alanyl-aspartyl-(O-methyl)-fluoromethylketone
CA-JNK1	Constitutively active JNK1, MKK7β2-JNK1α1
CA-JNK2	Constitutively active JNK2, MKK7β2-JNK2α2
CDKN2A	Cyclin dependent kinase inhibitor 2A
cDNA	Complementary DNA
CHCHD4	Coiled-coil-helix-coiled-coil-helix-domain-containing protein 4
cIAP1	Cellular IAP 1
cIAP2	Cellular IAP 2
CM-H_2DCFDA	Chloromethyl-2',7'-dichlorodihydrofluorescein diacetate
COX IV	Cytochrome c oxidase subunit 4 isoform 1
CQ	Chloroquine
Ct	C-terminus
CTL	Control
CYLD	Cylindromatosis
CYP	Cytochrome P540
CYP3A5	Cytochrome P450 3A5
Cyt c	Cytochrome c
DHAP	Dihydroxyacetone phosphate
DIABLO	Direct IAP binding protein with low pI
DISC	Death-associated signaling complex
DMEM	Dulbecco's modified Eagle medium
DN	Double negative

DNA	Deoxyribonucleic acid
DPC4	Deleted in pancreatic carcinoma locus 4
Drp1	Dynamin-related protein 1
DUSP4	Dual specificity phosphatase 4
EF-Ts	Elongation factor thermo stable
EF-Tu	Elongation factor thermo unstable
EGF	Epidermal growth factor
EGFR	Epidermal growth factor receptor
EMT	Epithelial-mesenchymal transition
ENO1	Enolase 1
ENO2	Enolase 2
ERK	Extracellular signal-regulated kinase
ETC	Electron transport chain
ETS-1	Erythroblastosis virus E26 oncogene homolog 1
F1,6BP	Fructose-1,6,-bisphosphate
F12	Ham's F-12 medium
F2,6BP	Fructose-2,6-bisphosphate
F6P	Fructose-6-phosphate
FAD/FAH_2	Flavin adenine dinucleotide/Reduced FAD
FADD	Fas-associated protein with death domain
Fas	First apoptosis signal/Apoptosis stimulating fragment
FBS	Fetal bovine serum
FCCP	Carbonyl cyanide *p*-trifluoro-methoxyphenyl hydrazone
G6P	Glucose 6-phoshate

GAP.....Glyceraldehyde 3-phosphate

GAPDH.....Glyceraldehyde 3-phosphate dehydrogenase

GDP.....Guanosine diphosphate

GEM.....Gemcitabine

GFP .....Green fluorescent protein

GGT1 .....Gamma-glutamyltransferase 1

GPx .....Glutathione peroxidase

GSH.....Glutathione

GST .....Glutathione S-transferase

GSTM1 .....Glutathione S-transferase mu 1

GTP .....Guanosine triphosphate

H2AX.....Histone 2A family member X

HA.....Hemagglutinin epitope

hGCLM .....Glutamate-cysteine ligase modifier subunit, human

hGGT1 .....Gamma-glutamyltransferase 1, human

hGSR.....Glutathione S-reductase, human

hGSTM1 .....Glutathione S-transferase mu 1

HIF .....Hypoxia-inducible factor

His.....Histidine

HK.....Hexokinase

HK1.....Hexokinase 1

HK2.....Hexokinase 2

hMOX1 .....Heme oxygenase 1, human

hMOX2 .....Heme oxygenase 2, human

HNF1A.....Hepatocyte nuclear factor 1, alpha

HNF4A.....Hepatocyte nuclear factor 4 alpha

hNQO1.....NAD(P)H quinone dehydrogenase 1, human

HRP.....Horseradish peroxidase

Hsp70.....70 kilodalton heat shock protein

HtrA2.....High temperature requirement protein A2

IAP.....Inhibitor of apoptosis

IL-1β.....Interleukin 1 β

IMM.....Inner mitochondrial membrane

IMS.....Intermembrane space

JNK.....c-Jun N-terminal kinase

JNK1.....c-Jun N-terminal kinase 1

JNK1α1.....c-Jun N-terminal kinase 1 α1

JNK2.....c-Jun N-terminal kinase 2

JNK2α2.....c-Jun N-terminal kinase 2 α2

JNK3.....c-Jun N-terminal kinase 3

kDa/kD.....Kilodalton

Keap1.....Kelch like ECH associated protein 1

KO.....Knockout

KRAS.....Kirsten rat sarcoma viral oncogene homolog

KRT81.....Cytokeratin 81

K-SFM.....Keratinocyte serum free medium

LC3.....Microtubule-associated protein 1A/1B light chain 3

LDHA.....Lactate dehydrogenase A

LKB1.....Liver kinase B1

MAP2K.....Mitogen-activated protein kinase kinase

MAP3K.....Mitogen-activated protein kinase kinase kinase

MAPK.....Mitogen-activated protein kinase

MEF.....Mouse embryonic fibroblast

MEM.....Minimum essential medium

MG132.....Carbobenzoxy-L-leucyl-L-leucyl-L-leucinal

MKK4.....Mitogen-activated protein kinase kinase 4

MKK7.....Mitogen-activated protein kinase kinase 7

MKK7β2.....Mitogen-activated protein kinase kinase 7 β2

MKP.....Mitogen-activated protein kinase phosphatase

MKP2.....Mitogen-activated protein kinase phosphatase 2

ML-IAP.....Melanoma IAP

MLS.....Mitochondrial localization sequence

MMP.....Matrix metalloproteinase

MNNG.....Methylnitronitrosoguanidine

MOMP.....Mitochondrial outer membrane permeabilization

MP2.....Control MIA PaCa-2

MP2-D.....2DG-adapted MIA PaCa-2

MP2-DW.....2DG-withdrawn MP2-D

mRNA.....Messenger RNA

MRPL18.....Mitochondrial ribosomal protein L18

MT-CO1.....Mitochondrially encoded cytochrome c oxidase I

MT-CO2.....Mitochondrially encoded cytochrome c oxidase II

MT-CYB.....Mitochondrially encoded cytochrome b

MT-ND1.....Mitochondrially encoded NADH:ubiquinone oxidoreductase core subunit 1

NAC.....N-acetylcysteine

NAD^+/NADH	Nicotinamide adenine dinucleotide/Reduced NAD
$NADP^+$/NADPH	Nicotinamide adenine dinucleotide phosphate/Reduced $NADP^+$
NAIP	Neuronal apoptosis inhibitory protein
NDI1	NADH dehydrogenase internal
NDUFA9	NADH:ubiquinone oxidoreductase subunit A9
NDUFB8	NADH:ubiquinone oxidoreductase subunit B8
NF-κB	Nuclear factor κ-light-chain-enhancer of activated B cells
Ni	Nickel
Ni-NTA	Nickel nitrilotriacetic acid
NLS	Nuclear localization sequence
NOX	NADPH oxidase
NP-40	Nonidet P40
NR1I2	Nuclear receptor subfamily 1 group I member 2
Nrf2	Nuclear factor, erythroid 2 like 2
NS	Nonspecific signal
OMM	Outer mitochondrial membrane
OXPHOS	Oxidative phosphorylation
PACO	Pancreatic adenocarcinoma (cell line)
PARP	Poly-ADP ribose polymerase
PBS	Phosphate buffered saline
PCa	Prostate cancer
PCNA	Proliferating cell nuclear antigen
PCR	Polymerase chain reaction
PD	Pulldown

PDAC.....Pancreatic ductal adenocarcinoma

PDH.....Pyruvate dehydrogenase complex

PDHA.....Pyruvate dehydrogenase complex, E1 α1 subunit

PDK1.....Pyruvate dehydrogenase kinase 1

PEP.....Phosphoenolpyruvate

PFK-1.....Phosphofructokinase-1

PFK-2.....Phosphofructokinase-2

PFKFB2.....6-Phosphofructo-2-kinase/fructose-2,6-bisphosphatase 2

PFKFB3.....6-Phosphofructo-2-kinase/fructose-2,6-bisphosphatase 3

PFKL.....Phosphofructokinase, liver

PFKM.....Phosphofructokinase, muscle

PFKP.....Phosphofructokinase, platelet

PGAM.....Phosphoglycerate mutase

PGAM1.....Phosphoglycerate mutase 1

PGAM5.....Phosphoglycerate mutase family member 5

$PGAM5_L$.....Phosphoglycerate mutase family member 5, long isoform

$PGAM5_S$.....Phosphoglycerate mutase family member 5, short isoform

PGK1.....Phosphoglycerate kinase

P_i.....Inorganic phosphate

PI.....Propidium iodide

PI3K.....Phosphoinositide 3-kinase

PINK1.....PTEN induced putative kinase 1

PKM.....Pyruvate kinase

PMSF .....Phenylmethylsulfonyl fluoride

polyHis.....Polyhistidine

PPP.....Pentose phosphate pathway

PRx.....Peroxiredoxin

PTEN.....Phosphatase and tensin homolog

PVDF .....Polyvinylidene fluoride

PXR.....Pregnane X receptor

Q.....Ubiquinone (coenzyme Q)

QM-PDA.....Quasimesenchymal

qPCR.....Quantitative PCR

RIP1 .....Receptor-interacting protein kinase 1

RIP3 .....Receptor-interacting protein kinase 3

RIPA .....Radioimmune precipitation assay buffer

RNA .....Ribonucleic acid

RNAi.....RNA interference

ROS.....Reactive oxygen species

RPMI 1640.....Roswell Park Memorial Institute 1640 medium

rRNA.....Ribosomal RNA

RT .....Reverse transcriptase

SDS .....Sodium dodecyl sulfate

SDS-PAGE .....Sodium dodecyl sulfate polyacrylamide gel electrophoresis

SEK1.....Stress-activated protein kinase kinase 1

shRNA.....Short hairpin RNA

Smac.....Second mitochondria-derived activator of caspases

Smad4 .....Smad family member 4

SOD1.....Superoxide dismutase 1

SOD2.....Superoxide dismutase 2

SRC.....Rous sarcoma viral oncogene homolog

STS-1.....Suppressor of T cell receptor signaling 1

STS-2.....Suppressor of T cell receptor signaling 2

tBHQ.....*tert*-butylhydroquinone

TCA.....Tricarboxylic acid

TGF-β.....Transforming growth factor β1

TMRM.....Tetramethylrhodamine ester

TNF.....Tumor necrosis factor

TNFR.....TNF receptor

TNFα.....Tumor necrosis factor α

TRAIL.....TNF-relatived apoptosis-inducing ligand

tRNA.....Transfer RNA

Ts.....Thermo stable

TSFM.....Mitochondrial elongation factor Ts

Tu.....Thermo unstable

TUFM.....Mitochondrial elongation factor Tu

TVA.....T263A/V300A mutation

Ub.....Ubiquitin

Ub_n.....Polyubiquitin

UT.....Untreated

WB.....Western blot

WT.....Wild-type

XIAP.....X-linked inhibitor of apoptosis

Zeb1 .....Zinc finger E-box binding homeobox 1

Zeb2 .....Zinc finger E-box binding homeobox 2

ZO-1.....Zona occludens 1

LIST OF SYMBOLS

α	Lowercase alpha, used to define intramolecular positions, protein subunits and isoforms
β	Lowercase beta, used to define intramolecular positions, protein subunits and isoforms
Δ	Uppercase delta, used to indicate a difference or describe protein deletions removing indicated amino acid residues
$\Delta\Psi_m$	Uppercase delta, uppercase Psi, m, indicates mitochondrial membrane potential
µ	Lowercase mu, used to abbreviate the *micro-* prefix (10^{-6})
°C	Degree symbol, used to define degrees Celsius

LIST OF APPENDIX TABLES

LIST OF APPENDIX FIGURES

I. INTRODUCTION

Mitochondria: Energy production, redox signals, and cell death

Mitochondrial structure and function

Long recognized for their roles as the powerhouses of the eukaryotic cell, mitochondria are key mediators of metabolism, homeostasis, survival, and death. In addition to providing cellular energy in the form of adenosine triphosphate (ATP), mitochondria also generate heat, regulate calcium storage and signaling, and house pro-apoptotic factors that are released into the cytosol to execute cell death programs following apoptotic stimuli [1]. Mitochondria are significant producers of reactive oxygen species (ROS), which are potentially toxic byproducts of cellular respiration that also function as second messengers to control signaling pathways that promote cellular homeostasis [2]. Together these diverse activities balance the fate of the cell, and their dysregulation is associated with a wide variety of pathologies, underscoring the fundamental impact of mitochondria upon human physiology and disease.

As shown in Figure 1.1, mitochondria are comprised of two membranes that define their suborganellar compartments. The outer mitochondrial membrane (OMM) separates the mitochondria from the cytosol and is permeable to small molecules (*e.g.*, H_2O, ATP, pyruvate), while the inner mitochondrial membrane (IMM) is a highly selective diffusion barrier between the intermembrane space (IMS) and the matrix. The matrix houses numerous metabolic processes including the TCA cycle, amino acid transamination, β-oxidation of fatty acids, and the initial stages of the urea cycle. ATP production via respiration occurs at the IMM, which is folded into cristae that increase IMM surface area and create localized pH pockets that drive respiration (discussed below).

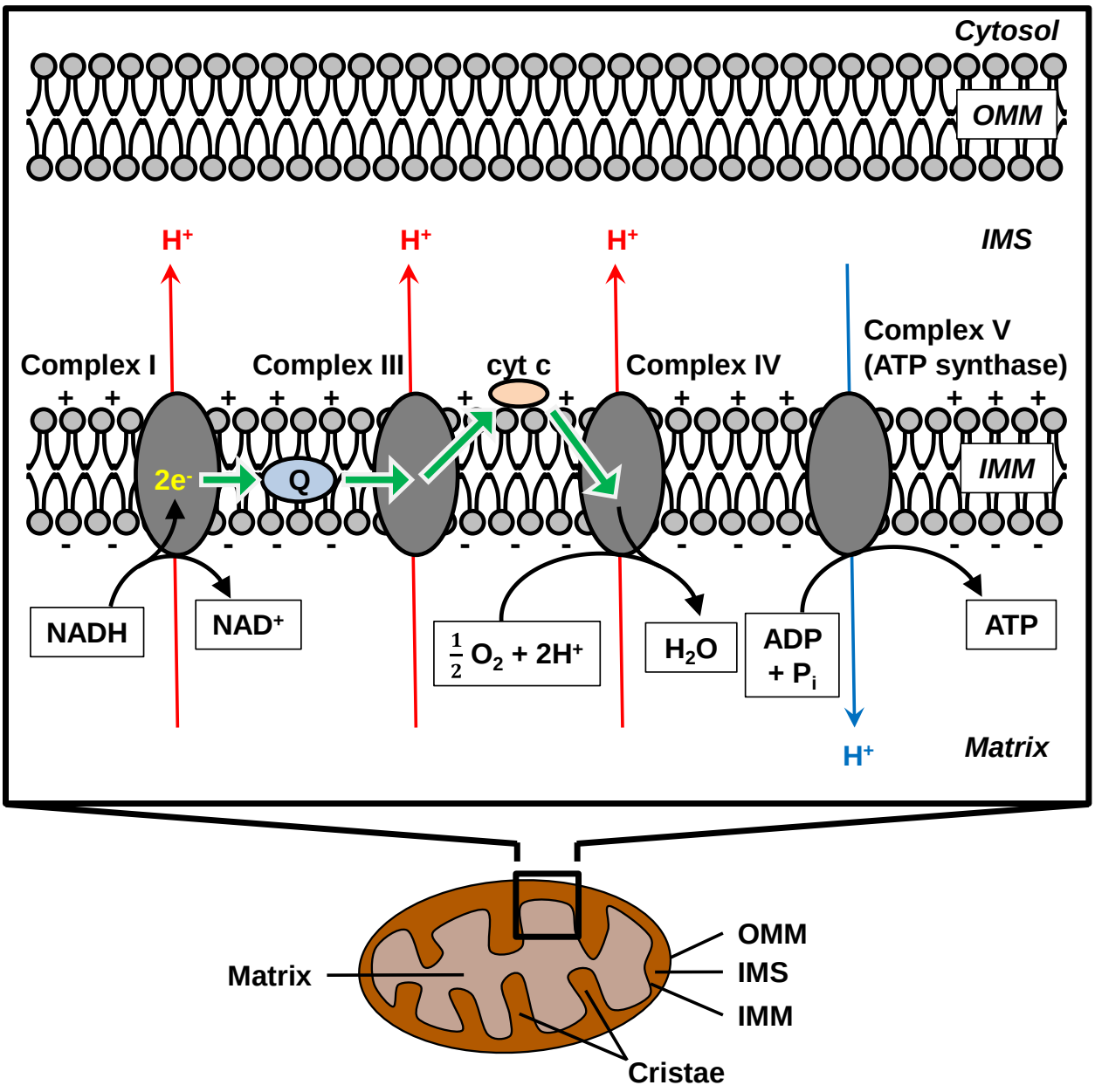

Figure 1.1. Mitochondrial structure and metabolism.
Mitochondria consist of two membranes (OMM and IMM) separating the IMS and the matrix, with the IMM folded into cristae. Inset: Following complex I-mediated oxidation of NADH, electrons are shuttled to complex III via ubiquinone/coenzyme Q (Q) and then to complex IV via cytochrome c (cyt c) with O_2 as the terminal electron acceptor. As electrons are shuttled through the ETC, complexes I, III, and IV pump protons from the matrix to the IMS to establish a proton gradient that is used by complex V to power ATP synthesis.

Aerobic and anaerobic metabolism

Much of the cell's fuel for ATP synthesis is derived from glucose. Upstream of mitochondrial ATP production, glucose is oxidized into two molecules of pyruvate during glycolysis as nicotinamide adenine dinucleotide (NAD^+) is reduced to NADH, yielding a relatively small amount of ATP. Subsequently pyruvate can be imported into the mitochondria for complete oxidation into CO_2 to produce substantially greater ATP quantities, or, depending on cellular metabolic needs, pyruvate may be reduced to lactate in the cytosol. Under conditions of abundant oxygen, pyruvate is broken down to CO_2 while its electrons reduce O_2 in order for mitochondria to generate ATP (Figure 1.2A). In oxygen-deprived anaerobic cells, such as rapidly contracting skeletal muscle or hypoxic tumor cells, ATP is produced entirely from glycolysis. In this situation, instead of delivery into the mitochondria, pyruvate is converted to lactate so that NAD^+ can be regenerated for continued glycolytic activity (Figure 1.2B).

Mitochondrial ATP production

Mitochondria are the main providers of ATP in eukaryotic cells. Among the many biochemical pathways of the cell, various fuel sources (carbohydrates, amino acids, lipids) are broken down to their basic building blocks (CO_2, H_2O, NH_3, etc.), while the energy released from these processes is used to power mitochondrial ATP synthesis. During the breakdown of reduced fuels, metabolites are enzymatically oxidized while their electrons are used to reduce NAD^+ to NADH or flavin adenine dinucleotide (FAD) to $FADH_2$. In the mitochondria, the electrons carried by NADH and $FADH_2$ are delivered into a series of protein complexes within the IMM known as the electron transport chain (ETC, alternatively called the respiratory chain). The ETC establishes a proton gradient across the IMM by means of redox reactions culminating in the reduction of O_2 to H_2O. Establishment of the proton gradient, a thermodynamically

difficult process requiring an input of free energy, is driven by the passage of electrons through cofactors of progressively increasing reduction potential. As electrons are transported through these assemblies, complexes I, III, and IV sequester potential energy by pumping protons (H^+) across the IMM from the matrix to the IMS. During oxidative phosphorylation (OXPHOS), ATP synthase (also known as complex V) harnesses this free energy by delivering protons across the IMM in the opposite direction, from high (IMS side) to low concentration (matrix side). Proton flux through complex V powers its ATP synthase activity, catalyzing the formation of ATP from ADP (adenosine diphosphate) and inorganic phosphate (P_i). The flow of electrons through the ETC and its coupling to ATP synthesis are diagrammed in Figure 1.1.

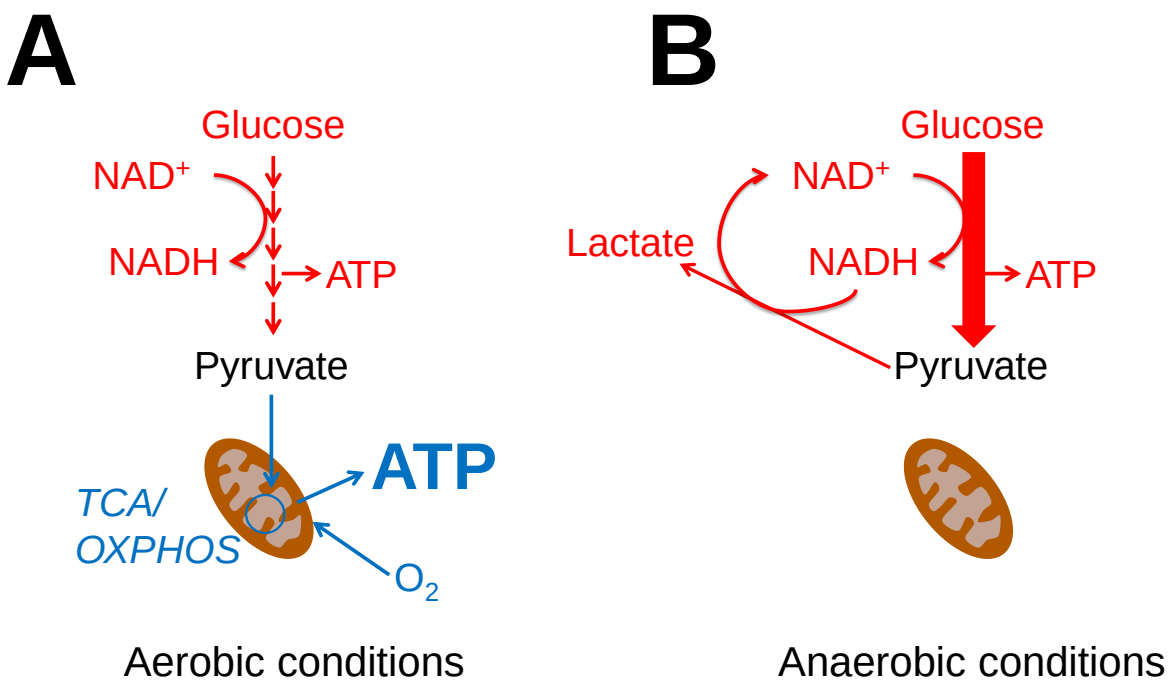

Figure 1.2. Glucose metabolism under aerobic and anaerobic conditions.
A) When O_2 is present, pyruvate is fully oxidized during the TCA cycle and used to generate ATP in the mitochondria. B) In the absence of O_2, pyruvate is converted to lactate in order for the cell to regenerate NAD^+ for continued glycolysis-derived ATP production.

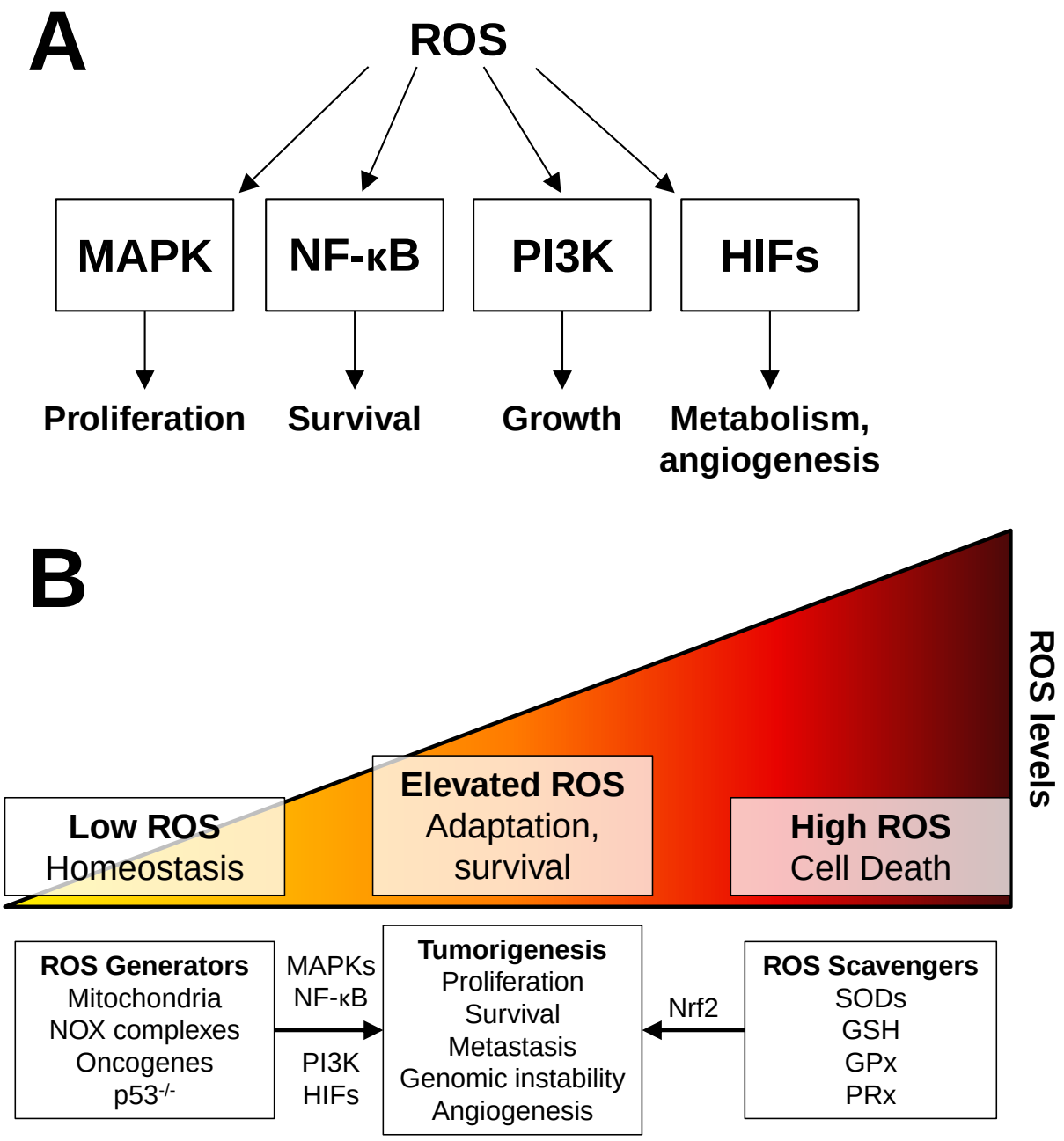

Figure 1.3. Cellular redox balance.
A) ROS regulate a variety of cell signaling pathways involved in metabolism and angiogenesis, growth, survival, and proliferation. B) Effects of altered ROS levels upon cell fate and tumorigenesis. Types of ROS generators and ROS scavengers are indicated. Different signaling molecules (MAPKs, NF-κB, PI3K, HIFs) can promote ROS or detoxify ROS to the benefit of tumorigenesis.

Mitochondria and reactive oxygen species

As potentially toxic by-products of cellular respiration, ROS are formed primarily by the aberrant leakage of electrons from the ETC. Mitochondrial ROS occur when electrons liberated from the respiratory chain partially reduce molecular oxygen to form superoxide anions, which are subsequently converted to hydrogen peroxide by mitochondrial superoxide dismutases 1 and 2 (SOD1, SOD2). Through the activity of glutathione peroxidase, hydrogen peroxide can then be neutralized during its reduction to H_2O. In addition to their production during normal mitochondrial respiration, ROS are also rapidly generated to high levels during ETC malfunction that is observed in cases of mitochondrial DNA mutation, complex I deficiency, or chemical ETC inhibition [3-5]. Additional sources of endogenous ROS include plasma membrane NADPH oxidase complexes, peroxisomes, and endoplasmic reticula, and cells may intentionally generate ROS in response to various stimuli including TNFα, EGF, IL-1β, hypoxia, and irradiation [6, 7].

High levels of ROS are biologically deleterious (Figure 1.3), leading to lipid peroxidation, protein damage, and enzymatic deactivation due to the oxidation of redox-sensitive cofactors. Critically, ROS cause oxidative damage to nucleic acids including base oxidation and strand breaks, creating potentially tumorigenic DNA lesions. In addition to their role in tumor initiation, high ROS levels are also involved with tumor progression, chronic inflammation, neurodegeneration, diabetes, and aging, among a host of other chronic conditions [8].

Historically ROS have been viewed as inevitable byproducts of metabolic reactions, but in the past two decades their essential roles in signal transduction to regulate normal cellular and physiological processes have become apparent [9]. Under normal cellular conditions, ROS are maintained at small amounts, as the ETC generates relatively low levels that are easily

neutralized by antioxidant enzymes. In healthy cells, a residual amount of ROS that escape enzymatic breakdown persists, and despite their potential for toxicity, these low ROS levels are predominantly beneficial (Figure 1.3). At basal levels ROS are essential for basic cell processes including proliferation, viability, and differentiation [10]. Moreover, while excessive ROS levels induce cellular toxicity, ROS overload is in fact often an intentionally produced active component of various programmed cell death pathways that are physiologically beneficial (*e.g.*, apoptosis).

Mitochondrial control of cell death

While actively respiring mitochondria are the predominant energy producers of the cell, mitochondria are also central to cell death, functioning as cellular stress sensors at the convergence of various cell death pathways. Although many distinct death pathways have been defined in various cell types and contexts, cell death is traditionally classified into three broad categories: apoptosis, autophagy, and necrosis [11]. These mechanisms are described in detail in appendix A.

Apoptosis (Greek, "*falling away*"), the most common and well-studied type of cell death, was named for the characteristic morphology of cells condensing and breaking into smaller apoptotic bodies that are phagocytosed by neighboring cells [12]. In contrast to premature or accidental cell death (necrosis), the quiet incorporation of apoptotic bodies into phagocytes allows immune evasion without inducing inflammation [13]. Biochemical hallmarks of apoptosis include the activation of pro-apoptotic Bcl-2 protein family members, caspase cleavage and activation, permeabilization of the mitochondrial membrane, flipping of phosphatidylserine membrane lipids, high ROS levels, DNA fragmentation and degradation, and rupture of the cell membrane [14]. Apoptosis is a routine event in multicellular organisms (>1 million cells per

second in humans), promoting normal development (*e.g.*, organ morphogenesis and lymphocyte maturation) and eliminating diseased cells, *e.g.*, those infected with pathogens or that have accumulated irreparable and potentially tumorigenic mutations [15, 16].

When cell death is a physiological necessity or cells become potentially tumorigenic, apoptosis is the most frequent biological outcome. Depending on stimulus and context, apoptosis can be activated through either an extrinsic or intrinsic pathway (Figure 1.4). Extrinsic apoptosis involves the binding of an external signaling ligand with its cognate receptor, in turn inducing toxic pathways within the cell. Intrinsic apoptosis is activated by cellular stresses such as radiation or chemical damage that are detected by the mitochondria, which respond by releasing apoptotic molecules that activate death pathways in the cytosol. Both extrinsic and intrinsic pathways are mediated by cascades of cysteine-aspartate proteases called caspases. Caspases activated by proteolytic cleavage serve as the executioners of apoptosis [17].

In the extrinsic pathway, cells respond to external signaling molecules that bind membrane-bound TNF receptors (TNFRs), leading to caspase activation and cell death. In contrast, the intrinsic pathway is activated by nonspecific internal stresses that directly or indirectly lead to changes in mitochondrial membrane permeability. Under nonstress conditions, the pro-survival proteins Bcl-2 and Bcl-X_L maintain mitochondrial membrane integrity by inhibiting their pro-apoptotic family members Bax, Bak, and Bid [18]. When the cell death pathway is induced, apoptotic proteins are activated through a variety of mechanisms relieving these inhibitory interactions. An example of this mitochondrial death protein activation can occur via the tumor suppressor p53. Following lethal signals, p53 is stabilized and can induce apoptotic genes as a nuclear transcription factor but also promote cell death proteins through direct interactions with Bcl-2 family members at the mitochondria [19]. Following apoptotic insult,

Bax and Bak oligomerize, causing the formation of pores in the OMM that increase its permeability [20]. Once the mitochondrial membrane has permeabilized, various death factors are released into the cytosol including Smac (second mitochondria-derived activator of caspases) and the ETC molecule cytochrome c [21]. Upon release from the mitochondria, Smac binds X-linked inhibitor of apoptosis (XIAP), neutralizing its ability to inhibit caspases, while cytosolic cytochrome c binds Apaf-1 and induces its oligomerization, forming the death complex known as the apoptosome [22]. The apoptosome recruits procaspase-9 and induces its cleavage into active caspase-9, which subsequently activates caspases-3 and 7 to mediate cellular disassembly [23].

Apoptosis-inducing factor: a microcosm of mitochondrial function

Overview of AIF architecture and activities

Common to the regulation of the diverse activities of the mitochondria is the NADH-dependent oxidoreductase known as apoptosis-inducing factor (AIF). As its name suggests, AIF was first characterized in the context of cell death [24]; however later studies have established the death-associated role of AIF is secondary to its widespread mitochondrial activities in controlling cellular metabolic and redox homeostasis [25, 26].

AIF (also known as *AIFM1* and *PCDC8*) is a ubiquitously expressed gene mapped to the X chromosome in mice and humans [27]. Phylogenetic analyses have revealed strong conservation of AIF among mammals with ~90% sequence identity, while AIF and AIF-like proteins originating from a universal common ancestor are found in eukaryotes, bacteria, and archaea [28-30]. The human *AIF* gene encodes a 613-amino acid (67 kDa) precursor polypeptide (Figure 1.5A) with an N-terminal mitochondrial localization sequence (MLS) that is cleaved at residue 54 upon mitochondrial import. This mature 62 kDa form of AIF (Δ1-54 AIF, Figure

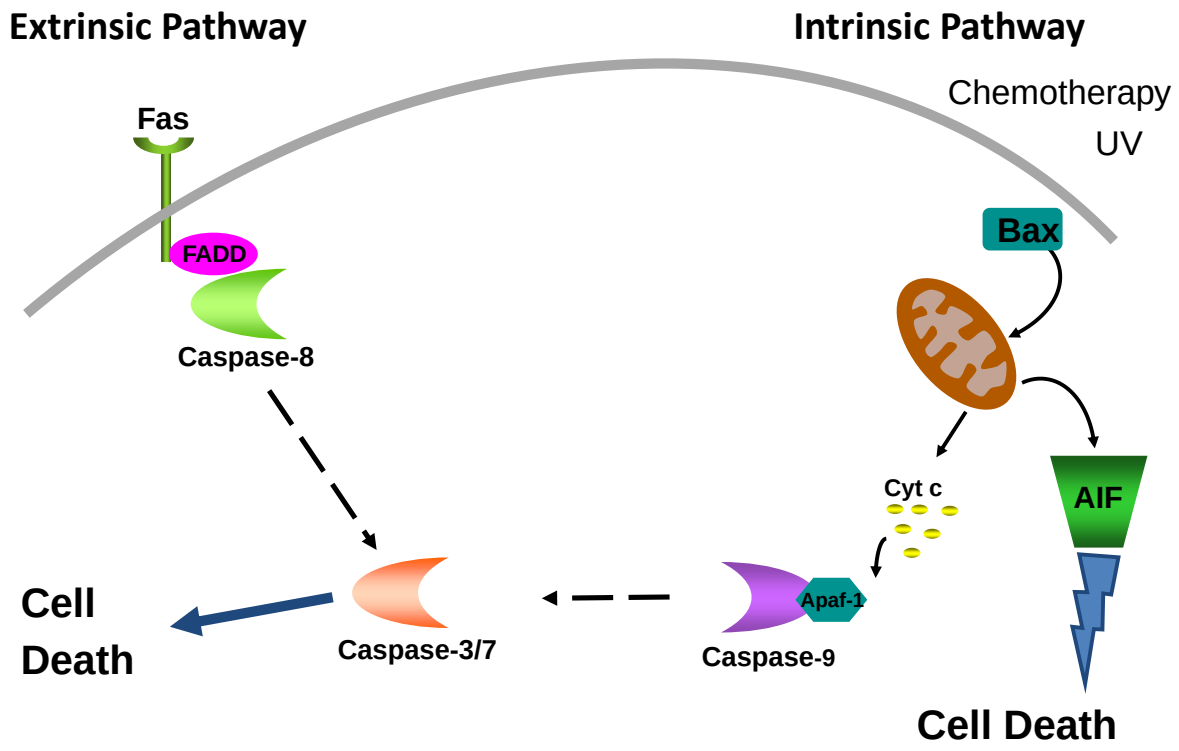

Figure 1.4. Extrinsic and intrinsic pathways of apoptosis.
The extrinsic apoptotic pathway is mediated by TNFs (*e.g.*, Fas ligand) and TNFRs (*e.g.*, Fas receptor), which recruit the adaptor molecule FADD to activate caspase-8. The intrinsic pathway, occurring through the mitochondria, involves OMM permeabilization followed by the release of cytochrome c and activation of caspase-9. Both pathways converge upon caspase-3 and caspase-7 activation. AIF can be released from the mitochondria and subsequently translocate to the nucleus in a caspase-independent manner.

1.5A) is tethered to the IMM by a small hydrophobic segment with the soluble protein surfaces extending into the IMS [24, 31]. Following import into the mitochondria, AIF acquires its oxidoreductase activity through the incorporation of an FAD moiety (Figure 1.5B) and adopts a glutathione reductase fold. Upon cell death stimuli and OMM permeabilization, AIF undergoes a second round of proteolytic cleavage at position 102 by cathepsins and/or calpains, freeing AIF from its IMM tether [24, 28, 31-33]. The liberated cytosolic form of AIF (Δ1-102 AIF, 57 kDa, Figure 5A) is targeted to the nucleus via its nuclear localization sequence (NLS), and its C-

terminal domain binds DNA to initiate chromatin condensation and DNA fragmentation characteristic of cellular demise [24, 34].

Role of AIF in cell death

AIF was first identified in 1996 as a soluble factor released from mouse mitochondria during apoptosis, causing isolated nuclei to undergo chromatin condensation and internucleosomal DNA fragmentation [35]. During this time knowledge of apoptotic signaling was limited, and the ability of AIF to trigger features of apoptosis independently of caspase activation (Figure 1.4) was an unprecedented discovery in the field of cell death research. Under conditions of cell death, OMM permeabilization induces the release of mitochondria-localized AIF into the cytosol (Figure 1.4), followed by its translocation to the nucleus and nonspecific DNA binding [24, 31, 32, 36-43]. In the nucleus AIF recruits additional factors including endonuclease G, cyclophilin A, and/or H2AX to form active DNAse complexes that induce chromatinolysis and DNA degradation [40, 41, 43]. The precise mechanistic details of this process remain unclear.

AIF-mediated toxicity is regulated by a variety of cell death inhibitors during various phases of the apoptotic cascade including Bcl-2, the heat shock protein Hsp70, and XIAP. AIF was first identified in the context of Bcl-2-mediated protection from apoptosis, and its release from the mitochondria is attenuated when Bcl-2 inhibits OMM permeabilization [24, 35]. Through its interaction with Apaf-1, Hsp70 promotes apoptotic resistance by suppressing the apoptosome complex and ensuing caspase activation [44, 45]. In a caspase-independent manner, Hsp70 also binds AIF, preventing its relocation to the nucleus [46, 47]. XIAP is an endogenous inhibitor of caspases but also functions as an E3 ubiquitin ligase [48]. Duckett and colleagues identified AIF as a binding partner of XIAP and target for ubiquitination [49]. Contrary to the

canonical association of ubiquitin modification with proteasomal targeting, XIAP-mediated ubiquitination of AIF at lysine 255 interferes with the ability of AIF to bind DNA and induce chromatin degradation [50]. It is notable that since AIF-mediated death is caspase independent, the actual mechanisms by which AIF causes toxicity more closely resemble necroptosis (appendix A).

Interestingly, we have identified the mitochondrial phosphatase PGAM5 as an AIF-associated factor that triggers a novel death pathway leading to mitophagic cell death. Similar to AIF, PGAM5 is ubiquitinated and inhibited by XIAP through a non-degradative mechanism [53]. This indicates the existence of a regulatory triad comprising AIF, PGAM5, and XIAP that could regulate the balance of cell death and survival. Therefore while AIF is not commonly a significant factor for the execution of "classical" apoptosis, AIF is likely to play a role in atypical death mechanisms associated with XIAP and PGAM5. Further exploration of this death triad and its control through non-canonical ubiquitination represents a significant area of research that may further explain how cells determine decisions of cell fate.

Despite an extensive number of studies defining the mechanisms by which AIF mediates cellular toxicity and its utility as a cell death marker [24, 31, 32, 36-43], the ability of AIF to kill is often insignificant [49, 51-54]. Rather, AIF activity is essential for the cell to die only under limited stimuli and to a narrow range of cell types, primarily neurons and cardiomyocytes in response to hypoxia-ischemia, DNA damage, and excitotoxicity [55-58]. Therefore, in sharp contrast to its name and initial characterization, AIF does not function as a universal effector of cell death.

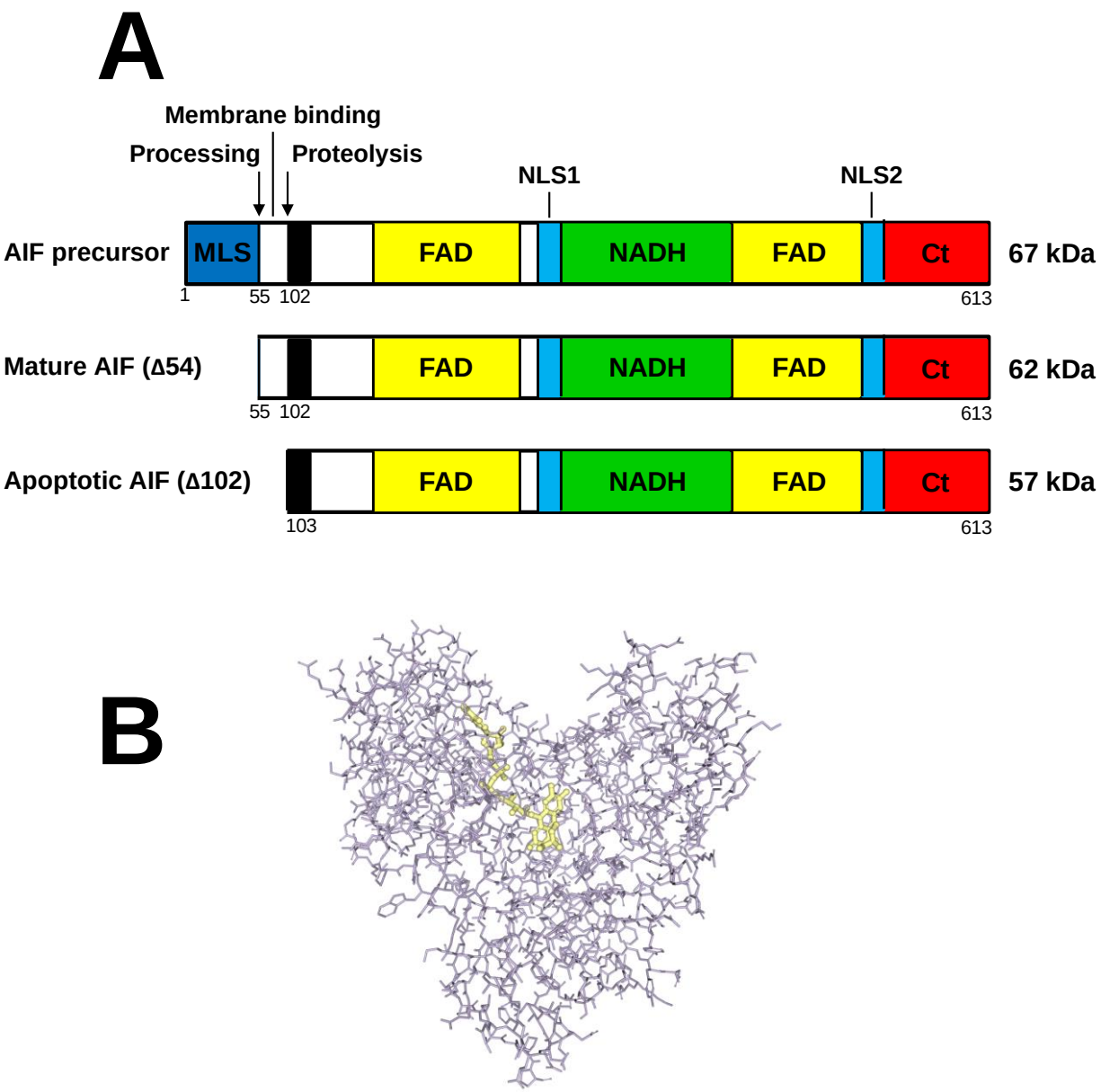

Figure 1.5. Domains and structure of AIF.
A) AIF is translated into a precursor polypeptide containing a mitochondrial localization sequence (MLS), two FAD-binding domains, an NADH binding domain, two nuclear localization sequences (NLS), and a C-terminal (Ct) DNA-binding domain. AIF is cleaved at the indicated positions during processing and mitochondrial release. B) Three-dimensional structure of AIF. Protein-bound FAD is shown in yellow. Image from the RCSB PDB (www.rcsb.org) of PDB ID 4BV6 [59].

Role of AIF in cell survival and homeostasis

Concurrently with studies of cell death mechanisms, AIF was also shown to possess an intrinsic redox activity dependent on FAD and NAD(P)H, similar to bacterial oxidoreductases, and that is independent of its death activity [24, 60]. AIF can catalyze the oxidization of both NADH and NADPH while reducing O_2 to superoxide *in vitro* [60], but the role of this NAD(P)H-oxidase activity *in vivo* is not well understood. These findings indicated additional activities distinct from AIF-mediated cell death and would first bring its dual nature to light. The enzymatic activity of AIF has been linked to control of mitochondrial structure and function [60, 61], and while a complete picture of how AIF promotes mitochondrial homeostasis remains elusive, it has become increasingly clear that the predominant cellular role of AIF maintains survival. The physiological significance of AIF in control of cell homeostasis and survival has been demonstrated in studies of AIF-null mice [26, 62], targeted AIF deletion experiments [63, 64], and cases of AIF mutation in humans [65-68] leading to a variety of mitochondrial respiratory chain and redox balance disorders. Inactivation of the *AIF* gene in mice causes embryonic lethality [62, 69], whereas the Harlequin mouse model exhibits severe and progressive neurodegeneration as a consequence of decreased AIF protein expression (>80%) in all tissues [26]. Tissue-specific AIF deletion studies demonstrated a series of physiological defects including skeletal muscle atrophy and dilated cardiomyopathy resulting from severe mitochondrial dysfunction and loss of cristae structure [63, 64]. More recent studies in humans have identified AIF mutations that lead to respiratory chain malfunction with a spectrum of clinical manifestations including mitochondrial encephalomyopathy [65], prenatal ventriculomegaly [66], and Cowchock syndrome [68]. While largely descriptive, these studies

collectively illustrate a role for AIF as a central regulator of cellular metabolism and redox balance.

Consistent with the phenotypes shared by AIF deficiency and mitochondrial respiratory chain disorders, ablation of AIF causes a loss of complex I of the ETC, resulting in impaired OXPHOS [25]. AIF is neither a part of complex I nor found to interact with any ETC subunits, but it has been suggested that AIF can transfer electrons from NADH to ubiquinone, functioning as a supplemental NADH oxidase to the ETC [70]. Other groups have reported that AIF mediates respiratory chain biogenesis by facilitating the co-translational mitochondrial import and stabilization of the ETC import factor CHCHD4 [71, 72]. It has been proposed that AIF serves as a sensor of cellular redox conditions, controlling mitochondrial respiration and/or cell death in response to the metabolic and oxidative environment [73]. These findings establish the centrality of AIF to control of the mitochondrial respiratory chain and energy production, and confirm AIF as a significant mediator of cell survival and homeostasis.

AIF functions as a pro-tumor molecule

Metabolism and redox control in cancer

Cancer arises when cells accumulate genomic mutations that render them incapable of controlling their own proliferation. To exhibit aggressive and invasive characteristics, cancer cells rewire their metabolic pathways in such a way that they produce high levels of both energy and macromolecular supplies supporting further proliferation. Otto Warburg first observed that cancer cells increase their glucose consumption despite sufficient O_2 levels relative to normal cells, hypothesizing that defective mitochondrial respiration contributes to tumorigenesis [74]. While elevated glucose consumption is a common characteristic of tumor cells, it is now well-established that many cancer cells rely on both glycolysis and mitochondrial energy metabolism

[75]. As Warburg noted, such changes indeed often involve a substantial increase in glycolytic activity ("aerobic glycolysis"), but rather than stemming from defective respiration, elevated glycolysis serves to supply the pentose phosphate pathway with intermediates used for macromolecule biosynthesis (Figure 1.6). These metabolic reprogramming events come at the cost of mitochondrial energy production, and the subsequent loss of metabolic leeway sensitizes cancer cells to metabolic perturbation relative to normal cells [76]. This "metabolism addiction" makes the disruption of cancer cells' delicate metabolic balance an attractive therapeutic goal.

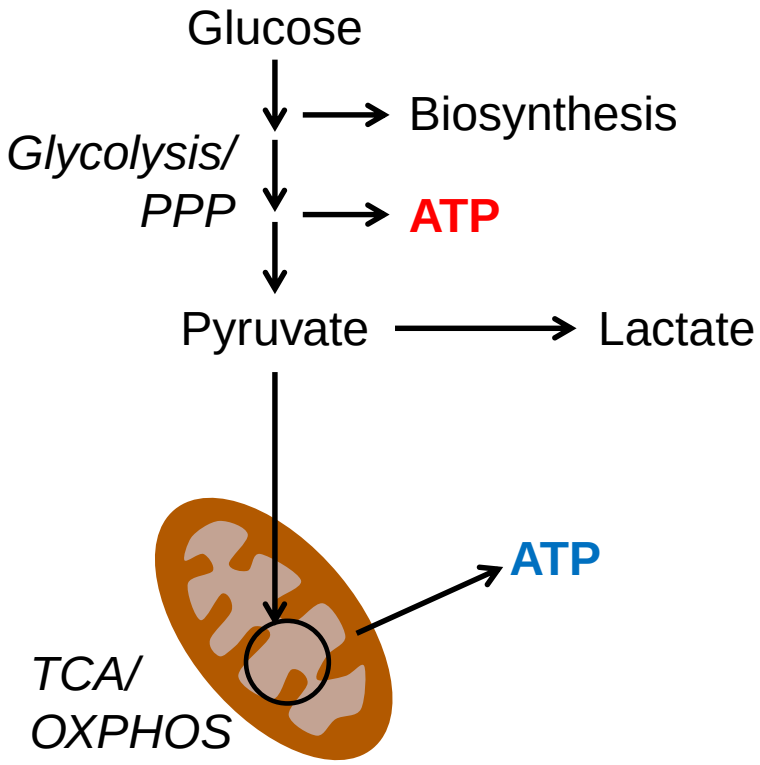

Figure 1.6. Metabolic fates of glucose.
Glucose may be catabolized to pyruvate during glycolysis, producing ATP, or glycolytic intermediates may enter biosynthesis reactions through the pentose phosphate pathway. If further glycolysis is required, pyruvate is converted to lactate. Alternatively pyruvate can be fully oxidized in the mitochondria to produce ATP. Metabolism addiction in cancer cells can result from the balancing act of upregulating these pathways simultaneously.

In addition to metabolic alterations supplying fuels necessary for aggressive growth, cancer cells also exhibit a moderate increase in ROS levels relative to normal cells that drive growth-promoting signaling events [77] and promote oxygen-independent metabolism in hypoxic tumor regions inaccessible to vasculature [78]. There exists a threshold for increased ROS, and this elevation of the cellular redox state must be carefully controlled since high ROS levels are lethal [79] (Figure 1.3). ROS-dependent signaling regulated by the mitogen-activated protein kinase (MAPK) family of proteins [80] is a significant example of how ROS levels impact cell fate. MAPKs operate as central signaling hubs to control a wide range of cellular activities in response to ROS and many other stimuli. Under conditions of elevated ROS, the MAPK known as c-Jun N-terminal kinase (JNK) can be activated through phosphorylation by upstream kinases (MAP2Ks) and relief of MAPK phosphatase (MKP)-mediated inhibition [80]. While it is recognized that exceptions exist, the generally held view is that in response to the cell's oxidative stress level, low levels of JNK activity promote proliferation, whereas high levels of JNK activity induce apoptosis [81]. Cancer cells elevate ROS to levels that drive pro-survival and proliferative activities through JNK and numerous other redox-sensitive signaling pathways. Although elevated ROS levels promote tumorigenic signal transduction, these increased ROS cause cancer cells to exhibit increased sensitivity to oxidative stress-induced toxicity relative to normal cells. Therefore there exists therapeutic potential for targeting redox balance in cancer treatment [82].

Tumorigenic activities of AIF

The pro-survival activity of AIF and its role in controlling metabolic and redox homeostasis in healthy cells is well positioned to be exploited by cancer cells in order to promote growth, invasiveness, and chemoresistance [51, 52, 54]. Indeed, increased AIF protein levels are

observed in a variety of cancer types including esophageal, skin, colorectal, gastric, lymphatic, pancreatic, and prostate cancers [51, 52, 83-88], suggestive of a prominent role in tumorigenesis. Despite its initial characterization as a death-associated molecule, the possibility of elevated AIF functioning as a tumor suppressor is unlikely. First, the requirement for AIF in cell death is exceedingly cell type and context specific: AIF-mediated toxicity is essential for cell death primarily in neurons and cardiomyocytes and in response to specific stimuli including hypoxia-ischemia, oxidative stress, DNA damaging agents, engagement of death receptors, and excitotoxins [55-58]. Second, in rare cases that AIF may induce lethality, endogenous AIF inhibitors (XIAP, Hsp70, Bcl-2) are also expressed at high levels in cancer [89-92] and could neutralize potentially toxic effects of AIF elevation. It is more likely that instead of a major role for AIF death function, the pro-survival activities of AIF would serve to mediate tumor-permissive metabolic and oxidative states.

How might the presence of AIF promote tumorigenesis? A supportive role of AIF in cancer would likely derive from its ability to regulate ETC/OXPHOS, which gains significance as cells become more aggressive and reliant on mitochondrial function. When tumors undergoing aerobic glycolysis reach advanced stages, cancer cells often continue to rely on mitochondria as a source of energy production [93] and suffer a metabolic disadvantage when mitochondrial function is lost. Indeed, several recent studies have identified paramount roles for OXPHOS in promoting the invasiveness of cancer cells [94-96]. A second mechanism for AIF support of cancer might involve increased ROS levels through AIF-mediated catalysis, which would serve as signaling molecules to promote proliferation and survival.

The work of Urbano *et al*. [54] was the first to demonstrate a pro-tumor role for AIF. Following ablation of AIF, Porter and colleagues observed reductions of complex I subunits and

decreased ROS levels in colorectal, breast, and lung cancer cell lines. These changes corresponded to impairments in both growth and resistance to chemical oxidative stress and DNA damaging agents in a manner dependent on the enzymatic activity of AIF. This demonstrated for the first time that *apoptosis-inducing factor* can function as an *anti-apoptotic* molecule that supports—rather than suppresses—tumorigenesis, likely through control of cellular metabolism and/or ROS-mediated survival signaling.

AIF enzymatic activity supports advanced prostate cancer

The work of our laboratory has further defined tumorigenic roles for the enzymatic activity of AIF in the context of advanced prostate cancer [51]. In a mouse model of prostate tumorigenesis [97], loss of the tumor suppressor PTEN in prostate tissue leads to increased AIF protein levels, indicating a possible role in the development of prostate tumorigenesis. Extending these data to human studies, increased AIF expression is observed at both the RNA and protein levels in prostate tumors relative to normal tissue. Notably, AIF protein levels become significantly more abundant with disease progression, and together these data show AIF levels can serve as a marker for disease and may promote prostate cancer (PCa) progression.

To test this hypothesis, AIF was stably suppressed in the PCa cell lines PC3, DU145, and LNCaP. While LNCaP cells are sensitive to androgen deprivation (a means of PCa treatment), PC3 and DU145 have developed resistance and are considered a model of further disease progression. Sensitivity to a variety of chemical death agents was unaffected following AIF ablation, further confirming the hypothesis that AIF is not a significant inducer of death in cancer. While proliferation was unaffected under nutrient-rich conditions *in vitro*, suppression of AIF severely impaired invasion, migration, and growth in Matrigel™ substrate. This AIF-dependent growth support was observed in PC3 and DU145 (advanced cells) but not LNCaP

cells. Xenograft studies of AIF-mediated tumorigenesis in mice were then conducted using PC3 cells, demonstrating that AIF is critical for tumor growth *in vivo*.

Metabolic assessment of PCa cells revealed that AIF-dependent growth support is directly related to its metabolic contribution. AIF knockdown led to decreased levels of complex I in PC3 and DU145 cells, yet subunits examined were unaffected in LNCaP cells. Notably, this was the first report of a context in which AIF does not regulate complex I. AIF-deficient PCa cells with decreased complex I also exhibited increased glucose consumption, increased lactate secretion, and decreased oxygen consumption. Together these data indicate that following suppression of AIF, mitochondrial OXPHOS expectedly decreases and is accompanied by an increase in glycolysis. The significance of this glycolytic elevation to survival was confirmed by sensitivity to glycolytic disruption, as cells treated with the glycolysis inhibitor 2-deoxyglucose exhibited substantially greater amounts of death when AIF was suppressed. Consistent with other metabolic analyses, these effects were only observed in PC3 and DU145 cells, while LNCaP cells were unaffected.

To determine if these observations are due to the enzymatic activity of AIF, cells were restored with either wild-type (WT) AIF or AIF with T263A/V300A mutations (TVA), which cause catalytic impairment. Restoration of AIF-deficient PC3 cells with WT-AIF but not TVA-AIF restored the metabolic and growth effects of AIF deficiency to control levels, demonstrating that the NADH-oxidase activity of AIF supports metabolism benefitting the growth and invasiveness of advanced prostate cancer cells. It is notable while only WT-AIF can restore growth and metabolism, both WT-AIF and TVA-AIF can restore complex I. This suggests that the enzymatic activity of AIF is not significant to complex I levels yet remains a critical factor for cellular metabolism, and the nature of metabolic switching following AIF ablation is not

limited to the effects of complex I expression alone. Altogether these experiments demonstrate the essential role of AIF enzymatic activity to the progression of PCa and prompt further investigation into AIF metabolic and redox activity in cancer.

Open questions and research objectives

Expanding studies of AIF metabolic activity to additional cancer types

Previous work in our laboratory [51] defined a novel pro-tumor metabolic role for the enzymatic activity of AIF in PCa. A natural question that arises is whether AIF expression and/or activity contribute to other cancer types, or if AIF is uniquely important to the development of limited cancers such as PCa and colorectal cancer [51, 54]. AIF expression and metabolic contribution to PCa both increase with disease progression. Extending this observation to other cancer types, does this suggest that AIF is important specifically to advanced-stage cancers?

This hypothesis forms the basis for our investigation of AIF activity in pancreatic ductal adenocarcinoma (PDAC), a disease almost universally advanced at diagnosis and consequently one of the most lethal malignancies across the world. Due to the anatomical position of the pancreas, tumors cannot be seen or felt during routine exams, and early detection methods for disease are scarce. Because symptoms typically do not manifest until the cancer has metastasized, tumors often become unresectable before diagnosis, and long-term survival after resection is poor. Moreover, current treatment options fail to prolong survival beyond several months that are accompanied by severe side effects, with PDAC mortality nearly identical to incidence [98]. The identification of AIF as a contributory factor for PDAC pathogenesis would extend its role beyond the context of PCa and also implicate AIF as a potential therapeutic target.

Pancreatic cancer as a setting to identify and predict which cells are sensitive to AIF

PDAC is one of the most bioenergetically sensitive and metabolically diverse known diseases [76]. In recent years several groups have subtyped PDAC based on gene expression signatures, oncogene addiction, and drug responses, which have been coined as classical, quasimesenchymal, and exocrine-like [99] and are described in Appendix B. Another study by Daemen *et al*. [100] demonstrated *metabolic* subtypes with strong correlation to the above groups. The "slow proliferating" metabolic subtype is especially low in carbohydrates and amino acids with substantially longer doubling times compared to the other two subtypes. The other two subtypes are classified as "glycolytic," corresponding to the quasimesenchymal subtype, and "lipogenic," corresponding to the classical subtype. The glycolytic subtype exhibits elevated activities of glycolysis and pentose phosphate pathways (PPP), whereas the lipogenic subtype displays increased lipid levels and, importantly, increased ETC/OXPHOS and mitochondrial redox activity.

Based upon our laboratory's previous work, AIF-mediated metabolism and growth support is clearly cell type-specific [51], but how/why AIF controls complex I and glucose metabolism in some cells but not others remains an open question. AIF is proposed to function as a metabolic/redox sensor of the mitochondria [73], and it therefore stands to reason that AIF activity may be regulated by the metabolic conditions and needs of the cell. The study of AIF among PDAC subtypes may reveal if AIF exhibits a subgroup preference, similar to PCa, and perhaps more importantly, demonstrate how AIF functions in different metabolic environments and elucidate predictive factors for AIF sensitivity.

A widespread role for the enzymatic activity of AIF

AIF is established to participate in both cell death and metabolism. AIF metabolic activity is limited to specific cell types, and essential roles for AIF in cellular toxicity are even more elusive. Do all AIF activities vary by cell type and context, or might AIF exhibit some yet to be identified universal cellular activity?

The significance of AIF enzymatic activity to mitochondrial homeostasis and survival has been demonstrated in a variety of descriptive studies [26, 62-68], and a possible widespread function may lie in the ability of AIF to produce ROS. The enzymatic activity of AIF has been demonstrated to generate superoxide *in vitro* [60], but AIF-mediated redox regulation in cells is an area largely unexplored. Altered ROS levels and ROS types control a variety of signaling pathways and cellular functions, and AIF-dependent differences in phenotypes among cells can be explained by cell type-specific methods of ROS regulation (*e.g.*, types and levels of antioxidants, other ROS producers, and/or endogenous regulators of redox signaling pathways). Such observations would confirm the long-speculated role of AIF as a central regulator of cellular oxidant signaling.

The implications of AIF as a signaling molecule

The identification of AIF as a control point for signal transduction would serve as a mechanistic milestone in understanding how AIF regulates cellular homeostasis, and explain how AIF can control nuclear gene expression from within the mitochondria. In the context of cancer, redox mechanisms through which AIF mediates tumorigenesis have yet to be identified. AIF levels increase in cancer, but upregulation typically does not exceed two- to threefold [51, 52]. This might represent a change that supports pro-tumor metabolic and redox activity but without inducing ROS overload or toxicity in the nucleus. Increased AIF levels could drive

redox signaling activity in cancer that promotes drug resistance [54], metabolism [51], or other tumorigenic properties such as metastasis (Figure 1.7).

How AIF metabolic and redox activities are integrated in cells remains an open question. Cellular metabolic and oxidative states are intertwined. Examples of the complex relationship between metabolism and oxidative stress include the production of NADPH (during PPP, a pathway branching from glycolysis) that regenerates glutathione for antioxidant defenses, and ROS production by actively respiring mitochondria. AIF-mediated regulation of ROS and redox signaling could occur through complex I, AIF itself, or both (Figure 1.7). Further definition of AIF ablation-sensitive and insensitive cell types (*e.g.*, PC3 vs. LNCaP) followed by comparison of metabolic vs. redox activities among cells would be a starting point to delineating AIF-associated metabolic regulation and control of oxidative state. If AIF-mediated redox signaling is independent of complex I and metabolism, then changes in cellular oxidative state should be observed in cells both sensitive and insensitive to AIF ablation. Additionally, experiments assessing redox effects of AIF suppression while retaining mitochondrial respiratory chain activity would further confirm whether AIF activities are related or independent.

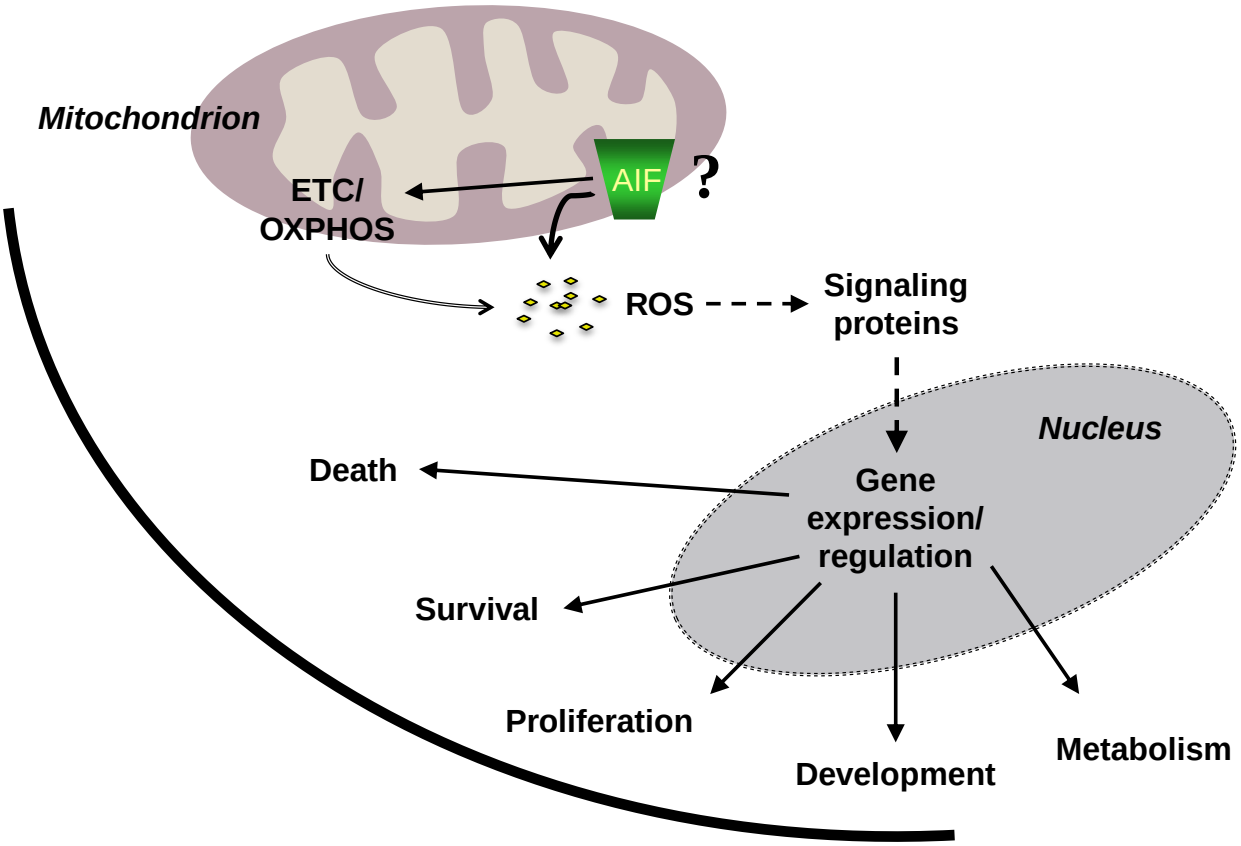

Figure 1.7. Involvement of AIF in cellular redox signaling.
AIF-mediated ROS production may result from the regulation of complex I and/or AIF enzymatic activity. Cellular ROS regulate a variety of genetic programs mediated by various signaling molecules.

Summary of research

The work of this study explores the metabolic and redox activities of AIF and their relationship in the context of both normal and tumorigenic cells. While AIF is not typically critical for cell death, experiments of this work demonstrate an involvement of AIF with PGAM5 and XIAP. PGAM5 suppresses XIAP-mediated ubiquitination of AIF, and XIAP and PGAM5 oppose one another to mediate cell death-survival balance. Studies of metabolically reconditioned PDAC cells show that metabolic adaptation plays a significant role in the acquisition of increased tumorigenesis through the mitochondria, indicating a likely role for AIF as a mediator of PDAC metabolic plasticity. AIF is then revealed to play a substantial role to the

growth and survival of PDAC cells through a metabolic mechanism that depends on cellular metabolic needs. OXPHOS-dependent PDAC cells require the metabolic activity of AIF for growth and survival, whereas glycolytic cells that do not rely on OXPHOS are metabolically insensitive to AIF. This suggests that basal metabolic state governs AIF-dependent growth support and demonstrates for the first time a potential explanation for different AIF sensitivity among cell types. Building upon these findings, the ability of AIF to mediate oxidative stress-induced signaling is then assessed in a broad panel of both normal and cancer cells. Regardless of AIF-mediated metabolic control, AIF is required for oxidative stress-induced activation of the MAP kinases JNK1, p38, and ERK. The role of AIF as a novel signal transduction protein is confirmed through its ability to trigger the metastatic event known as cadherin switch through JNK1, and genetic reversal of the cadherin switch in the absence of AIF is lethal. Finally, the abilities of AIF to regulate redox signaling and metabolism are shown to be functionally uncoupled, demonstrating novel routes through which AIF mediates growth and survival and underscoring their significance to human health and disease.

II. REVERSIBLE ADAPTATION OF PANCREATIC CANCER CELLS TO GLYCOLYSIS INHIBITION INDUCES A PERSISTENT INCREASE IN DRUG RESISTANCE

Abstract

Pancreatic ductal adenocarcinoma (PDAC) is one of the deadliest forms of cancer, due in part to altered metabolism that contributes to invasion and drug resistance. PDAC cells are among the most metabolically diverse and adaptable cancer types, and a better understanding of how metabolic adaptation impacts drug resistance may be used to further identify molecular targets. Here we demonstrate that while several PDAC cell types exhibit resistance to glycolytic inhibition with 2-deoxyglucose (2DG), MIA PaCa-2 cells are highly sensitive with a strong dependence upon glycolysis for survival. Prolonged exposure to 2DG causes MIA PaCa-2 cells to adapt by upregulating mitochondrial activity, which is accompanied by increased ROS and oxidative stress sensitivity, altered growth and invasion, and increased drug resistance. Remarkably, these metabolic and growth effects reverse when conditions of glycolytic suppression are relieved. However, increased drug resistance persists when cells are removed from 2DG pressure. This demonstrates that metabolism directly regulates drug resistance and that transient metabolic alterations can lead to long-term effects upon chemoresistance.

Introduction

Pancreatic ductal adenocarcinoma (PDAC) is one of the most lethal malignancies across the world, with mortality nearly identical to incidence. Because symptoms are often detected late into disease progression, tumors become unresectable prior to diagnosis, and long-term survival after resection is poor, with current treatment options failing to prolong survival beyond several months [101].

Relative to other cancers, PDACs often encounter more demanding *in vivo* metabolic constraints that stem from hypovascular and fibrotic microenvironments leading to hypoxia and limited nutrient availability. Therefore PDAC cells acquire metabolic capabilities not seen in other cancer types. These metabolic changes contribute significantly to invasion and resistance to treatment [76, 102].

PDAC is one of the most bioenergetically sensitive and metabolically diverse known diseases [76]. In order to grow aggressively and invade through the body, cancer cells undergo metabolic reprogramming events producing both energy and macromolecular supplies at high levels supporting further proliferation and resistance to treatment. Otto Warburg first observed that relative to normal cells, cancer cells exhibit highly increased glycolytic activity under conditions of abundant oxygen. It was hypothesized that defective mitochondrial respiration is a cause for this "aerobic glycolysis" and contributes to tumorigenesis [74]. However, it is clear now that many cancer cells rely on both glycolysis and mitochondrial energy metabolism [75].

Cancer cells additionally exhibit increased ROS levels relative to normal cells that drive growth-promoting signaling events [77] and promote oxygen-independent metabolism in hypoxic tumor regions inaccessible to vasculature [78]. However, because high ROS levels are lethal, cancer cells often exhibit increased sensitivity to oxidative stress-induced toxicity relative to normal cells. ROS elevation in cancer is attributed in part to altered metabolism [79, 103].

PDAC is stratified into three subtypes (classical, quasimesenchymal, and exocrine-like) according to gene expression signatures, oncogene addiction, and drug responses [99]. Notably, these subtypes correspond to defined metabolic phenotypes [100]. The quasimesenchymal subtype exhibits a dependence upon glycolysis for growth and survival, while the classical subtype displays increased lipid levels, ETC/OXPHOS, and mitochondrial redox activity.

Drug responses and mean survival rates differ significantly among subtypes (Appendix B) and are likely due to intrinsic differences in metabolic characteristics. Here we show that glycolytic PDAC cells subjected to prolonged glycolysis inhibition undergo metabolic changes that lead to increased mitochondrial activity and dependence. These alterations confer resistance to a variety of chemotherapeutic agents, and cells remarkably revert back to a glycolytic phenotype following relief of anti-glycolytic conditions. Interestingly, while the metabolic phenotype can reverse, drug resistance persists. Altogether this demonstrates by proof of principle that PDAC cells undergoing transient metabolic adaptations can acquire long-term drug resistance.

Materials and methods

Materials

MEM, DMEM, RPMI 1640, GlutaMAX, trypsin, fetal bovine serum (FBS), and phosphate buffered saline (PBS) were from Thermo Scientific; QuantiChrom™ Glucose Assay Kit was from BioAssay Systems; Matrigel™ was from BD Biosciences; Matrigel Recovery Solution was from Corning; all other materials were from Sigma.

Cell culture

PANC-1, BxPC-3, HPAF-II, and MIA PaCa-2 cells were from ATCC (kind gift of Dr. Sanku Mallik, NDSU). Cells were grown in an atmosphere of 95% air and 5% CO_2 at 37 °C. All media was supplemented with 2 mM GlutaMAX. Cell lines were grown and cultured with the following media formulations: PANC-1 cells in DMEM supplemented with 10% FBS; MIA PaCa-2 in DMEM supplemented with 10% FBS and 2.5% horse serum; BxPC-3 in RPMI 1640 supplemented with 10% FBS; HPAF-II in MEM supplemented with 10% FBS.

Metabolic conditioning with 2-deoxyglucose

MIA PaCa-2 cells were exposed to 500 μM 2DG for 72 h and then at progressively increasing concentrations every 3-4 d until cells grew in 10 mM 2DG. Once cells were in 10 mM 2DG, cells were treated with progressively increasing concentrations of 2DG in cycles of 3-4 d of 2DG exposure and 3-4 d of growth in the absence of 2DG. Once cells (MP2-D) could be cultured in 50 mM 2DG for 48 h without substantial toxicity (~3 mo of treatment), cells were cultured in alternating normal media conditions and media containing 50 mM 2DG. Fractions of cells from these cultures were then grown in normal media without 2DG for ~3 mo to generate MP2-DW cells.

Drug treatments

Cells seeded at equal densities were treated with 0-50 mM 2-deoxyglucose (2DG) for 0-96 h, 1 μM gemcitabine for 72 h, 10 μM FCCP for 48, 10 μM oligomycin A for 24 h, 90 μM tBHQ for 24 h, 10 mM N-acetylcysteine for 24 h, 1 μg/mL docetaxel for 48 h, 1 μM paclitaxel for 48 h, or 100 μg/mL etoposide for 24 h.

Cell viability

Cells treated as indicated above were harvested by trypsinization, washed, and resuspended in PBS containing 2 μg/mL propidium iodide. Cell viability was determined by flow cytometry.

Measurements of mitochondrial $\Delta\Psi_m$ and abundance

Staining for mitochondrial membrane potential was carried out as described previously [104] by resuspending harvested cells in PBS containing 200 nM TMRM followed by flow cytometry. Staining for mitochondrial abundance was carried out by incubating cells with 100 nM MitoTracker™ Red at 37 °C for 20 min. Cells were then harvested and resuspended in PBS,

followed by assessment of stain intensity using an Accuri C6 flow cytometer. Mitochondrial heterogeneity was defined as the sum of right and left histogram peak shoulders.

ROS measurements

Cells were incubated with 2.5 μM MitoSOX™ Red (for mitochondrial superoxide), or 10 μM CM-H_2DCFDA (for general cellular ROS) at 37 °C for 20 min. Cells were then harvested and resuspended in PBS, followed by assessment of stain intensity using an Accuri C6 flow cytometer.

Glucose consumption measurements

Cells were harvested by trypsinization, washed, resuspended in fresh medium, and seeded at equal densities in replicate 6-well plates. Cells were grown at 37 °C for 72 h. Media was then collected from each well, and total glucose was measured using the QuantiChrom™ Glucose Assay Kit (BioAssay Systems). Total cell number in each sample was determined by Coulter™ counting. To determine glucose consumed per cell, total glucose consumption per sample was divided by its corresponding cell count.

Phase contrast microscopy

Images were captured by phase contrast microscopy using the 10× and 20× objectives of a Nikon TS100F microscope equipped with a Nikon DS-Fi1 digital camera detection system and NIS Elements 4.0 software.

Matrigel™ experiments

Equal volumes of cold Matrigel™ were added to each well in 24-well plates and then allowed to solidify at 37 °C for 1 h. Cells were added to Matrigel™ layers at equal densities and exposed to substrate conditions for up to 5 days in the absence or presence of GEM. Detached cells were collected and quantified by Coulter™ counting; attached cells were extracted from

substrate using Matrigel recovery solution (Corning) and quantified by Coulter™ counting. Percent viability was defined as the number of attached cells divided by total cells. Glucose assay was performed as described above.

Cell growth rate measurements

Cells were harvested by trypsinization, washed, resuspended in fresh medium, and seeded at equal densities in replicate 6-well plates. Cells were harvested and quantified by Coulter™ counting every 24 h for 96 h.

Scratch assay

Cells were harvested by trypsinization, washed, resuspended in fresh media, and seeded in replicate 6-well plates. Cells were allowed to attach overnight, and a single scratch was made through the middle of each well using a P200 pipette tip [105]. Cells were immediately washed, fresh media was added, and each scratch was imaged. Cells were then incubated for 24 h before final assessment of scratch width. All images were captured by phase contrast microscopy using the 10× objective of a Nikon TS100F microscope equipped with a Nikon DS-Fi1 digital camera detection system and NIS Elements 4.0 software.

Results

Assessment of metabolic plasticity and drug resistance in pancreatic cancer cells

Pancreatic cancer is a highly aggressive disease with 5-year survival rates of only 5-10%. Based on factors such as KRAS activation, *in vivo* microenvironments, and fluctuations in nutrient and oxygen availability, PDAC cells exhibit a remarkable metabolic plasticity that has been implicated as a cause of intense therapeutic resistance [76, 102, 106]. To assess the ability of PDAC cells to adapt to metabolic perturbation, four pancreatic cancer cell lines (PANC-1, BxPC-3, HPAF-II, MIA PaCa-2) were treated with 2-deoxyglucose (2DG), an inhibitor of

glycolysis. Cells able to meet the metabolic demands of growth and survival under conditions of impaired glycolysis will therefore display increased resistance to treatment. Following treatment cells showed various sensitivities to glycolysis inhibition (Figure 2.1A). PANC-1 and BxPC-3 cells demonstrated high levels of survival (>80%) when treated with 2DG, while HPAF-II cells exhibited moderate survival rates of ~70%. In contrast, MIA PaCa-2 cells were highly sensitive to 2DG, with only ~20% survival following glycolytic disruption (Figure 2.1A). This demonstrates a variety of metabolic requirements among PDAC cell types that agrees with previous findings [52, 100].

Metabolism is a significant contributor to the survival and aggressiveness of PDAC cells. Therefore we questioned if sensitivity to glycolytic disruption is related to therapeutic resistance. Gemcitabine (GEM) is a nucleoside analog and the current first-line treatment for patients [107]. Viability following GEM treatment was then evaluated using PANC-1 and MIA PaCa-2 cells, which exhibit the highest resistance and highest sensitivity to 2DG (Figure 2.1A), respectively. MIA PaCa-2 cells were substantially more sensitive to GEM than PANC-1 cells, with a difference of >30% in GEM resistance between cell types (Figure 2.1B).

Acquired resistance to glycolytic disruption is accompanied by an upregulation of mitochondrial activity

Since MIA PaCa-2 cells show the highest sensitivity both to metabolic disruption and GEM treatment among cell types used (Figure 2.1), this raised the question of whether the two are related. Therefore we generated MIA PaCa-2 cells resistant to 2DG. MIA PaCa-2 cells were exposed to progressively increasing 2DG concentrations over a period of ~3 months until cells exhibited no significant death at 50 mM 2DG for 48 h. Quantification of control non-conditioned

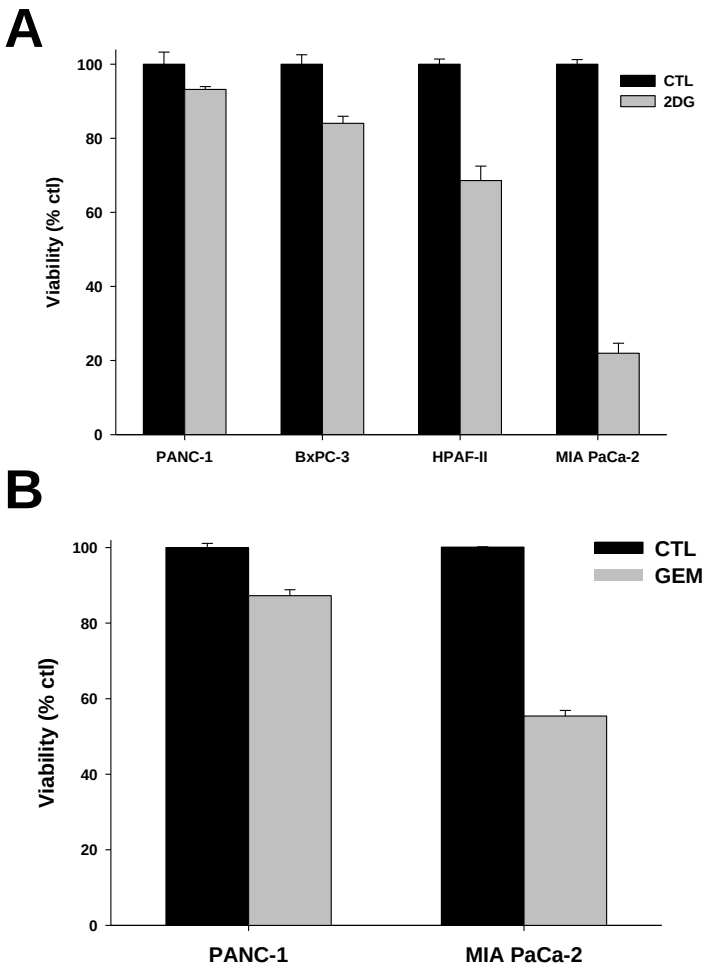

Figure 2.1. Sensitivity of PDAC cells to glycolysis inhibition and gemcitabine.
The indicated cell types were seeded at equal densities and treated with either A) 50 mM 2-deoxyglucose or B) 1 uM gemcitabine for 72 h, followed by PI stain and flow cytometry. Data are shown as average ± standard deviation.

cells (MP2) vs. 2DG-conditioned cells (MP2-D) demonstrated that MP2-D cells are capable of survival in 2DG for more time (Figure 2.2A) and at higher concentrations (Figure 2.2B).

In order to survive glycolysis inhibition, cells must acquire energy through alternative means, in particular by upregulating mitochondrial ATP production [108]. Therefore MP2 and MP2-D cells were assessed for mitochondrial activity by staining with tetramethylrhodamine ester (TMRM, an indicator of mitochondrial membrane potential). When MP2 cells were stained

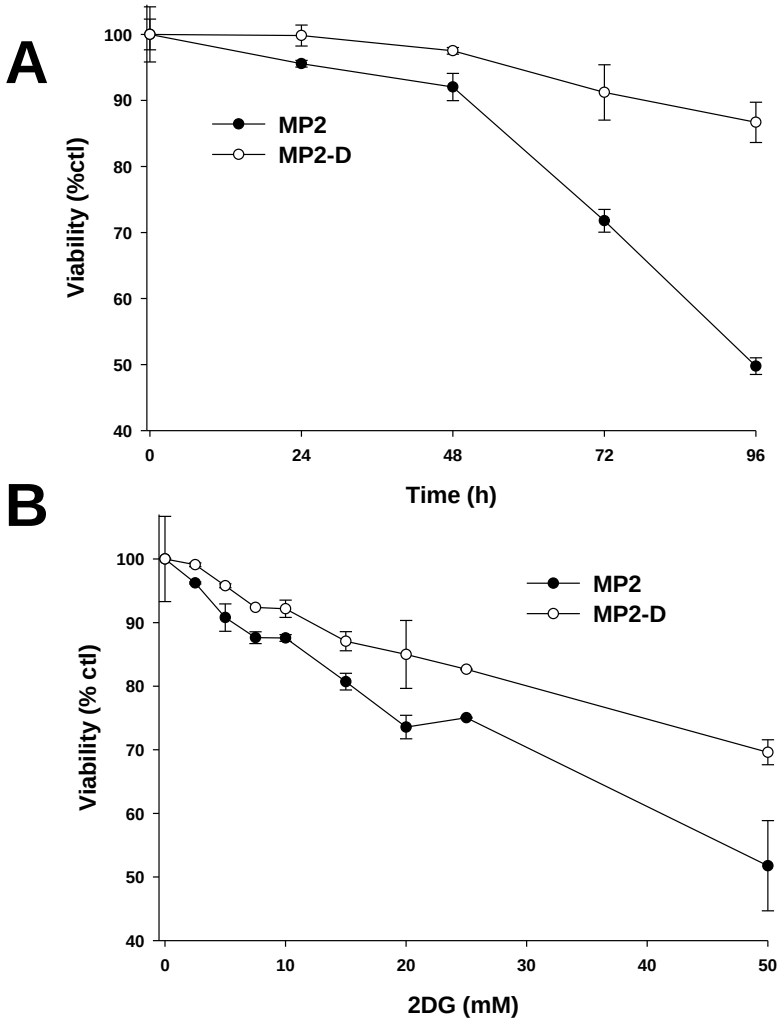

Figure 2.2. Establishment of MP2-D cells.
Cells were seeded at equal densities and then treated with A) 50 mM 2-deoxyglucose for 0-96 h or B) 0-50 mM 2-deoxyglucose for 72 h, followed by PI staining and flow cytometry. Data are shown as average ± standard deviation.

with TMRM, populations of low, medium, and high stain intensity were observed (Figure 2.3A). Staining of MP2-D cells revealed increased fractions with high membrane potential (Figure 2.3A, B). Mitochondria are more efficient producers of ATP than the pathway of glycolysis, and this ~10% increase in mitochondrial activity is approximately that which would be predicted to compensate for glycolytic deficiency. To determine if this increase in mitochondrial activity is

due to an increase in mitochondrial biogenesis, cells were stained with MitoTracker™ Red, an indicator of mitochondrial abundance. Interestingly, average stain intensity did not increase in MP2-D cells (Figure 2.3A). However, histogram peaks were narrower with fewer cell populations deviating from the mean in MP2-D samples when compared with MP2 controls (Figure 2.3A). This indicates a decrease in mitochondrial heterogeneity (Figure 2.3C), suggesting that cells become more selective for active mitochondria. The magnitude of this difference (~10%) agrees with TMRM experiments demonstrating increased mitochondrial activity in MP2-D cells. Notably, this ability of cells to upregulate mitochondrial activity shows that the mitochondria of MIA PaCa-2 cells are not impaired despite a metabolic preference for glycolysis. The reason MIA PaCa-2 cells fail to survive acute 2DG treatment remains an open question.

Cells that undergo a metabolic shift from glycolysis to OXPHOS will exhibit decreased glucose consumption and altered sensitivity to metabolic inhibitors. Glucose consumption was therefore assessed, showing decreased levels in MP2-D cells (Figure 2.4A). Similar changes in glucose uptake levels were observed when cells were exposed to Matrigel™ growth substrate (Figure 2.4B), which approximates an *in vivo* environment. These data suggest decreased levels of glycolysis in MP2-D cells, a phenotype that would be expected for cells exhibiting increased mitochondrial activity to survive 2DG treatment.

MP2 and MP2-D cells were then treated with two inhibitors of mitochondrial metabolism. Carbonylcyanide-*p*-trifluoromethoxyphenylhydrazone (FCCP) is a lipophilic weak acid that shuttles protons across membranes, leading to impairment of the proton gradient generated by the ETC and a subsequent loss of mitochondrial ATP production. Oligomycin A inhibits ATP synthase by blocking its proton channel. MP2-D cells exhibited significantly

increased death following treatment with either agent (Figure 2.4C, D), further demonstrating a shift from glycolysis to OXPHOS in MP2-D cells.

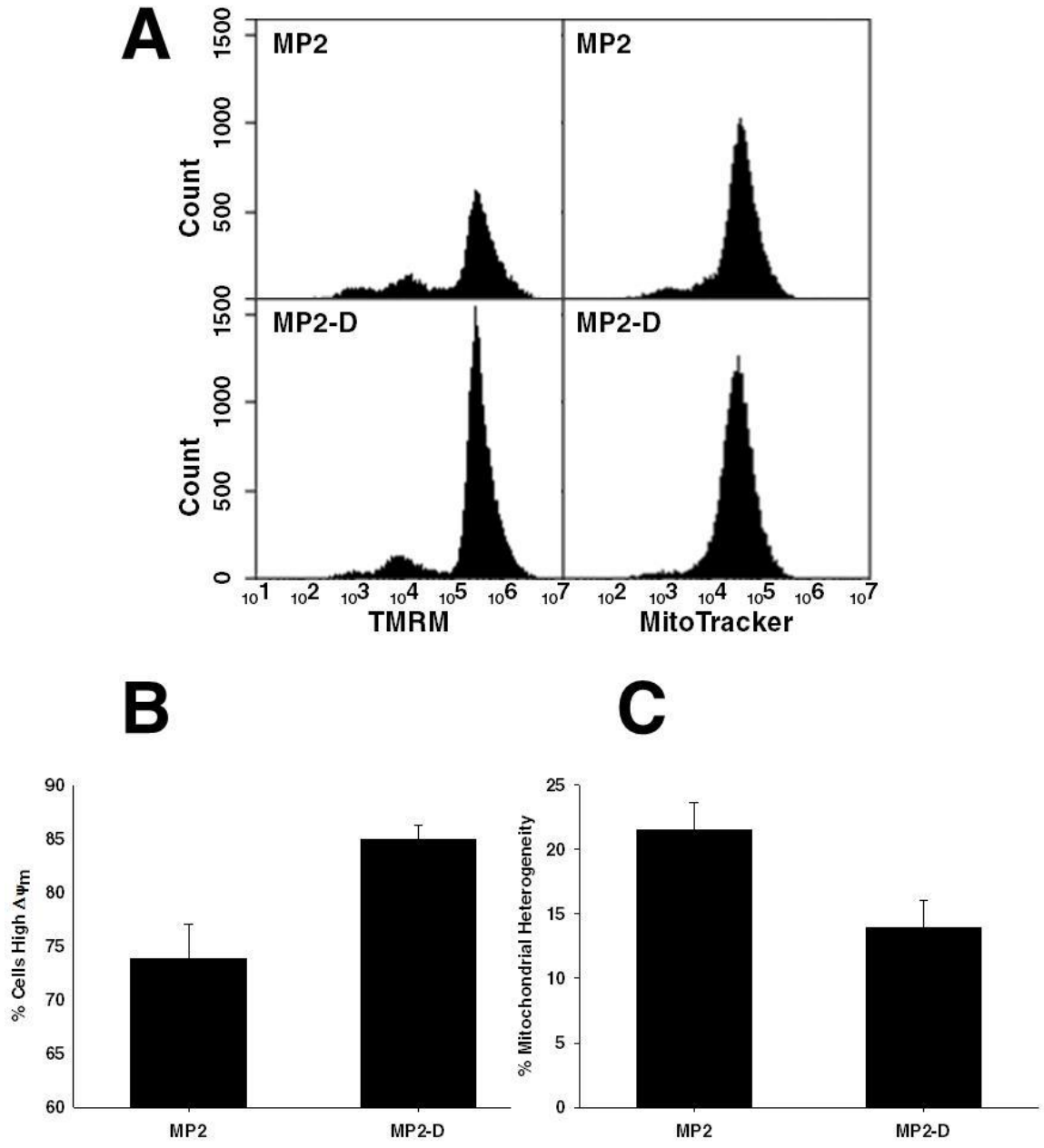

Figure 2.3. Acquired 2DG resistance leads to increased mitochondrial activity.
Cells were stained with either TMRM or MitoTracker™ Red and then assessed by flow cytometry. A) Representative histograms. B) Percentages of cells exhibiting high TMRM stain intensities. C) Mitochondrial heterogeneity was determined by the sum of high and low outliers of cell samples stained with MitoTracker™ Red. Data are shown as average ± standard deviation.

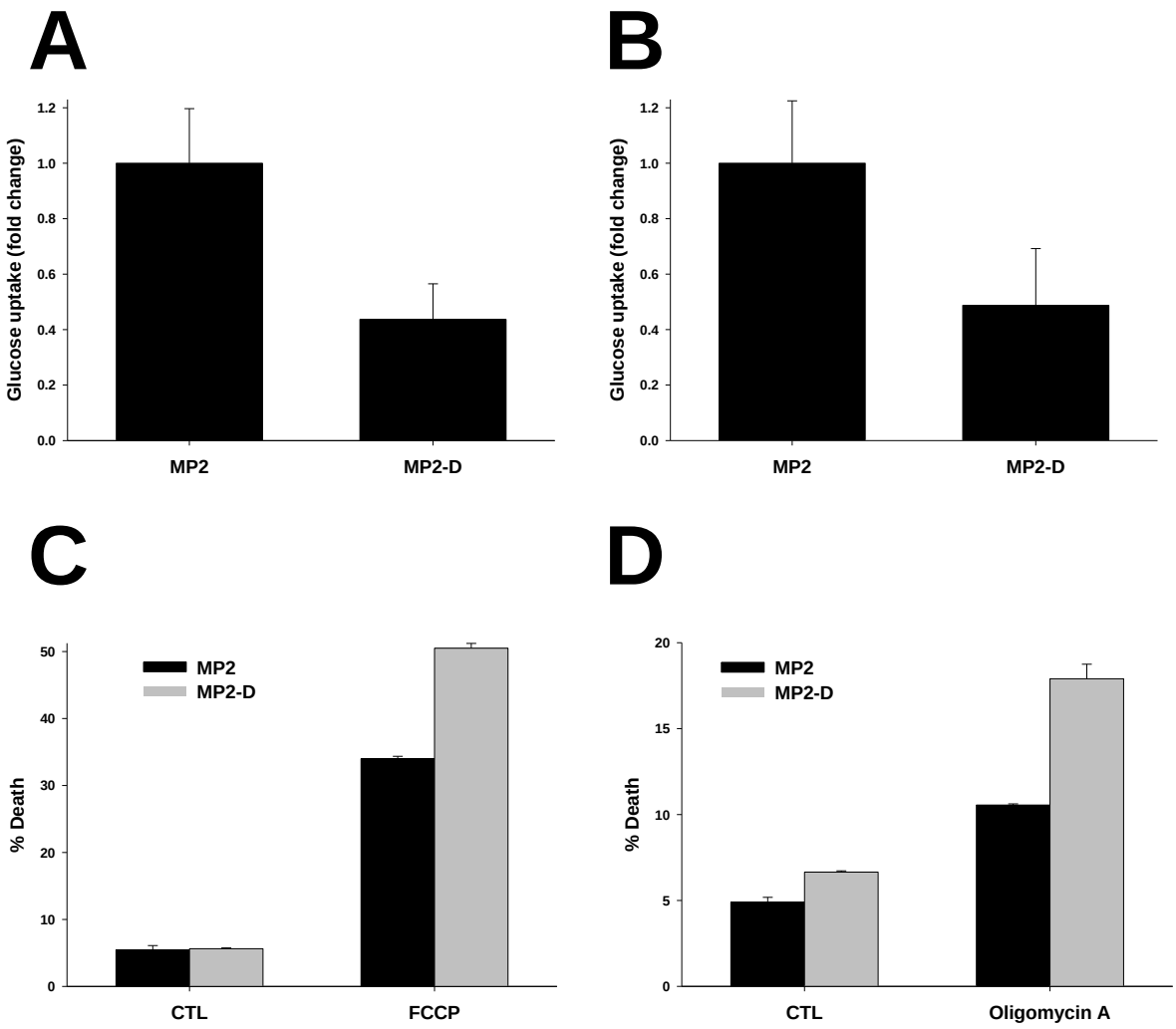

Figure 2.4. 2DG-conditioned cells shift from glycolysis to OXPHOS dependence for survival.
Glucose consumption was assessed A) *in vitro* and B) in Matrigel™ substrate using the QuantiChrom™ Glucose Assay Kit (BioAssay Systems). C) Cells were treated with control vehicle or 10 μM FCCP for 48 h, stained with PI, and assessed by flow cytometry. D) Cells were treated with either control vehicle or 10 μM oligomycin A for 24 h and then assessed as in (C). Data are shown as average ± standard deviation.

2DG-resistant cells exhibit increased ROS and oxidative stress sensitivity

Mitochondria are a major source of intracellular ROS due to leakage of electrons from the ETC. During tumorigenesis increased ROS levels can stimulate signaling pathways

promoting growth and survival, but can also induce toxicity if the cellular threshold is exceeded (Figure 1.3). Since MP2-D cells contain more active mitochondria than control MP2 cells, we questioned if ROS levels and/or redox sensitivity were also altered. Cells were stained with MitoSOX™ Red, an indicator of mitochondrial superoxide, followed by flow cytometry. Relative to MP2 cells, MP2-D cells exhibited ~40% greater mitochondrial superoxide levels (Figure 2.5A). Cells were then stained with chloromethyl-2',7'-dichlorodihydrofluorescein diacetate (CM-H_2DCFDA), a general detector of many ROS species not including superoxide that could indicate the extramitochondrial redox state. Similar to staining with MitoSOX™, cells showed increased ROS levels by >50% greater than controls following metabolic reconditioning (Figure 2.5B). Overall these data suggest that MP2-D cells contain increased mitochondrial and cytosolic ROS levels.

Since MP2-D cells have substantially higher levels of ROS, this raises the possibility that cells are closer to an oxidative stress-induced death threshold than controls. To test this hypothesis cells were treated with the oxidative stress agent *tert*-butylhydroquinone (tBHQ). Measurements of viability demonstrated resistance in control cells, but almost no survival (<10%) in MP2-D cells (Figure 2.5C), suggesting a dramatically increased sensitivity to oxidative stress that agrees with increased ROS levels.

Having observed that MP2-D cells show a severe sensitivity to oxidative stress, we then tested the inverse hypothesis that cells are more resistant to antioxidant treatment. While antioxidants can protect against ROS-induced cell death [109], neutralization of ROS at high amounts can also induce toxicity due to decreased pro-survival signaling [110]. Cells were treated with N-acetylcysteine (NAC), a ROS scavenger, at lethal concentrations. While MP2 cells showed reduced survival following NAC treatment, MP2-D cells were resistant to NAC

(Figure 2.5D), further demonstrating altered ROS responses in MP2-D cells. Altogether these data show that MP2-D cells increase ROS levels that can impact survival, either due to increased oxidative stress, decreased antioxidant defenses, or both.

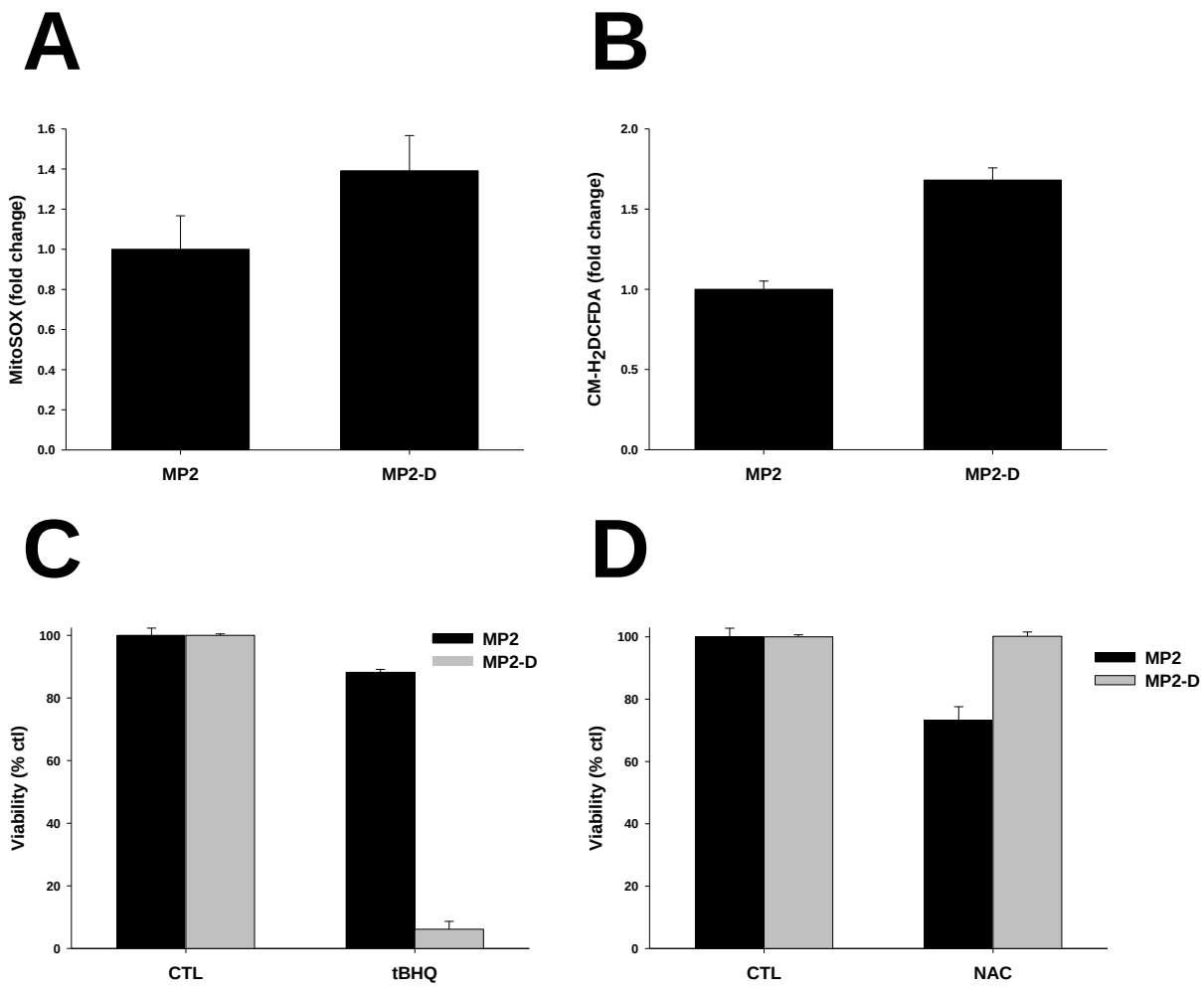

Figure 2.5. 2DG-conditioned cells exhibit increased ROS levels and sensitivity to oxidative stress.
Cells were stained with either A) MitoSOX™ Red or B) CM-H_2DCFDA and then assessed by flow cytometry. C) Cells were treated with control vehicle or 90 μM tBHQ for 24 h, stained with PI, and assessed by flow cytometry. D) Cells were treated with either control vehicle or 10 mM NAC for 24 h and then assessed as in (C). Data are shown as average ± standard deviation.

2DG-induced metabolic reconditioning alters cell growth and migration

Since acquired resistance to 2DG alters mitochondrial metabolism and cellular redox state, we then hypothesized that metabolic changes would impact tumorigenic phenotypes. In support of this hypothesis, MP2-D cells exhibited morphological differences from controls. MP2 cells showed web-like structures with projections extending to contact neighboring cells, while MP2-D cells formed clustered cobblestone structures (Figure 2.6A). Cells were then seeded in Matrigel™ substrate and further visualized. Control cells formed large, dense structures with numerous arm-like projections and tight cell-cell contacts, whereas MP2-D cells dispersed across the substrate with fewer projections and looser intercellular positioning (Figure 2.6B).

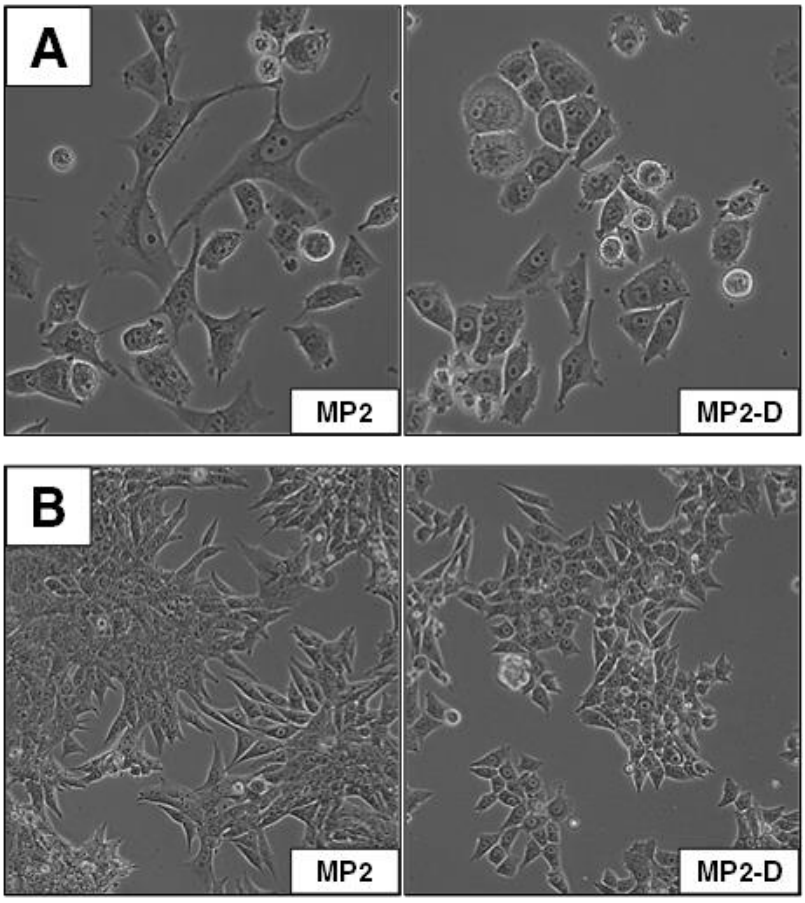

Figure 2.6. Acquired resistance to glycolysis inhibition induces morphological changes. Cells were seeded at equal densities and then imaged using confocal microscopy A) in vitro or B) in Matrigel™ substrate.

Changes in morphology are indicative of altered cell behavior. To determine if MP2-D cells are likely to exhibit different tumorigenic properties, MP2 and MP2-D cells were seeded at equal densities and then quantified after 5 days. Quantification of MP2-D cells revealed reduced numbers compared to controls, indicating a moderately reduced proliferation rate (Figure 2.7A). Migration of cells was then assessed by scratch assay. Following mechanical wound of cells at high densities, cells migrate across the wound and towards each at different rates, indicating different migratory properties. When MP2 and MP2-D were subjected to the wound-healing assay, MP2-D cells rapidly migrated across the wells at substantially higher rates than controls (Figure 2.7B), completely covering the wound within 48 hours (data not shown). This increased migration of MP2-D cells is in contrast to decreased proliferation, suggesting that acquired resistance to glycolysis inhibition promotes motility but not growth rates.

Metabolic and growth effects of 2DG conditioning are reversible

Metabolic alterations in PDAC are highly diverse, and changes in response to different metabolic stresses occur at levels not seen in other cancer types [76]. To determine if it is possible to restore the MP2-D phenotype to that of MP2 cells, MP2-D cells were withdrawn from 2DG and cultured in normal media for the same period of time as 2DG conditioning (~3 months). After ~3 months following 2DG withdrawal, cells were then treated with 2DG followed by viability assay. Remarkably, cells previously conditioned to prolonged 2DG exposure and then withdrawn (MP2-DW) exhibited a significant reduction in resistance to 2DG (Figure 2.8A), suggesting a reversion to a glycolytic phenotype. To determine if mitochondrial activity was affected, cells were then treated with oligomycin A and assessed for cell death levels. Consistent with changes observed with 2DG treatment, MP2-DW cells showed reduced levels of death compared to MP2-D cells when mitochondrial ATP production was impaired (Figure 2.8B).

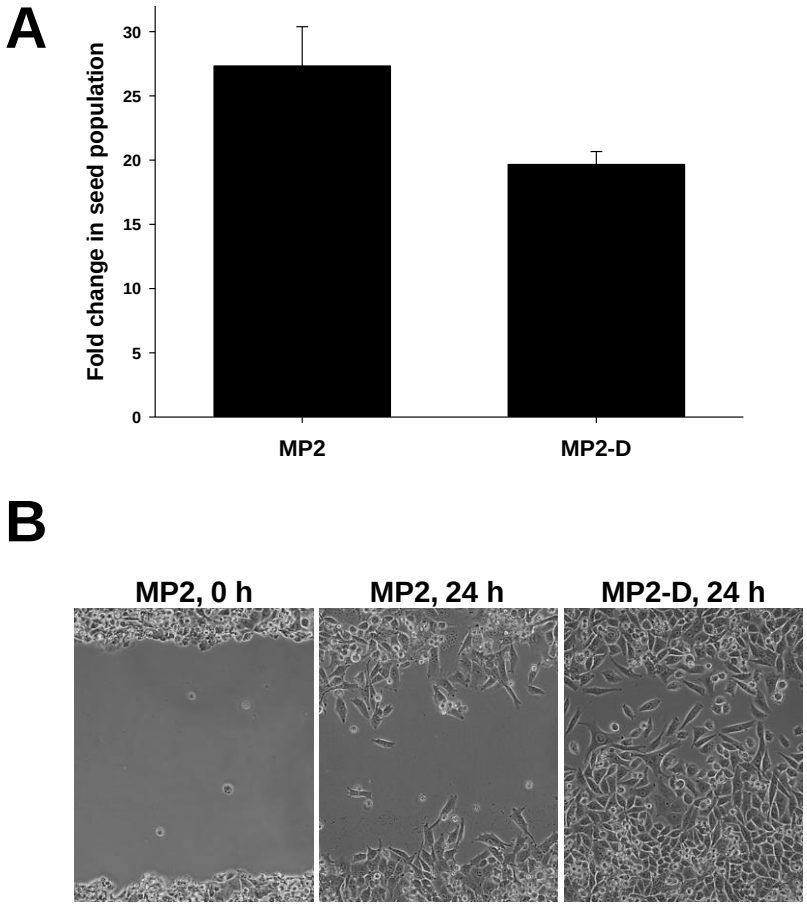

Figure 2.7. 2DG-conditioned cells exhibit altered proliferation and migration.
A) Cells were seeded and equal densities and then quantified after 96 h. B) Cells plated at high density were subjected to mechanical wound and then allowed to heal for 24 h followed by phase contrast microscopy. Data are shown as average ± standard deviation.

The effects of 2DG withdrawal upon proliferation *in vitro* were then assessed. Cells were seeded at equal densities and quantified every 24 h for 4 d. MP2 cells exhibited doubling times of ~24, and MP2-D cells showed moderately reduced rates of proliferation with doubling times of ~28 h (Figure 2.8C). Consistent with a metabolic reversion to glycolysis similar to MP2 cells, MP2-DW cells displayed doubling times of ~24 h that were identical to controls (Figure 2.8C).

Cells were next assessed for proliferation rates under Matrigel™ growth conditions. Cells were seeded at equal densities and then incubated for 5 d prior to extraction and quantification.

MP2-D cells grew to populations of <50% of controls (Figure 2.8D), consistent with decreased doubling times (Figure 2.8C). However, MP2-DW cells with restored metabolism exhibited increased rates of proliferation in substrate (Figure 2.8D), further demonstrating the reversibility of 2DG conditioning.

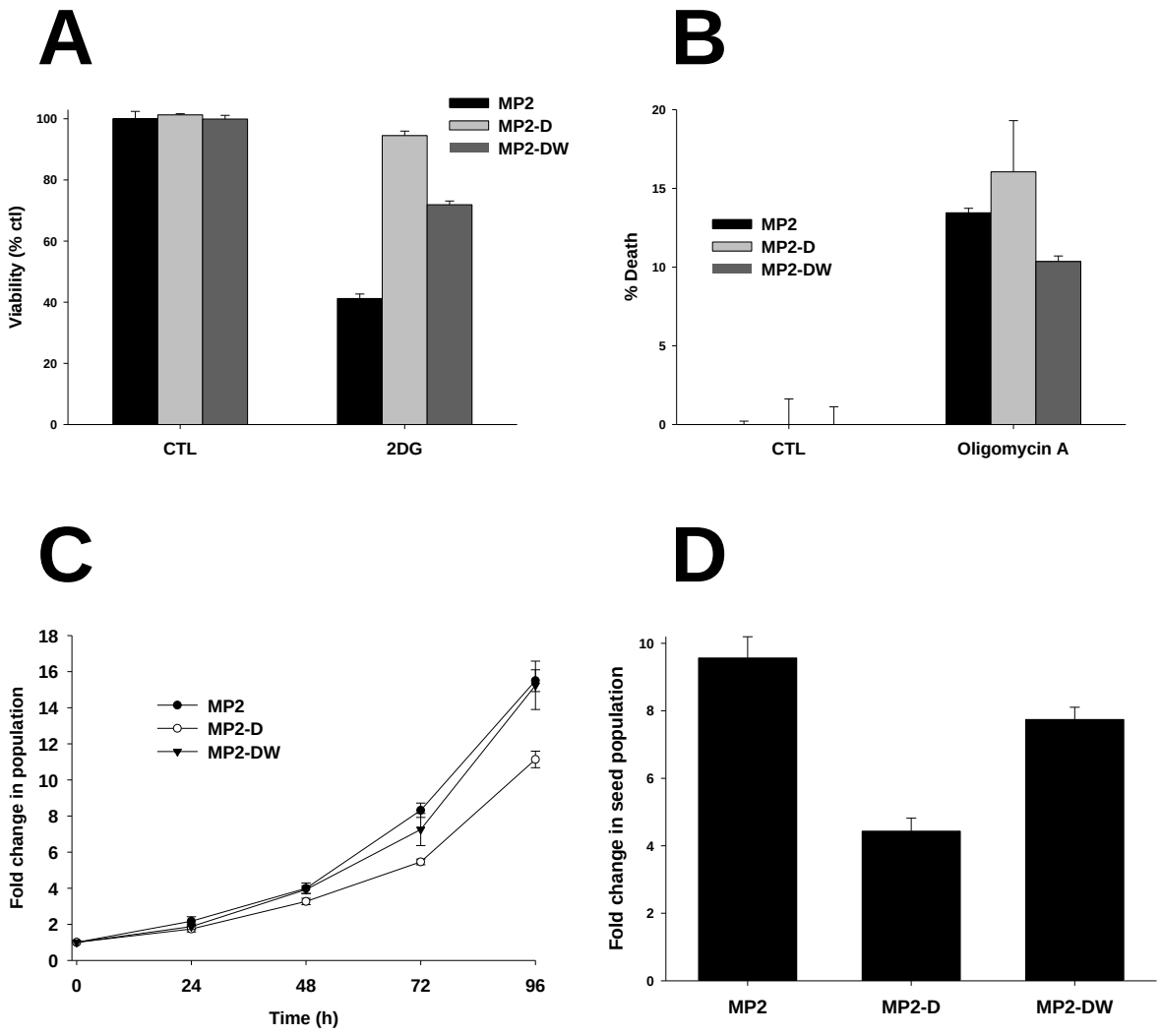

Figure 2.8. The metabolic and growth effects of acquired resistance to glycolysis inhibition are reversible.
A) Cells were left untreated or treated with 50 mM 2DG for 48 h, stained with PI, and assessed by flow cytometry. B) Cells treated with control vehicle or 10 μM oligomycin A for 24 h were subjected to PI staining and flow cytometry. C) Cells were seeded and equal densities and then quantified every 24 h for 96 h. D) Cells were seeded at equal densities in Matrigel™ and incubated for 5 d. Cells were then extracted and quantified. Data are shown as average ± standard deviation.

2DG conditioning causes the acquisition of persistent drug resistance

Having derived 2DG-resistant MIA PaCa-2 cells and characterized altered metabolism and growth, we then wondered if resistance to glycolysis inhibition was related to GEM sensitivity (Figure 2.1B). Therefore MP2 and MP2-D cells were treated with GEM and subjected to viability assay. Interestingly, 2DG conditioning caused a ~15% increase in resistance to GEM *in vitro* (Figure 2.9A), demonstrating that metabolic alterations can play a significant role in survival following treatment. Since MP2-D cells displayed increased GEM resistance *in vitro*,

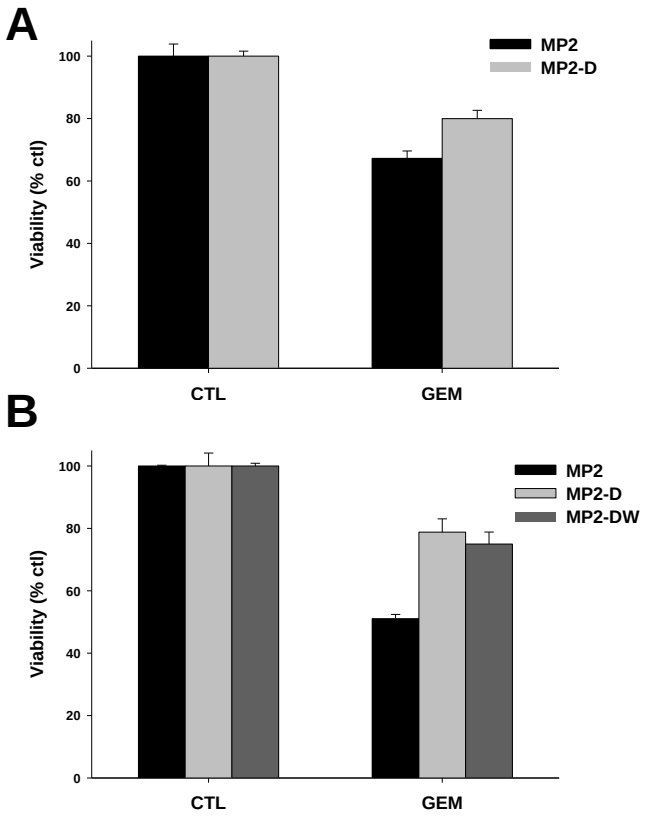

Figure 2.9. 2DG conditioning increases GEM resistance that is unaffected by reversion to a glycolytic phenotype.
A) Cells were treated with control vehicle or 1 μM GEM for 72 h and then assessed for viability levels by PI stain and flow cytometry. B) Cells were seeded at equal densities in Matrigel™ substrate and then allowed to incubate overnight. Cells were then treated with control vehicle or 1 μM GEM for 72 h. Attached and detached cells were then extracted and quantified. Viability was defined by cells remaining attached by total cells. Data are shown as average ± standard deviation.

we next assessed viability in Matrigel™ substrate and the potential for reversibility in MP2-DW cells. MP2, MP2-D, and MP2-DW cells were seeded in Matrigel™ and then treated with GEM for 3 d. Similar to *in vitro* experiments, 2DG-conditioned cells displayed elevated GEM resistance (Figure 2.9B), but at greater levels than cells treated *in vitro* (>25%). Strikingly, GEM resistance remained increased in MP2-DW cells (Figure 2.9B) despite metabolic and growth reversions (Figure 2.8).

To determine if this increased drug resistance is specific to GEM or extends to other death-inducing molecules, cells were additionally treated with three agents commonly used in cancer treatment. Paclitaxel and docetaxel interfere with microtubules during cell division through different mechanisms [111], and etoposide is a topoisomerase inhibitor [112]. Notably, MP2-D cells exhibited increased resistance to all three agents (Figure 2.10) at varying magnitudes (~10-30% increases relative to controls). Similar to GEM treatment, cells did not decrease resistance to docetaxel following metabolic reversion (Figure 2.10). In contrast, resistance to paclitaxel and etoposide significantly decreased in MP2-DW cells relative to MP2-D cells. This indicates that withdrawal from 2DG conditioning does not lead to a general pro-survival effect but promotes survival in a manner depending on therapeutic mechanism. Altogether these data raise the intriguing possibility that undergoing transient metabolic alterations can have long-term consequences upon drug resistance.

Discussion

Metabolism and tumorigenesis

Collectively these data demonstrate the effects of forced glycolytic downregulation upon metabolism, proliferation, migration, and chemoresistance in PDAC cells. Our experiments

suggest that mitochondria can promote tumorigenesis and resistance to therapy, further highlighting the importance of mitochondrial function to disease progression.

Mitochondrial defects in cancer cells are not uncommon, and elevated rates of glycolysis are frequently observed in tumors. However, elevated glycolysis is usually not due to mitochondrial impairment but occurs to promote macromolecule biosynthesis. MIA PaCa-2 cells are an example of a cancer cell line exhibiting a classical Warburg phenotype. This cell type does not appear to exhibit mitochondrial impairment, but why mitochondria are not readily employed to produce energy remains unknown.

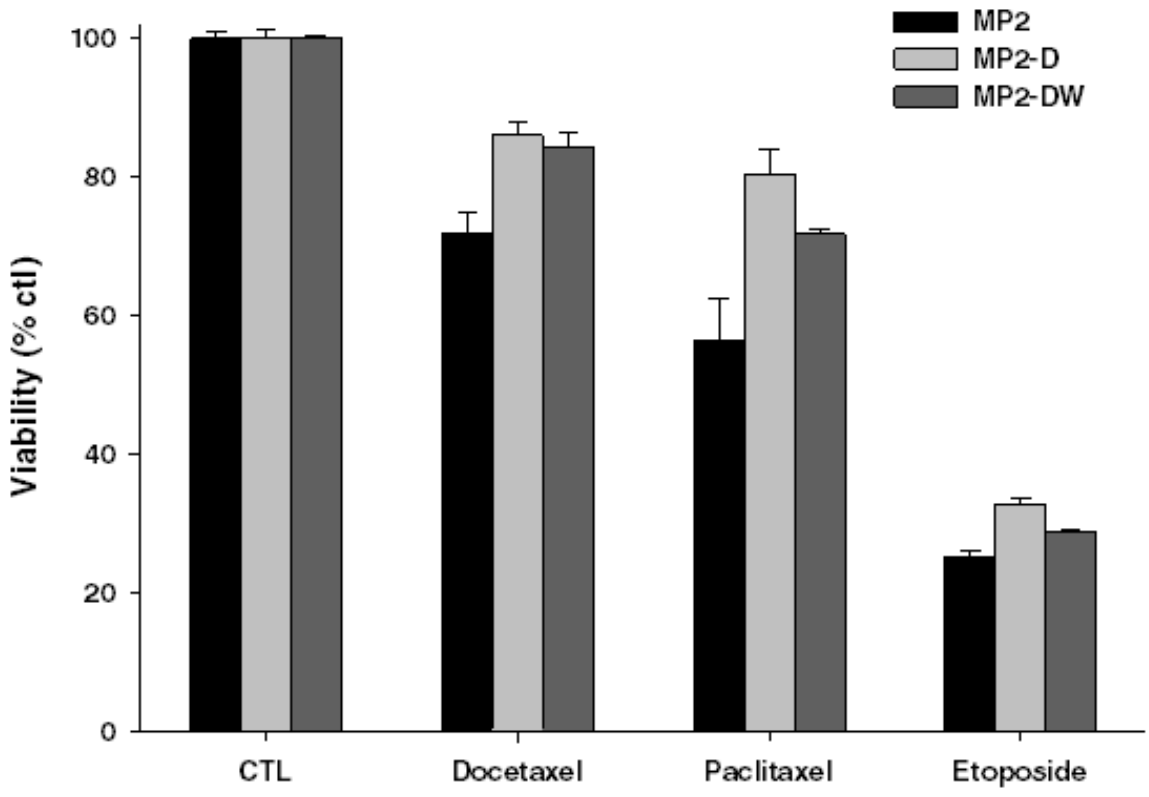

Figure 2.10. Adaptation to glycolysis inhibition increases resistance to docetaxel, paclitaxel and etoposide.
A) Cells were treated with control vehicle or the indicated drugs (docetaxel, 1 μg/ml for 48 h; paclitaxel, 1 μM for 48, etoposide, 100 μg/mL for 24 h) and then assessed for viability levels by PI stain and flow cytometry. Data are shown as average ± standard deviation.

Table 2.1. Characteristics of metabolically reconditioned PDAC cells.

	MP2	MP2-D	MP2-DW
Glycolysis dependence	High	Low	High
Mitochondrial activity	Low	High	Low
Doubling time	24 h	28 h	24 h
GEM resistance	*	****	****
Docetaxel resistance	*	****	****
Paclitaxel resistance	*	****	***
Etoposide resistance	*	****	**

Glycolysis dependence is defined by sensitivity to 2DG (Figure 2.8A), mitochondrial activity is defined by sensitivity to FCCP and oligomycin A (Figure 2.8B), and doubling time was determined as shown in Figure 2.8C. Drug resistance levels were assessed as shown in Figures 2.9 and 2.10. Values were scaled to the difference between MP2 and MP2-D cells and ranked as follows: * 0-25%, ** 25-50%, *** 50-75%, **** 75-100%.

2DG-adapted cells exhibit altered growth and drug resistance

MIA PaCa-2 cells adapted to 2DG demonstrated decreased glucose consumption, increased mitochondrial activity, and increased sensitivity to mitochondrial inhibitors. As would be expected with increased mitochondrial activity, ROS levels were additionally elevated to levels that strongly sensitized cells to oxidative stress. Furthermore, proliferation rates decreased while migratory characteristics were enhanced.

Notably, metabolic and growth changes were reversible when 2DG pressure was relieved, while changes in drug resistance persisted (Table 2.1). This suggests that short-term metabolic alterations can have lasting effects on tumorigenesis. For example, cells undergoing an energetically demanding situation (*e.g.*, matrix invasion) may upregulate mitochondrial activity that is accompanied by increased drug resistance, and this acquired resistance is unchanged when cells revert to glycolysis (*e.g.*, under hypoxic conditions).

This study is the first to generate 2DG-resistant human cells, showing that sustained glycolytic inhibition leads to increased therapeutic resistance that does not subside following metabolic reversion to a glycolytic phenotype. This further demonstrates the close interplay of metabolism and chemoresistance, indicating an additional tumorigenic mechanism that could guide therapeutic intervention. Altogether this work defines a pivotal role for transient tumorigenic metabolic adaptations to the progression of advanced disease.

III. BASAL METABOLIC STATE GOVERNS AIF-DEPENDENT GROWTH SUPPORT IN PANCREATIC CANCER CELLS

Abstract

Apoptosis-inducing factor (AIF), named for its involvement in cell death pathways, is a mitochondrial protein that regulates metabolic homeostasis and plays a contributory role to the development of cancer through its enzymatic activity. Having previously implicated AIF as pro-tumor factor selectively beneficial to advanced PCa, we assessed the role of AIF in the context of pancreatic cancer, a disease setting that most often presents at an advanced stage by the time of diagnosis. Archival gene expression data revealed a modest elevation of AIF transcript levels in subsets of pancreatic tumor specimens, suggesting a possible role in disease progression. AIF expression was then suppressed in a panel of five pancreatic cancer cell lines that display diverse metabolic phenotypes. AIF ablation selectively crippled the growth of cells *in vitro* in a manner that directly correlated with the loss of mitochondrial respiratory chain subunits and altered glucose metabolism, and these effects were exacerbated in the presence of Matrigel™ substrate. This suggests a critical metabolic role for AIF to pancreatic tumorigenesis, while the spectrum of sensitivities to AIF ablation depends on basal cellular metabolic phenotypes. Altogether these data indicate that AIF supports the growth and survival of metabolically defined pancreatic cancer cells and that this metabolic function may derive from a novel mechanism so far undocumented in other cancer types.

Introduction

In the context of prostate cancer, AIF preferentially supports metabolism benefitting the aggressiveness of advanced-stage cells. Given these previous findings, we questioned the role of AIF in the pathogenesis of pancreatic ductal adenocarcinoma (PDAC), a disease which almost

always reaches an advanced stage before diagnosis [98]. As mentioned in Chapters 1 and 2, late detection of PDAC makes it one of the most lethal cancers with a grim 5-year survival rate of 5-10% [101]. As tumors progress to advanced stages, reliance upon specific metabolic pathways for growth and survival increases substantially while cells become vulnerable to death by metabolic disruption, a trait known as metabolism addiction. As one of the most metabolically diverse and bioenergetically sensitive forms of cancer, mitochondrial function is often crucial to pancreatic tumorigenesis [76, 94], suggesting a possible role for AIF metabolic activity in supporting the growth and survival of PDAC cells.

Here AIF is identified as a major contributor to the growth-promoting metabolic state of pancreatic tumor cells. The contribution of AIF to PDAC metabolism in a panel of cell lines was directly related to their basal metabolic preferences. While cells that employ both glycolysis and mitochondrial energy metabolism rely on AIF for survival, those that rely only upon glycolysis cannot benefit from AIF metabolic activity. Through a mechanism that appears distinct from that observed in prostate cancer, AIF facilitates a metabolic balance that maintains survival. Further, this role could extend to normal tissues and may explain the selective sensitivity to AIF suppression among cell types. Altogether these findings suggest that AIF is a significant support molecule to the development and progression of specific pancreatic cancer specimens and further shed light upon the ability of AIF to function in a pro-tumor fashion.

Materials and methods

Materials

MEM, DMEM, RPMI 1640, DMEM/F12, GlutaMAX, horse serum, insulin, transferrin, epidermal growth factor, trypsin, 4-12% bis-tris polyacrylamide gels, and nitrocellulose membranes were obtained from Life Technologies; fetal bovine serum (FBS), phosphate

buffered saline (PBS), and Pierce ECL 2 Western Blotting Substrate were from Thermo Scientific; QuantiChrom™ Glucose Assay Kit was from BioAssay Systems; Matrigel™ was from BD Biosciences; Matrigel Recovery Solution was from Corning; protease inhibitor tablets were from Roche Applied Science; all other materials were from Sigma. Antibodies were obtained as follows: anti-AIF (Santa Cruz Biotechnology, sc-13116), anti-complex I 39 kDa (Life Technologies, 459100), anti-complex I 20 kDa (Life Technologies, 459210), anti-complex I 17 kDa (Life Technologies, A21359), anti-COX IV (Life Technologies, A21347) anti-β-actin (Sigma, A5316), and peroxidase-conjugated anti-mouse (Amersham Biosciences, NA931V).

Oncomine data analysis

Data sets examining AIF mRNA expression in pancreatic tumors versus normal pancreatic tissue from 7 studies [113-119] were analyzed using Oncomine [120]. Statistical calculations and normalization techniques are given by the Oncomine website (http://www.oncomine.org).

Cell culture

PANC-1, BxPC-3, HPAF-II, HPAC, and MIA PaCa-2 cells were from ATCC (kind gift of Dr. Sanku Mallik, NDSU). HEK293T cells were as described [51]. Cells were grown in an atmosphere of 95% air and 5% CO_2 at 37 °C. All media was supplemented with 2 mM GlutaMAX. Cell lines were grown and cultured with the following media formulations: HEK293T and PANC-1 cells in DMEM supplemented with 10% FBS; MIA PaCa-2 in DMEM supplemented with 10% FBS and 2.5% horse serum; BxPC-3 in RPMI 1640 supplemented with 10% FBS; HPAF-II in MEM supplemented with 10% FBS; and HPAC in a 1:1 mixture of DMEM and Ham's F12 medium supplemented with 5% FBS, 2 μg/mL insulin, 5 μg/mL transferrin, 40 ng/mL hydrocortisone, and 10 ng/mL epidermal growth factor.

Lentivirus production and infection

FG12-derived plasmids for targeting of AIF and LacZ by RNA interference (RNAi) have been rigorously assessed and used as described [51, 121, 122]. Lentiviral packaging plasmids pRRE, pRSV-rev, and pHCMV-G are as described [123]. RNAi plasmids and equal amounts of lentiviral packaging plasmids were transfected into HEK293T cells using the calcium phosphate precipitation method [124]. Supernatants of transfected HEK293T cultures were then filtered through 0.45-μm PVDF Millex-HV filters (Millipore) and concentrated by centrifugation at 20,000 x g for 90 min at 4 °C. Viral pellets were resuspended in PBS and then incubated overnight at 4 °C prior to use. Cell lines were then infected as described [51]. PANC-1 and MIA PaCa-2 cells were infected with lentiviruses carrying shLacZ-GFP or shAIF-GFP, after which infection was verified by fluorescence microscopy and flow cytometry with an Accuri C6 flow cytometer. BxPC-3, HPAC, and HPAF-II cells were infected with lentiviruses carrying shLacZ-puro or shAIF-puro and then selected using 2 μg/mL puromycin.

Cell viability

Cells were seeded in equal replicate densities in 6-well plates and allowed to attach overnight. Cells were then left untreated or treated with 1 μg/mL actinomycin D, 1 μM gemcitabine, or 50 mM 2-deoxyglucose for 24-72 h. Cells were then harvested by trypsinization, washed, and resuspended in PBS containing 2 μg/mL propidium iodide. Cell viability was determined by flow cytometry.

SDS-PAGE and immunoblot

Cells were harvested by trypsinization, washed, and resuspended in radioimmune precipitation assay lysis buffer (PBS containing 1% Nonidet P-40, 0.5% sodium deoxycholate, 0.1% sodium dodecyl sulfate, 1 mM dithiothreitol, 1 mM phenylmethanesulfonyl fluoride, and 1

protease inhibitor mixture tablet per 10 mL). Lysates were then normalized for protein content, separated by SDS-PAGE, and transferred to nitrocellulose membranes. Membranes were blocked with 5% milk in Tris-buffered saline with 0.1% Tween-20 and incubated with primary antibodies for 1 h at room temperature. Membranes were then washed and incubated with peroxidase-conjugated anti-mouse IgG secondary antibody for 45 min at room temperature, followed by washing and visualization using enhanced chemiluminescence with a MyECL imaging system (Thermo Scientific).

Cell growth rate measurements

Cells were harvested by trypsinization, washed, resuspended in fresh medium, and seeded at equal densities in replicate 6-well plates. Cells were harvested and quantified by Coulter™ counting after 72 h. Fold change in growth was determined by dividing populations of AIF-deficient cells by corresponding control populations.

Scratch assay

Cells were harvested by trypsinization, washed, resuspended in fresh media, and seeded in replicate 6-well plates. Cells were allowed to attach for 12-36 h, and a single scratch was made through the middle of each well using a P200 pipette tip [105]. Cells were immediately washed, fresh media was added, and each scratch was imaged. Cells were then incubated for 6-48 h before final assessment of scratch width. All images were captured by phase contrast microscopy using the 10× objective of a Nikon TS100F microscope equipped with a Nikon DS-Fi1 digital camera detection system and NIS Elements 4.0 software.

Glucose consumption measurements

Cells were harvested by trypsinization, washed, resuspended in fresh medium, and seeded at equal densities in replicate 6-well plates. Cells were grown at 37 °C for 72 h. Media was then

collected from each well, and total glucose was measured using the QuantiChrom™ Glucose Assay Kit (BioAssay Systems). Total cell number in each sample was determined by Coulter™ counting. To determine glucose consumed per cell, total glucose consumption per sample was divided by its corresponding cell count.

Matrigel™ experiments

Equal volumes of cold Matrigel™ were added to each well in 24-well plates and allowed to solidify at 37 °C for 1 h. Cells were harvested, washed, resuspended in fresh medium, and seeded in equal densities on solidified Matrigel™ layers. Cells were grown in Matrigel™ for up to 21 days with media replenished following each week of growth and imaged using phase contrast microscopy as described above. Cells were then extracted from substrate with the Matrigel Recovery Solution (Corning), and glucose consumption and growth measurements were performed as described above.

Results

AIF transcripts are increased in pancreatic cancer

To determine a potential involvement of AIF in pancreatic cancer, archived expression data were retrieved from the cancer gene expression database Oncomine (oncomine.com). Archival data from a total of 7 data sets comparing relative AIF expression in pancreatic adenocarcinomas to normal pancreatic tissue are currently available [113-119]. When average AIF expression was compared between groups (cancer vs. normal) and for each data set, a trend towards elevated AIF transcripts in pancreatic cancer tissue was apparent (values ranging from essentially unchanged to an increase of 1.54 fold in cancer relative to normal). However, the observed increase in average expression was only statistically significant in one of the seven data sets, which indicated a 1.45-fold increase in AIF expression in pancreatic cancer tissue ([113],

p=0.024; for all other studies p=0.068-0.956). Representative data are shown in Figure 3.1A-D. At first glance these data suggested that altered AIF expression is not a global trend in pancreatic cancer, but that in a small fraction of tissue cohorts a modest (less than 2-fold) elevation of AIF expression can be observed.

To further explore AIF expression changes in these cohorts of cancer vs. normal tissues we compared individual expression data from each sample within each cohort (Figures 3.1E-H). Interestingly, in 5 of the 7 data sets there appears a subtype within each cancer group that displays elevated AIF expression significantly beyond the 90% confidence interval defined for normal tissues [113-116, 119]. This subtype represents ~36% of the total among these five cohorts, and while elevated AIF is observed, the magnitude of this elevation remains modest (less than 3-fold relative to control tissue). These data are in close agreement with similar analyses examining AIF mRNA and protein expression in prostate cancer tissues [51]. Taken together these data suggest that while elevated AIF expression is not a global feature of pancreatic cancer, there exists a subtype of pancreatic tumors (approximately one-third of the total samples assessed) in which AIF expression is significantly elevated. That increased expression is modest likely reflects potential toxicity associated with AIF-mediated cell-killing when levels exceed a certain threshold [24].

Establishment of AIF-deficient cell lines

The above analysis of AIF gene expression data from clinically derived pancreatic cancer tissues suggested a connection between elevated AIF expression and subtypes of pancreatic tumors. In order to evaluate the role of AIF in the growth and survival of pancreatic cancer cells, we generated a panel of AIF-deficient PDAC cell lines. Given the metabolic activity of AIF in other systems, we targeted AIF in a panel of five cell types (PANC-1, BxPC-3, HPAC, HPAF-II,

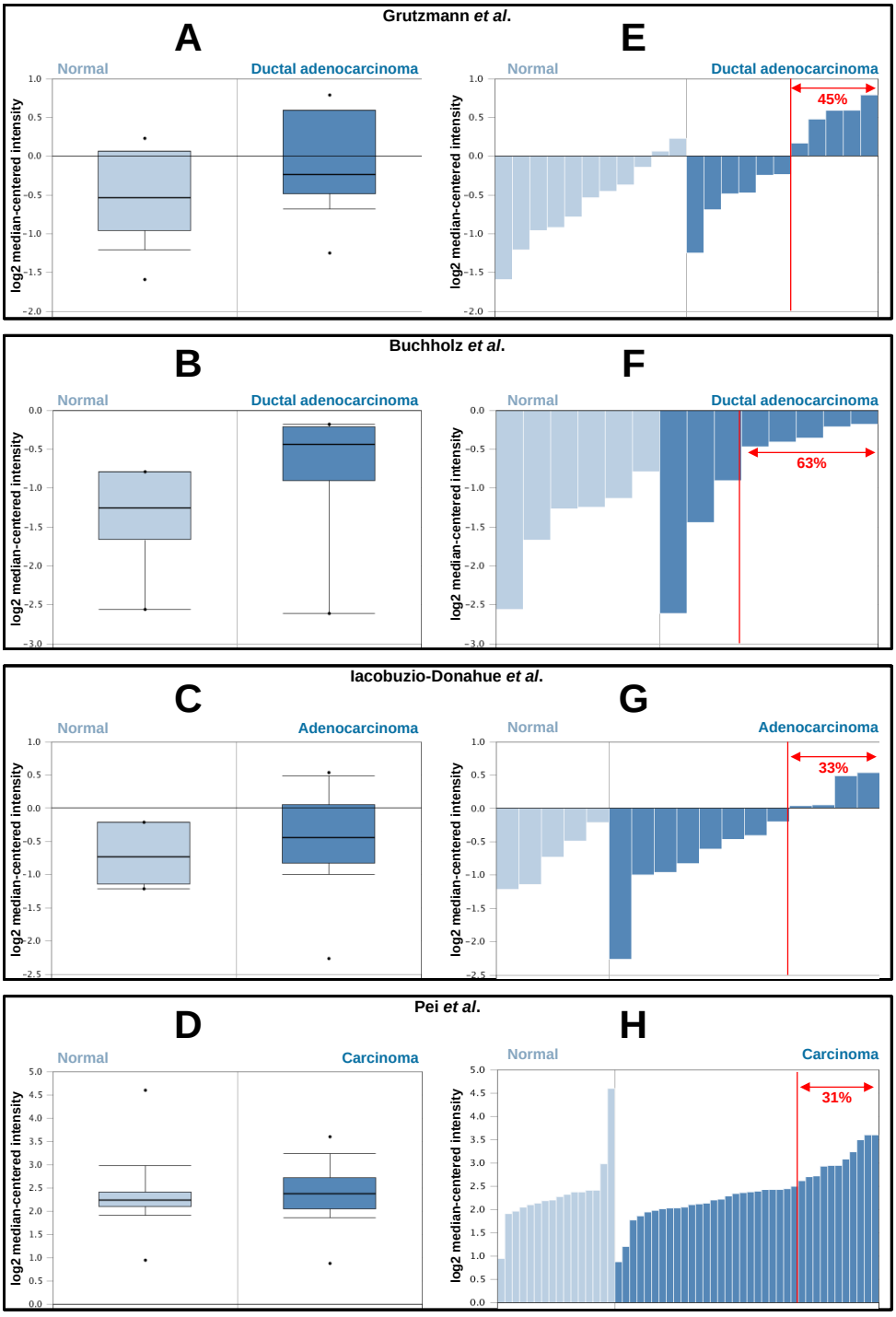

Figure 3.1. AIF transcript levels are increased in pancreatic cancer.
Data comparing AIF mRNA transcript expression in normal pancreatic tissues vs. pancreatic tumors was retrieved from the Oncomine database and assessed as shown in representative studies [113-115, 119]. A-D) Average relative AIF mRNA expression in normal pancreatic tissues vs. pancreatic tumors. E-H) Relative AIF mRNA levels among individual samples within each cohort. Fractions of tumor specimens within each cohort exhibiting statistically significant AIF expression changes relative to normal tissue are indicated in red.

and MIA PaCa-2) that display diverse metabolic characteristics (Figure 3.2). Previously, metabolic phenotyping of PDAC cells was rigorously established by gene expression analysis, sensitivity to metabolic inhibitors, and metabolite profiling [100]. PANC-1 and BxPC-3 cells balance the metabolic requirements derived from glycolysis, pentose phosphate pathway, and mitochondrial energy metabolism, while HPAC cells display a pronounced bias towards lipid metabolism; HPAF-II cells also require mitochondrial energy pathways but are more reliant upon glycolysis than those previously described, and MIA PaCa-2 cells are highly glycolytic (Table 3.1). Within this panel of cell lines oncogene status (Table 3.2) varies slightly: all cells except

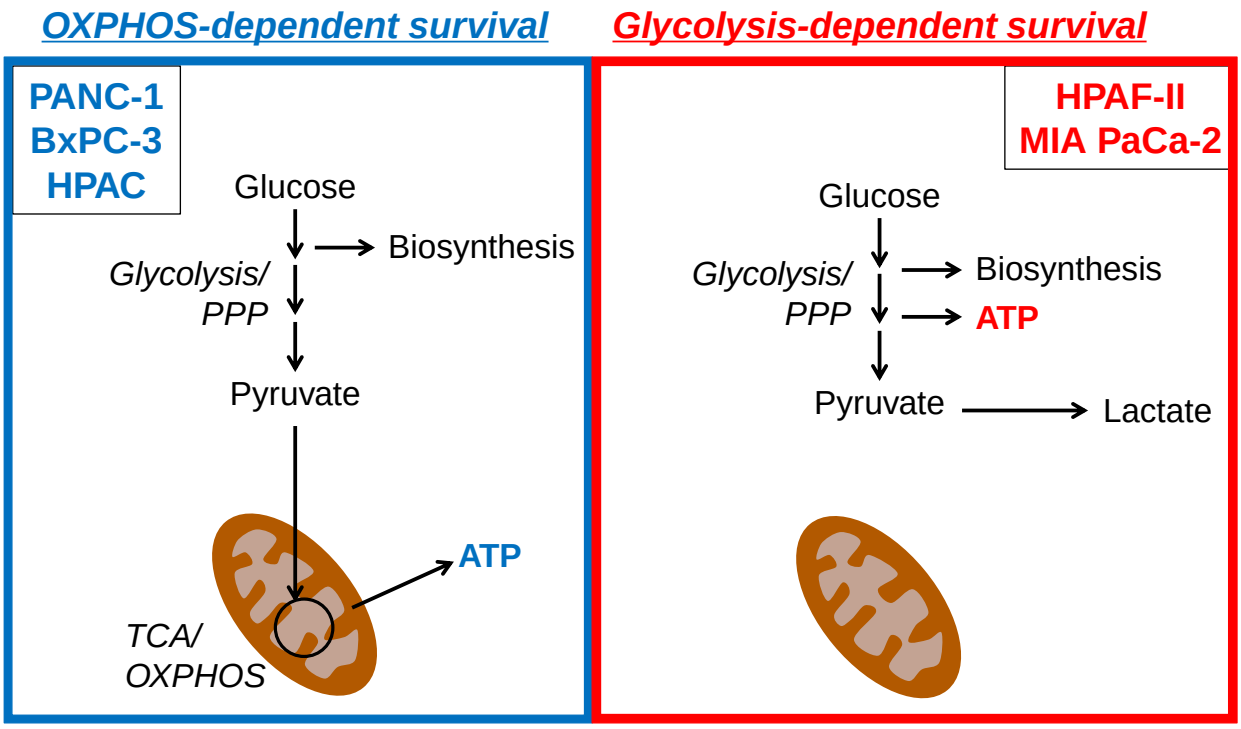

Figure 3.2. Pancreatic cancer cell lines exhibit distinct metabolic phenotypes.
PANC-1, BxPC-3, and HPAC cells acquire energy predominantly from mitochondrial OXPHOS. Relative to OXPHOS-dependent cells, the glycolytic cell lines HPAF-11 and MIA PaCa-2 cells produce most ATP from glycolysis [100].

Table 3.1. Metabolic phenotypes are associated with sensitivity to AIF ablation.

	Relative metabolic phenotype [100]		Sensitivity to glycolytic disruption	Sensitivity to AIF ablation
	Glycolysis/PPP	Fatty acid/ OXPHOS		
PANC-1	Moderate	Moderate	Insensitive	Sensitive
BxPC-3	Moderate	Moderate	Insensitive	Sensitive
HPAC	Low	High	Insensitive	Sensitive
HPAF-II	High	Moderate	Moderately sensitive	Moderately sensitive
MIA PaCa-2	High	Low	Sensitive	Insensitive

Table 3.2. Oncogene status of PDAC cell lines.

	Patient, age	KRAS	p53	CDKN2A/p16	Smad4/DPC4
PANC-1	Caucasian male, 56	G12D	R273H	-/-	WT
BxPC-3	Caucasian female, 61	WT	Y220C	WT	-/-
HPAC	Caucasian female, 64	G12D	WT	112 amber stop	WT
HPAF-II	Caucasian male, 44	G12D	P151S	Δ29-34	WT
MIA PaCa-2	Caucasian male, 65	G12C	R248W	-/-	WT

BxPC-3 express mutant KRAS, and all cells except HPAC express mutant p53 [125-131]. Silencing of AIF expression by RNAi was achieved through infection with lentiviruses harboring short-hairpin RNA (shRNA) sequences targeting either AIF (shAIF) or LacZ (shLacZ) as a control. PANC-1 and MIA PaCa-2 cells were infected with lentiviruses that carried GFP expression cassettes which served to confirm stable integration and subsequent knockdown of targeted genes. Success of lentiviral infection was evaluated by observation of at least 95% GFP

positivity using fluorescence microscopy and flow cytometry (Figure 3.3A, B). Due to lower infection efficiencies, BxPC-3, HPAC, and HPAF-II cells were infected with lentiviruses carrying puromycin resistance as a selectable marker instead of GFP, and stably infected cells were derived by treatment with puromycin. To control for differences between lentiviruses bearing puromycin resistance vs. GFP, we additionally established PANC-1 cells via puromycin selection that were indistinguishable from GFP-infected cells in all assays performed (data not shown). To determine the extent of AIF protein ablation in our cell line panel, immunoblot analysis was employed, which demonstrated AIF knockdown levels greater than 95% in all cases when compared to either uninfected cells or shLacZ negative controls (Figure 3.3C).

AIF ablation does not affect chemical death induction

In various cell types, AIF has been suggested to promote both death induction and survival in response to toxic chemical triggers. To determine the role of AIF in regulating cell death in pancreatic cancer, two death-inducing agents with distinct mechanisms of action were employed: actinomycin D, an inhibitor of protein synthesis; and gemcitabine, a nucleoside analog and the first-line treatment for PDAC [107, 132]. Following treatment viability was measured by propidium iodide fluorescence exclusion assay. When compared to controls, AIF-deficient cell lines showed neither increased resistance (to actinomycin D) nor increased sensitivity (to gemcitabine) following treatment (Figure 3.4). Similar results were obtained by treatment with etoposide, MNNG, arsenic trioxide, menadione, and hydrogen peroxide (data not shown). These data demonstrate that AIF does not play a significant regulatory role in the promotion of cell death in pancreatic cancer cells, and is consistent with previous studies evaluating AIF-mediated cell death [51].

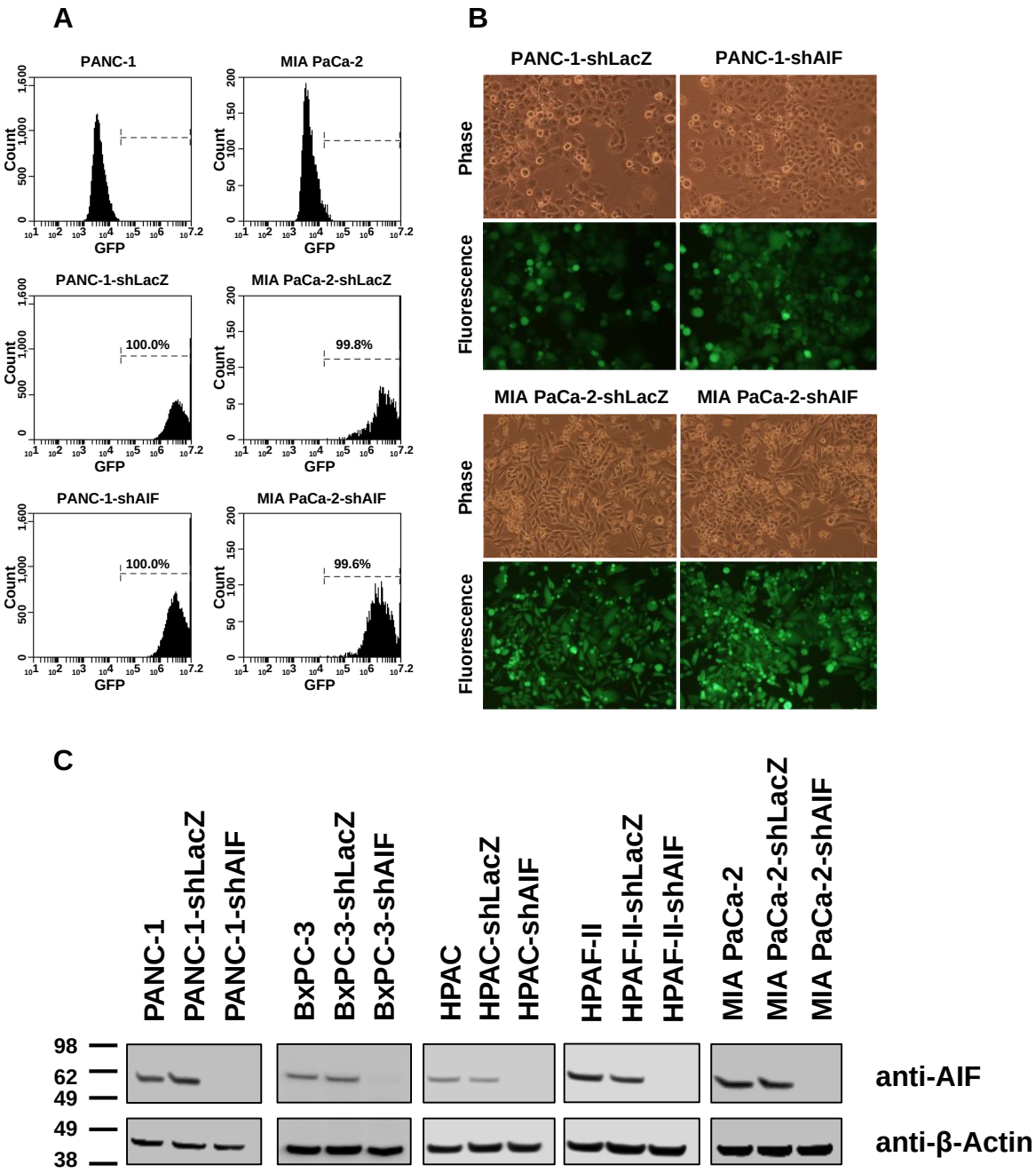

Figure 3.3. Establishment of AIF-deficient PDAC cell lines.
PANC-1 and MIA PaCa-2 cells were stably infected with shRNA hairpins targeting LacZ or AIF with GFP as a selectable marker via lentiviral delivery. GFP positivity of infected cell lines was assessed by flow cytometry (A) and fluorescence microscopy (B). Equivalent targeting in BxPC-3, HPAC, and HPAF-II cells was achieved by puromycin selection; suppression of AIF protein expression was verified by immunoblot analysis (C).

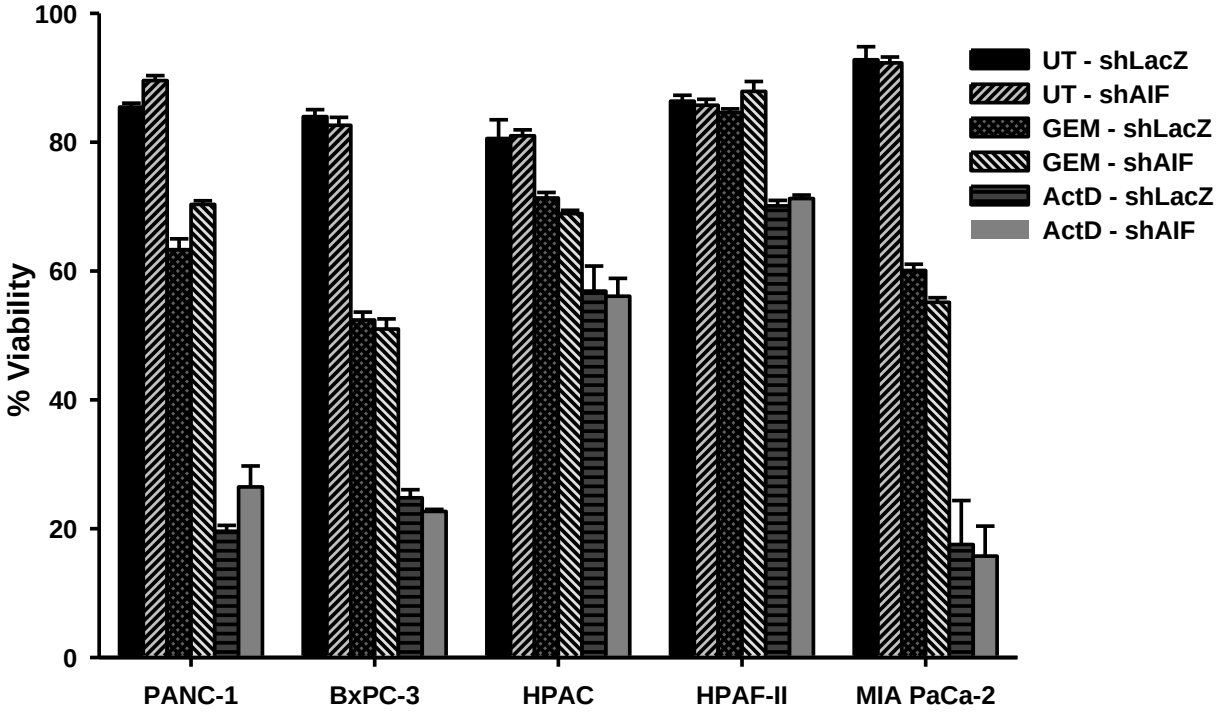

Figure 3.4. AIF ablation does not impact chemical death induction.
Equal numbers of cells were harvested, washed, and allowed to attach overnight. Cells were then left untreated (UT) or treated with 1 µg/mL actinomycin D (ActD) for 24 h or 1 µM gemcitabine (GEM) for 48-72 h. Cell viability was then determined by propidium iodide staining and flow cytometry. Data are shown as average ± standard deviation.

AIF selectively supports PDAC cell growth and migration

In order to determine whether AIF ablation impacts the rate of proliferation of pancreatic cancer cells, *in vitro* growth rates of AIF-deficient PDAC cells were assessed. Equal populations of cells were seeded in fresh media and allowed to proliferate for 72 h before quantification by Coulter™ counting. Notably, 4 of the 5 cell lines (PANC-1, BxPC-3, HPAC, and HPAF-II) showed a reduction in growth rate following ablation of AIF. After 3 days of proliferation, AIF-deficient PANC-1, BxPC-3, and HPAC cells exhibited ~60% of growth compared to shLacZ controls. AIF ablation resulted in a less substantial reduction in proliferation in HPAF-II cells

(~75%), while growth was unaffected in MIA PaCa-2 cells (Figure 3.5A). These results are distinct from previous observations: in prostate cancer the growth rates of cells are largely unaffected by AIF ablation under nutrient-rich conditions *in vitro*, and it is not until exposure to Matrigel™ or growth stress *in vivo* that AIF-deficient prostate cancer cells exhibit substantial reductions in growth. This suggests that AIF is either more important in advanced PDAC vs. prostate cancer, and/or functions via alternative/additional mechanisms.

To further define the role of AIF in controlling the aggressiveness of pancreatic tumor cells, the migration of AIF-deficient cells was assessed by scratch assay. High densities of cells were plated in replicate and allowed to attach for 12-36 h, and a scratch was made across the middle of each well with a P200 pipette tip. Scratch width was assessed immediately following cell displacement and 6-48 h later. AIF-deficient PANC-1, BxPC-3, and HPAC cells showed reduced migration, while little change was observed in AIF-deficient HPAF-II or MIA PaCa-2 cells (Figure 3.5B), in agreement with our proliferation rate data. It is notable that while MIA PaCa-2-shAIF cells displayed similar migration compared to controls, when plated at the high densities used in the migration assay these cells took longer to adhere to plate surfaces. This suggests that AIF may be involved in cellular adhesion in this cell type; further studies are needed to define this function more clearly and determine the cancer specificity of this observation. Altogether, these data indicate that 1) the impact of AIF ablation upon pancreatic tumor cells is more severe than that observed in prostate cancer, 2) there is a spectrum of sensitivities to AIF ablation that is reflected by changes in cell growth patterns, and 3) AIF supports pancreatic tumorigenesis through a mechanism distinct from that shown in prostate cancer.

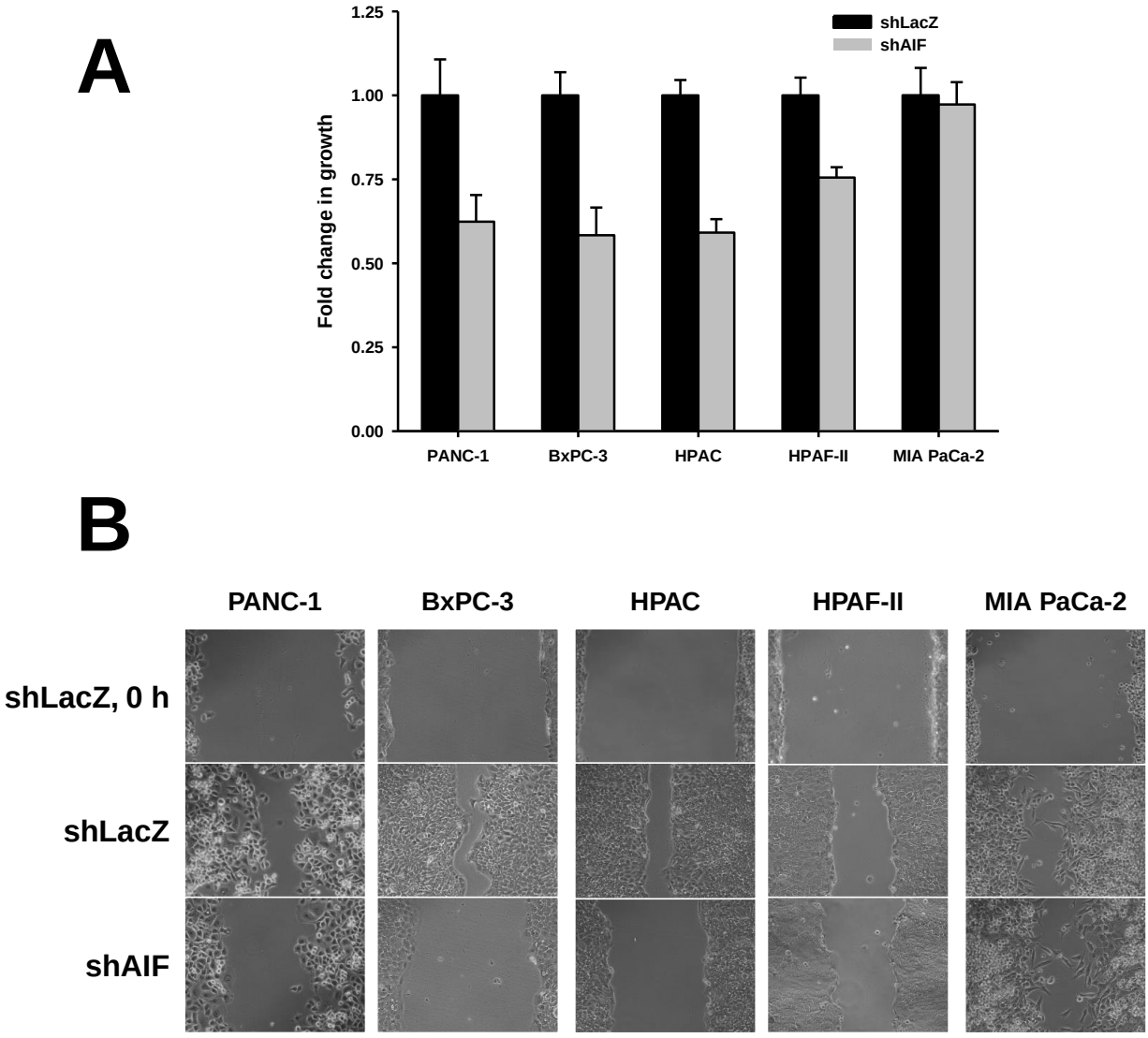

Figure 3.5. AIF selectively supports the growth and migration of PDAC cells.
A) Cells were plated in equal densities in replicate, harvested, and quantified by Coulter™ counting after 72 h of growth. Data are shown as average ± standard deviation. B) High densities of cells were seeded in replicate wells and allowed to attach for 12-36 h. A single scratch was made through the middle of each well, and width was assessed at 0 h (all cell lines), 6 h (HPAC), 10 h (HPAF-II), 24 h (PANC-1), and 48 h (BxPC-3 and MIA PaCa-2). Representative images are shown; all images were captured at 10× magnification.

Cellular energy phenotype determines the ability of AIF to promote growth and survival of PDAC cells

Having found that AIF selectively contributes to the rates of both cellular proliferation and migration *in vitro*, we sought to determine how AIF supports cell growth in pancreatic cancer and distinguish these effects based on cellular metabolic state. A common feature of cells that require AIF for basal metabolic activity is a loss of expression in protein subunits of complex I of the respiratory chain [25, 51]. To determine whether respiratory chain regulation is related to AIF-mediated cell growth, cells were lysed and probed for complex I subunits by immunoblot analysis. Following knockdown of AIF the concomitant changes in respiratory chain protein levels were diverse and directly correlated with both metabolic phenotype and changes in growth. AIF-deficient PANC-1, BxPC-3, and HPAC cells exhibited substantial reductions in 39-kDa, 20-kDa, and 17-kDa complex I subunits (Figure 3.6). Interestingly, when AIF was suppressed in BxPC-3 cells, the expression of not only complex I subunits but also COX IV was reduced (Figure 3.6), a change that has not been previously reported in cancer and may suggest a more global alteration in the mitochondrial proteome in this cell type. Changes in respiratory chain status were minimal when AIF was depleted from HPAF-II and MIA PaCa-2 cells (Figure 3.6). These data indicate that loss of complex I in pancreatic cancer cells following AIF ablation is dependent on metabolic phenotype.

A common adaptation following impairment of the mitochondrial respiratory chain is an increase in glucose consumption, allowing cells to meet ATP demands directly through glycolysis. To further define the role of AIF in pancreatic cancer cells, metabolic changes associated with AIF ablation were first evaluated by measuring glucose consumption rates. In agreement with the spectrum of respiratory deficiencies observed, AIF-deficient PANC-1,

BxPC-3, and HPAC cells consumed ~2-5-fold more glucose than their corresponding controls, while HPAF-II-shAIF and MIA PaCa-2-shAIF cells exhibited glucose consumption levels that were essentially unchanged when compared to controls (Figure 3.7A). Notably, the magnitudes of altered glucose consumption in our panel of cell lines directly correlated with the severity of respiratory chain deficiency that followed ablation of AIF (Figure 3.6). This correlation suggests that differences in sensitivity to AIF ablation among cell types may stem from differential metabolic requirements prior to AIF ablation. For example, due to a pre-existing decrease in respiratory chain activity [133], MIA PaCa-2 and HPAF-II cells have already adapted by upregulating glycolysis such that further impairment of the respiratory chain via AIF ablation has no additional effects upon glucose consumption.

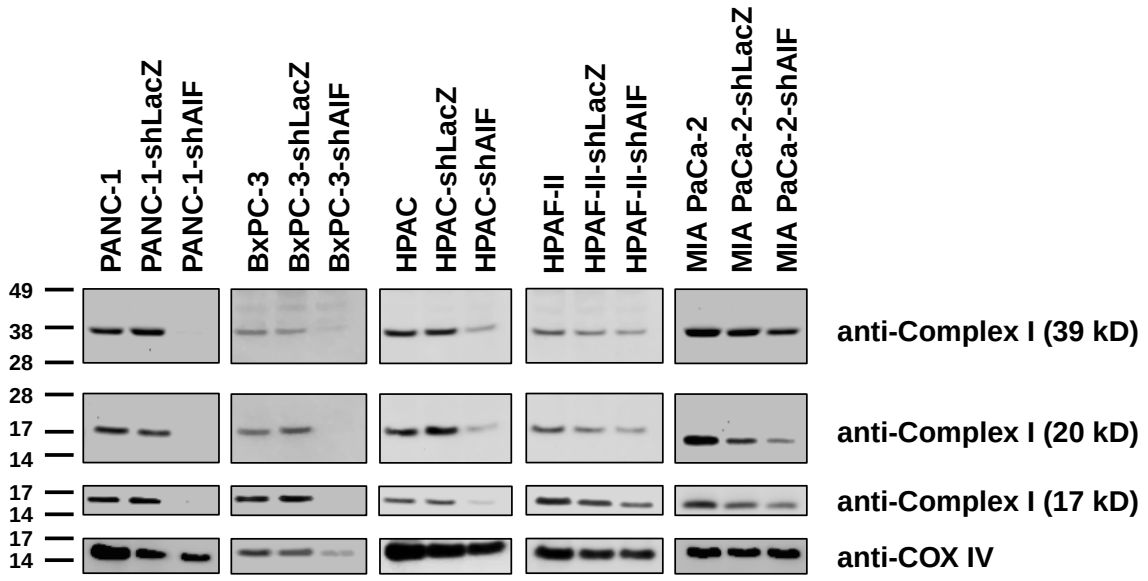

Figure 3.6. AIF selectively controls protein levels of nuclear-encoded respiratory chain subunits.
Following suppression of AIF, respiratory chain status was assessed by immunoblot analysis of complex I (39-, 20-, and 17-kDa subunits) and COX IV. Corresponding β-actin immunoblots are shown in Figure 3.3.

To test this hypothesis and to determine the benefit of AIF-mediated glucose metabolism to cell survival, we next inhibited glycolysis in our panel of cell lines by treatment with 2-deoxyglucose. Glycolytic cell lines will exhibit a higher sensitivity to treatment than those that remain capable of using other pathways (OXPHOS, lipid catabolism, glutaminolysis, etc.) to compensate for this metabolic deficiency. To assess sensitivity, cell viability was measured using propidium iodide staining followed by flow cytometry. Results revealed that while control PANC-1 and BxPC-3 cells are entirely resistant to 2-deoxyglucose for the duration of treatment, those that lack AIF exhibit substantial sensitivity with only ~40-50% survival following treatment (Figure 3.7B). Taken together with the corresponding respiratory statuses of these cell lines (Figure 3.6), AIF is likely to regulate a balance between glycolysis and OXPHOS that is critical to the growth and survival of PANC-1 and BxPC-3 cells. In contrast, AIF ablation did not affect sensitivity to treatment in HPAC cells despite their complex I deficiency and elevated glucose consumption levels (Figure 3.7B). This is not surprising given the lipogenic nature of the HPAC cell line [100], which allows cells to circumvent the metabolic requirement for AIF and complex I but at the expense of their proliferative capacity (Figure 3.5). When compared to the resistant PANC-1, BxPC-3, and HPAC cell lines, control HPAF-II and MIA PaCa-2 cells both displayed a high basal sensitivity to 2-deoxyglucose, reflecting their dependence on glycolysis that is likely due to long-term adaptations to basal mitochondrial dysfunction. AIF ablation modestly increased sensitivity to glycolytic disruption in HPAF-II cells, but MIA PaCa-2 cells displayed a pre-existing addiction to glycolysis [100, 134] that could not be amplified by AIF suppression. This sensitivity was comparable to PANC-1-shAIF and BxPC-3-shAIF cells following treatment (Figure 3.7B) and is consistent with glucose consumption data (Figure 3.7A). In this context loss of AIF has little to no additional metabolic effect, an observation that

further confirms the hypothesis that differences in glucose uptake among cell types following AIF ablation derive from differences in the intrinsic activities of their respiratory chains.

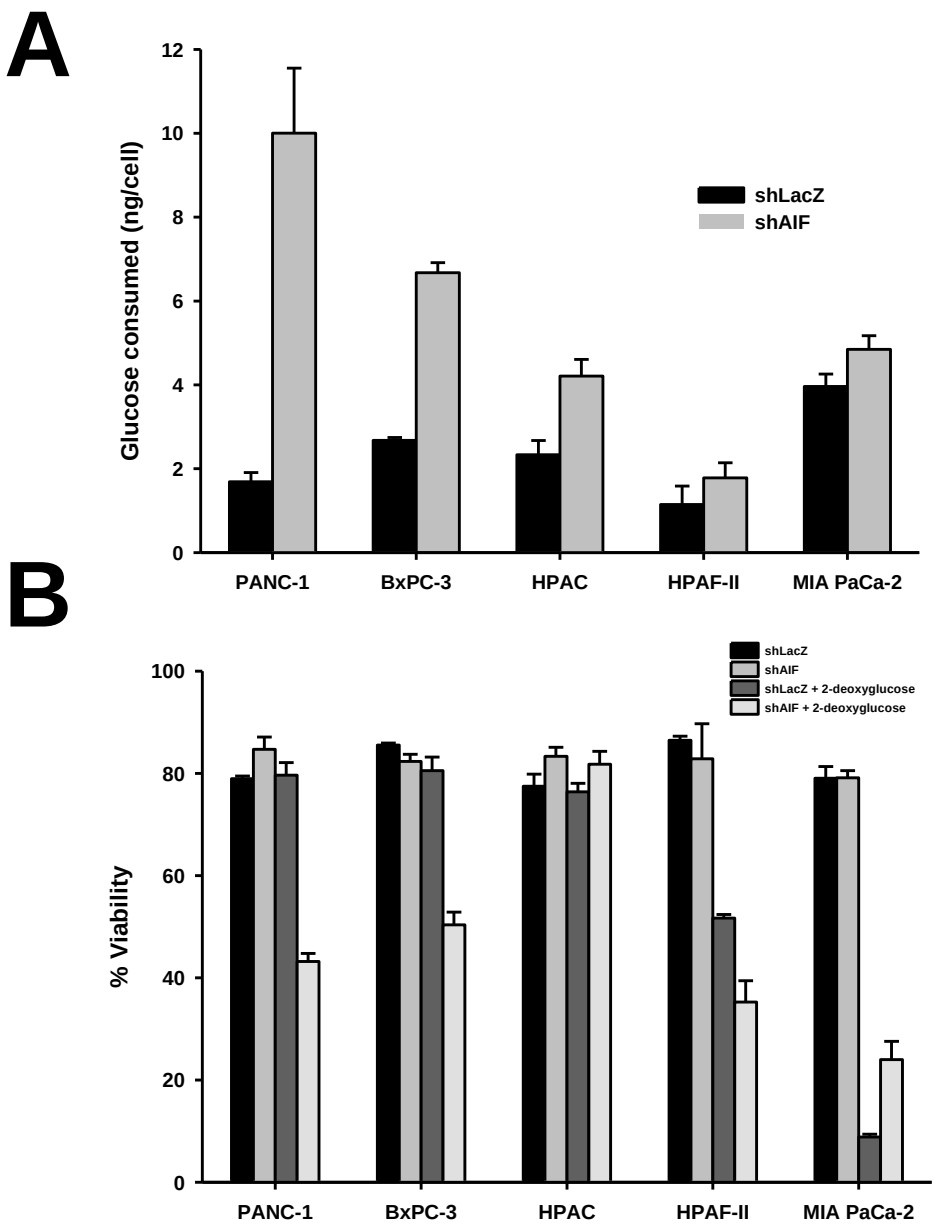

Figure 3.7. Glycolytic dependence predicts metabolic sensitivity to AIF ablation.
A) Equal densities of cells were plated in fresh media, and total glucose was measured using the QuantiChrom™ Glucose Assay Kit (BioAssay Systems) 72 h after seeding. Total numbers of cells in each well were used to determine glucose consumption per cell. B) Cells were seeded in equal densities and allowed to attach overnight before treatment with 50 mM 2-deoxyglucose. After 48 h cells were collected, and viability was determined by propidium iodide staining and flow cytometry. Data are shown as average ± standard deviation.

Matrigel™ growth conditions amplify AIF dependence

Following the observations that AIF supports metabolism benefiting the growth and survival of non-glycolytic pancreatic cancer cells *in vitro*, we next explored the metabolic function of AIF in an environment that more closely resembles conditions found *in vivo*. Matrigel™ is a cell growth substrate that consists of matrix protein polymers and proteoglycans found in natural extracellular environments and is often used as a model for studying tumorigenesis in a setting that approximates *in vivo* cell growth and survival. To assess the role of AIF in the growth and metabolism of pancreatic cancer cells under such conditions, glucose consumption and growth were measured following exposure to Matrigel™ substrate. Results were strikingly similar to those found in the absence of Matrigel™, except that the differences between control and AIF-deficient cells were amplified. When introduced into substrate, cells displayed a dependence upon AIF expression for aggressive growth and normal glucose consumption. While control PANC-1, BxPC-3, and HPAC cells grew into spheroidal tumor-like structures, those without AIF exhibited substantial reductions in both size (Figure 3.8A) and proliferation rate (Figure 3.8B). Furthermore, AIF-deficient PANC-1, BxPC-3, and HPAC cells consumed ~3-7-fold more glucose than those with AIF (Figure 3.8C), suggesting that glycolysis becomes critical for growth and survival under Matrigel™ growth conditions when AIF is depleted. In the HPAF-II cell line, which exhibited modest changes in growth and metabolism following AIF ablation *in vitro*, both shLacZ controls and shAIF failed to invade the substrate to the extent of other cell lines, yet HPAF-II-shAIF cells showed a substantial reduction in growth rate and a 2-fold increase in glucose consumption. Taken together with previous data, this suggests that AIF plays a minor role in HPAF-II glucose metabolism under nutrient-rich conditions but that this role becomes more important upon exposure to Matrigel™. In contrast,

MIA PaCa-2-derived cell lines did not display significant changes (Figure 3.8), consistent with *in vitro* measurements. Following growth in Matrigel™ changes in both glucose uptake and growth in substrate were more severe but directly proportional to those found *in vitro*. Altogether, these data indicate that AIF supports the growth and survival of some pancreatic cancer cells by facilitating a metabolic balance, and this metabolic function is most beneficial OXPHOS-dependent populations.

Discussion

AIF elevation in cancer promotes survival without affecting death induction

When functioning in a pro-death role, AIF can undergo nuclear translocation followed by the induction of chromatin condensation and DNA degradation during various forms of cell death [135-139]. As a promoter of caspase-independent death, it is formally possible that AIF could act in a tumor-suppressive manner. Yet while AIF nuclear translocation has been observed in cancer [140, 141], this study and others [51, 54] show that loss of AIF suppresses tumorigenesis and that AIF's nuclear function is unlikely to make a significant contribution to death pathways despite overexpression in tumors [51, 83-88]. AIF elevation in cancer is modest (typically less than 3-fold), suggesting a threshold exists above which AIF expression is either no longer beneficial or actively disadvantageous. Despite this threshold, AIF elevation in cancer is both sufficient and necessary for AIF to promote survival through its enzymatic activity [51, 54].

Pathogenic AIF mechanisms

Presently, AIF enzymatic activity has been demonstrated to support tumorigenesis through at least two distinct mechanisms. In colorectal cancer cells, AIF elevates the cellular oxidative state to protect against chemical stress-induced apoptosis [54]. In prostate cancer, AIF promotes a metabolic state that selectively supports the growth and survival of cells that have

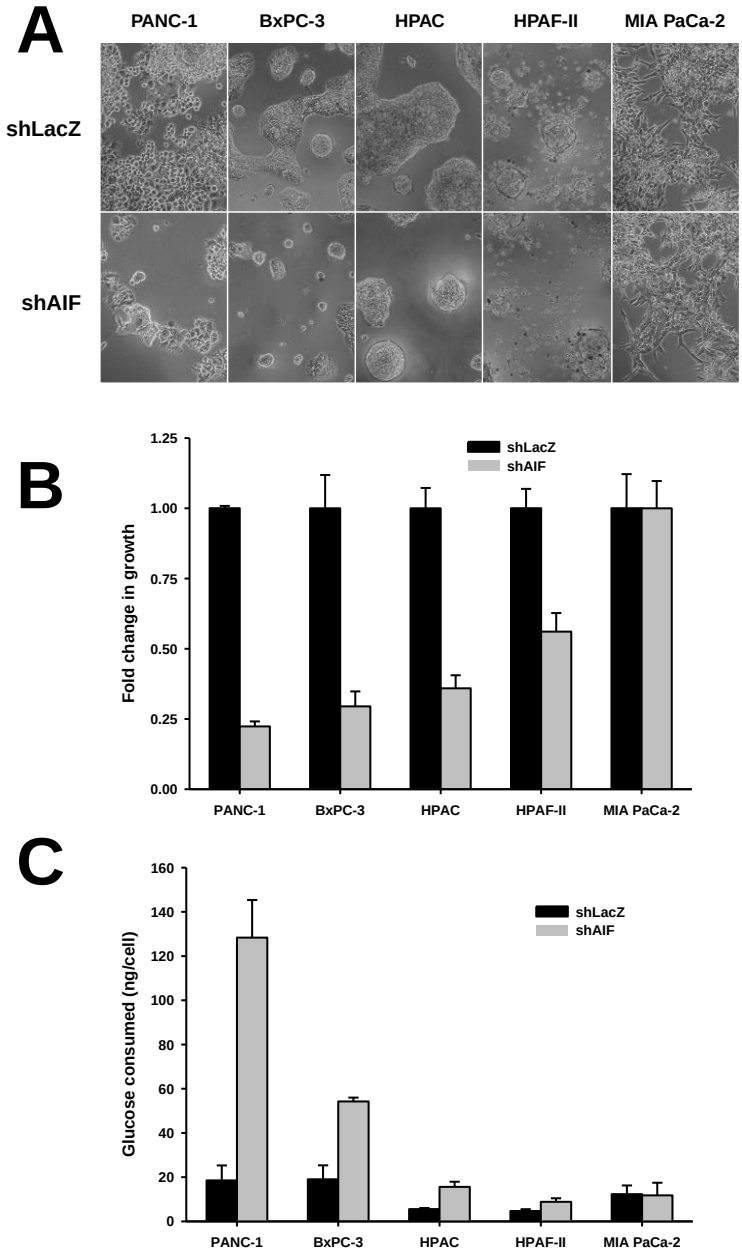

Figure 3.8. Matrigel™ environment amplifies dependence upon AIF-mediated growth and metabolism.

A) Cells were plated in replicate Matrigel™ layers and allowed to grow for up to 21 days. Representative images (captured at 10× magnification) are shown. B) Cells were extracted from substrate and quantified by Coulter™ counting. C) Cells were exposed to Matrigel™ conditions prior to media collection and total glucose measurements using the QuantiChrom™ Glucose Assay Kit (BioAssay Systems). Cells were extracted from substrate with the Matrigel Recovery Solution (Corning) and quantified by Coulter™ counting. Total numbers of cells in each well were used to determine glucose consumption per cell. Data are shown as average ± standard deviation.

achieved advanced status [51], suggesting that AIF addiction in cancer manifests as tumors become increasingly aggressive. Data presented here agree with a similarly important contribution for AIF to pancreatic cancer progression, a disease setting that most often presents at an advanced stage by the time of diagnosis. However, in contrast to observations in prostate cancer, the selectivity of AIF support of different pancreatic cancer cell types was directly related to their cellular energy preferences.

Differences in AIF sensitivity among cell types

PANC-1, BxPC-3, and HPAC cells, all of which display a metabolic phenotype not solely reliant upon glycolysis (Figure 13B, Table 1, [100]), exhibited a remarkably similar reduced growth phenotype (~60% of controls) following AIF ablation that also included respiratory chain depletion and elevated glucose consumption levels ranging from ~2-5-fold. When introduced into Matrigel™ substrate, more severe changes in both growth (20-30% of controls) and glucose uptake (~3-7-fold increases) were observed. PANC-1 and BxPC-3 cell lines were also sensitized to glycolytic disruption, suggesting that glycolysis becomes critical for survival following AIF ablation. This change was not observed in the HPAC cell line, likely due to a metabolic flexibility that derives from its lipogenic phenotype [100]; in this context AIF supports aggressive growth, yet cells remain capable of maintaining survival in the absence of AIF's metabolic activities.

HPAF-II cells, which exhibit a greater dependence on glycolysis than PANC-1, BxPC-3, or HPAC cells (Figure 3.7B, Table 3.1, [100]), also showed changes following AIF ablation, although less severe. Cells did not lose complex I subunits, nor did they exhibit significantly increased glucose consumption *in vitro*. Despite this apparent lack of metabolic consequence *in vitro*, AIF ablation further increased sensitivity to 2-deoxyglucose while modestly compromising

growth. Moreover, introduction to Matrigel™ caused HPAF-II-shAIF cells to elevate glucose consumption by 2-fold while significantly reducing growth rate. No changes in either growth or glucose metabolism were identified in MIA PaCa-2 cells, which displayed a severe pre-existing addiction to glycolysis (Figure 3.7B, Table 3.1, [100]) that could not be further exacerbated by AIF ablation.

AIF is a potential mediator of metabolic flexibility

While our data suggest that AIF is selectively beneficial to metabolically "flexible" PDAC cells that use both glycolysis and OXPHOS for energy production, the basis for the selective sensitivity of different cell types to AIF ablation has not been firmly established. It has been proposed that AIF functions as a metabolic sensor through binding and oxidizing NADH ligands [59]. In light of this hypothesis and extending current data to other cell types, AIF may regulate respiratory chain expression and metabolic flux in response to $NADH/NAD^+$ availability (established by the overall metabolic state). By implication, AIF is consequently central to a self-regulating metabolic balance.

Our data suggest that AIF expression is necessary to mediate a metabolic balance in certain pancreatic cancer cells (*e.g.*, PANC-1, BxPC-3, and HPAC), and AIF ablation induces cellular adaptations that lead to a greater reliance upon glycolysis for survival in these cell types. Other cell types that exhibit a pre-existing addiction to glycolysis (*e.g.*, HPAF-II and MIA PaCa-2) are therefore less sensitive to AIF ablation. This further emphasizes the impact of metabolic balance in support of pancreatic tumorigenesis, specifically through the expression of AIF (Figure 3.9).

Summary

In this study we established a pro-tumorigenic role for AIF in pancreatic cancer that derives from its metabolic activities. The selectivity of AIF dependence in tumorigenesis appears independent of oncogene/tumor suppressor status (Table 3.2) and instead stems from the overall cellular metabolic state, which results from the cumulative effect of genetic alterations. We found a direct relationship between basal metabolic state and dependence upon AIF expression (Table 3.1): as cells become aggressive such that they require a critical balance between mitochondrial energy metabolism and glycolysis, they become more dependent upon AIF. A recent report identified PDAC subtypes based upon metabolic requirements [100]. This extensive study characterized the metabolic states of all cell lines used in our study (Table 3.1) as well as numerous other cell lines, and their data strongly support our model. These data and our previous studies suggest that AIF's metabolic impact upon tumorigenesis increases with disease progression. Previously we showed that AIF promotes a metabolic state permitting progression to advanced stages. Based on our current data, we propose that in the most advanced tumor cells (such as in PDAC), which critically rely on metabolic reprogramming for growth and survival, AIF activity is maximally exploited and becomes entwined within the overall metabolic state, a situation in which the only limiting factor to AIF dependence is how the cell utilizes mitochondrial energy metabolism.

Altered AIF expression is not a general feature of cancerous tissues and AIF activity is not universally supportive to cancer development and progression. However, in studies presented here we have identified a subpopulation of pancreatic cancer samples in which AIF expression is elevated, and using a panel of cancer cell lines with defined metabolic phenotypes we have correlated AIF activity to basal metabolic state. At present the molecular mechanisms defining

AIF sensitivity remain to be elucidated, yet the experiments presented outline a framework for determining those cells in which AIF activity is critical, based on criteria such as metabolic phenotype and fuel source preference/requirements. The promise of this framework is the potential for AIF-mediated therapy. Development of such therapy, either as a stand-alone approach or more likely in combination with other modalities, will depend on better understanding of AIF mechanism and accurate metabolic assessment, but offers significant potential for increasing our treatment arsenal for cancer patients suffering from advanced disease.

Altogether this study highlights the metabolic significance of AIF to PDAC and expands the range of AIF function in tumorigenesis. We found that the basal energetic requirements of PDAC cells determine the ability of AIF to support metabolic plasticity that benefits growth and survival. As a metabolic linchpin in cancer, AIF therefore represents a novel therapeutic target.

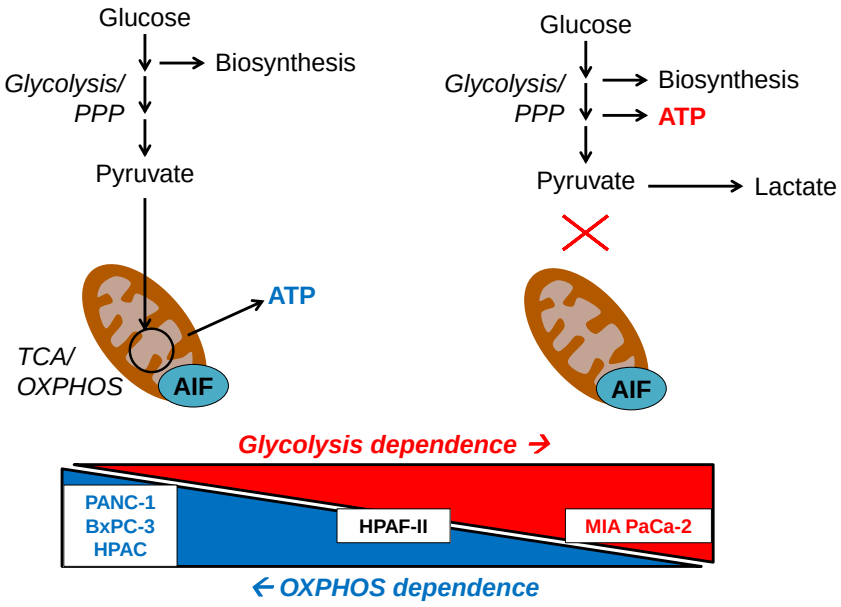

Figure 3.9. Basal metabolic state governs AIF-dependent growth support.
AIF is required for complex I and metabolism benefitting the growth and survival of OXPHOS-dependent cells, but dispensable for metabolism and independent of complex I in glycolytic cells.

IV. AIF IS A ROTENONE-RESPONSIVE TRANSLATION FACTOR FOR MITOCHONDRIAL GENE EXPRESSION BALANCING RESPIRATORY CHAIN ACTIVITY WITH GLYCOLYSIS

Abstract

AIF is critical for the regulation of metabolism, especially in the context of tumorigenesis. Altered metabolism and sensitivity to metabolic disruption are observed following AIF ablation, but how AIF regulates energy production remains largely unknown. One of the key questions surrounding AIF metabolic activity is why complex I protein levels decrease following AIF ablation, and how AIF mechanistically maintains subunits of the ETC. Here we define a role for AIF as a mediator of mitochondrial gene expression. AIF interacts with both mitochondrial EF-Tu (TUFM) and the mitochondrial ribosome, promoting their association with each other. Knockdown of TUFM demonstrates loss of both nuclear and mitochondria-encoded proteins, indicating that impairment of mitochondrial translation leads to decreased nuclear protein expression in the mitochondria and explains how AIF can control protein levels of the ETC encoded both by nuclear and mitochondrial genomes. AIF knockdown and loss of complex I alters glucose metabolism, and experiments here demonstrate that levels of a variety of glycolysis enzymes increase when AIF expression is suppressed. Altogether these experiments identify novel mechanisms through which AIF controls mitochondrial metabolism and extra-mitochondrial responses to AIF ablation.

Introduction

The mitochondrial protein known as AIF has been demonstrated to control complex I and cellular metabolism to the benefit of tumorigenesis. However, a mechanistic understanding of how AIF serves this metabolic function remains to be determined. Determining how AIF

controls levels of ETC subunits would solve a longstanding open question in the field of AIF biology and provide a further understanding of the regulation of cellular metabolism. Following AIF ablation, select cell types exhibit decreases in subunits of complex I, and a variety of explanations can be envisioned. AIF may regulate stability, import, translation, and/or transcription of ETC proteins.

If AIF regulates complex I at the post-translational level, this would suggest that complex I is degraded following loss of AIF. This could be due either to improper import and/or assembly of complex I. Within cells turnover of defective, old, and/or unnecessary proteins occurs through two general mechanisms, involving degradation via either proteasomes or lysosomes. Prior to proteasomal degradation, proteins are modified by covalent attachment of ubiquitin residues to form polyubiquitin chains. Within polyubiquitin chains, ubiquitin units are linked at lysine residue 48, which signals for proteasomal targeting. Ubiquitin linkages at alternative residues have also been reported [142], which serve to regulate protein activity rather than degradation. Following the attachment of K48-linked polyubiquitin chains to the target protein, the protein is recognized by the proteasome and subsequently degraded. During lysosomal degradation, proteins and other intracellular components are engulfed into the acidic lysosome and broken down by lysosomal hydrolases. Lysosome-mediated degradation of cellular components is often mediated by the catabolic cellular recycling process known as autophagy [143].

If complex I is degraded either by proteasomes or lysosomes following AIF ablation, this would suggest that AIF is essential for respiratory chain stability. Additionally or alternatively, AIF may regulate transcription and/or translation of mitochondria-encoded proteins, integrating the cellular metabolic environment with mitochondrial activity. Mitochondria contain their own circular double-stranded genome encoding 37 genes. Of these 37 genes, 13 encode ETC protein

subunits, 22 encode mitochondrial tRNAs, and 2 encode rRNAs. It is thought that mitochondria evolved from an ancestral prokaryote that was engulfed by a larger cell and shared a symbiotic relationship, with the mitochondrial ancestor eventually losing independence from the host's nuclear genome [144]. Over time mitochondria retained only a handful of their own genes, now integrating their expression with nuclear-encoded proteins. If AIF is a necessary factor for mitochondrial gene expression, then loss of AIF and subsequent losses of mitochondria-encoded proteins would prevent translation, import, and/or assembly of nuclear-encoded ETC subunits, which usually happen concurrently.

Similar to translation in the cytosol, mitochondrial translation involves ribosomes, tRNAs, and elongation factors. The mitochondrial ribosome (mitoribosome) functions similarly to cytosolic ribosomes, but differs in composition with higher ratios of protein to rRNA. The mitochondrial ribosome is comprised of a large 39S subunit and a small 28S subunit, which together form a 55S mitoribosome that synthesizes proteins encoded within the mitochondrial genome [145].

Mitochondrial translation requires accessory factors for the ribosome to synthesize proteins. One of these elongation factors known as EF-Tu (known as TUFM in the mitochondria) is bound to GDP in its inactive state, and this GDP is released upon binding with EF-Ts (TSFM in the mitochondria). As a G-protein, EF-Tu then binds GTP to become active. When complexed with GTP, EF-Tu can then bind an aminoacyl-tRNA (aa-tRNA). Subsequently EF-Tu guides the aa-tRNA to the ribosome, where the tRNA anticodon binds the codon of ribosome-associated mRNA. Correct codon-anticodon pairing then induces the ribosome to activate the GTPase domain of EF-Tu, causing GTP hydrolysis. Following GTP hydrolysis, EF-Tu undergoes a conformational change that leads to the release of EF-Tu from the aa-tRNA and ribosome. The

ribosome then catalyzes the transfer of the growing polypeptide onto the amino acid. The liberated EF-Tu (now GDP-bound) is able to be reactivated by EF-Ts and repeat the cycle [146].

Here we find that AIF is a critical factor for mitochondrial translation. Ablation of AIF does not lead to either proteasomal or lysosomal degradation of complex I, further suggesting an absence of protein translation rather than increased turnover. AIF knockdown in our panel of PDAC cell lines demonstrates that AIF is required for mitochondria-encoded protein expression in specific cell types, similar to our observations of nuclear-encoded subunits. Mechanistic examination suggests that AIF stimulates the association of TUFM with the mitoribosome to promote translation of mitochondrial genes. The AIF-TUFM-mitoribosome complex is disrupted by rotenone, suggesting that AIF serves as an adaptor protein that is sensitive to changing metabolic conditions. Loss of AIF metabolic activity leads to the upregulation of the metabolic transcription factor c-Myc and a variety of glycolysis enzymes, suggesting altered glycolysis in AIF-deficient cells is due to additional changes in nuclear encoded proteins beyond the ETC. Altogether these experiments shed light upon how AIF can control the ETC and the effects upon nuclear gene expression, furthering our understanding of the regulation of cellular metabolism.

Materials and methods

Materials, plasmids and antibodies

MEM, DMEM, RPMI 1640, DMEM/F12, GlutaMAX, horse serum, insulin, transferrin, epidermal growth factor, trypsin, 4-12% bis-tris polyacrylamide gels, and nitrocellulose membranes were obtained from Life Technologies; fetal bovine serum (FBS), phosphate buffered saline (PBS), Ni-NTA agarose, and Pierce ECL 2 Western Blotting Substrate were from Thermo Scientific; protease inhibitor tablets were from Roche Applied Science; all other materials were from Sigma.

Lentiviral plasmids FG12-shLacZ-GFP, FG12-shAIF-GFP, FG12-shLacZ-puro, and FG12-shAIF-puro were described previously [51, 52, 121, 147]. Lentiviral packaging plasmids pHCMV-G, pRRE, and pRSV-rev are as described [123]. The pcDNA3.1-Myc/His-MRPL18 plasmid [148] was kindly provided by Dr. Shu-Bing Qian (Cornell University). To create pEBB-TUFM-HA, TUFM cDNA was subcloned from pcDNA3 into the pEBB-HA backbone. Lentiviral pLKO plasmids were obtained as follows: psPAX2 and pMD2.G-vsv-G from Dr. Didier Trono (Addgene plasmids #12260 and 12259); and pLKO.1-puro-scramble [149] from Dr. David Sabatini (Addgene plasmid #1864); pLKO.1-puro-shTUFM #1 (TRCN0000280863) and pLKO.1-puro-shTUFM #2 (TRCN0000280864) were from Sigma.

Antibodies were obtained as follows: anti-AIF (Santa Cruz Biotechnology, sc-13116), anti-NDUFA9 (Life Technologies, 459100), anti-NDUFB8 (Life Technologies, 459210), anti-COX IV (Life Technologies, A21347), anti-polyubiquitin conjugated protein (Enzo Life Sciences, PW8805), anti-LC3 (Cell Signaling, 12741), anti-TUFM (Thermo, PA5-27511), MT-ND1 (Abcam, ab181848), anti-MT-CYB (Abcam, ab81215), anti-MT-CO1 (Abcam, ab14705), anti-MT-CO2 (Abcam, ab79393), anti-HK1 (Cell Signaling, 2024), anti-HK2 (Cell Signaling, 2867), anti-PFKP (Cell Signaling, 8164), anti-PFKFB2 (Cell Signaling, 13045), anti-PFKFB3 (Cell Signaling, 13123), anti-ALDOA (Cell Signaling, 8060), anti-GAPDH (Cell Signaling, 5174), anti-PGAM1 (Cell Signaling, 12098), anti-ENO1 (Cell Signaling, 3810), anti-ENO2 (Cell Signaling, 8171), anti-PKM1/2 (Cell Signaling, 3190), anti-PKM2 (Cell Signaling, 4053), anti-PDHA1 (Cell Signaling, 3205), anti-PDK1 (Cell Signaling, 3820), anti-LDHA (Cell Signaling, 3582), anti-c-Myc (Cell Signaling, 5605), anti-β-actin (Sigma, A5316), anti-HA (Covance, MMS-101P), peroxidase-conjugated anti-HA (Sigma, H-6533), peroxidase-conjugated anti-

FLAG (Sigma, A8592), peroxidase-conjugated anti-mouse (Amersham Biosciences, NA931V), and HRP-conjugated anti-rabbit IgG (Amersham Biosciences, NA934B).

Cell culture

PANC-1, BxPC-3, HPAF-II, HPAC, and MIA PaCa-2 cells were from ATCC (kind gift of Dr. Sanku Mallik, NDSU). PC3 and HEK293T cells were as described [51]. Cells were grown in an atmosphere of 95% air and 5% CO_2 at 37 °C. All media was supplemented with 2 mM GlutaMAX. Cell lines were grown and cultured with the following media formulations: HEK293T and PANC-1 cells in DMEM supplemented with 10% FBS; MIA PaCa-2 in DMEM supplemented with 10% FBS and 2.5% horse serum; BxPC-3 and PC3 in RPMI 1640 supplemented with 10% FBS; HPAF-II in MEM supplemented with 10% FBS; and HPAC in a 1:1 mixture of DMEM and Ham's F12 medium supplemented with 5% FBS, 2 μg/mL insulin, 5 μg/mL transferrin, 40 ng/mL hydrocortisone, and 10 ng/mL epidermal growth factor.

Lentiviral production and stable infection of cell lines

FG12-derived plasmids for targeting of AIF and LacZ by RNA interference (RNAi) have been rigorously assessed and used as described [51, 121, 122]. Lentiviral packaging plasmids pRRE, pRSV-rev, and pHCMV-G are as described [123]. RNAi plasmids and equal amounts of lentiviral packaging plasmids were transfected into HEK293T cells using the calcium phosphate precipitation method [124]. Supernatants of transfected HEK293T cultures were then filtered through 0.45-μm PVDF Millex-HV filters (Millipore) and concentrated by centrifugation at 20,000 x g for 90 min at 4 °C. Viral pellets were resuspended in PBS and then incubated overnight at 4 °C prior to use. Cell lines were then infected as described [51]. PANC-1 and MIA PaCa-2 cells were infected with lentiviruses carrying shLacZ-GFP or shAIF-GFP, after which infection was verified by fluorescence microscopy and flow cytometry with an Accuri C6 flow

cytometer. BxPC-3, HPAC, and HPAF-II cells were infected with lentiviruses carrying shLacZ-puro or shAIF-puro and then selected using 2 μg/mL puromycin.

For establishment of cell lines stably suppressing TUFM, pLKO.1-based lentiviruses were generated by transfecting HEK293T cells with pMD.2, psPAX2, and pLKO.1-scramble or pLKO.1-shTUFM using the calcium phosphate method. Viral supernatant was collected at 48 h and 72 h post-transfection and then filtered using 0.45 μm-pore size Millex HV PVDF filter units. Target cells were then incubated with viral supernatant and 8 μg/mL polybrene for 24 h. Stably infected cells were selected using 1 μg/mL puromycin.

Cell lysis, immunoprecipitation, and nickel affinity precipitation

Cell lysates were prepared in radioimmune precipitation assay (RIPA) lysis buffer (PBS containing 1% NP-40, 0.5% sodium deoxycholate, 0.1% SDS, 1 mM dithiothreitol, 1 mM PMSF, 1 mM sodium fluoride, 1 mM sodium orthovanadate, and 1 protease inhibitor mixture tablet per 10 mL).

For immunoprecipitation experiments, RIPA cell lysates were normalized for protein content and then incubated with indicated antibodies for 2 h at 4 °C. Protein G-coupled agarose beads were then added and incubated for 1 h. Agarose beads were then recovered by centrifugation and washed in RIPA buffer. Precipitated protein was eluted by adding lithium dodecyl sulfate sample buffer followed by heating samples at 95 °C for 5 min. Samples were then analyzed by immunoblot as described below.

For nickel affinity precipitation experiments, RIPA cell lysates were normalized for protein content and then incubated with Ni-NTA agarose for 2 h at 4 °C. Agarose beads were then recovered by centrifugation and washed in RIPA buffer. Precipitated protein was eluted by

adding lithium dodecyl sulfate sample buffer followed by heating samples at 95 °C for 5 min. Samples were then analyzed by immunoblot as described below.

Immunoblot analysis

For immunoblot experiments, protein samples were separated by SDS-PAGE using 4-12% gradient SDS-polyacrylamide gels followed by electrotransfer to nitrocellulose membranes. Membranes were blocked with 5% milk or bovine serum albumin in tris-buffered saline containing 0.02 to 0.2% Tween-20 and then incubated with the indicated primary antibodies. Membranes were then washed three times and incubated with HRP-conjugated anti-mouse or anti-rabbit followed by visualization using enhanced chemiluminescence.

Replicate immunoblots were quantified at multiple exposures for linearity using myImage Analysis™ software (Thermo Scientific). Band intensities for phosphorylated proteins were divided by intensities for the corresponding total proteins; all protein values and phospho-protein/total protein ratios were then normalized to β-actin values. To determine fold changes among lanes, all ratios were then normalized to control lanes (leftmost lanes).

Drug treatments

Cells were seeded at equal densities and allowed to attach overnight. Cells were then treated with either control solvent, 50 μM MG132 for 3-6 h, 0-50 μM chloroquine overnight, or 100 μM rotenone for 1 h. Following treatment cells were subjected to lysis and immunoblot as described above.

Results

Complex I is not degraded following AIF ablation

AIF regulates protein levels of complex I [25, 73], but the mechanisms underlying this regulatory process are not well established. One possibility is that AIF could regulate import or

folding of complex I. Based upon cell type and metabolic requirements, mitochondria may exhibit different sensitivities to defective complex I following loss of AIF. For example, MIA PaCa-2 cells are glycolytic and do not appear to acquire significant amounts of ATP from mitochondrial ETC/OXPHOS [52]. In this context complex I malfunction would not substantially impact metabolism. However, in cells that utilize OXPHOS to obtain energy (*e.g.*, PC3 and PANC-1 cells) [51, 52], defective complex I could signal for either proteasomal or lysosomal degradation as a mechanism to replace ETC subunits (which is a futile process without AIF).

To test the hypothesis that AIF ablation triggers degradation of complex I, AIF-proficient and deficient PC3 cells were used. PC3 cells exhibit complex I deficiency following AIF ablation and were therefore treated with MG132, a proteasomal inhibitor. If complex I is degraded by the proteasome, MG132 should restore complex I in AIF-deficient cells. Immunoblot for ubiquitinated proteins (Figure 4.1) demonstrated substantial protein ubiquitination (a signal for proteasomal degradation and indicator of MG132 efficacy) following treatment. However, the 39-kDa subunit (NDUFA9) of complex I remained at low levels upon proteasomal inhibition (Figure 4.1), suggesting that complex I is not degraded by the proteasome when AIF is suppressed.

An alternative means by which complex I depletion may occur is through lysosomal degradation. Autophagy, a cellular process serving to degrade and recycle cellular components, uses lysosomes to turn over intracellular molecules and organelles. During this process the autophagic protein LC3-I is conjugated with phosphatidylethanolamine, forming LC3-II and leading to its association with lysosomes to promote membrane expansion and fusion events. LC3-II is then degraded within the lysosome [143]. When lysosomes are neutralized by

lysosomotropic agents such as chloroquine, LC3-II accumulates, leading to an increased LC3-II/LC3-I ratio that can be visualized via immunoblot. Therefore, similar to our experiment with MG132, we treated cells with chloroquine to determine if complex I is lysosomally degraded, using LC3 as a marker for lysosomal inhibition. Following treatment with chloroquine, LC3-II substantially increased (Figure 4.2) and indicates lysosomal neutralization. However, similar to our observations of proteasomal inhibition, suppression of lysosomal activity did not restore complex I (Figure 4.2) and suggests that complex I is neither degraded by the proteasome nor lysosome following AIF ablation. It is notable that less LC3-II accumulation was observed in AIF-deficient cells (Figure 4.2), suggesting a possible involvement of AIF in regulating autophagy.

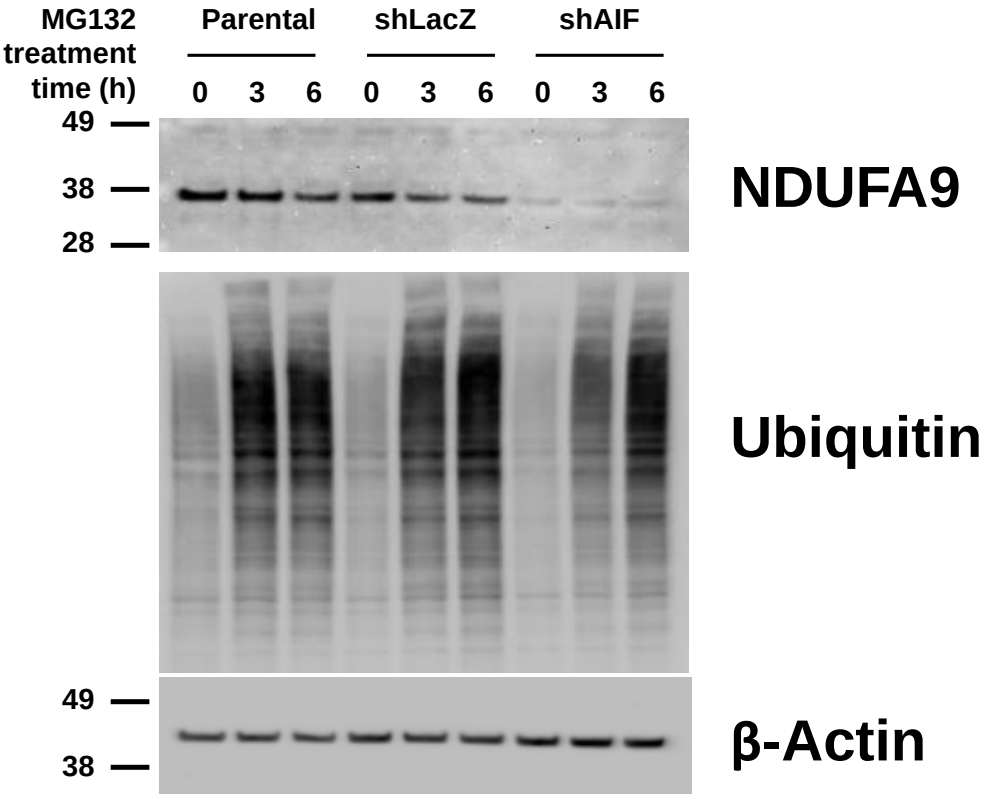

Figure 4.1. Complex I is not degraded by the proteasome following AIF ablation.
PC3-derived cells were treated with control solvent or 50 μM MG132 for 3 or 6 h, then lysed and assessed for the indicated proteins by immunoblot.

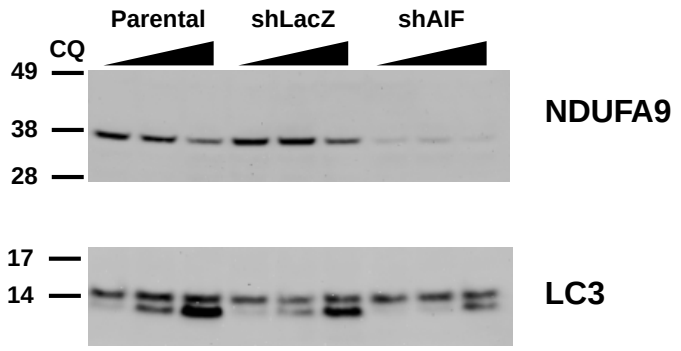

Figure 4.2. AIF ablation does not induce lysosomal degradation of complex I.
PC3-derived cells were treated with 0, 10, or 50 μM chloroquine (CQ), lysed, and assessed for the indicated proteins by immunoblot.

Proteasomal and lysosomal degradation are the two major general mechanisms for protein turnover. Proteases are capable of degrading specific protein targets, but the multitude of ETC proteins associated with AIF ablation make this an unlikely mode of complex I deficiency. Rather, it appears that complex I is not translated. It remains to be determined how AIF impacts ETC subunits at the RNA level.

AIF regulates mitochondria-encoded protein levels

Complex I is not degraded following AIF ablation, suggesting that ETC deficiency occurs at or prior to protein translation. While most respiratory chain proteins are encoded by the nucleus, 13 are encoded within the mitochondrial genome. Therefore we wondered if AIF could control protein levels of mitochondria-encoded genes, similar to what is observed for AIF-dependent control of nuclear-encoded ETC genes [52]. If mitochondrially encoded proteins are impaired by AIF ablation, this could lead to a loss of translation and import of nuclear encoded proteins. To interrogate the possibility that AIF is involved with mitochondrial gene expression, lysates of our panel of AIF-deficient PDAC cells (Chapter 3) were probed for 4 different mitochondria-encoded proteins: MT-ND1 (complex I), MT-CYB (complex III), MT-CO1

(complex IV), and MT-CO2 (complex IV). Immunoblot analysis revealed that following AIF ablation cells exhibited decreased levels of mitochondria-encoded proteins that varied with cell type (Figure 4.3A). PANC-1 cells showed decreases in MT-ND1 and MT-CO2; and BxPC-3 cells demonstrated losses in MT-CYB, MT-CO1, and MT-CO2; while HPAC cells showed reduced levels of all 4 proteins assessed following AIF knockdown. HPAF-II and MIA PaCa-2 cells did not exhibit substantial changes in mitochondria-encoded proteins, similar to a lack of response for nuclear-encoded proteins. It is also notable that in general HPAF-II and MIA PaCa-2 exhibit lower levels of mitochondria-encoded proteins prior to AIF ablation, raising the possibility that these two cell types may have fewer and/or less metabolically active mitochondria. Altogether, these data show that in specific cell types AIF controls both mitochondria- and nuclear-encoded ETC proteins. It is possible AIF may control mitochondrial gene expression, and when mitochondrial gene expression is impaired by AIF ablation, translation and/or import of nuclear-encoded ETC proteins is halted [150].

AIF promotes formation of a mitochondrial translation complex containing mitochondrial EF-Tu and the mitoribosome

ETC impairment due to AIF deficiency stems from loss of both nuclear and mitochondria-encoded ETC subunits, which is not due to increased protein turnover and rather appears to involve control mitochondrial gene expression. Previously we identified the mitochondrial ribosomal protein L18 (MRPL18) and the mitochondrial elongation factor Tu (TUFM) in a biochemical screen for mitochondrial AIF binding partners [53], providing a starting point to explore potential mechanisms through which AIF mediates ETC protein levels. Therefore we questioned the ability of AIF to control translation of the respiratory chain, which could be in part through interactions with the mitochondrial translation machinery.

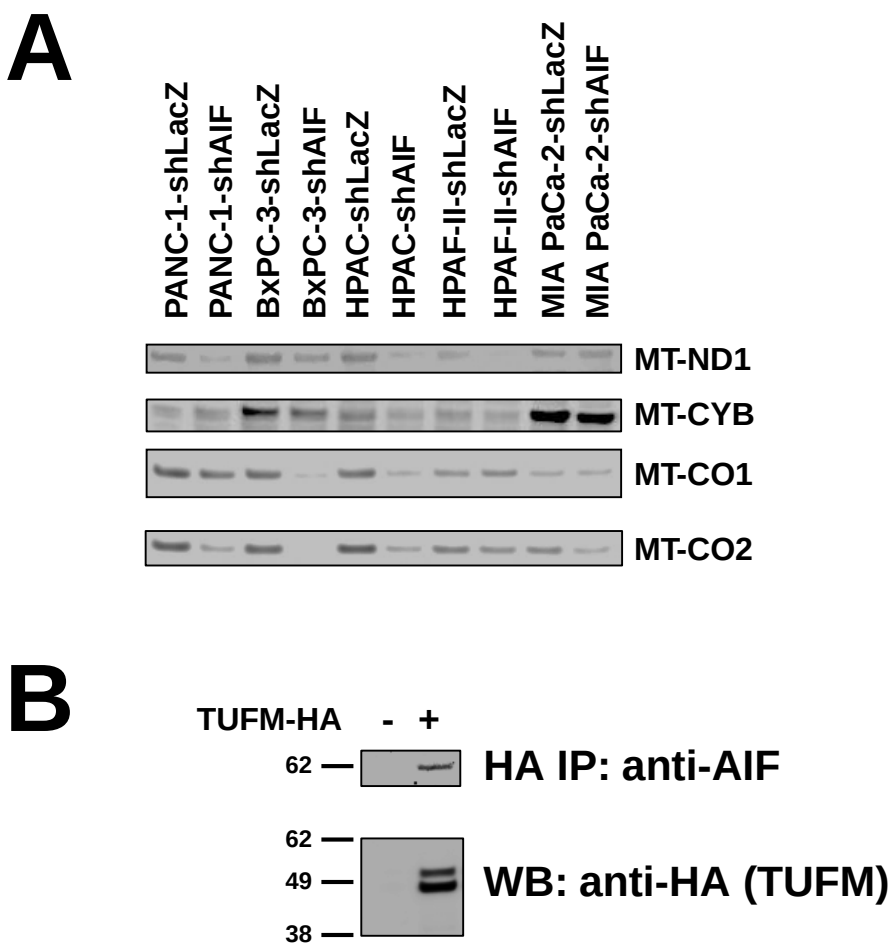

Figure 4.3. AIF interacts with the mitochondrial translation factor TUFM and controls protein levels of mitochondria-encoded genes.
A) Following suppression of AIF, levels of mitochondria-encoded proteins (MT-ND1, MT-CYB, MT-CO1, and MT-CO2) were assessed in the indicated cell types by immunoblot analysis. Corresponding β-Actin immunoblots are shown in Figure 3.3. B) HEK293T cells were transfected with control plasmids or plasmids encoding HA-tagged TUFM and subjected to co-immunoprecipitation using an anti-HA antibody followed by immunoblot.

To verify if TUFM physically associates with AIF, HEK293T cells were transfected with HA-tagged TUFM followed by immunoprecipitation using an anti-HA antibody. Immunoblot analysis demonstrated the presence of AIF in the precipitated samples containing exogenous TUFM (Figure 4.4B), showing that TUFM binds endogenous AIF.

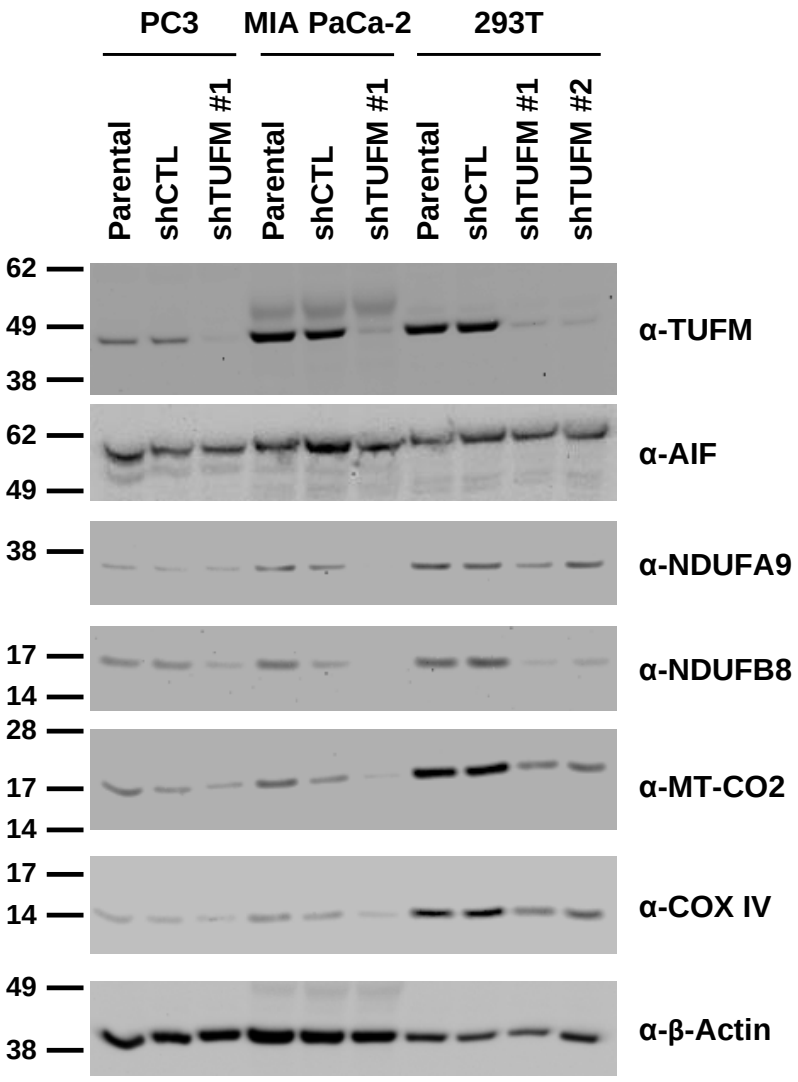

Figure 4.4. TUFM ablation induces the loss of both mitochondria- and nuclear-encoded ETC proteins.
The indicated cell types were either uninfected or stably infected with either control lentiviruses (shCTL) or lentiviruses harboring TUFM targeting sequences (shTUFM #1, 2), then lysed and assessed for the indicated proteins by immunoblot.

To determine the role of TUFM in controlling protein levels of mitochondrial proteins, we then stably suppressed TUFM expression using lentivirus-mediated shRNA induction and puromycin selection. Three different cell lines exhibiting different ETC responses to AIF ablation were targeted: AIF-deficient PC3 cells show decreased ETC subunit levels, whereas

AIF-deficient MIA PaCa-2 and HEK293T cells do not show changes in ETC proteins [51-53]. To ensure results were not due to nonspecific shRNA targeting effects, two different TUFM targeting sequences (shTUFM #1, shTUFM #2) were used in HEK293T cells. Immunoblot for TUFM was used to verify stable infection and knockdown (Figure 4.5). AIF levels were unaffected following TUFM knockdown, but decreases in complex I subunits NDUFA9 (39 kDa) and NDUFB8 (20 kDa), COX IV, and MT-CO2 were observed. Similar to mitochondria-encoded ETC proteins, nuclear-encoded proteins were additionally reduced, demonstrating that loss of mitochondrial gene expression triggers the loss of nuclear-encoded ETC subunits. Therefore this may explain the loss of nuclear-encoded ETC proteins following AIF ablation. Interestingly, decreases in ETC protein levels were substantially more apparent in MIA PaCa-2 and HEK293T cells, whereas little to no change in ETC proteins was observed in PC3 cells. This is particularly notable since PC3 cells, but not MIA PaCa-2 or HEK293T cells exhibit ETC deficiency following AIF knockdown. While this observation requires further experimentation to provide a mechanistic explanation, it may suggest that AIF can promote mitochondrial protein expression without TUFM, but TUFM cannot promote translation without AIF.

We then tested the possibility that AIF and TUFM could regulate ETC translation through interaction with the mitochondrial ribosome. Having previously identified the mitoribosomal protein MRPL18 as another AIF-associated factor [53], we then transfected HEK293T cells with either empty control plasmids or plasmids encoding FLAG-tagged AIF with HA-tagged TUFM and/or 6x-His-tagged MRPL18. The 6x-His tag exhibits a high affinity for nickel and can therefore be used for purification/precipitation. Transfected cells were lysed and then subjected to nickel affinity precipitation followed by immunoblot for FLAG (AIF) and HA (TUFM). Both AIF and TUFM precipitated with MRPL18 (Figure 4.5), suggesting that both

proteins are MRPL18 binding partners. Additionally, overexpression of AIF increases TUFM-MRPL18 binding. Since AIF binds both TUFM (Figure 4.3) and MRPL18 (Figure 4.5), this raises the possibility that AIF serves as an adaptor protein promoting delivery of aminoacyl-tRNAs from EF-Tu to the mitochondrial ribosome, a process that is indispensable for protein synthesis.

Binding of AIF and TUFM with MRPL18 was additionally tested following treatment with rotenone, a complex I inhibitor that disrupts respiratory chain function and cellular metabolism. The TUFM-MRPL18 interaction was unaffected by treatment, but binding of AIF with MRPL18 showed a robust increase in the presence of rotenone. Interestingly, when both AIF and TUFM were simultaneously overexpressed with MRPL18, rotenone treatment caused a strong reduction in binding of both proteins. The mechanisms and biochemical logic underlying this altered binding remain to be determined, but these data demonstrate that the AIF-mediated mitochondrial translation complex is sensitive to respiratory chain activity, further suggesting that AIF responds to metabolic changes within the cell (Chapter 3).

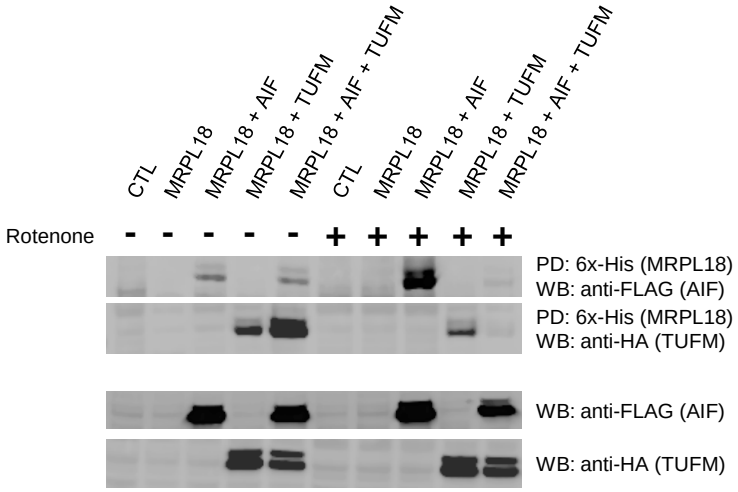

Figure 4.5. AIF facilitates the formation of a mitochondrial translation complex containing TUFM and MRPL18 that is responsive to rotenone.
HEK293T cells were transfected with the indicated plasmids and then treated with either control solvent or 100 μM rotenone, followed by nickel affinity precipitation and immunoblot.

Loss of AIF leads to an increase of glycolysis enzymes

Having identified the existence of an AIF-associated translation complex likely to control protein levels of ETC subunits within the mitochondria, we then questioned the mechanism by which cells produce ATP in the absence of complex I following AIF knockdown. Previous observations of increased glucose consumption and lactate section combined with decreased oxygen consumption levels in the absence of AIF [51, 52] strongly suggest a metabolic switching event to glycolysis. One mechanism by which cells increase the flux of metabolites through different pathways is via changes in protein levels of metabolic enzymes, in particular those catalyzing thermodynamically irreversible conversions. Therefore protein levels of glycolytic enzymes were assessed in AIF-proficient and deficient PC3 cells, which have been thoroughly evaluated for AIF-dependent metabolic phenotypes [51].

Enzymes assessed function in both the preparatory and payoff phases of glycolysis, and we additionally evaluated the status of enzymes regulating the conversion of pyruvate to acetyl-CoA for oxidation in the mitochondria, or pyruvate to lactate for sustained glycolysis (Figure 4.6A). Interestingly, increases in glycolysis enzyme levels in AIF-deficient cells were observed throughout the glycolytic pathway (Figure 4.6B, C), with changes ranging from ~2-3-fold that are consistent with the magnitude of glucose consumption changes observed in PC3 cells [51].

Within the initial stage of glycolysis, changes in levels of at least three enzymes were observed (Figure 4.6B, C). Hexokinase (HK) catalyzes the ATP-dependent phosphorylation of glucose, which is the rate-limiting first step of glycolysis. Levels of HK1, the most ubiquitously expressed HK isoform, approximately doubled following knockdown of AIF, whereas levels of the HK2 isoform were unaffected. It is notable that the role of HK2 in coupling glycolysis to OXPHOS is thought to drive tumorigenic growth [151], while HK1 is the only HK isoform

expressed in cells that rely most heavily upon glucose metabolism, such as the brain and red blood cells [152].

Significant changes were additionally observed at the level of the conversion of fructose-6-phosphate to fructose-1,6-bisphosphate, which is the commitment step of glycolysis catalyzed by phosphofructokinase-1 (PFK-1) and the most heavily regulated step of the pathway [153]. Three isozymes of PFK-1 exist in humans [154]: platelet (PFKP), liver (PFKL), and muscle (PFKM). PFKL was not expressed at detectable levels in PC3 cells (data not shown), while PFKM levels remain to be assessed. However, protein levels of PFKP increased substantially following AIF ablation, consistent with elevated glucose consumption and glycolytic activity. We additionally noted changes in PFK-2, which is one of the most important regulators of glycolysis. PFK-2 is a bifunctional enzyme that mediates both the synthesis and degradation of fructose-2,6-bisphosphate (F2,6BP). F2,6BP is a strong allosteric activator of PFK-1, and whether PFK-2 predominantly exhibits kinase (F2,6BP synthesis) or phosphatase (degradation) activity depends on the cell's metabolic needs. Two isoforms of PFK-2, known as PFKFB2 and PFKFB3, were assessed. Levels of PFKFB2 were unaffected by suppression of AIF, but a robust increase in levels of PFKFB3 was observed. Interestingly, PFKFB3 is induced by hypoxia, has substantially higher kinase activity than other PFK-2 isoforms [155, 156], and exhibits almost no phosphatase activity [157], which strongly suggest that elevated PFKFB3 levels serve to promote, and not inhibit, glycolysis.

Within the payoff phase of glycolysis, changes were found in protein levels of phosphoglycerate mutase (PGAM1) and two widely expressed isoforms of enolase (ENO1, ENO2). Upregulation of both enzymes serves to promote glycolysis benefitting survival in cancer [158-160]. In the context of AIF ablation, elevation of PGAM1 and ENO1/2 are likely to

aid in accelerating the conversion of glucose-derived metabolites to pyruvate for increased ATP production mediated by phosphoglycerate kinase (PGK1) and pyruvate kinase (PKM).

Following the oxidation of glucose during glycolysis, the pyruvate product can either be converted to acetyl-CoA for subsequent oxidation, or reduced to lactate in order to replenish NAD^+ sustaining further glycolysis. Changes in levels of neither the E1 α1 subunit (PDHA) of the pyruvate dehydrogenase complex (PDH) nor the PDH inhibitor PDH kinase 1 (PDK1) were observed in AIF-deficient cells. However, protein levels of lactate dehydrogenase (LDHA) notably increased, strongly agreeing with increased lactate production following AIF ablation [51]. Altogether these data suggest that when AIF is lost from cells, glycolysis is upregulated and metabolic flux is shuttled through lactate generation in order to produce ATP in the absence of mitochondrial energy production. Moreover, this increased glycolytic activity occurs through the elevation of various glycolytic enzymes.

Glycolysis enzyme levels are regulated through a variety of genetic control mechanisms. One of the predominant means cells use to control the expression of glycolysis enzymes is through the transcription factor known as c-Myc, a master regulator of metabolism that can stimulate glycolysis through the expression of target genes including LDHA, PFK-1, enolase, and numerous others [161]. It is notable that these genes increase following AIF ablation which could be due to elevated c-Myc activity. Therefore AIF-proficient and deficient cells were additionally probed for c-Myc protein levels. Interestingly, c-Myc levels were upregulated in response to AIF ablation (Figure 4.6B, C) and may indicate a mechanism through which AIF-deficient cells upregulate glycolytic activity. Collectively these data further support increased glycolytic activity observed in AIF-deficient cells and begin to shed light upon survival mechanisms in the absence of AIF.

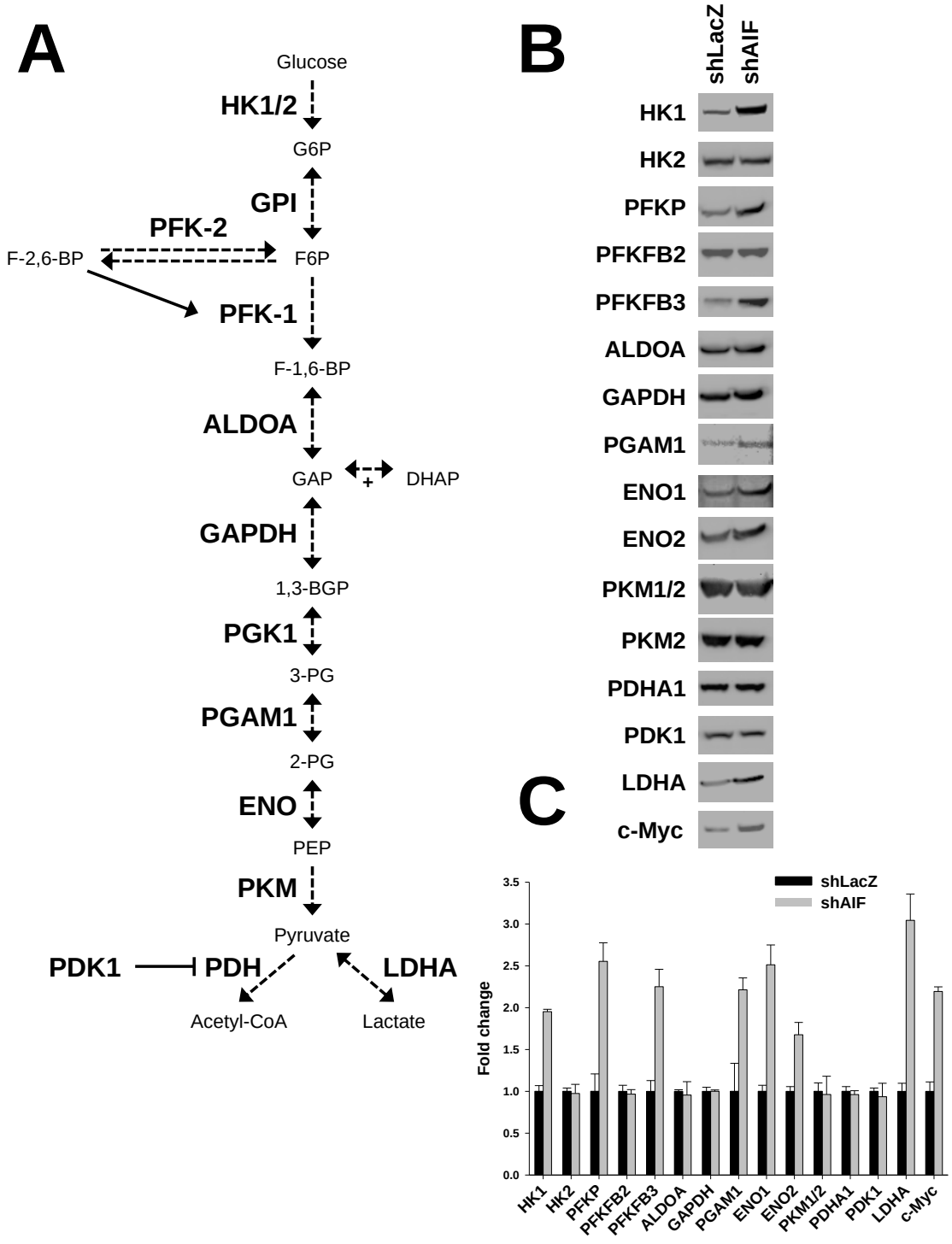

Figure 4.6. AIF ablation increases levels of glycolysis enzymes.
A) Schematic of glycolysis. Dashed arrows indicated chemical conversations; solid lines indicate activation. B) The indicated PC3-derived cells were lysed and probed for the indicated proteins by immunoblot. C) Replicate immunoblots from panel b were quantified and normalized to β-actin. Data are presented as average ± standard deviation.

Discussion

AIF mediates mitochondrial protein translation

This study demonstrates for the first time that AIF controls protein levels of not only nuclear-encoded ETC subunits but also proteins encoded by the mitochondrial genome. AIF-mediated control of mitochondria-encoded proteins occurs in specific cell types (*e.g.*, HPAC) but not others (*e.g.*, MIA PaCa-2), similar to our observations of nuclear-encoded subunits. These differences could stem from differences in mitochondrial activity and/or metabolic requirements among cell types (Chapter 3).

Assessment of the mechanisms underlying AIF ablation-induced metabolic switching revealed several intriguing events associated with AIF mitochondrial activity. Following AIF suppression, complex I could not be restored either by the proteasomal inhibitor MG132 or the lysosomal inhibitor chloroquine. Other than through protein target-specific proteases, proteasomal and lysosomal degradation are the two major general mechanisms for protein turnover. When AIF is suppressed, complex I is not degraded; rather, it appears likely that complex I deficiency occurs because complex I subunits are not translated.

This hypothesis is supported by our observations of AIF binding with MRPL18 and TUFM, which are essential components of the mitochondrial translation machinery. Through these interactions AIF could promote mitochondrial translation from the inner membrane. Mitoribosomes are frequently localized to the IMM [162, 163], likely because all mitochondria-encoded proteins are membrane-bound. It appears that AIF forms a complex with TUFM and MRPL18 that promotes TUFM-MRPL18 association. This is notable since EF-Tu proteins are required to bind ribosomes in order to supply the ribosome with aminoacyl-tRNAs. Therefore if AIF is suppressed, decreased TUFM-MRPL18 binding is likely to decrease mitochondrial

translation, leading to a reduction in ETC subunits. Subsequently an impairment of mitochondria-encoded proteins could cause the cell to halt translation and/or import of nuclear-encoded ETC subunits. Indeed, knockdown of TUFM induces the loss of both mitochondria- and nuclear-encoded proteins.

Interestingly, TUFM ablation-induced loss of ETC proteins is the most apparent in MIA PaCa-2 and HEK293T cells, whereas PC3 cells exhibit lower magnitudes of ETC deficiency. This is in contrast with the effects of AIF ablation, which induces ETC deficiency in PC3 cells, but not MIA PaCa-2 or HEK293T cells. Reasons for this inverse relationship can only be speculated at this point. Perhaps AIF can promote mitochondrial protein expression without TUFM, but TUFM cannot promote translation without AIF activity. We hypothesize that AIF exhibits lower activity in MIA PaCa-2 cells, which have lower requirements for mitochondrial energy production (Chapter 2, 3). Moreover, disruption of mitochondrial activity with rotenone disrupts the AIF-mediated translation complex, further supporting the concept of metabolic conditions governing AIF activity. This would explain why AIF ablation but not TUFM ablation causes the loss of ETC subunits in PC3 cells, while TUFM ablation but not AIF ablation causes ETC loss in MIA PaCa-2 and HEK293T cells (exhibiting different metabolic requirements). This hypothesis merits further interrogation.

Metabolic effects of AIF ablation

When AIF and complex I levels are impaired, cells switch from OXPHOS to glycolysis in order to produce ATP. Further assessment of this metabolic switch reveals that a variety of glycolytic enzymes are upregulated at the protein levels including HK1, PFKP, PFKFB3, PGAM1, ENO1, ENO2, and LDHA. This suggests that increased glycolysis following AIF ablation occurs at least in part through elevation of glycolysis enzyme levels. It is also interesting

that AIF ablation increases levels of c-Myc, a critical regulator of metabolism. This hints to the existence of AIF-dependent signal transduction events regulating metabolism, and to our knowledge this is the first report of AIF involvement with an oncogene.

Summary

Altogether this study shows that AIF serves as a regulator of mitochondrial translation and suggests that ETC deficiency following AIF ablation is triggered by impairments in mitochondrial gene expression. Remarkably, AIF appears to promote TUFM-MRPL18 binding in order to synthesize mitochondria-encoded proteins, and this activity is sensitive to metabolic changes induced by rotenone. When AIF activity is impaired, cells upregulate glycolysis enzymes to increase glycolytic flux, a requirement for cells to obtain ATP without proper respiratory chain activity. Collectively, these data confirm the ability of AIF to physically associate with the mitochondrial translation machinery and identify a potential mechanism through which AIF controls protein levels of the mitochondrial respiratory chain.

V. THE ENZYMATIC ACTIVITY OF AIF ELEVATES OXIDATIVE STRESS LEVELS REGULATING REDOX-SENSITIVE SIGNAL TRANSDUCTION

Abstract

Apoptosis-inducing factor (AIF) is a mitochondrial flavoprotein occasionally involved in cell death that primarily regulates mitochondrial energy metabolism under normal cellular conditions. AIF catalyzes the oxidation of NADH *in vitro*, yet the significance of this redox activity in cells remains unclear. Here we show that through its enzymatic activity AIF is a critical factor for the induction of ROS. Moreover, AIF-mediated ROS levels correspond to changes in the antioxidant response, suggesting AIF regulates cellular ROS and subsequent nuclear responses to oxidative stress. Assessment of the ability of AIF to regulate other redox-sensitive pathways shows that AIF is required for oxidative stress-induced activation of the mitogen-activated protein kinases JNK1, p38, and ERK. Altogether these data demonstrate for the first time the ability of AIF to serve as a significant redox signaling protein.

Introduction

The known roles of AIF in cell death and survival exemplify the duality of mitochondria in life/death decisions: nuclear translocation of AIF is occasionally observed under conditions of cell death [24], whereas under non-stress conditions AIF is essential to mitochondrial energy production through regulation of the respiratory chain and glucose metabolism [25, 51, 52]. Through high levels of ROS production, mitochondria can induce cell death but at low to moderate ROS levels promote pro-survival pathways. AIF generates ROS *in vitro*, but the ability of AIF to mediate ROS levels in cells is not well understood.

The ability of AIF to regulate metabolism and complex I (both capable of altering ROS levels), as well as its ROS-generating enzymatic activity, strongly suggests that AIF is likely to

play an important role in the regulation of intracellular ROS. While AIF enzymatic activity has been shown to produce superoxide anions *in vitro*, these findings have not been extended to the context of an intracellular environment, and the role of AIF enzymatic activity in control of cellular ROS levels and its significance to cell biology is not well understood.

ROS serve as second messengers to promote a variety of redox-sensitive signaling pathways. A potential biological purpose for AIF regulation of ROS in cells may be to induce these pathways, serving as a transmitter of extra-mitochondrial signaling cues. The contribution of AIF enzymatic activity to cellular homeostasis has remained largely elusive, and the ability of mitochondria-localized AIF to control intracellular redox signaling has long been speculated [54]; yet to date no studies have definitively shown the existence of such pathways. Since actively respiring mitochondria are an important ROS source for pro-oxidant signaling, this suggests that AIF could sense and/or promote ROS through its NADH-oxidase activity in addition to regulating respiratory chain biogenesis.

We and others have defined contributory roles for AIF metabolic activity to the growth and survival of cancer cells, but AIF-mediated redox control and its involvement in the process of tumorigenesis are not well understood. Notably, ROS levels have been shown to change with loss of AIF, but whether ROS levels increase or decrease appears dependent upon cell type and context. For example, Harlequin mice, which express low levels of AIF due to a proviral insertion with the *Aif* promoter, exhibit increased ROS levels leading to cell death and neurodegeneration that can be rescued by antioxidant treatment [26]. In contrast, ROS levels decrease following AIF knockout in colorectal cancer cells, leading to increased sensitivity to apoptosis [54]. Among different cell types, these differences in AIF redox function could be due to different ETC protein and activity levels, basal ROS levels influencing the direction of AIF-

mediated catalysis, or other factors. These findings collectively demonstrate a significant role for AIF to cellular redox control, but mechanistic details and pathways involved remain undefined.

Various purposes for AIF redox activity have been proposed. Urbano *et al*. [54] posited that AIF promotes oxidative stress signaling that can promote the survival of cancer cells, whereas Sevrioukova [73] put forth a model in which AIF senses oxidative stress levels and can respond (*e.g.*, by regulating complex I, translocating to the nucleus, generating or suppressing ROS, etc.) depending on stimulus. Here we tested both models and found that AIF is required for various stimuli to induce high ROS levels, and that AIF is additionally required for oxidative stress-induced signaling pathways in a variety of cell types. AIF-mediated redox control regulates both antioxidant defenses and MAPK phosphorylation, which demonstrate that AIF promotes intracellular ROS and for the first time identifies the existence of AIF-dependent signal transduction pathways. Based on the diversity of ROS signaling activities, these findings open the door to a broad range of potential AIF functions in cell biology and disease.

Materials and methods

Materials, plasmids and antibodies

DMEM, RPMI 1640, DMEM/F12, K-SFM, GlutaMAX, horse serum, insulin, transferrin, epidermal growth factor, trypsin, 4–12 % bis-tris polyacrylamide gels, nitrocellulose membranes, fetal bovine serum (FBS), phosphate buffered saline (PBS), and Pierce ECL 2 Western Blotting Substrate were from Thermo Fisher Scientific; immunoglobulin G-Sepharose was from Amersham; all other materials were from Sigma.

Lentiviral plasmids FG12-shLacZ-puro and FG12-shAIF-puro were described previously [51, 52, 121, 147]. To generate RNAi-resistant AIF restoration pSL4-hygro plasmids, AIF cDNA was subcloned from pEBB-siMut-AIF^{WT} and pEBB-siMut-AIF^{TVA} [51] into pSL4-hygro [164].

Lentiviral packaging plasmids pHCMV-G, pRRE, and pRSV-rev are as described [123]. Additional constructs were kind gifts obtained as follows: pcDNA3-ASK1-HA [165] from Dr. Jonathan D. Ashwell; pcDNA3-Flag-MKK7β2-JNK1α1 and pcDNA3-Flag-MKK7β2-JNK2α2 [166] from Dr. Roger Davis (Addgene plasmids #19726 and 19727).

Antibodies were obtained as follows: anti-AIF (Santa Cruz, sc-13116), anti-Nrf2 (Santa Cruz, sc-13032), anti-HMOX1 (Santa Cruz, sc-136960), anti-GSTM1 (Santa Cruz, sc-517262), anti-GGT1 (Santa Cruz, sc-100746), anti-β-actin (Sigma, A5316), anti-α/β-tubulin (Cell Signaling, 2148), anti-PCNA (Cell Signaling, 2586), anti-MLK1 (Cell Signaling, 5029), anti-phospho-MKK4/SEK1 S257 (Cell Signaling, 4514), anti-MKK4/SEK1 (Cell Signaling, 9152), anti-phospho-JNK T183/Y185 (Cell Signaling, 4668), anti-JNK (Cell Signaling, 9252), anti-JNK1 (Cell Signaling, 3708), anti-JNK2 (Cell Signaling, 9258), anti-phospho-p38 T180/Y182 (Cell Signaling, 9216), anti-p38α (Santa Cruz, sc-535), anti-phospho-ERK T202/Y204 (Cell Signaling, 4377), anti-ERK1/2 (Cell Signaling, 9107), anti-DUSP4/MKP2 (Cell Signaling, 5149), anti-phospho-c-Jun S73 (3270), anti-c-Jun (Cell Signaling, 9165), anti-GAPDH (Cell Signaling, 5174), anti-histone H3 (Cell Signaling, 9715), horseradish peroxidase (HRP)-conjugated anti-Flag (Sigma, A8592), HRP-conjugated anti-HA (Sigma, A6533), HRP-conjugated anti-mouse IgG (Amersham Biosciences, NA391B), HRP-conjugated anti-rabbit IgG (Amersham Biosciences, NA934B), and HRP-conjugated anti-rabbit native IgG (Sigma, R3155).

Cell culture

Cells were cultured in an atmosphere of 95% air and 5% CO_2 at 37 °C. All media formulations were supplemented with 2 mM GlutaMAX. HEK293T and MRC-5 cells were cultured in DMEM supplemented with 10% FBS; PC3 and HCT 116 cells in RPMI 1640 medium supplemented with 10% FBS; MIA PaCa-2 cells in DMEM supplemented with 10%

FBS and 2.5% horse serum; and HPAC cells in a 1:1 mixture of DMEM and Ham's F12 medium supplemented with 5 % FBS, 2 μg/mL insulin, 5 μg/mL transferrin, 40 ng/mL hydrocortisone, and 10 ng/mL EGF. RWPE-1 cells were cultured in K-SFM (Thermo Scientific, 17005042) supplemented with 0.05 mg/mL bovine pituitary extract and 5 ng/mL EGF. Cells were harvested by trypsinization, washed in PBS, and seeded at equal densities and then allowed to attach overnight prior to all assays.

Drug treatments

Cells were subjected to chemical treatments as follows: menadione at 100 μM for 1 h (for ROS assays) or 50 μM overnight (for viability assays); antimycin A at 50 μM for 1 h (for ROS assays) or 48 h (for viability assays); tBHQ at 90 μM overnight (for Nrf2 and antioxidant gene expression assays), 500 μM overnight (for viability assays), or 0-2 mM for 1 h (for phospho-JNK assays); and anisomycin at 0-5 μM for 1 h. Following treatment cells were harvested and assessed in the indicated assays.

Transfections

Plasmids were transfected into cells using Lipofectamine™ 2000 as described by the manufacturer. Cells were then harvested 48-72 h following transfection and either lysed as described below or quantified by Coulter™ counting.

ROS measurements

Following treatments described above, cells were incubated with 2.5 μM MitoSOX™ Red (for mitochondrial superoxide), or 10 μM CM-H_2DCFDA (for general cellular ROS) at 37 °C for 20 min. Cells were then harvested and resuspended in PBS, followed by assessment of stain intensity using an Accuri C6 flow cytometer.

Cell viability

Following drug treatments described above, attached and floating cells were harvested, washed, and resuspended in PBS containing 2 μg/mL propidium iodide. Cell viability was then determined by flow cytometry using an Accuri C6 flow cytometer.

Lentiviral production and stable infection of cell lines

To establish cell lines stably suppressing or overexpressing AIF, lentiviral particles were produced by transfecting equal amounts of pHCMV-G, pRRE, pRSV-rev, and FG12- or pSL4-derived plasmids into HEK293T cells using the calcium phosphate method [124]. Following incubation at 37 °C for 48 h, supernatants were collected, filtered using 0.45 μm-pore size Millex HV PVDF filter units (Millipore) and concentrated by centrifugation at 20,000 x g. Viral pellets were then resuspended in PBS at 4 °C overnight. Resuspended virus was added to cells in the presence of 4 μg/mL polybrene for 4 h at 37 °C in an environment of 93% air and 7% CO_2. Cell lines used for stable RNAi targeting of AIF were infected with either control lentivirus (shLacZ) or lentivirus harboring an AIF target sequence (shAIF) followed by selection with 1 μg/mL puromycin. To establish "restoration" cell lines expressing either wild-type AIF or a catalytically impaired mutant, cells were infected with empty vector, AIF^{WT}, or AIF^{TVA} and then selected with 500 μg/mL hygromycin B.

Cell lysis, fractionation, immunoprecipitation, and immunoblot analysis

Cell lysates were prepared in radioimmune precipitation assay (RIPA) lysis buffer (PBS containing 1% NP-40, 0.5% sodium deoxycholate, 0.1% SDS, 1 mM dithiothreitol, 1 mM PMSF, 1 mM sodium fluoride, 1 mM sodium orthovanadate, and 1 protease inhibitor mixture tablet per 10 mL) or Laemmli buffer (62.5 mM tris-HCl pH 6.8, 2% SDS, 10% glycerol, and 5% β-mercaptoethanol).

For cell fractionation experiments, cytosolic and nuclear extracts were prepared by adding hypotonic buffer (20 mM HEPES pH 7.9, 10 mM KCl, 10 mM KCl, 1 mM EDTA, 10% glycerol, 1 mM dithiothreitol, 0.2% NP-40, 1 mM PMSF, and 1 protease inhibitor tablet per 10 mL) to cells with gentle vortexing. Supernatants (constituting the cytosolic fraction) were extracted, and nuclear extracts were then prepared by resuspending insoluble fractions in extraction buffer (hypotonic buffer containing 20% glycerol and 420 mM NaCl). Fractions were then analyzed by immunoblot as described below.

For immunoprecipitation experiments, RIPA cell lysates were normalized for protein content and then incubated with indicated antibodies for 2 h at 4 °C. Protein G-coupled agarose beads were then added and incubated for 1 h. Agarose beads were then recovered by centrifugation and washed in RIPA buffer. Precipitated protein was eluted by adding lithium dodecyl sulfate sample buffer followed by heating samples at 95 °C for 5 min. Samples were then analyzed by immunoblot as described below.

For immunoblot experiments, protein samples were separated by SDS-PAGE using 4-12% gradient SDS-polyacrylamide gels followed by electrotransfer to nitrocellulose membranes. Membranes were blocked with 5% milk or bovine serum albumin in tris-buffered saline containing 0.02 to 0.2% Tween-20 and then incubated with the indicated primary antibodies. Membranes were then washed three times and incubated with HRP-conjugated anti-mouse or anti-rabbit followed by visualization using enhanced chemiluminescence.

Replicate immunoblots were quantified at multiple exposures for linearity using myImage Analysis™ software (Thermo Scientific). Band intensities for phosphorylated proteins were divided by intensities for the corresponding total proteins; all protein values and phospho-

protein/total protein ratios were then normalized to β-actin values. To determine fold changes among lanes, all ratios were then normalized to control lanes.

Quantitative RT-PCR

Gene expression analysis was carried out as described [167] using the relative standard curve method for quantification. Briefly, real time PCR was carried out on the ABI Prism 7000 sequence detection system (Applied Biosystems, Foster City, CA). Total RNA was isolated from the indicated cell lines using TRIzol reagent according to the manufacturer's instructions. 30 μg of RNA isolated from each sample was treated with 30 units of DNase I (Promega) for 30 min at 37 °C. After DNase I digestion, RNA was purified using an RNeasy mini purification kit (Qiagen) following the manufacturer's protocol. An oligo (dT) primer was used in cDNA synthesis. 200 ng of RNA was reverse transcribed in a total volume of 50 μl using the TaqMan reverse transcription reagents kit (Applied Biosystems). To make a standard curve, serial dilutions of RNA from one sample (160, 40, 10, and 2.5 ng/μL final concentrations) were added to the RT reaction. Aliquots (3.5 μl) of cDNA were added to a 31.5-μl reaction mixture containing 17.5 μl of 2× SYBR® Green PCR Master Mix (Applied Biosystems) and 200–400 nm primers; quadruplicate samples were prepared for each RNA source. Absence of DNA contamination was verified by performing amplification from cDNA without reverse transcriptase. The primers for PCR were designed with IDT PrimerQuest software (Integrated DNA Technologies, Inc.). Sequences are shown in Table D1. Primers to either β-Actin or GAPDH were used in order to determine normalization factors between AIF proficient (shLacZ) and AIF deficient (shAIF) cell lines, and variation in β-actin/GAPH levels between cell lines was less than 10% in all cases.

Results

AIF promotes cellular ROS via its enzymatic activity

The known roles of AIF in the regulation of respiratory chain proteins and superoxide production suggest that AIF activity may control mitochondrial redox balance. Therefore we tested the effects of AIF ablation upon cellular ROS responses, focusing on PC3 and HeLa cells that exhibit different respiratory chain responses following knockdown [25, 51]. In order to assess the ability of AIF to regulate ROS levels and associated signaling pathways, we began by establishing PC3 and HeLa cells in which AIF expression is stably suppressed using a lentiviral RNAi approach described previously [51, 52]. Lentiviruses harboring either control sequences (shLacZ) or AIF targeting sequences (shAIF) were generated and then used to infect cells. Cells were then subjected a second round of lentiviral infection in order to generate AIF restoration cell lines stably expressing either an empty vector, wild type AIF (AIF^{WT}), or a catalytically inactive AIF mutant [51, 54] containing the substitutions T263A and V300A (AIF^{TVA}). Lentiviral cDNA constructs additionally harbored a silent mutation resistant to shRNA-mediated targeting of AIF [51].

Following derivation of cell lines (shLacZ + empty, shAIF + empty, shAIF+AIF^{WT}, shAIF+AIF^{TVA}), cellular ROS levels were compared following acute oxidative stress triggers using two chemical agents with differing mechanisms of action: menadione, a naphthoquinone derivative that potentiates redox cycling and is linked to AIF redox activity [168]; and antimycin A, an inhibitor of the ETC targeting complex III. Staining with MitoSOX™ Red (an indicator of mitochondrial superoxide levels) demonstrated that menadione induces a rapid increase of mitochondrial superoxide in both cell types that requires AIF to different extents. Suppression of AIF in HeLa cells did not substantially affect stimulation levels (data not shown), whereas in

PC3 cells AIF ablation almost entirely abolished superoxide production. Having observed significant changes in PC3 cells, we tested the effect of AIF enzymatic activity on superoxide production using our panel of AIF-restored PC3 cells. We observed that AIF^{WT}, but not AIF^{TVA} restored mitochondrial superoxide production following treatment (Figure 5.1A), demonstrating that the enzymatic activity of AIF is essential for the increase of mitochondrial superoxide in response to acute menadione exposure. To determine if altered mitochondrial ROS production was connected to the extramitochondrial redox state of cells, we then measured general cellular ROS by detection with chloromethyl-2',7'-dichlorodihydrofluorescein diacetate (CM-H_2DCFDA, a general detector of many ROS species not including superoxide) following antimycin A stimulation. The enzymatic activity of AIF was required for the production of intracellular ROS in HeLa cells (Figure 5.1B), whereas PC3 cells exhibited antimycin A-stimulated ROS that were independent of AIF (data not shown).

To determine if AIF-mediated ROS protection is related to sensitivity to the oxidative stress triggers examined, viability of PC3 and HeLa cells were then evaluated following overnight treatment (Figure 5.1C, D). Consistent with decreased ROS levels following AIF ablation, the loss of AIF decreased cell deaths levels when cells were treated with menadione and antimycin A. Taken together these data indicate that in both cell types the NADH-oxidase activity of AIF facilitates acute ROS generation in response to chemical redox agents, which can regulate sensitivity to oxidative stress.

AIF-mediated ROS activate antioxidant responses under basal and stimulated conditions

The above data indicate that AIF promotes acute ROS generation. We therefore hypothesized that AIF could also regulate basal ROS and low-dose/nonlethal ROS stimulation with downstream signaling effects. If AIF-dependent ROS can activate signal transduction

pathways, then differences in molecular signaling responses (such the antioxidant response) should be observed when AIF is suppressed. To test the role of AIF in control of such signaling pathways, we stimulated HeLa and PC3 cells with *tert*-butylhydroquinone (tBHQ) as an exogenous source of ROS to activate redox-sensitive pathways in a mitochondria-independent fashion.

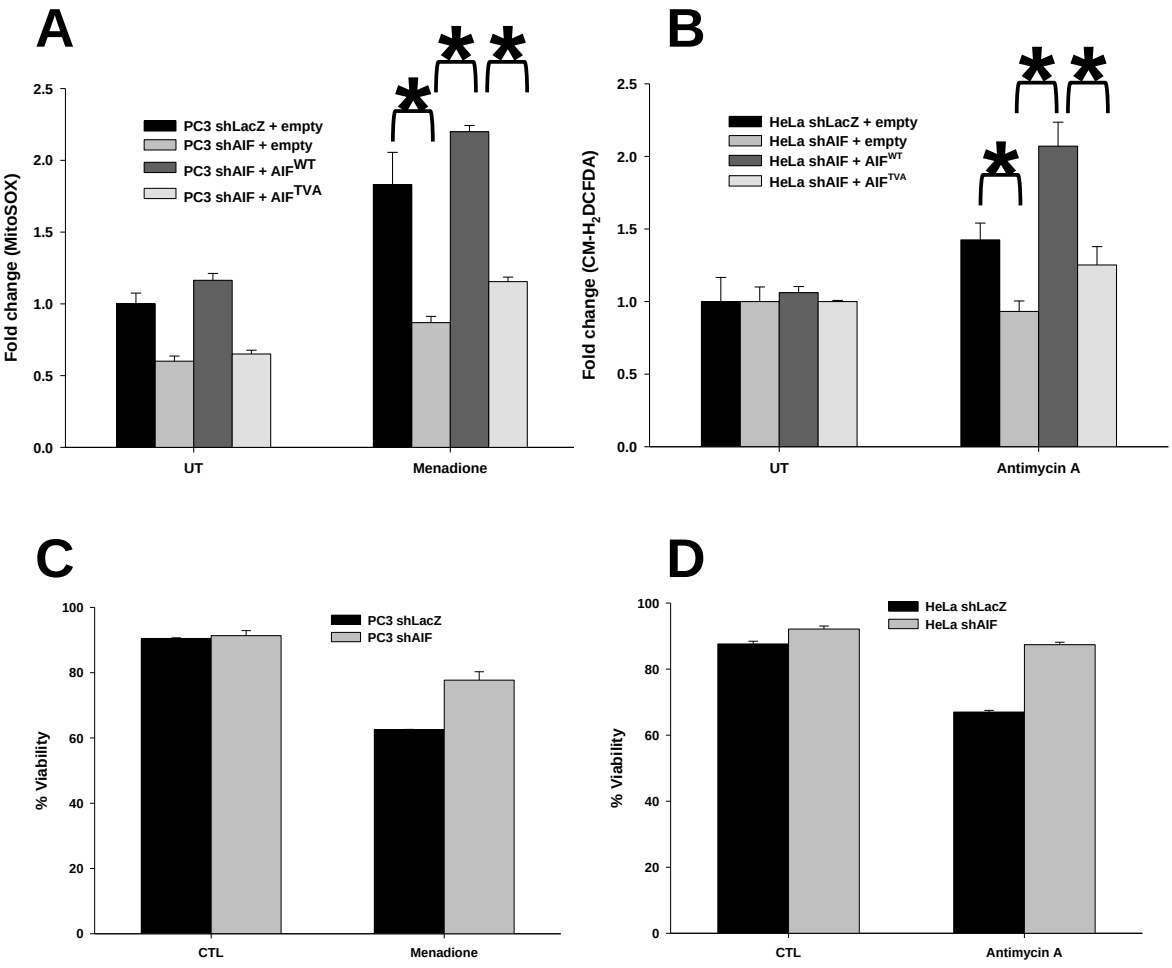

Figure 5.1. AIF enzymatic activity regulates cellular ROS.
A) Effect of AIF enzymatic activity on mitochondrial superoxide production: The indicated cell lines were left untreated (UT) or treated with menadione, stained with MitoSOX™ Red, and assessed by flow cytometry. B) Effect of AIF enzymatic activity on general cellular ROS production: Relative fluorescence intensity was measured by flow cytometry following antimycin A treatment and subsequent CM-H_2DCFDA staining. C-D) Viability levels of the indicated cell types treated with either menadione or antimycin A were determined by PI exclusion assay. Data are presented as average ± standard deviation. *$p<0.05$.

As a measure of cellular response to AIF redox function, activities of the antioxidant response (Nrf2 activity and antioxidant gene expression levels) were assessed. Under conditions of oxidative stress, the antioxidant transcription factor Nrf2 is stabilized from proteasomal degradation and accumulates in the nucleus [169]. Following treatment with tBHQ, nuclear accumulation of Nrf2 was dependent upon AIF in HeLa but not PC3 cells (Figure 5.2A, B), which may be related to varied AIF-dependent ROS levels observed above (Figure 5.1). To further interrogate altered nuclear Nrf2 in HeLa cells, cells were stimulated with tBHQ and/or treated with the proteasome inhibitor MG132, followed by immunoblot analysis of total cellular protein. AIF-deficient cells demonstrated decreased total Nrf2 levels under both basal and stimulated conditions. MG132 increased Nrf2 levels independently of tBHQ, but to a lesser extent in AIF-deficient cells (Figure 5.2C). Together these data suggest altered Nrf2 responses in HeLa cells result from decreased Nrf2 protein levels, increased Nrf2 degradation rate, or both.

To further characterize the role of AIF in control of cellular redox activity, we additionally assessed levels of Nrf-2 dependent antioxidant genes under basal conditions by RT-qPCR. In agreement with our measurements of ROS production, substantial changes in mRNA transcripts encoding a variety of antioxidant genes under basal conditions were observed in both cell types (Figure 5.3A, B). Almost all genes assessed under basal conditions decreased following AIF knockdown, whereas one gene increased and notably was different between cell types (GGT1 in HeLa cells, GSTM1 in PC3 cells). We further assessed levels of antioxidant transcripts following treatment with tBHQ. Following stimulation, either no change or decreased upregulation was observed in AIF-deficient cells; and hMOX1 is common for both cell lines as the most upregulated and most affected by AIF loss (Figure 5.3C, D).

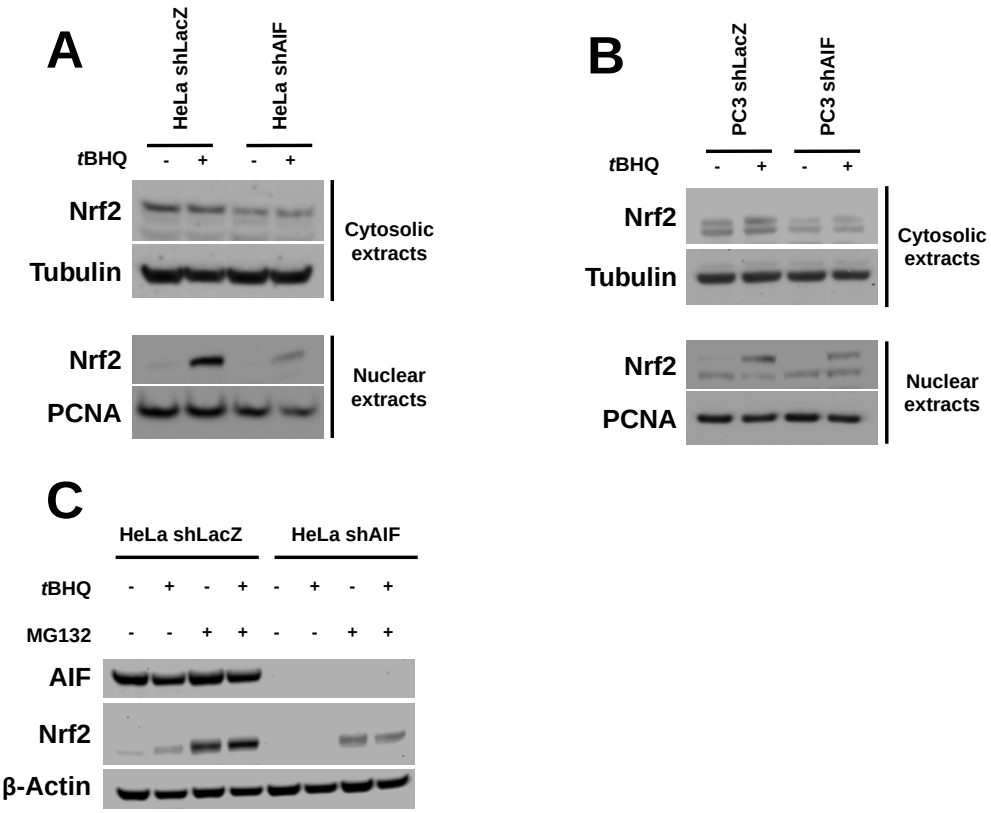

Figure 5.2. AIF-mediated redox signaling regulates Nrf2 levels and translocation.
A, B) Effect of AIF ablation on Nrf2 translocation: The indicated cell lines were treated with control solvent or tBHQ and then fractionated into cytosolic and nuclear extracts followed by immunoblot for Nrf2. Tubulin and PCNA were used as loading controls for cytosolic and nuclear extracts, respectively. C) Effect of AIF ablation on Nrf2 levels: Cells were treated with control solvent or tBHQ in the absence or presence of MG132, lysed, and subjected to immunoblot with the indicated antibodies.

Having observed notable differences in GGT1, GSTM1, and hMOX1 mRNA transcript levels that appear cell type-specific, protein levels were then assessed by immunoblot analysis (Figure 5.3E), which generally agreed with RT-qPCR data. In HeLa cells, tBHQ induced an increase in hMOX1 that was not substantially affected by AIF ablation, whereas GSTM1 was generally unaffected by either tBHQ or AIF levels. In contrast, levels of GGT1 increased dramatically following AIF ablation in HeLa cells relative to undetectable control levels, both in the absence and presence of tBHQ. Consistent with mRNA assessment, AIF-dependent antioxidant protein levels in PC3 cells differed from HeLa cells. Control PC3 cells upregulated

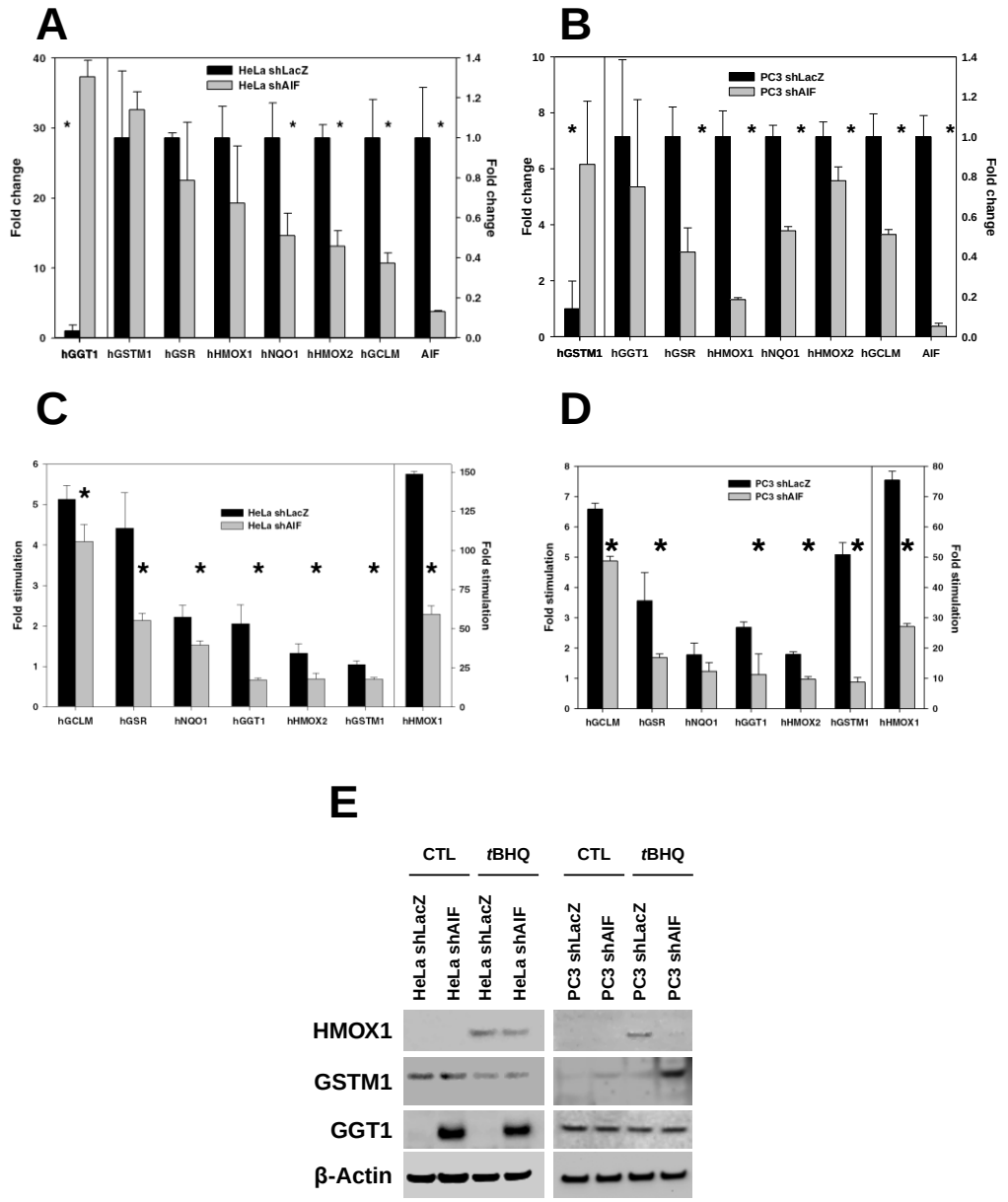

Figure 5.3. AIF levels control antioxidant responses.
A, B) Effect of AIF ablation on basal levels of antioxidant gene transcripts: Quantitative PCR (qPCR) was used to determine basal levels of antioxidant transcripts in the indicated cell lines. C, D) Effect of AIF ablation on tBHQ-stimulated levels of antioxidant transcripts: Fold stimulation of antioxidant transcripts in tBHQ-treated cells relative to vehicle-only controls were measured by qPCR. qPCR data were acquired by A.S. Wilkinson. E) Cells treated with control solvent or tBHQ were lysed and assessed for levels of the indicated proteins by immunoblot. Quantitative data are presented as average ± standard deviation. *$p<0.05$.

hMOX1 following tBHQ stimulation, but this upregulation was impaired following loss of AIF. GSTM1 levels increased under basal conditions following AIF knockdown, and increased further under tBHQ-induced conditions, while GGT1 did not show any changes with either tBHQ or AIF ablation. Further experimentation is required to account for mechanisms and differences between cell types, but data presented here show for the first time the ability of AIF to serve as a redox control protein that produces ROS in cells with observable downstream effects.

In an effort to determine if altered ROS production and redox signaling following AIF ablation affect sensitivity to oxidative stress, PC3- and HeLa-derived cell lines were then subjected to lethal concentrations of tBHQ and assessed for viability levels. PC3 and HeLa cells exhibited notably different sensitivities to tBHQ, which may in part explain different antioxidant responses when AIF is suppressed. In both cell types and consistent with the above viability data (Figure 5.1C, D), AIF ablation protected against tBHQ-induced cell death (Figure 5.4A, B), which may be due to decreased oxidative stress levels (Figure 5.1A, B). This indicates that AIF-mediated ROS elevation and/or altered antioxidant responses can impact sensitivity to oxidative stress following a variety of stimuli.

Suppression of AIF decreases MAPK phosphorylation

We then wondered if AIF-mediated ROS signaling impacts pro-tumor proliferative and survival pathways. We have shown previously that AIF promotes the growth and invasiveness of advanced-stage prostate [51] and pancreatic cancer cells [52]. PC3 cells, an androgen-independent prostate cancer line commonly used as a model for advanced prostate cancer [170], serve as a well-characterized system for studying AIF-dependent tumorigenic activity. AIF knockdown substantially reduces the aggressiveness of PC3 cells [51], but the mechanism(s) underlying AIF-dependent growth and survival are presently unclear.

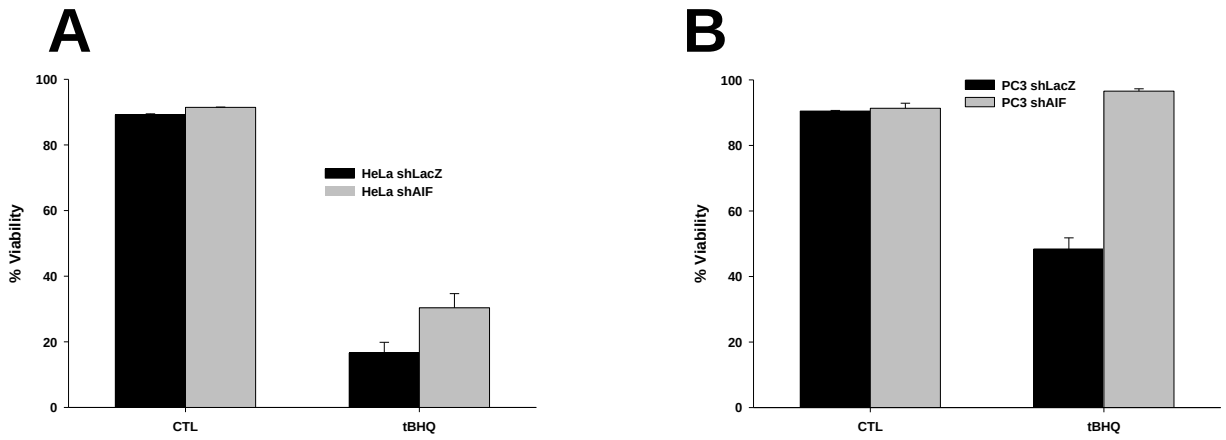

Figure 5.4. AIF knockdown decreases sensitivity to oxidative stress.
HeLa- (A) and PC3-derived (B) cell lines were treated with control vehicle or tBHQ and assessed for viability levels by PI staining and flow cytometry.

To determine if AIF plays a role in regulating intracellular signal transduction associated with this growth phenotype, we evaluated the activation status of MAPK signaling molecules following AIF ablation. Upon stimulation by a variety of signals including oxidative stress, MAP3Ks phosphorylate and activate MAP2Ks, which subsequently phosphorylate and activate MAPKs (Figure 5.5). MAPKs can additionally be activated when their endogenous inhibitors, the MAPK phosphatases (MKPs), are suppressed (Figure 5.5). This MAPK phospho-activation allows activity levels to be assessed by immunoblot. When AIF expression was suppressed, phosphorylation levels of three MAPKs (JNK, p38, ERK), as well as the JNK target c-Jun, were markedly reduced under basal conditions (Figure 5.6A, B). When upstream factors (MLK1, MKK4/SEK1) of the MAP2K and MAP3K families were assessed, neither protein levels nor phosphorylation were altered. We additionally evaluated protein levels of the endogenous MAPK inhibitor dual specificity phosphatase 4 (DUSP4). DUSP4 dephosphorylates JNK, p38, and ERK to suppress their activities, but is inactivated and degraded under conditions of oxidative stress [171]. Notably, DUSP4 protein levels increased two-fold following AIF ablation

(Figure 5.6A, B). This observation may be an indicator of decreased oxidative stress levels and a possible explanation for MAPK impairment when AIF expression is suppressed.

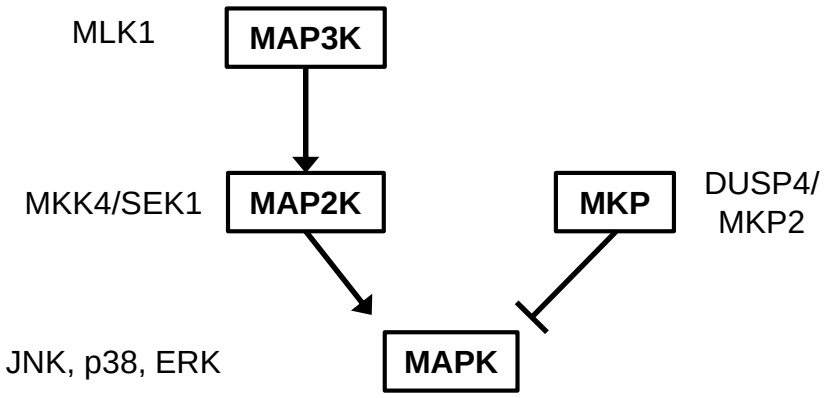

Figure 5.5. MAPK signal transduction.
MAP3Ks (*e.g.*, MLK1) phosphorylate and activate MAP2Ks (*e.g.*, MKK4/SEK1), which subsequently phosphorylate and activate MAPKs (JNK, p38, ERK). MAPK activity is suppressed by dephosphorylation mediated by MKPs (*e.g.*, DUSP4/MKP2).

We additionally tested the response of JNK and p38 to the chemical MAPK activator anisomycin [172] following AIF ablation. Anisomycin-stimulated phosphorylation of both JNK and p38 required AIF expression (Figure 5.6C), suggesting that AIF is required for MAPK activation both under basal and stimulated conditions. We further explored the AIF-dependent phosphorylation capacity of MAPKs by overexpressing apoptosis signal-regulating kinase 1 (ASK1), a redox-sensitive MAP3K that phosphorylates both JNK and p38 under conditions of oxidative stress [173] but that is activated in a ROS-independent manner when overexpressed [53]. HA-tagged ASK1 was transfected into PC3-derived cells followed by immunoblot for HA to verify overexpression (Figure 5.6D). When ASK1 was overexpressed, phosphorylation of JNK and p38 increased both in the presence and absence of AIF (Figure 5.6D). This strongly suggests that while AIF ablation impairs MAPK activation, the intrinsic activity of neither JNK nor p38 is inherently compromised.

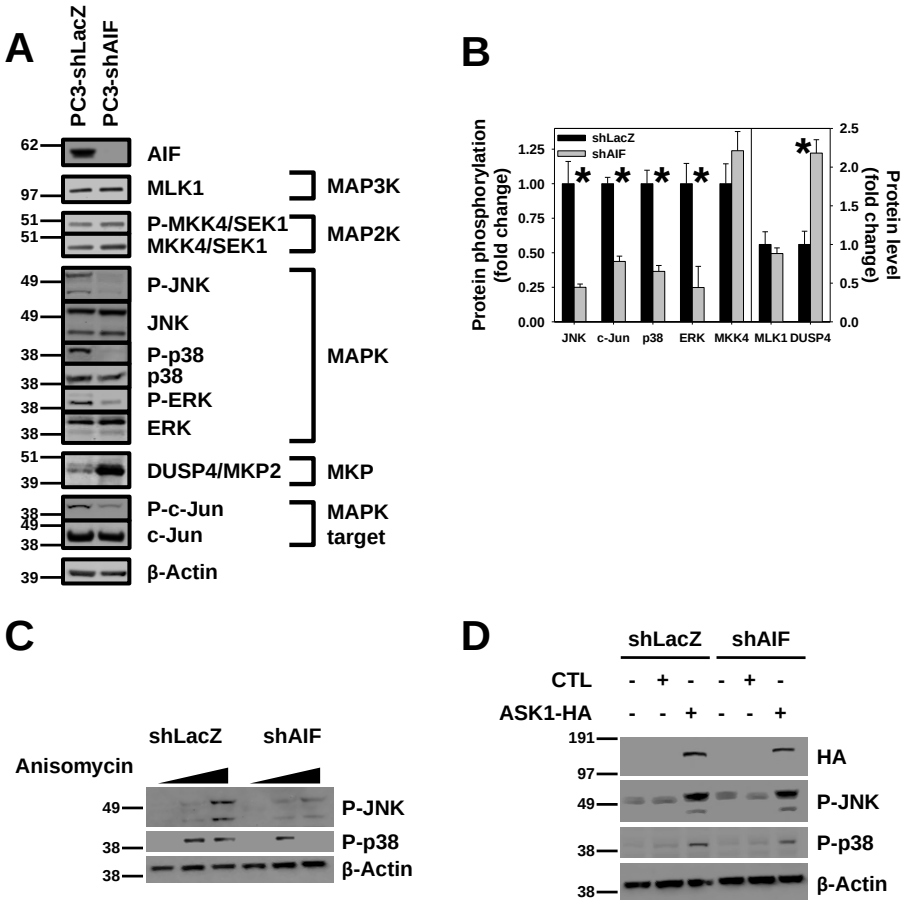

Figure 5.6. AIF knockdown impairs MAPK signaling.
A) PC3-derived cells were seeded at equal densities and then subjected to immunoblot using the indicated antibodies. (B) Replicate immunoblots from *panel a* were quantified and normalized to β-actin. Phosphoprotein quantities were normalized both to their corresponding total protein quantities and β-actin. Data are presented as average ± standard deviation. *$p<0.05$. C) Cells treated with increasing concentrations of anisomycin for assessed for the indicated proteins by immunoblot. D) PC3-derived cells were transfected with either empty control (CTL) or ASK1-HA encoding plasmids and then assessed by immunoblot using the indicated antibodies.

Redox-dependent JNK phosphorylation requires AIF

Based upon its ROS-generating enzymatic activity [60] and having observed that AIF influences multiple levels of MAPK signaling pathways, we then questioned whether AIF influences signal transduction under conditions of redox stimulation, concentrating our efforts on the JNK pathway. We therefore assessed the effects of AIF ablation on oxidative stress-induced

activation of JNK in a broad panel of cell types derived from both normal and cancerous tissues: PC3 (prostate cancer), HPAC (pancreatic cancer), MRC-5 (normal lung), HCT 116 (colorectal cancer), and MIA PaCa-2 (pancreatic cancer). Following acute, nonlethal redox stimulation with increasing concentrations of *tert*-butylhydroquinone (tBHQ), we assessed levels of phosphorylated JNK. While the exact patterns of JNK phosphorylation with respect to oxidative stress sensitivity varied among cell lines, AIF was required for this oxidant-induced phosphorylation in all cells tested (Figure 5.7).

AIF-dependent changes in JNK phosphorylation were observed under basal conditions, under oxidative stress conditions, or both. Cell lines exhibited variable JNK sensitivity to tBHQ, with some cells readily phosphorylating JNK at low doses and others requiring substantially higher tBHQ concentrations. PC3, HPAC, and HCT 116 cells exhibited modest basal phospho-JNK levels that further increased with treatment; when AIF was suppressed cells were unable to phosphorylate JNK following tBHQ stimulation. Conversely, in MIA PaCa-2 and MRC-5 cells JNK was relatively insensitive to the treatment conditions used yet showed AIF-dependent changes at the highest levels of tBHQ tested (Figure 5.7). However, despite cell type-specific differences in basal phospho-JNK levels and pre-existing differences in sensitivity to tBHQ, AIF was critical for all cell types to phosphorylate JNK. This suggests the ability of AIF to regulate JNK phosphorylation is widespread among cell types.

To determine if altered phosphorylation was involved with subcellular redistribution of JNK, we subjected PC3-derived cells to acute tBHQ treatment and then separated cells into cytosolic and nuclear extracts. Total levels of JNK1 and JNK2 were unchanged in both cytosolic and nuclear fractions, but within both fractions levels of phospho-JNK were decreased in AIF-

deficient cells (Figure 5.8). This suggests that AIF ablation does not affect distribution of total JNK, but that altered JNK phosphorylation occurs in both the cytosol and nucleus.

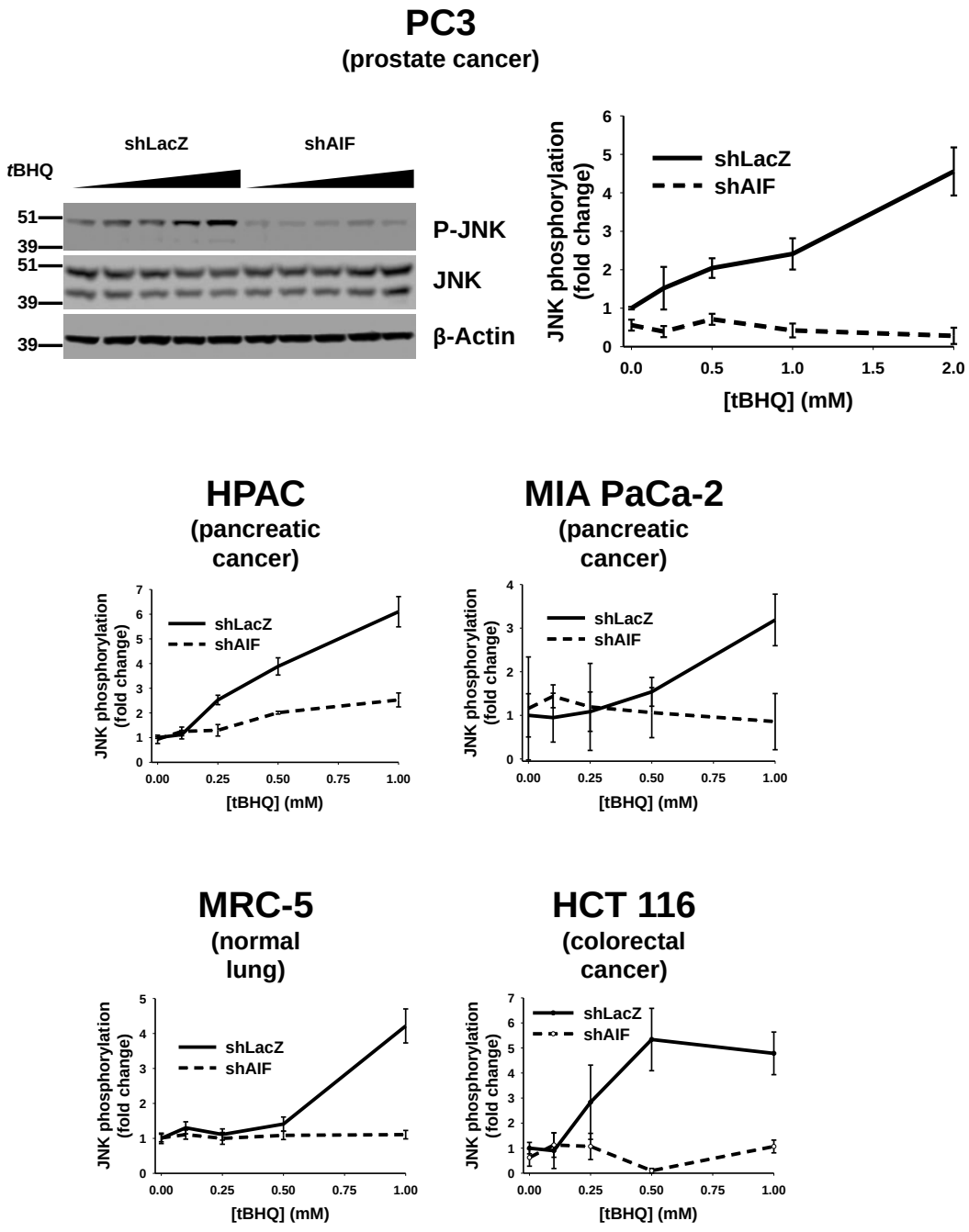

Figure 5.7. AIF is required for oxidative stress-induced JNK phosphorylation.
AIF proficient (shLacZ, shGFP) and deficient (shAIF) cells derived from the indicated cell lines were treated with increasing concentrations of tBHQ as follows: 0, 0.2, 0.5, 1, 2 mM (PC3); 0, 0.1, 0.25, 0.5, 1 mM (HCT 116, HPAC, MIA PaCa-2, MRC-5). Following treatment immunoblots were performed with the indicated antibodies and quantified by densitometry.

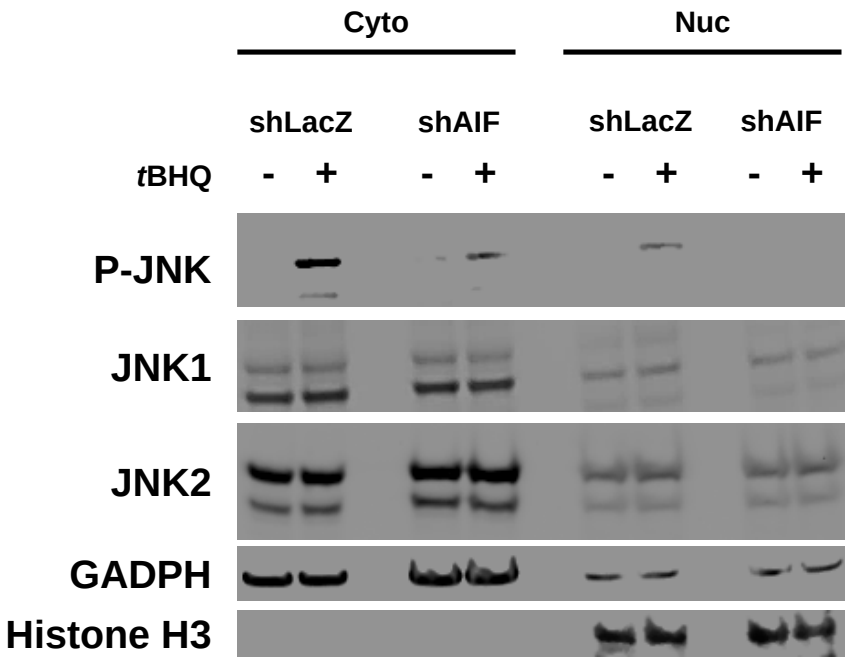

Figure 5.8. AIF promotes cytosolic and nuclear JNK phosphorylation without influencing JNK redistribution.
PC3-derived cells treated with either 0 or 2 mM tBHQ were separated into cytosolic and nuclear fractions followed by immunoblot for phospho-JNK, JNK1, and JNK2. GADPH and histone H3 were used as cytosolic and nuclear markers, respectively.

AIF enzymatic activity promotes the activation of JNK1

Since the enzymatic activity generates ROS *in vitro* [60] and elevates cellular ROS levels (Figure 5.1A, B), we then questioned whether this enzymatic activity is responsible for oxidative stress-induced JNK phosphorylation (Figure 5.7). Therefore PC3-, HPAC-, and RWPE-1-shAIF cells stably infected with either empty-hygro lentivirus, AIF^{WT}, and AIF^{TVA} were treated with tBHQ and then assessed for JNK phosphorylation by immunoblot. As shown in Figure 5.9A, restoration of AIF-deficient PC3 cells with AIF^{WT}, but not AIF^{TVA}, increased phospho-JNK levels in all cell types following tBHQ stimulation and demonstrated that the enzymatic activity of AIF is required for oxidant-induced JNK phosphorylation.

JNK proteins are encoded by three separate genes (JNK1, JNK2, JNK3) that give rise to one of ten different isoforms, and alternative splicing of the carboxyl terminus results in their long (54 kD) and short (46 kD) molecular weight variants for all three JNK species. JNK1 and JNK2 are ubiquitously expressed, whereas JNK3 is expressed primarily in the brain and to a lesser extent in the heart and testis [174]. To determine which JNK isoform responds to AIF activity, we first employed constitutively active forms of JNK (CA-JNK) fused with the JNK activator MKK7 that have been characterized previously [166]. Under basal conditions the introduction of CA-JNK1 and CA-JNK2 enhanced proliferation, and AIF was required for CA-JNK1 to drive cell growth (Figure 5.9B, left). Immunoblot for Flag epitope confirmed comparable transfection efficiency within cell lines (Figure 5.9B, right). To determine which endogenous JNK isoform is under AIF control, we then used an isoform non-specific antibody to precipitate total phosphorylated JNK from tBHQ-treated cells followed by isoform specific immunoblotting for JNK1 and JNK2. Only JNK1 was phosphorylated in response to acute oxidant stimulation, suggesting JNK1 is the target of tBHQ. Additionally, this phosphorylation event was AIF-dependent (Figure 5.9C), demonstrating that AIF is required for the activity of JNK1 but not JNK2.

Discussion

AIF regulates cellular ROS levels

The NADH-oxidase activity of AIF has been studied *in vitro* [60], but the biochemical consequences of AIF-mediated superoxide production within cells and the contribution of AIF ROS signaling to disease have remained largely descriptive. Experiments described here show that elevation of ROS by AIF is required for cellular redox signaling, and it is conceptually

satisfying that this activity controls signaling pathways well known for both pro- and anti-apoptotic downstream effects.

Data presented in this study show decreased ROS levels following loss of AIF, consistent with altered antioxidant responses that are largely decreased in a manner that depends on cell type and context. It is notable that AIF ablation moderately protected cells from the oxidative stress agents menadione, antimycin A, and tBHQ. While this indicates a pro-death function for AIF, cell death is likely due to toxic ROS levels, rather than AIF nuclear translocation. Indeed, AIF has been shown to trigger cell death under lethal oxidative stress conditions induced by menadione without translocating to the nucleus [168], which is in agreement with our findings.

Impact of AIF-mediated ROS in cancer

A large body of data demonstrating AIF upregulation in tumors [51, 52, 83-88, 175] suggest a possible role for AIF-mediated redox signaling in the context of cancer. One possibility is that within normal cells AIF functions as a ROS sensor that mediates responses to oxidative stress, and can be harnessed by cancer cells to promote tumorigenesis. In addition to AIF-mediated metabolic control, the ability of AIF to regulate cellular redox signaling provides further insight into overexpression levels. For example this may explain why AIF elevation in cancer rarely exceeds 2-fold compared to normal cells [51, 52]. Rather than AIF nuclear death activity it may instead be AIF ROS amplification, uncoupled from the "classic" death mechanism, which must be held in check by tumors.

Effects of AIF redox activity upon MAPK signaling

In addition to promoting oxidative stress and the antioxidant response, AIF-mediated redox signaling induces MAPK phosphorylation. It is notable that MAPKs can both promote and inhibit cell death, depending on phosphorylation levels and context [80]. Under oxidative stress

conditions, JNK1 is phosphorylated in an AIF-dependent manner in a variety of cell types. In PC3 cells, overexpression of CA-JNK1 promotes proliferation that requires AIF, suggesting that JNK1 serves as a pro-tumor molecule under AIF control. Based on the wide range of cellular activities regulated by JNK and other MAPKs, it is tempting to speculate a variety of phenotypes that result from AIF-dependent signal transduction. For example, increased invasiveness due to elevated AIF levels observed in advanced prostate cancer cells [51] could be due to JNK-induced changes in metastatic genes (explored in chapter 7).

Summary

Collectively the data here form a mechanistic starting point for AIF-mediated regulation of growth and survival [51, 52, 54], suggesting that through its catalytic function AIF primes MAPK activity by moderating cell redox state. It is likely that the biological consequences of AIF-induced signaling are diverse and dependent upon intracellular contexts [51, 52]. Oncogene status, cellular metabolic activity, and levels of oxidative stress proteins (*e.g.*, superoxide dismutase) and MAPK regulators are potential factors in the variability of AIF-mediated redox signaling. While a number of outcomes for AIF-mediated ROS production can be envisioned, experiments here demonstrate for the first time that AIF serves as an essential signal transduction protein.

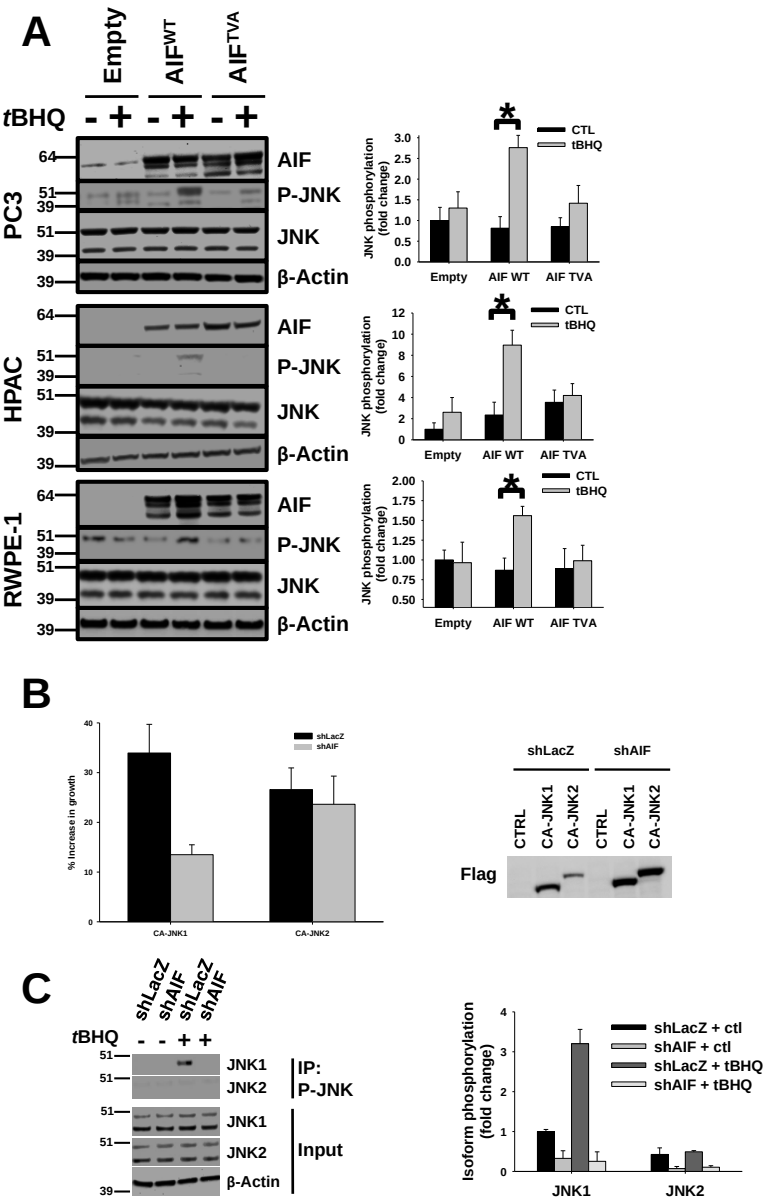

Figure 5.9. The enzymatic activity of AIF promotes JNK1 phosphorylation and activity. A) AIF-deficient PC3, HPAC, and RWPE-1 cells (shAIF) restored with either empty vector, AIF^{WT}, or AIF^{TVA} were treated with tBHQ as follows: 0 or 2 mM (PC3), 0 or 0.25 mM (HPAC), or 0.5 mM (RWPE-1); treatment was followed by immunoblot for phosphorylated JNK. Replicate immunoblots were quantified and normalized to total JNK and β-actin. B) PC3-shLacZ or shAIF cells were transfected with either control plasmid or plasmids expressing either CA-JNK1 or CA-JNK2. 48 h post-transfection totals cells were determined by Coulter^{TM} counting. Change in growth relative to empty control plasmid is shown. Protein expression was verified by immunoblot for Flag epitope. C) Total phosphorylated JNK was enriched from PC3-derived cells treated with 0 or 2 mM tBHQ by immunoprecipitation using an isoform non-specific P-JNK antibody, and precipitated material was analyzed by immunoblot for JNK1 and JNK2. Phospho-JNK was quantified by normalizing precipitated material to JNK1 or JNK2 and β-actin of input samples. Data are presented as average ± standard deviation. *$p<0.05$.

VI. AIF SIGNALS JNK1 TO INDUCE THE CADHERIN SWITCH, A KEY METASTATIC EVENT THAT IS LETHAL IN THE ABSENCE OF AIF-MEDIATED METABOLIC CONTROL

Abstract

AIF is a mitochondrial regulator of cellular homeostasis that controls both metabolic state and oxidative stress levels. Through the ROS-generating enzymatic activity of AIF, cells can activate signaling proteins and regulate the expression of nuclear genes. Therefore we sought to define AIF-mediated signaling pathways and their impact upon cell phenotype. Here we show that AIF regulates the expression of a variety of genes associated with the epithelial-mesenchymal transition (EMT) through JNK-dependent and independent mechanisms. Strikingly, by activating JNK1, AIF promotes the cadherin switch, an important metastatic event in cancer cells in which E-cadherin levels are reduced and N-cadherin levels increase. Inducing the cadherin switch causes AIF-deficient cells to undergo apoptosis, and this cell death corresponds to changes in glucose consumption and phosphorylation of the metabolic signaling molecule known as AMPK. Collectively, these data suggest that AIF loss-induced apoptosis occurs due to a metabolic imbalance with cancer cell aggressiveness. Therefore these observations highlight the ability of AIF to promote tumorigenesis by driving metastatic progression while simultaneously supplying its heavy energetic demand.

Introduction

AIF is an essential mitochondrial regulator of both cellular metabolic and redox conditions [73]. In addition to its involvement in cell death and critical role in maintaining mitochondrial ETC components, AIF additionally possesses an intrinsic enzymatic activity [60] that increases cellular ROS levels. These AIF-induced ROS control both antioxidant responses

and MAPK phosphorylation (Chapter 5). However, the downstream effects of AIF-dependent signaling, their impact upon tumorigenesis, and their balance with AIF-mediated metabolism remain unknown.

A variety of cellular effects for signaling by AIF can be envisioned. A potential downstream process of particular significance to tumorigenesis is the epithelial-mesenchymal transition (EMT), which can be influenced by ROS levels, mitochondrial signaling, metabolic conditions, and MAPK activation [176, 177]. These stimuli are not the only factors contributing to the series of biochemical changes involved but are shared with AIF and point to a possible role for AIF in the process of EMT.

During an EMT, a polarized epithelial cell undergoes extensive biochemical alterations in order to acquire a mesenchymal phenotype. The basement membrane interacting with the cell is then degraded, while the mesenchymal cell migrates away from the epithelial layer. EMTs serve to segregate cells, occurring in a variety of physiological events including embryonic implantation and formation, organ development, wound healing, tissue regeneration, and organ fibrosis. Cancer cells can additionally employ the EMT machinery to acquire an invasive and metastatic phenotype. This cancer-associated EMT is capable of promoting metastasis, migration, chemoresistance, metabolic alterations, immune evasion, and tumor cell interactions [177, 178]. Therefore the EMT represents a pivotal tumorigenic event capable of substantially increasing patient mortality.

EMTs are induced by a variety of stimuli including growth factors, cytokines, extracellular matrix conditions, and ROS. The sequence of cellular events occurring upon these cues involves dissociation of cell junctions, loss of polarity, cytoskeletal reorganization, upregulation of matrix metalloproteinases (MMPs), basement membrane degradation and

subsequent invasion. These events require a large-scale change in gene expression, with some of the central molecular players involved including β-catenin, Snail, Slug, Twist, Vimentin, Zeb1, E-cadherin, and N-cadherin. While the signaling and genetic events associated with EMT are complex, a key event of this process is the cadherin switch. During the cadherin switch, cells decrease expression of the tumor suppressor E-cadherin and increase levels of the mesenchymal marker known as N-cadherin, representing an important transition point at which cells gain further aggressiveness. This phenotype associated with the cadherin switch is due to inappropriate protein interactions with intra- and extracellular signaling molecules and altered communication with neighboring cells [176-178].

Here we show that AIF ablation alters EMT-associated genes both at the RNA and protein levels. Notably, the cadherin switch reverses when AIF is suppressed, due to impaired JNK1 signaling. Reversal of E-cadherin levels in AIF-deficient cells induces apoptosis, which may be due to a failure to metabolically adapt to E-cadherin ablation. Interestingly, the pattern of death observed corresponds to changes in phosphorylation of AMP-activated protein kinase (AMPK), a central regulator of metabolic signaling. Therefore this study links AIF to a variety of novel signaling molecules involved in both EMT and metabolism, further expanding the breadth of cellular activities mediated by AIF.

Materials and methods

Materials, plasmids and antibodies

DMEM, RPMI 1640, GlutaMAX, horse serum, trypsin, 4–12 % bis-tris polyacrylamide gels, nitrocellulose membranes, fetal bovine serum (FBS), phosphate buffered saline (PBS), and Pierce ECL 2 Western Blotting Substrate were from Thermo Fisher Scientific; Matrigel™ was from BD Biosciences; Matrigel recovery solution was from Corning; protease inhibitor tablets

were from Roche Applied Science; bVAD-fmk was from Enzyme Systems Products; all other materials were from Sigma.

Lentiviral plasmids FG12-shLacZ-GFP, FG12-shAIF-GFP, FG12-shLacZ-puro, and FG12-shAIF-puro were described previously [51, 52, 121, 147]. Lentiviral packaging plasmids pHCMV-G, pRRE, and pRSV-rev are as described [123]. Additional constructs pcDNA3-Flag-MKK7β2-JNK1α1 and pcDNA3-Flag-MKK7β2-JNK2α2 [166] were provided by Dr. Roger Davis (Addgene plasmids #19726 and 19727). Lentiviral pLKO plasmids were obtained as follows: psPAX2 and pMD2.G-vsv-G from Dr. Didier Trono (Addgene plasmids #12260 and 12259); pLKO.1-puro-scramble [149] from Dr. David Sabatini (Addgene plasmid #1864); and pLKO.1-puro-shE-cadherin [179] from Dr. Robert Weinberg (Addgene plasmid #18801); pLKO.1-puro-shJNK1 (DTRCN0000010580) and pLKO.1-puro-shJNK2 (TRCN0000000945) were from Dharmacon. All shRNA sequences have been rigorously assessed for off-target effects and used as described previously [51, 52, 121, 122, 179-183].

Antibodies were obtained as follows: anti-AIF (Santa Cruz, sc-13116), anti-β-actin (Sigma, A5316), anti-phospho-JNK T183/Y185 (Cell Signaling, 4668), anti-JNK (Cell Signaling, 9252), anti-JNK1 (Cell Signaling, 3708), anti-JNK2 (Cell Signaling, 9258), anti-phospho-c-Jun S73 (3270), anti-E-cadherin (Cell Signaling, 4065), anti-N-cadherin (Cell Signaling, 4061), anti-β-Catenin (Cell Signaling, 8480), anti-Vimentin (Cell Signaling, 5741), anti-Claudin-1 (Cell Signaling, 13255), anti-Snail (Cell Signaling, 3879), anti-Slug (Cell Signaling, 9585), anti-Zeb1 (Cell Signaling, 3396), anti-Zeb2 (Santa Cruz, sc-271984), anti-ZO-1 (Cell Signaling, 8193), anti-AMPKα (Cell Signaling, 4186), anti-phospho-AMPKα T172 (Cell Signaling, 2535), anti-AMPKα/β (Cell Signaling, 4150), anti-phospho-AMPKβ1 S182 (Cell Signaling, 4186), anti-ETS-1 (Santa Cruz, sc-350), horseradish peroxidase (HRP)-conjugated

anti-Flag (Sigma, A8592), HRP-conjugated anti-mouse IgG (Amersham Biosciences, NA391B), and HRP-conjugated anti-rabbit IgG (Amersham Biosciences, NA934B).

Cell culture

Cells were cultured in an atmosphere of 95% air and 5% CO_2 at 37 °C. All media formulations were supplemented with 2 mM GlutaMAX. HEK293T and MRC-5 cells were cultured in DMEM supplemented with 10% FBS; PC3, and LNCaP cells in RPMI 1640 medium supplemented with 10% FBS; and MIA PaCa-2 cells in DMEM supplemented with 10% FBS and 2.5% horse serum. Cells were harvested by trypsinization, washed in PBS, and seeded at equal densities and then allowed to attach overnight prior to all assays.

Transfections

Plasmids were transfected into cells using Lipofectamine™ 2000 as described by the manufacturer. Cells were then harvested 48-72 h following transfection and assessed as indicated.

Drug treatments

Cells were treated with SP600125 at 0-40 μM for 72 h, or bVAD-fmk at 50 μM at time of seeding and then every 48 h for 7 days. Following treatment cells were harvested and assessed in assays as described below.

Lentiviral production and stable infection of cell lines

To establish cell lines stably suppressing or overexpressing AIF, lentiviral particles were produced by transfecting equal amounts of pHCMV-G, pRRE, pRSV-rev, and FG12- or pSL4-derived plasmids into HEK293T cells using the calcium phosphate method [124]. Following incubation at 37 °C for 48 h, supernatants were collected, filtered using 0.45 μm-pore size Millex HV PVDF filter units (Millipore) and concentrated by centrifugation at 20,000 x g. Viral pellets

were then resuspended in PBS at 4 °C overnight. Resuspended virus was added to cells in the presence of 4 μg/mL polybrene for 4 h at 37 °C in an environment of 93% air and 7% CO_2. Cell lines used for stable RNAi targeting of AIF were infected with either control lentivirus or lentivirus harboring an AIF target sequence as follows: shLacZ-puro or shAIF-puro (PC3, MRC-5) followed by selection with 1 μg/mL puromycin, shLacZ-GFP or shAIF-GFP (LNCaP, MIA PaCa-2). LNCaP-derived cells were established as described previously [51].

For establishment of cell lines stably suppressing JNK1, JNK2, or E-cadherin, pLKO.1-based lentiviruses were generated by transfecting HEK293T cells with pMD.2, psPAX2, and pLKO-shRNA using the calcium phosphate method. Viral supernatant was collected at 48 h and 72 h post-transfection and then filtered using 0.45 μm-pore size Millex HV PVDF filter units. Target cells were then incubated with viral supernatant and 8 μg/mL polybrene for 24 h. Stably infected cells were selected using 1 μg/mL puromycin.

Cell lysis, SDS-PAGE and immunoblot analysis

Cell lysates were prepared in radioimmune precipitation assay (RIPA) lysis buffer (PBS containing 1% NP-40, 0.5% sodium deoxycholate, 0.1% SDS, 1 mM dithiothreitol, 1 mM PMSF, 1 mM sodium fluoride, 1 mM sodium orthovanadate, and 1 protease inhibitor mixture tablet per 10 mL) or Laemmli buffer (62.5 mM tris-HCl pH 6.8, 2% SDS, 10% glycerol, and 5% β-mercaptoethanol). Protein samples were separated by SDS-PAGE using 4-12% gradient SDS-polyacrylamide gels followed by electrotransfer to nitrocellulose membranes. Membranes were blocked with 5% milk or bovine serum albumin in tris-buffered saline containing 0.02 to 0.2% Tween-20 and then incubated with the indicated primary antibodies. Membranes were then washed three times and incubated with HRP-conjugated anti-mouse or anti-rabbit followed by visualization using enhanced chemiluminescence.

Replicate immunoblots were quantified at multiple exposures for linearity using myImage Analysis™ software (Thermo Scientific). Band intensities for phosphorylated proteins were divided by intensities for the corresponding total proteins; all protein values and phospho-protein/total protein ratios were then normalized to β-actin values. To determine fold changes among lanes, all ratios were then normalized to control lanes (leftmost lanes).

Quantitative RT-PCR

Gene expression analysis was carried out as described [167] using the relative standard curve method for quantification. Briefly, real time PCR was carried out on the ABI Prism 7000 sequence detection system (Applied Biosystems, Foster City, CA). Total RNA was isolated from the indicated cell lines using TRIzol reagent according to the manufacturer's instructions. 30 μg of RNA isolated from each sample was treated with 30 units of DNase I (Promega) for 30 min at 37 °C. After DNase I digestion, RNA was purified using an RNeasy mini purification kit (Qiagen) following the manufacturer's protocol. An oligo (dT) primer was used in cDNA synthesis. 200 ng of RNA was reverse transcribed in a total volume of 50 μl using the TaqMan reverse transcription reagents kit (Applied Biosystems). To make a standard curve, serial dilutions of RNA from one sample (160, 40, 10, and 2.5 ng/μL final concentrations) were added to the RT reaction. Aliquots (3.5 μl) of cDNA were added to a 31.5-μl reaction mixture containing 17.5 μl of 2× SYBR® Green PCR Master Mix (Applied Biosystems) and 200–400 nm primers; quadruplicate samples were prepared for each RNA source. Absence of DNA contamination was verified by performing amplification from cDNA without reverse transcriptase. The primers for PCR were designed with IDT PrimerQuest software (Integrated DNA Technologies, Inc.). Primer sequences are shown in Table D1. Primers to either β-Actin or GAPDH were used in order to determine normalization factors between AIF proficient (shLacZ)

and AIF deficient (shAIF) cell lines, and variation in β-actin/GAPH levels between cell lines was less than 10% in all cases.

Phase contrast microscopy

Images were captured by phase contrast microscopy using the 10× objective of a Nikon TS100F microscope equipped with a Nikon DS-Fi1 digital camera detection system and NIS Elements 4.0 software.

Matrigel™ experiments

Equal volumes of cold Matrigel™ were added to each well in 24-well plates and then allowed to solidify at 37 °C for 1 h. Cells were added to Matrigel™ layers at equal densities and exposed to substrate conditions for 3-7 days in the absence or presence of bVAD-fmk. Detached cells were collected and quantified by Coulter™ counting; attached cells were extracted from substrate using Matrigel recovery solution (Corning) and either lysed as described above or quantified by Coulter™ counting. Percent death was defined as the number of detached cells divided by total cells.

Results

AIF promotes the cadherin switch

Through control of redox signaling, AIF is capable of inducing the phosphorylation of JNK. As a central signaling hub at the convergence of cellular programs regulating death, survival, proliferation, and differentiation [184], JNK contributes to a variety of tumorigenic processes when phosphorylated. An important cellular activity influenced by JNK in cancer is the epithelial-mesenchymal transition (EMT) [176], a large-scale series of gene expression changes that increase the metastatic proclivity of cells. A key event of EMT is the cadherin switch, whereby cells reduce expression of the tumor suppressor E-cadherin and elevate N-

cadherin to invade distal tissues [185]. To determine if AIF and JNK are involved with control of EMT, we assessed expression levels of EMT-associated genes in AIF deficient PC3 cells via RT-PCR. AIF ablation did not globally alter EMT transcripts, but we observed a striking elevation in E-cadherin mRNA (25-fold increase, Figure 6.1A) that was confirmed at the protein level by immunoblot in PC3 and MRC-5 cells (Figure 6.1). To further determine the role of AIF in the cadherin switch, we probed lysates for N-cadherin and observed decreased levels following AIF ablation in both cell types (Figure 6.1B). The effects of AIF upon the cadherin switch were also examined in LNCaP and MIA PaCa-2 cells (Figure 6.1B). As a cell line derived from a less aggressive (androgen sensitive) prostate cancer [186], LNCaP cells do not exhibit a cadherin switch, expressing high levels of E-cadherin and low N-cadherin. Since pre-existing cadherin levels in LNCaP cells are similar to those associated with AIF ablation in PC3 and MRC-5 cells, cadherin levels expectedly did not change with AIF knockdown in LNCaP cells (Figure 6.1B). This is consistent with our previous observations that LNCaP cells are metabolically insensitive to the loss of AIF [51]. In contrast, MIA PaCa-2 cells displayed a cadherin profile similar to PC3 and MRC-5 cells but that was unaffected by suppression of AIF (Figure 6.1B). We previously demonstrated that MIA PaCa-2 cells do not rely on either their mitochondria or AIF to survive and grow [52], thus it was not surprising that cadherin levels were unaffected by AIF ablation in this cell type.

AIF ablation and JNK suppression converge to similar molecular phenotypes and reveal novel AIF signaling targets

To determine if JNK is responsible for the cadherin switch in PC3 cells, we suppressed JNK activity by two independent approaches: pharmacological inhibition or genetic knockdown. For chemical inhibition experiments, AIF proficient and deficient PC3 cells were treated with the

pan-JNK inhibitor SP600125 [187]. AIF deficient cells exhibit subtle differences in morphology when compared to controls that may represent a more epithelial phenotype [51]. Notably, exposure to SP600125 induced morphological changes in AIF proficient cells, including increased size and length, converging on the appearance of PC3-shAIF cells (Figure 6.2). JNK inhibition by SP600125 was confirmed by immunoblot for phospho-c-Jun (Figure 6.3A). c-Jun phosphorylation in AIF-deficient cells was expectedly reduced prior to treatment and further impaired by SP600125 to a greater extent than in AIF proficient cells; this corresponds to our observations that AIF is an upstream effector of JNK (Chapter 5).

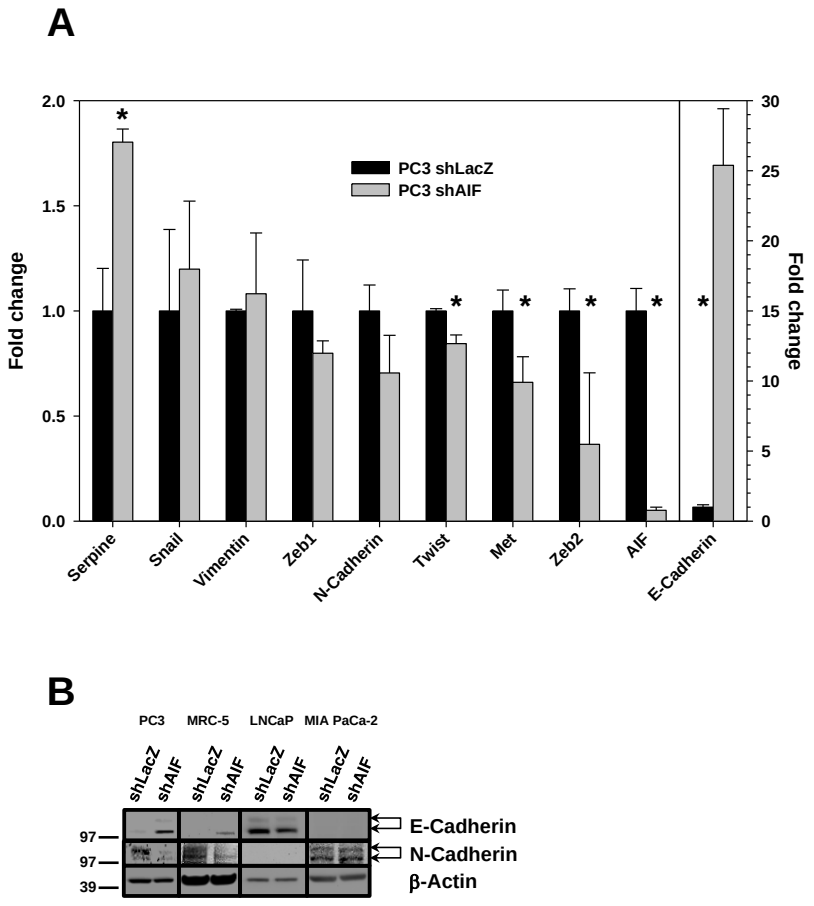

Figure 6.1. AIF promotes the cadherin switch.
A) Transcript levels of EMT-associated genes in PC3-derived cells were assessed by qPCR. Data acquired by A.S. Wilkinson. B) Protein levels of E-cadherin and N-cadherin in the indicated cell types were determined by immunoblot analysis. Data are presented as average ± standard deviation. *$p<0.05$.

To further characterize the observed changes in morphology at the molecular level, immunoblots were performed for 11 proteins linked to both morphological phenotype and EMT: E-cadherin, N-cadherin, β-catenin, vimentin, claudin-1, Snail, Slug, Zeb1, Zeb2, ZO-1, and ETS-1 (Figure 6.3A). Similar to the biochemical effects of AIF ablation, SP600125 increased E-cadherin and decreased N-cadherin protein to levels comparable to those associated with AIF deficiency, demonstrating their regulation by both AIF and JNK. Furthermore, our screen revealed 7 additional genetic targets of AIF-mediated mitonuclear signaling: vimentin, a cytoskeletal molecule expressed in mesenchymal cells that maintains cell shape and integrity [188]; Snail, Slug, Zeb1, Zeb2, and ZO-1, which are central transcriptional regulators of EMT [176]; and ETS-1, an EMT-associated factor linked to mitonuclear retrograde signaling that regulates invasion by controlling the expression of matrix metalloproteinases [150, 176].

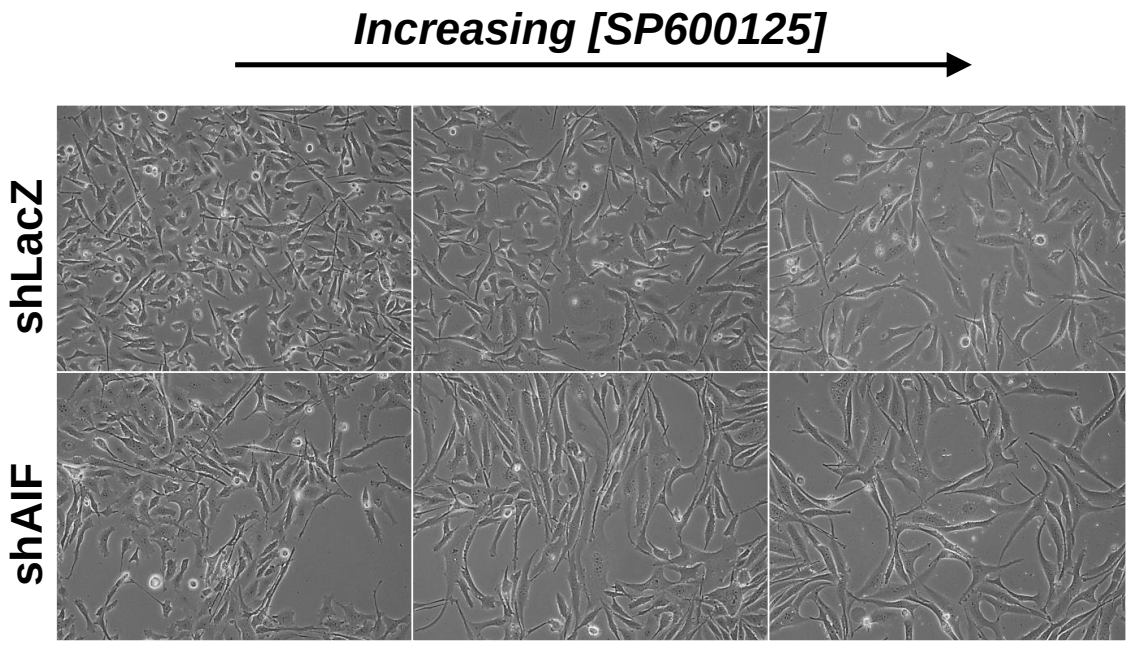

Figure 6.2. AIF ablation and JNK inhibition converge to similar cellular morphologies. PC3-derived cells were treated with 0, 10, and 40 μM SP600125 for 72 h and then imaged by phase contrast microscopy.

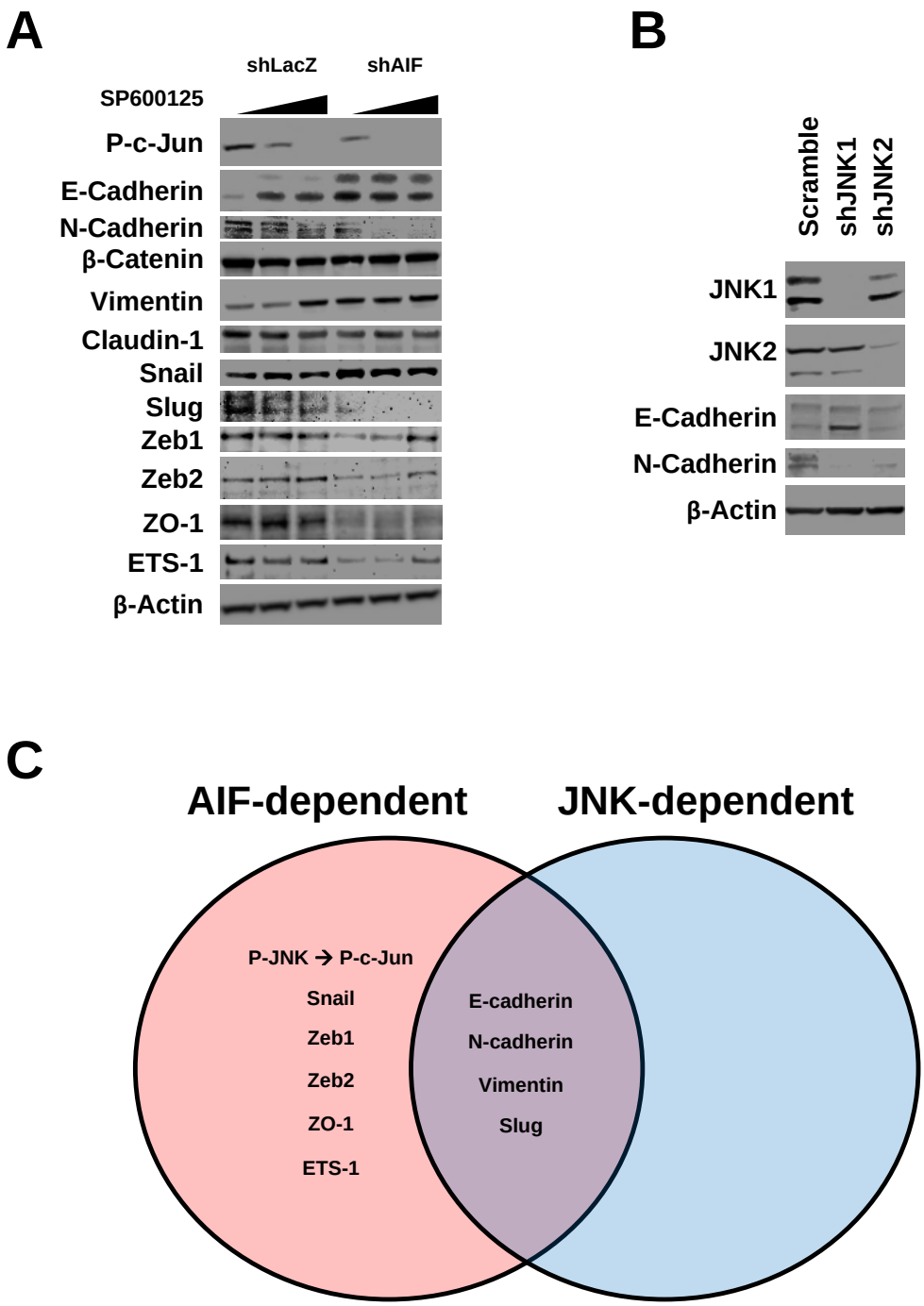

Figure 6.3. AIF ablation and JNK suppression converge to similar molecular phenotypes and reveal novel AIF signaling targets.
(A) PC3-derived cells were treated with 0, 10, and 40 μM SP600125 for 72 h, lysed and probed with the indicated antibodies by immunoblot analysis. B) Stable knockdown of JNK1 and JNK2 in PC3 cells and their effects on E-cadherin and N-cadherin were determined by immunoblot analysis. C) Venn diagram depicting the convergence of AIF-dependent and JNK-dependent signaling determined from panels A and B.

To further assess the involvement of JNK in the cadherin switch and to define isoform specificity, we next generated PC3 cells stably deficient in JNK1 or JNK2 by lentivirus-mediated shRNA induction (Figure 6.3B). In agreement with the effects of SP600125, we observed changes in E-cadherin and N-cadherin following JNK knockdown that were isoform specific. Knockdown of JNK2 decreased N-cadherin expression, while the loss of JNK1 phenocopied the previously observed effects of AIF ablation, triggering both an elevation in E-cadherin and a reduction in N-cadherin levels (Figure 6.3B).

Taken together, these data suggest that AIF functions upstream of JNK, and through JNK activity AIF can control the cadherin switch as well as expression of specific morphological and EMT-associated genes. As an example of this specificity, AIF and JNK suppress E-cadherin without affecting levels of β-catenin (Figure 6.3A), a critical reciprocal regulator of E-cadherin [189]. Notably, while levels of not all AIF-dependent proteins required JNK, all JNK-dependent proteins identified were also dependent upon AIF (Figure 6.3C). This further demonstrates that AIF is essential for basal JNK activity, and also reveals the existence of additional AIF-dependent signaling pathways.

AIF-mediated signal transduction triggers the cadherin switch via JNK1

Collectively these data show that AIF enzymatic activity induces JNK1 signaling, and that AIF and JNK1 share E-cadherin as a target. The ability of AIF to promote both JNK1 activation and the cadherin switch raised the possibility that if JNK1 functions as a conduit for AIF-mediated signaling, then restoration of JNK activity in AIF-deficient cells would reverse E-cadherin to control levels. In order to restore JNK activity in the absence of AIF, we employed constitutively active forms of JNK (CA-JNK) fused with the JNK activator MKK7 and tagged with Flag epitope that have been characterized previously [166]. Plasmids encoding CA-JNK1 or

CA-JNK2 were transfected into PC3-shLacZ and PC3-shAIF cells followed by immunoblot for Flag and phospho-c-Jun (Figure 6.4), demonstrating both expression and activity of each CA-JNK protein. When CA-JNK1 was introduced into PC3-shAIF cells, E-cadherin reversed to near-control (shLacZ) levels (Figure 6.4), confirming that AIF regulates the cadherin switch by activating JNK1.

Failure to induce E-cadherin causes AIF-deficient cells to undergo apoptosis

We have shown previously that AIF ablation severely impairs tumorigenesis [51, 52]. Seeking to link these results to our current data defining an AIF-dependent signaling pathway, we employed the use of a Matrigel™-based assay as an *in vitro* approximation of molecular responses that may occur *in vivo*. We began by growing PC3-shLacZ and PC3-shAIF cells in Matrigel™ followed by extraction from substrate after 3 days. Similar to our data acquired from cells grown under nutrient-rich conditions *in vitro*, phosphorylation of JNK was impaired in AIF-deficient cells grown in Matrigel™ (Figure 6.5A). This suggests that AIF-mediated JNK phosphorylation occurs under physical and chemical environments encountered by tumor cells *in vivo*.

Since we observed that AIF ablation leads to a loss of JNK1-mediated control of E-cadherin, we then explored the effects of reverting E-cadherin to control levels in AIF-deficient cells. Lentiviruses harboring either control scramble shRNA or shRNA against E-cadherin [179] were generated and then used to infect PC3-shLacZ and PC3-shAIF cells. Stable knockdown of E-cadherin in AIF-deficient PC3 cells (PC3-shAIF/shE-cadherin) increased levels of N-cadherin (Figure 6.5B), suggesting N-cadherin levels can be altered by E-cadherin [179] in an AIF-dependent manner.

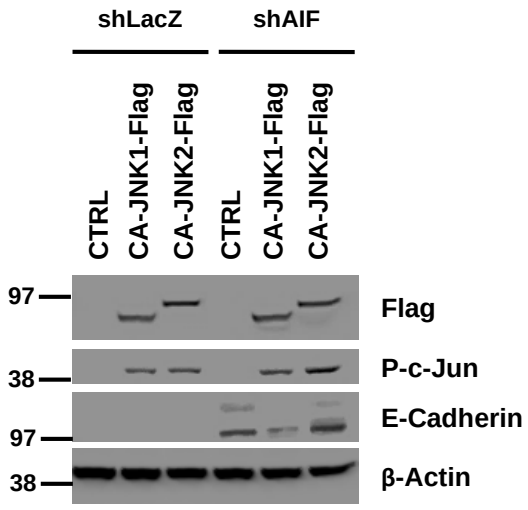

Figure 6.4. AIF signals JNK1 to downregulate E-cadherin.
PC3-derived cells were transfected with either empty control (CTL) plasmids or plasmids encoding either CA-JNK1-Flag or CA-JNK2-Flag, followed by immunoblot analysis with the indicated antibodies.

To determine if E-cadherin is involved with these changes, we next subjected PC3-shLacZ/scramble, PC3-shAIF/scramble, and PC3-shAIF/shE-cadherin cells to Matrigel™. Cells were seeded at three different densities (low, medium, high) and then incubated at 37 °C for 7 days (Figure 6.5C, D). In agreement with our previous observations [51], AIF proficient cells (PC3-shLacZ/scramble) demonstrated population increases ranging from 4-8 fold, indicating an ability to survive growth stress conditions. As expected, PC3-shAIF/scramble cells showed no increase in total viable numbers, with seed populations remaining essentially unchanged over the duration of the experiment. Notably, this AIF-deficient phenotype was further exacerbated in PC3-shAIF/shE-cadherin cells, which exhibited net reductions of 25-75% compared to controls (Figure 6.5C, D).

During this incubation, significant fractions of PC3-shAIF/scramble cells condensed and detached from the substrate (hallmarks of cell death), and the severity of this phenotype increased for PC3-shAIF/shE-cadherin cells. This raised the possibility that the absence of AIF

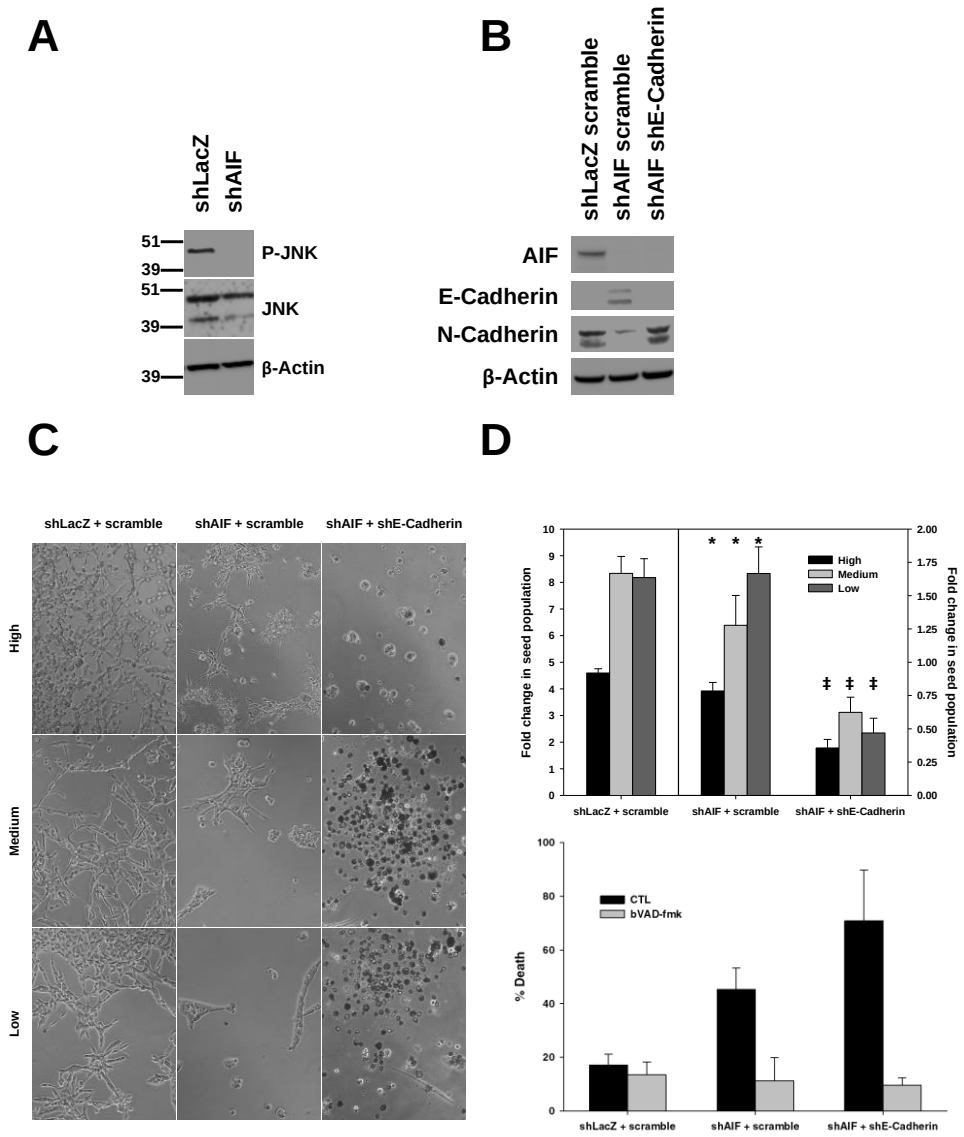

Figure 6.5. Suppression of E-cadherin reverses N-cadherin levels and triggers apoptosis in AIF-deficient PC3 cells in Matrigel™ environment.

A) Immunoblot analysis of phospho-JNK in PC3 shLacZ and shAIF cells recovered from Matrigel™ substrate. B) PC3-derived cells were stably infected with lentiviruses harboring either control scramble shRNA or shE-cadherin followed by immunoblot for AIF, E-cadherin, and N-cadherin. C) Phase contrast images of PC3-derived cells seeded at high, medium, and low densities in Matrigel™ substrate and grown for 7 days. D) Following 7 days of growth on Matrigel™, attached cells were recovered from and then quantified by Coulter™ counting. *$p<0.05$ compared with shLacZ scramble cells seeded at respective initial densities; ‡$p<0.05$ compared with shAIF scramble cells at corresponding seed populations. E) Cells were seeded in Matrigel™ substrate and treated with 50 μM bVAD-fmk immediately following seeding and then every 48 h for 7 days. Attached and detached cells were then recovered and quantified by Coulter™ counting; percent death is defined as the fraction of detached cells within each sample. All quantitative data are presented as average ± standard deviation.

leads to an active form of cell death under growth stress conditions that is amplified by E-cadherin loss. To test this possibility, we repeated the Matrigel™ experiment in the absence and presence of the caspase inhibitor bVAD-fmk. Detached populations of Matrigel™-exposed cells were harvested and viability was quantified (Figure 6.5D). PC3-shLacZ/scramble cells did not demonstrate appreciable cell death, and therefore were insensitive to caspase inhibition. In contrast, the cell death observed for both PC3-shAIF/scramble and PC3-shAIF/shE-cadherin cells was substantially reduced following caspase inhibition. These results strongly suggest that under growth stress conditions *Apoptosis-Inducing Factor* ablation triggers apoptosis that is made more severe by the inability to upregulate E-cadherin. Altogether these data show that when activated by the enzymatic activity of AIF, JNK1 suppresses E-cadherin to promote invasiveness, but suppression of AIF-dependent E-cadherin levels in the absence of AIF is lethal.

AIF and E-cadherin ablation-induced cell death corresponds to changes in AMPK phosphorylation and glucose consumption

Following the observations that AIF ablation induces apoptosis that is increased by knockdown of E-cadherin in Matrigel™ (Figure 6.5), we hypothesized that E-cadherin serves to inhibit cell death in the absence of AIF-mediated ATP production [51]. A pivotal endogenous sensor of cellular energetic state that is also linked to mechanotransduction (*e.g.*, due to Matrigel™-induced stresses) is the heterotrimeric protein complex known as AMP-activated protein kinase (AMPK). Notably, AMPK functions downstream of E-cadherin, stimulating glucose consumption and ATP production that allow the cell to resist mechanical forces imposed by the physiological environment [190]. In contrast to this pro-glycolytic role for AMPK associated with E-cadherin, the loss of AMPK triggers a metabolic switch to aerobic glycolysis

[191], which is consistent with the notion of a shared metabolic regulatory pathway between AMPK and AIF.

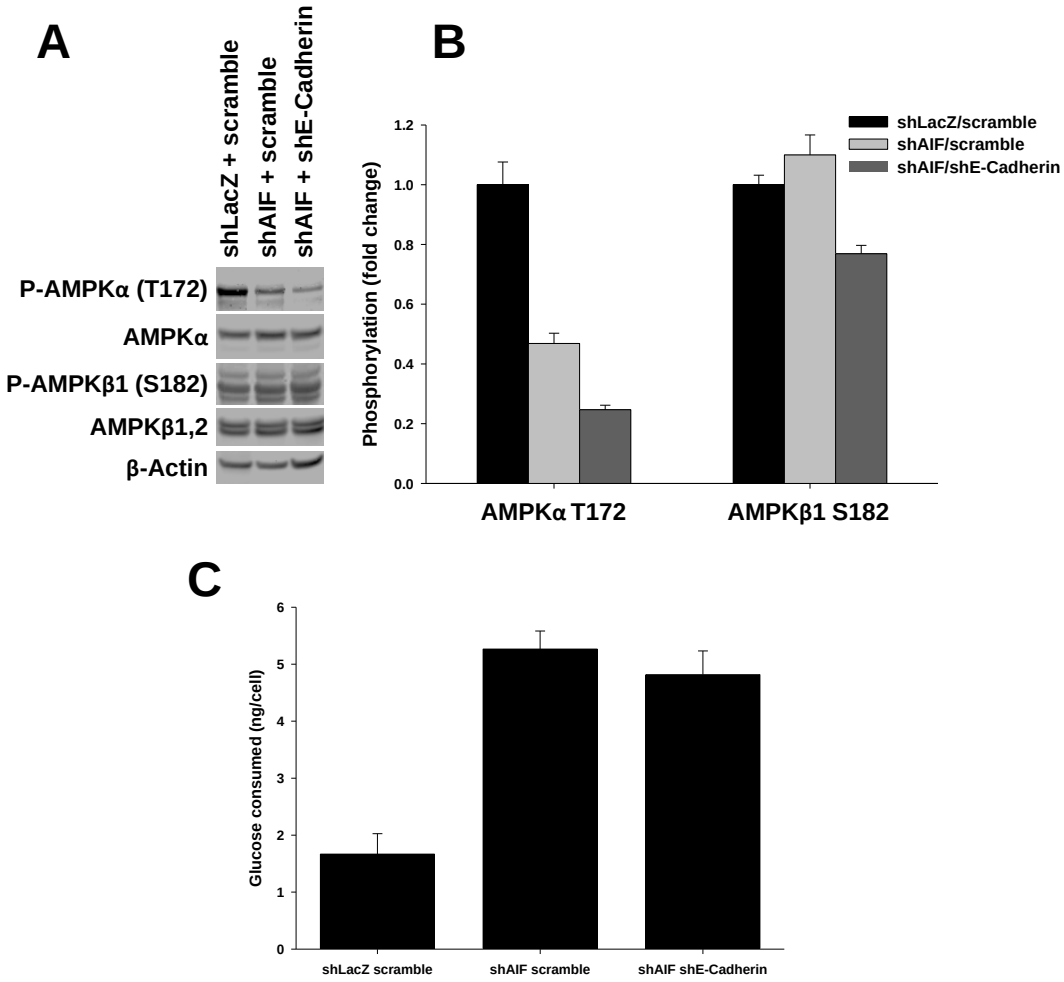

Figure 6.6. Loss of AIF and E-cadherin alters AMPK phosphorylation and glucose consumption.
A) The indicated cell lines were lysed and assessed for the indicated proteins by immunoblot. B) Replicate immunoblots from *panel a* were quantified and normalized to total AMPKα or AMPKβ1,2 and β-actin. C) Equal densities of cells were plated in fresh media, and total glucose was measured using the QuantiChrom™ Glucose Assay Kit (BioAssay Systems) 72 h after seeding. Total numbers of cells in each well were used to determine glucose consumption per cell. All quantitative data are presented as average ± standard deviation.

Based on the shared pathways of AIF, E-cadherin, and AMPK, the status of AMPK was then evaluated in the context of AIF and E-cadherin ablation. While many regulatory

mechanisms for AMPK have been identified, two notable post-translational modifications are essential for protein activity and localization. The α subunit of AMPK is phosphorylated by LKB1 at T172 in the activation loop, and this phosphorylation is required for activation [192-194]. AMPK activity is additionally regulated through protein localization; phosphorylation at S182 of the β1 subunit inhibits nuclear redistribution without affecting enzyme activity [195]. Therefore phosphorylation levels of AMPKα T172 and AMPKβ1 S182 were assessed by immunoblot analysis in PC3-derived cell lines (shLacZ/scramble controls, shAIF/scramble, and shAIF/shE-cadherin). Interestingly, AIF-deficient cells exhibited substantial decreases in AMPKα phosphorylation (Figure 6.6A, B), which may be a potential trigger for the metabolic switching event that occurs following AIF ablation [51, 192-194]. It is notable that this phosphorylation was further reduced upon loss of E-cadherin (Figure 6.6A, B), consistent with an exacerbated AIF-deficient apoptotic phenotype observed above (Figure 6.5). No substantial changes in phosphorylation levels of AMPKβ1 S182 were observed, suggesting that this residue is not strongly involved with either AIF or E-cadherin signaling. Collectively these data strongly correlate with the pattern of cell death observed and suggest that AMPK responds both to AIF ablation and AIF/E-cadherin ablation, in particular with respect to phospho-activation at α-T172.

If AMPK is associated with the protective function of E-cadherin in the context of AIF ablation, why do cells die despite further dephosphorylation of AMPK when E-cadherin is suppressed? We wondered if following AIF ablation cells have met a glycolytic threshold that cannot be exceeded upon additional metabolic demand, for example when E-cadherin growth suppressive activity is lost. If this is the case, AMPK could respond to such a change (through further phosphorylation change) yet still fail to protect cells. To test the validity of this idea, glucose consumption levels were assessed in PC3-derived cells. AIF-deficient cells increased

glucose uptake levels (Figure 6.6C), consistent with previous data [51] that indicate an upregulation of glycolysis to meet ATP demands. Notably, ablation of E-cadherin in AIF-deficient cells did not further increase glucose consumption (Figure 6.6C). This observation provides evidence that loss of E-cadherin induces death in AIF-deficient cells due to a drastic loss of metabolic plasticity.

Discussion

Identification of a novel signal transduction pathway under AIF control

This study is the first both to define the steps of an AIF-dependent signaling pathway and to show AIF promotes the cadherin switch. The reversal of the cadherin switch following AIF ablation in some cells raises the possibility that AIF may influence metastasis [51] by triggering E-cadherin suppression and N-cadherin elevation. Experiments presented here focus primarily on the cadherin switch in the context of altered AIF/JNK activity, but all MAPKs (JNK, p38, and ERK) have been implicated in the cadherin switch and metastatic progression [176]; whether and how AIF can regulate cadherin levels through p38 and ERK represent significant future questions.

In light of the wide diversity of cell functions mediated by JNK, a variety of different signaling activities for AIF as an upstream messenger can be envisioned. In addition to the EMT and cadherin switch, JNK is additionally involved with apoptosis, differentiation, proliferation, survival, inflammation, and DNA repair. Through control of JNK activity, AIF is positioned to serve as a regulator as one or more of these activities and could therefore function in a significantly greater range of cellular activities than originally assumed.

Balance of AIF-mediated signaling with metabolism

Interestingly, we observed that while AIF promotes the cadherin switch via JNK1 activation, reversing this switch in AIF-deficient cells is lethal under Matrigel™ growth conditions. AMPK, a regulator of both metabolism and E-cadherin signaling, exhibits decreased phosphorylation following AIF loss that is further impaired when E-cadherin is suppressed, while glucose consumption cannot further increase with dual knockdown. This suggests that induction of the tumor suppressor E-cadherin following AIF ablation is a potential survival adaptation in the absence of AIF-mediated mitochondrial ATP production [51]. This might occur to slow cell growth to rates that can match metabolic availability of macromolecules and cell fuel sources [196], altogether demonstrating the roles of AIF, JNK, and E-cadherin as double-edged swords in cancer [197-199]. Cancer cells may use AIF to activate pro-tumor signaling pathways (such as JNK1-mediated suppression of E-cadherin), but their activation in the absence of AIF can in some situations be lethal, possibly due to altered AIF-dependent metabolism [25, 51, 52]. In the context of our experiments, AIF loss-induced upregulation of E-cadherin (due to impaired JNK activity) could serve as a brake on cell growth, which must remain in check when cells are unable to meet the metabolic demand of survival and invasion in growth substrate. Cells may alter AMPK status in response to dual knockdown of AIF and E-cadherin, but glycolysis cannot further increase with E-cadherin loss if a maximal level of glycolytic activity is already met following AIF ablation.

Summary

Experiments here show that through JNK1 activity AIF promotes the cadherin switch. Loss of AIF and subsequent impairment of JNK signaling induce E-cadherin upregulation, and knockdown of E-cadherin induces apoptosis when AIF is suppressed. This cell death observed

appears to be related to a loss of balance between growth and metabolic demand; these data merit further investigation to confirm this hypothesis. Altogether, these findings define a novel signaling pathway comprising AIF, JNK1, and E-cadherin, and highlight their roles in controlling metabolism and redox signals with significant impact upon decisions of cell fate.

VII. AIF-MEDIATED REDOX SIGNALING IS UNCOUPLED FROM STABILIZATION OF THE MITOCHONDRIAL RESPIRATORY CHAIN

Abstract

The mitochondrial flavoprotein AIF controls both cellular metabolism and redox signaling. Regulation of metabolism and oxidative stress levels are often related, and it remains unknown if the redox effects of AIF ablation are due to altered metabolism, or if these effects are independent of AIF-mediated metabolic control. Suppression of AIF in 13 different cell lines from a variety of cancer types and tissues reveals that AIF-mediated stabilization of the respiratory chain is restricted to cell type, which is in contrast to the widespread role of AIF in redox-dependent activation of JNK. Interestingly, in cells that do exhibit complex I deficiency following AIF ablation, complex I levels are variably dependent upon the enzymatic activity of AIF, and further metabolic analysis shows that mitochondrial activity and abundance are not substantially impaired. Since no correlation appears to exist between metabolic sensitivity to AIF ablation and impaired redox signaling, this strongly suggests that AIF-mediated metabolism and oxidative stress responses are independent. We confirm this model by enhancing ETC activity with the yeast oxidoreductase NDI in AIF-deficient cells, which restores glucose consumption but not JNK signaling or the cadherin switch. Altogether these data demonstrate functional uncoupling of AIF-mediated control of the respiratory chain from AIF-dependent redox signaling.

Introduction

Cellular metabolic and redox states are closely related. The pentose phosphate pathway (PPP) is a metabolic route diverging from glycolysis that generates NADPH which can be used to detoxify free radicals. The ETC generates ROS during respiration due to electron leakage.

Additionally, ROS can inhibit various control points of glucose oxidation. Therefore changes in cellular metabolic conditions are frequently accommodated by changes in oxidative stress levels. This raises the question of whether impaired redox signaling following AIF ablation is due to loss of AIF or alteration of cellular metabolism.

AIF is a mitochondrial oxidoreductase that controls both metabolism and cellular ROS levels with substantial impact upon intracellular signaling. Following AIF ablation, cells decrease protein levels of complex I subunits and exhibit a metabolic shift from OXPHOS to glycolysis that is reflected by increased glucose uptake and lactate secretion accompanied by decreased oxygen consumption. When AIF is suppressed, glycolysis increases in order to generate ATP in the absence of mitochondrial energy production. Additionally, it is thought that impaired growth is in part due to a downregulation of the PPP, which normally supplies the cell with macromolecular precursors for biosynthetic reactions. Rather than shuttling into the PPP, glycolytic intermediates may be instead destined for pyruvate so that ATP is generated at a level sufficient for survival.

This metabolic switching event adds complexity to the observation that AIF enzymatic activity promotes cellular redox signaling. While AIF generates ROS *in vitro*, a number of explanations for decreased ROS levels and altered redox signaling following AIF suppression are possible. The ability of AIF enzymatic activity to produce ROS directly is one potential explanation for AIF-dependent ROS changes in cells; however, it is also plausible that changes in ROS and redox signaling stem from changes in complex I levels. Since complex I functions at the start of the ETC, loss of complex I could lead to decreased ROS levels due to decreased transport of electrons. Alternatively, ETC malfunction can also increase ROS levels due to electron backup within the ETC. In addition to AIF enzymatic activity and AIF-dependent

complex I levels, a third rationale for altered oxidative state can be envisioned. Since glycolysis is upregulated following AIF ablation, changes in the PPP would likely alter NADPH levels, which could consequently have significant impact upon cellular redox state.

Interestingly, not all cells exhibit ETC deficiency or metabolic switching following AIF knockdown. This selective metabolic sensitivity to AIF loss seems to depend upon cellular metabolic preferences. Therefore assessment of redox signaling and metabolic status in cells that are metabolically insensitive to AIF ablation may clarify whether AIF-mediated redox signaling results from AIF metabolic regulation. Moreover, in cells that exhibit a metabolic switch following AIF ablation, reversal of this switch followed by evaluation of redox signaling would further establish a relationship between AIF-mediated metabolism and redox control.

To address the relationship between AIF enzymatic activity, AIF-dependent complex I levels, and AIF-mediated redox signaling, experiments here focus on mitochondrial responses to AIF ablation, followed by assessment of JNK activity in the context of AIF ablation and altered metabolism. Remarkably, AIF-dependent signal transduction is uncoupled from stabilization of the mitochondrial respiratory chain and cellular metabolism. Altogether these findings show functional independence of the metabolic and redox activities of AIF, further demonstrating the versatility of AIF in homeostatic control and tumorigenesis.

Materials and methods

Materials, plasmids and antibodies

MEM, DMEM, RPMI 1640, DMEM/F12, GlutaMAX, horse serum, insulin, transferrin, epidermal growth factor, trypsin, 4–12 % bis-tris polyacrylamide gels, nitrocellulose membranes, fetal bovine serum (FBS), phosphate buffered saline (PBS), and Pierce ECL 2 Western Blotting

Substrate were from Thermo Fisher Scientific; QuantiChrom™ Glucose Assay kit was from BioAssay Systems; all other materials were from Sigma.

Lentiviral plasmids FG12-shLacZ-GFP, FG12-shAIF-GFP, FG12-shLacZ-puro, and FG12-shAIF-puro were described previously [51, 52, 121, 147]. To generate RNAi-resistant AIF restoration pSL4-hygro plasmids, AIF cDNA was subcloned from pEBB-siMut-AIF^{WT} and pEBB-siMut-AIF^{TVA} [51] into pSL4-hygro [164]. Lentiviral packaging plasmids pHCMV-G, pRRE, and pRSV-rev are as described [123]. pMXs-NDI1 [200] was from Dr. David Sabatini (Addgene plasmid #72876). To generate pEBB-NDI1-Flag, NDI1 cDNA was amplified by PCR from pMXs-NDI1 using primers containing NotI and KpnI restriction sites (sequences available upon request) and then inserted into the pEBB-Flag backbone using standard cloning techniques. Lentiviral pLKO plasmids were obtained as follows: psPAX2 and pMD2.G-vsv-G from Dr. Didier Trono (Addgene plasmids #12260 and 12259); pLKO.1-puro-scramble [149] from Dr. David Sabatini (Addgene plasmid #1864); and pLKO.1-puro-shE-cadherin [179] from Dr. Robert Weinberg (Addgene plasmid #18801).

Antibodies were obtained as follows: anti-AIF (Santa Cruz, sc-13116), anti-NDUFA9 (Invitrogen, 459100), anti-NDUFB8 (Invitrogen, 459210), anti-citrate synthase (Cell Signaling, 14309), anti-β-actin (Sigma, A5316), anti-phospho-JNK T183/Y185 (Cell Signaling, 4668), anti-JNK (Cell Signaling, 9252), anti-E-cadherin (Cell Signaling, 4065), anti-N-cadherin (Cell Signaling, 4061), anti-Flag (Sigma, F3165), HRP-conjugated anti-mouse IgG (Amersham Biosciences, NA391B), and HRP-conjugated anti-rabbit IgG (Amersham Biosciences, NA934B).

Cell culture

Cells were cultured in an atmosphere of 95% air and 5% CO_2 at 37 °C. All media formulations were supplemented with 2 mM GlutaMAX, except for K-SFM as described below.

HEK293T, MRC-5, PANC-1, PL45, and HeLa cells were cultured in DMEM supplemented with 10% FBS; PC3, DU145, LNCaP, BxPC-3, and HCT 116 cells in RPMI 1640 medium supplemented with 10% FBS; HPAF-II cells in MEM supplemented with 10% FBS; MIA PaCa-2 cells in DMEM supplemented with 10% FBS and 2.5% horse serum; and HPAC cells in a 1:1 mixture of DMEM and Ham's F12 medium supplemented with 5 % FBS, 2 μg/mL insulin, 5 μg/mL transferrin, 40 ng/mL hydrocortisone, and 10 ng/mL EGF. RWPE-1 cells were cultured in K-SFM (Thermo Scientific, 17005042) supplemented with 0.05 mg/mL bovine pituitary extract and 5 ng/mL EGF. Cells were harvested by trypsinization, washed in PBS, and seeded at equal densities and then allowed to attach overnight prior to all assays.

Transfections

Plasmids were transfected into cells using Lipofectamine™ 2000 as described by the manufacturer. Cells were then harvested 48-72 h following transfection and either lysed as described below or quantified by Coulter™ counting.

Drug treatments

Cells were subjected to chemical treatments as follows: tBHQ at 0-2 mM for 1 h, and staurosporine at 1 μM for 16 h. Following treatment cells were harvested and assessed in assays as indicated.

Lentiviral production and stable infection of cell lines

To establish cell lines stably suppressing or overexpressing AIF, lentiviral particles were produced by transfecting equal amounts of pHCMV-G, pRRE, pRSV-rev, and FG12- or pSL4-derived plasmids into HEK293T cells using the calcium phosphate method [124]. Following incubation at 37 °C for 48 h, supernatants were collected, filtered using 0.45 μm-pore size Millex HV PVDF filter units (Millipore) and concentrated by centrifugation at 20,000 x g. Viral pellets

were then resuspended in PBS at 4 °C overnight. Resuspended virus was added to cells in the presence of 4 μg/mL polybrene for 4 h at 37 °C in an environment of 93% air and 7% CO_2. Cell lines used for stable RNAi targeting of AIF were infected with either control lentivirus or lentivirus harboring an AIF target sequence as follows: shLacZ-puro or shAIF-puro (PC3, HPAC, MRC-5, RWPE-1, HeLa, PANC-1, BxPC-3, PL45, HPAF-II) followed by selection with 1 μg/mL puromycin; shLacZ-GFP or shAIF-GFP (DU145, LNCaP, HCT 116, MIA PaCa-2). To establish "restoration" cell lines (PC3, HeLa) expressing either wild-type AIF or a catalytically impaired mutant, cells were infected with empty vector, AIF^{WT}, or AIF^{TVA} and then selected with 500 μg/mL (PC3) or 1000 μg/mL (HeLa) hygromycin B.

For establishment of cell lines stably suppressing E-cadherin, pLKO.1-based lentiviruses were generated by transfecting HEK293T cells with pMD.2, psPAX2, and pLKO-shE-cadherin using the calcium phosphate method. Viral supernatant was collected at 48 h and 72 h post-transfection and then filtered using 0.45 μm-pore size Millex HV PVDF filter units. Target cells were then incubated with viral supernatant and 8 μg/mL polybrene for 24 h. Stably infected cells were selected using 1 μg/mL puromycin.

Cell lysis, fractionation and immunoblot analysis

Cell lysates were prepared in radioimmune precipitation assay (RIPA) lysis buffer (PBS containing 1% NP-40, 0.5% sodium deoxycholate, 0.1% SDS, 1 mM dithiothreitol, 1 mM PMSF, 1 mM sodium fluoride, 1 mM sodium orthovanadate, and 1 protease inhibitor mixture tablet per 10 mL). Mitochondrial extracts were prepared as described [201]. Briefly, cells were resuspended in buffer A (250 mM sucrose, 20 mM HEPES-KOH pH 7.9, 10 mM KCl, 1.5 mM $MgCl_2$, 1 mM EDTA, 1 mM EGTA, 1 mM dithiothreitol, 1 mM PMSF, and 1 protease inhibitor mixture tablet per 10 mL) and equilibrated on ice for 20 min, followed by homogenization with a

Dounce tissue grinder (Kimble™ Kontes™). Samples were then centrifuged at 400 x g for 10 min at 4 °C. Supernatants were then collected and further centrifuged at 10,000 x g for 10 min at 4 °C. Precipitated material (constituting the mitochondrial fraction) was then washed in buffer A and resuspended in NP-40 lysis buffer (1% NP-40, 10% glycerol, 25 mM HEPES pH 7.9, 100 mM NaCl, 1 mM EDTA, 1 mM dithiothreitol, 1 mM sodium fluoride, 1 mM sodium orthovanadate,1 mM PMSF, and 1 protease inhibitor tablet per 10 mL).

For immunoblot experiments, protein samples were separated by SDS-PAGE using 4-12% gradient SDS-polyacrylamide gels followed by electrotransfer to nitrocellulose membranes. Membranes were blocked with 5% milk or bovine serum albumin in tris-buffered saline containing 0.02 to 0.2% Tween-20 and then incubated with the indicated primary antibodies. Membranes were then washed three times and incubated with HRP-conjugated anti-mouse or anti-rabbit followed by visualization using enhanced chemiluminescence.

Replicate immunoblots were quantified at multiple exposures for linearity using myImage Analysis™ software (Thermo Scientific). Band intensities for phosphorylated proteins were divided by intensities for the corresponding total proteins; all protein values and phospho-protein/total protein ratios were then normalized to β-actin values. To determine fold changes among lanes, all ratios were then normalized to control lanes (leftmost lanes).

Measurements of mitochondrial $\Delta\Psi_m$ and abundance

Staining for mitochondrial membrane potential was carried out as described previously [104] by resuspending harvested cells in PBS containing 200 nM TMRM followed by flow cytometry. Staining for mitochondrial abundance was carried out by incubating cells with 100 nM MitoTracker™ Red at 37 °C for 20 min. Cells were then harvested and resuspended in PBS, followed by assessment of stain intensity using an Accuri C6 flow cytometer.

Glucose consumption measurements

Following transfections, fresh media was replenished, and cells were grown at 37 °C for 72 h. Media glucose levels were then assessed using the QuantiChrom™ Glucose Assay kit (BioAssay Systems). Cells in each sample were quantified by Coulter™ counting and used to determine glucose consumption levels per cell.

Results

AIF-mediated respiratory chain stabilization is limited to cell type

Our data demonstrate that AIF-mediated signaling promotes a JNK1-dependent cadherin switch. In addition to this activity, AIF is essential for mitochondrial homeostasis under healthy cellular conditions [25, 26, 62]. AIF controls both protein levels within mitochondrial complex I and metabolic flux, yet the role of AIF-mediated redox control in these metabolic activities remains unclear. Moreover, it is presently unclear whether the ability of AIF to influence mitochondrial metabolism (through complex I protein expression) and redox/ROS signaling are related properties, or if these are separate features of AIF activity that govern distinct cellular responses. To begin addressing this question, we evaluated AIF-mediated control of complex I and mitochondrial activity (potential sources of intracellular ROS) in a broad panel of human cell lines. Suppression of AIF protein by lentivirus-mediated RNAi was verified by immunoblot (Figure 7.1A), and following ablation of AIF we observed cell line specific losses of complex I subunits NDUFA9 and NDUFB8 (Figure 7.1A). Previously we have tested the effect of AIF ablation on respiratory chain protein levels [51, 52] in some cell types employed here (PC3, DU145, LNCaP, PANC-1, BxPC-3, HPAC, HPAF-II, MIA PaCa-2), which are consistent with our current data. Following AIF ablation 7 of the 13 cell lines (MRC-5, PC3, DU145, PANC-1, BxPC-3, HPAC, PL45) exhibited reductions in levels of complex I subunits NDUFA9 and

NDUFB8 to variable extents, whereas in HeLa cells a reduction of only NDUFB8, but not NDUFA9, was observed. In the remaining 5 cell lines (RWPE-1, HCT 116, LNCaP, HPAF-II, MIA PaCa-2), levels of neither NDUFA9 nor NDUFB8 were affected following suppression of AIF (Figure 7.1A), indicating AIF is not universally required to maintain expression of respiratory chain proteins.

AIF enzymatic activity variably controls complex I levels

To determine if AIF-mediated control of respiratory protein levels is dependent on AIF's NADH-oxidase activity, we next generated AIF restoration cell lines expressing either wild type AIF (AIF^{WT}) or a catalytically inactive AIF mutant [51, 54] containing the substitutions T263A and V300A (AIF^{TVA}). Lentiviruses harbored cDNA constructs with a silent mutation resistant to shRNA-mediated targeting of AIF [51], and the introduction of hygromycin B resistance was used to select stably infected cells. Expression of both wild type AIF and the enzymatically deficient mutant restored complex I to control levels in PC3 cells (Figure 7.1B), suggesting that the NADH-oxidase activity of AIF is not required for complex I protein expression. These findings are in agreement with our previously derived PC3 cell lines in which GFP and puromycin resistance were used as selection markers [51]. Interestingly, when AIF was reintroduced to HeLa-shAIF cells (which exhibited a reduction of only NDUFB8), AIF^{TVA} failed to restore NDUFB8 to control levels (Figure 7.1B). This indicates that the enzymatic activity of AIF is essential for complex I regulation only for certain ETC subunits and/or in specific cell types. While the mechanism of AIF-mediated mitochondrial control remains poorly understood, the above analyses show that the ability of AIF to control respiratory chain subunit levels is highly variable and dependent upon context.

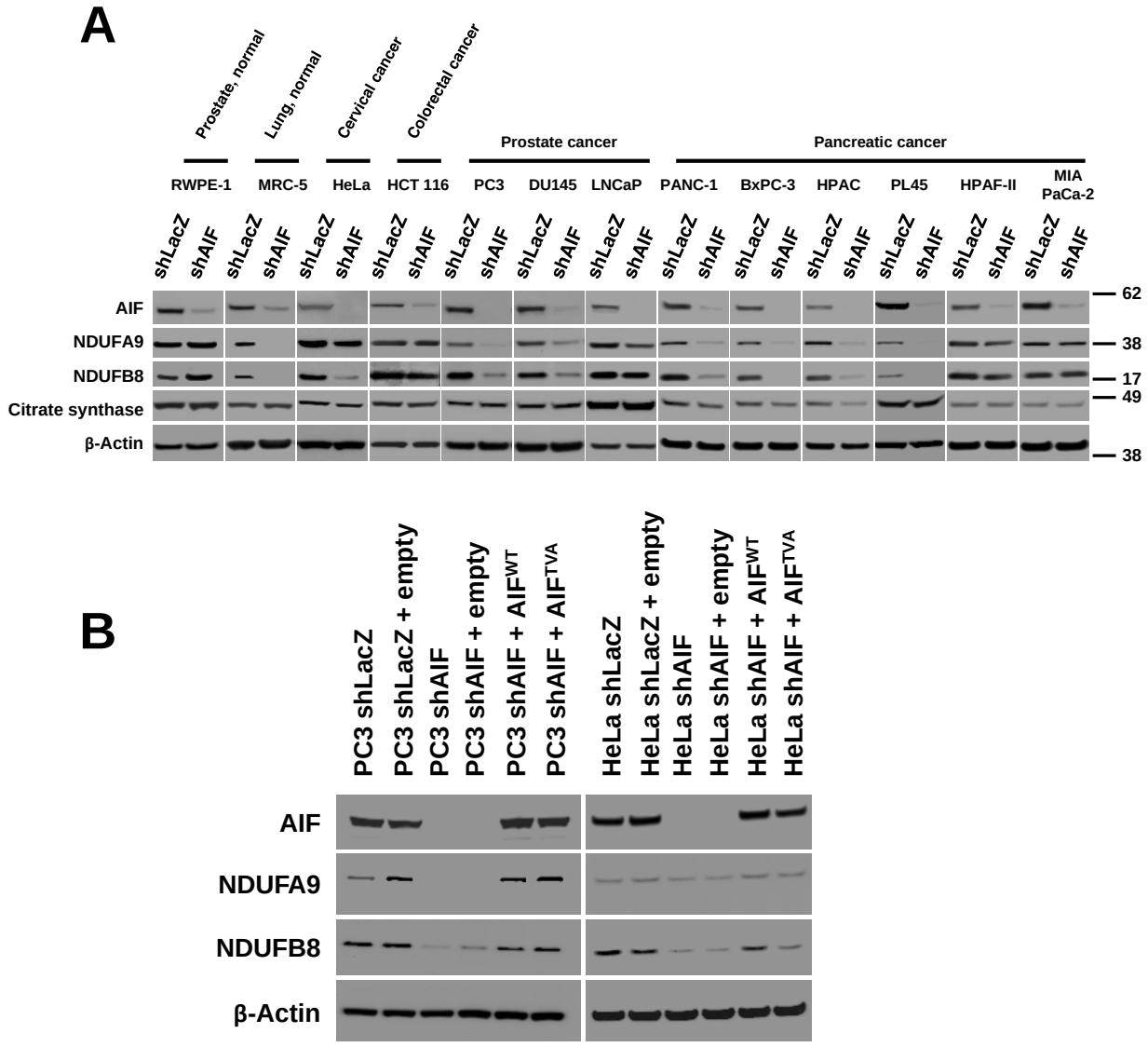

Figure 7.1. AIF-mediated control complex I levels is restricted to cell type and variably requires AIF enzymatic activity.

A) Immunoblot analysis was performed on a panel of AIF proficient (shLacZ) and deficient (shAIF) human cell lines from diverse tissue types. Antibodies recognizing AIF, complex I subunits NDUFA9 and NDUFB8, and citrate synthase were employed; β-actin was used as a loading control. B) Immunoblot analysis for AIF, NDUFA9, NDUFB8, and β-actin was performed as in panel A on "restored" PC3 and HeLa cell lines.

Table 7.1. Effect of AIF ablation on mitochondrial $\Delta\Psi_m$ and abundance.

	Change in $\Delta\Psi_m$ (%)	*p*	Change in abundance (%)	*p*
HeLa	20.9	0.020	9.7	0.587
HPAC	16.3	0.007	34.2	0.002
MRC-5	15.5	0.007	19.6	0.026
DU145	13.9	0.064	23.4	0.147
MIA PaCa-2	13.7	0.128	-13.8	0.212
HCT 116	12.6	0.079	21.7	0.315
PL45	8.5	0.149	30.2	0.120
BxPC-3	8.5	0.001	26.2	0.004
PANC-1	5.6	0.178	-12.7	0.007
LNCaP	4.7	0.553	-13.2	0.376
PC3	-2.0	0.595	2.6	0.272
RWPE-1	-7.7	0.040	-2.6	0.168
HPAF-II	-10.5	0.389	-0.2	0.987
Staurosporine treatment	-59.3	0.000	-30.1	0.045

Staining with either TMRM or MitoTracker™ Red was used to determine $\Delta\Psi_m$ and abundance of mitochondria, respectively, in cells proficient (shLacZ) and deficient in AIF (shAIF). Changes following AIF ablation compared to control cells are shown; p-values were determined by two-tailed homoscedastic Student's t-tests. Changes between staurosporine-treated and control-treated cells were used as a comparative reference to the effects of AIF ablation (bottom row).

AIF is not critical for general mitochondrial fitness

Since some cell types exhibited complex I deficiency following AIF ablation, we evaluated mitochondrial status in our panel of cell lines to determine if mitochondrial function and/or biogenesis (possible triggers for oxidative stress signaling) were impaired. Citrate synthase, a mitochondrial matrix enzyme and marker for mitochondrial abundance, was unchanged when AIF was suppressed (Figure 7.1A). Furthermore, assessment of mitochondrial status by staining with tetramethylrhodamine ester (TMRM, an indicator of mitochondrial $\Delta\Psi_m$) and MitoTracker™ Red (an indicator of mitochondrial abundance) suggests that AIF ablation does not substantially dissipate the mitochondrial electrochemical gradient nor decrease mitochondrial abundance in any cell types tested (Table 7.1). It is therefore likely that while AIF controls complex I in some cell types, AIF is not critical for mitochondrial fitness. Strikingly, all cell types examined required AIF for JNK signaling (Chapters 5, 6) regardless of whether AIF deficiency led to changes in complex I (Figure 7.1A).

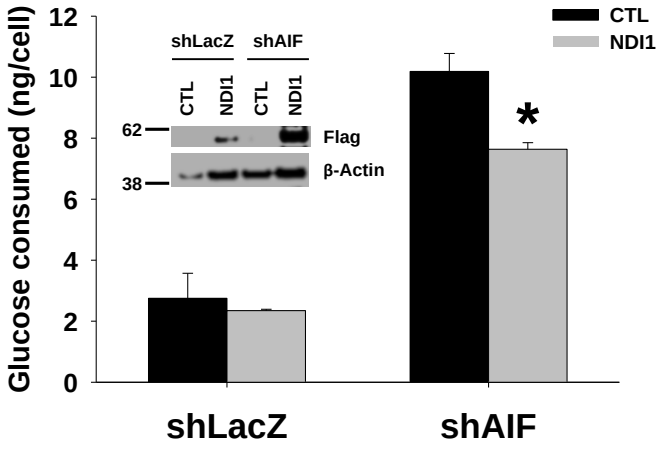

Figure 7.2. NDI1 reduces glucose consumption in AIF-deficient cells.
Glucose consumption levels of PC3-derived cells transfected with either control plasmid (CTL) or NDI1 were measured using the QuantiChrom™ Glucose Assay kit (BioAssay Systems) and normalized to cell numbers. Data are presented as average ± standard deviation. *$p<0.05$. Inset: Protein expression levels of NDI1 in transfected PC3-derived cells were determined by immunoblot for Flag epitope in mitochondrial extracts.

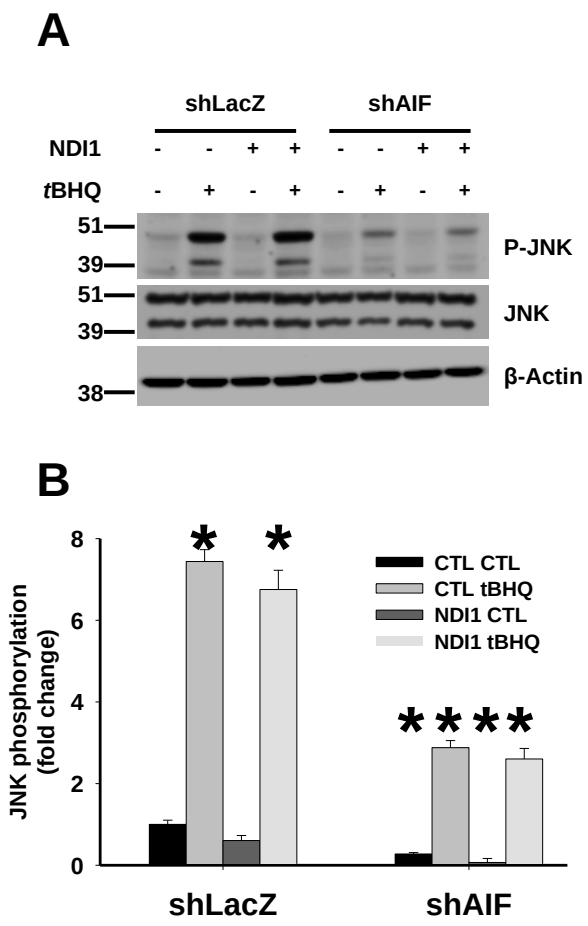

Figure 7.3. NDI1 does not affect JNK phosphorylation in AIF-deficient cells.
A) PC3-derived cells transfected with either control plasmid or NDI1 were treated with 0 or 2 mM tBHQ followed by immunoblot for phosphorylated JNK. B) Replicate phospho-JNK immunoblots from *panel a* were quantified and normalized to total JNK and β-actin. *$p<0.05$ compared with shLacZ CTL plasmid + 0 mM (CTL CTL). Data are presented as average ± standard deviation.

Respiratory chain repair restores AIF ablation-induced metabolic switching but not oxidative stress signaling

We then questioned whether the AIF-dependent signaling factors (*e.g.*, ROS) regulating JNK are directly produced by AIF or an indirect effect of AIF-mediated control of mitochondrial complex I activity. If re-establishment of mitochondrial respiration in AIF-deficient cells restores the signaling effects observed above, then this would suggest that AIF drives redox signaling

through complex I. Therefore we sought to restore functionality of ETC/OXPHOS while maintaining knockdown of AIF. To accomplish this, we expressed an epitope-tagged form of NDI1 in AIF proficient and deficient cells. NDI1 is a single-subunit NADH:ubiquinone oxidoreductase expressed by yeast and known to enhance and/or restore mitochondrial respiratory activity in human cells with complex I defects. NDI1 can therefore be used to determine if an AIF-deficient phenotype is due to the specific loss of AIF or the more general loss of complex I function [202-204]. Control vectors and NDI1 plasmids were transfected into PC3-derived cells and then assessed for NDI1 expression. Immunoblot of mitochondrial extracts for Flag epitope showed that NDI1 protein is expressed in transfected PC3-derived cells (Figure 7.2). A critical metabolic effect of AIF ablation is an increase in glucose consumption that supports energy production required for cell survival [51, 52]. When NDI1 was transfected into AIF-deficient PC3 cells, glucose consumption decreased significantly (Figure 7.2) and indicates an improvement in mitochondrial metabolic activity resulting from the introduction of a functional NDI1 protein.

Despite restoration of the ETC with NDI1, oxidant-induced JNK phosphorylation remained unaffected by respiratory enhancement (Figure 7.3), and changes in the cadherin switch were not altered when AIF-deficient cells were transfected with NDI1 (Figure 7.4). Therefore, in addition to the finding that JNK requires AIF enzymatic activity across cell types regardless of AIF-dependent complex I status, these data demonstrate that AIF redox signaling is uncoupled from its roles in control of complex I and cellular metabolism.

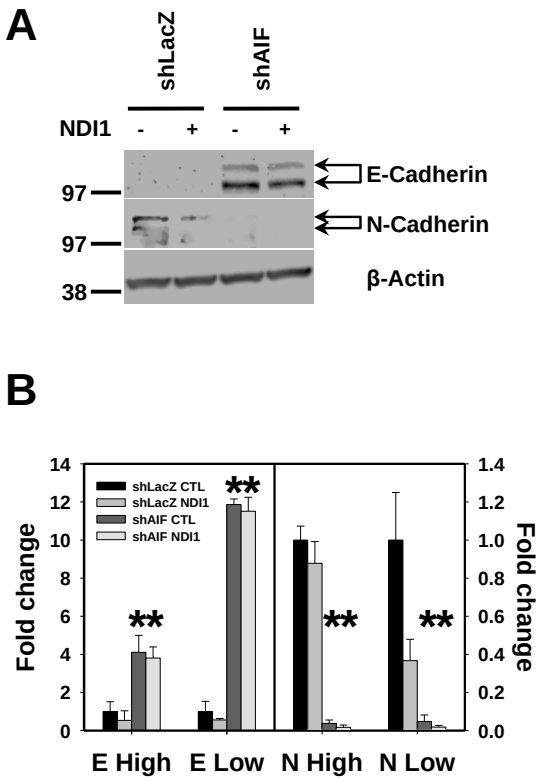

Figure 7.4. The cadherin switch is unaffected by NDI1 introduction in AIF-deficient cells. A) PC3-derived cells transfected with either control plasmid or NDI1 were subjected to immunoblot for E-cadherin and N-cadherin. B) Replicate immunoblots from *panel a* were quantified and normalized to β-actin. E/N-cadherin upper band, E/N high; lower band, E/N low. *p<0.05 compared to shLacZ CTL. Data are presented as average ± standard deviation.

Discussion

AIF, ROS, and metabolic regulation

The multitude of roles for AIF in controlling cellular metabolic and redox conditions prompted our investigation into why decreased redox signaling is observed following AIF ablation. ROS can be produced directly by AIF enzymatic activity or by the flow of electrons through the ETC, which is also dependent upon AIF [25, 60]. Additionally, cellular ROS levels may vary with changes in metabolic conditions; for example, the metabolic switching from OXPHOS to glycolysis that occurs following AIF ablation could be a trigger for altered ROS.

Does AIF directly promote ROS or are decreased ROS following AIF ablation due to altered metabolism?

AIF promotes redox signaling independently of metabolic state

It is notable that AIF ablation does not substantially decrease mitochondrial $\Delta\Psi_m$, which could be maintained by low but remaining complex I levels and/or ETC activity initiated by complex II or fatty acid β-oxidation. Similarly, AIF does not appear to substantially control mitochondrial abundance, a potential ROS source that could activate JNK. The enzymatic activity of AIF generates ROS (Chapter 5) in both PC3 and HeLa cells (exhibiting different ETC responses following AIF ablation) but does not universally control complex I (Figure 7.1), which is the first evidence that the cellular redox effects of AIF result specifically from its enzymatic activity and are not only a side-effect of AIF-mediated complex I function. These findings are further supported by experiments showing that respiratory chain enhancement in AIF-deficient cells restores glucose consumption but not JNK phosphorylation or E-cadherin levels. It is striking that the ability of AIF enzymatic activity to promote oxidative stress-induced JNK activation is independent of complex I status and cellular metabolic state, especially since metabolism and ROS levels are both controlled by this AIF activity.

Summary

Altogether this study shows the ability of AIF to promote redox signaling is uncoupled from metabolic control. These findings further support a highly multifunctional nature for AIF and suggest a significant capacity to separately regulate metabolism and redox state to the benefit of tumorigenesis. This finding that AIF regulates both cellular functions through a single enzymatic activity highlights the therapeutic promise of targeting AIF enzymatic activity in cancer.

VIII. AIF BINDING PROTEINS XIAP AND PGAM5 REGULATE DECISIONS OF CELL FATE THROUGH UBIQUITINATION-DEPENDENT MUTUAL ANTAGONISM

Abstract

AIF is a mitochondrial protein that exhibits dissociable activities in cellular homeostasis and caspase-independent cell death. AIF has been implicated in a variety of atypical cell death pathways and physically associates with the caspase-independent cell death regulators PGAM5 and XIAP, but the mechanisms and functional significance of these interactions remain unclear. Here we show that the association of PGAM5 with AIF protects AIF from XIAP-mediated inhibition, and that PGAM5 triggers PINK1-dependent mitophagic cell death when overexpressed. Binding of PGAM5 with Keap1 and Bcl-X_L facilitates XIAP-mediated ubiquitination and inhibition. Because XIAP ubiquitinates PGAM5 at a C-terminal lysine residue unique to the long isoform, XIAP fails to protect against toxicity induced by the short PGAM5 isoform. Reciprocally, PGAM5 can prevent XIAP from dimerizing and self-ubiquitinating, which leads to altered XIAP activity. Overexpression of PGAM5 in embryonic fibroblasts demonstrates acute toxicity that is inhibited by XIAP, while long-term overexpression of PGAM5 in surviving cells protects against arsenic trioxide through an XIAP-dependent mechanism. Altogether these data illuminate a novel AIF-PGAM5-XIAP regulatory triad that determines cell fate decisions.

Introduction

The mitochondrial flavoprotein known as AIF is essential for cellular metabolism and the regulation of oxidative stress [25, 51, 52, 205]. In contrast to these pro-survival activities, AIF is additionally involved in cell death when released from the mitochondria [24]. In a caspase-independent manner, liberated AIF translocates to the nucleus where it binds DNA and

associates with other factors (Endonuclease G, H2AX, Cyclophilin A) to form active DNase complexes, inducing chromatin condensation and internucleosomal DNA cleavage [24, 31, 32, 36-43].

AIF-mediated chromatin degradation is inhibited by the multifunctional survival molecule known as XIAP. While serving as a potent suppressor of caspase activation and the execution of apoptosis, XIAP exhibits additional roles in copper homeostasis and the modulation signaling cascades including TGF-β, NF-κB, and JNK [48]. XIAP possesses an E3 ubiquitin ligase activity involved in a variety of activities including the regulation of cell death. Notable death-associated ubiquitination targets of XIAP include XIAP itself, Smac, and AIF [49, 206, 207]. XIAP ubiquitinates AIF at a lysine residue essential for DNA binding, and this ubiquitination event occurs through alternative linkages that do not induce protein degradation [50]. Similar to AIF, the mitochondrial phosphatase PGAM5 is another non-degradative ubiquitination target of XIAP. Interestingly, PGAM5 is an AIF-associated factor [53], suggesting that AIF, PGAM5, and XIAP may form a regulatory axis that mediates decisions of cell fate.

As the name indicates, PGAM5 contains a PGAM domain yet lacks mutase activity. PGAM5 is only distantly related to the phosphoglycerate mutase family, with the characteristic phosphohistidine motif within the PGAM domain poorly conserved in PGAM5 [208]. The closest relatives of PGAM5 are STS-1 and STS-2, which are ubiquitin-binding phosphatases involved in receptor-mediated signaling [209, 210]. Rather than functioning as a mutase, PGAM5 uses the PGAM catalytic region to operate as a phosphatase. While the purpose of PGAM5 phosphatase activity is unclear, PGAM5 has been shown to dephosphorylate ASK1, leading to the activation of JNK and p38 [211], consistent with initially characterized roles for PGAM5 in cell death and oxidative stress responses [212-214].

PGAM5 was first identified as a Bcl-X_L binding partner [214], and the first functional studies of PGAM5 revealed that PGAM5 is a substrate for Keap1-dependent ubiquitination [212]. PGAM5 regulates antioxidant responses within a mitochondrial ternary complex containing Keap1 and Nrf2 (also a Keap1 target), and Keap1-mediated ubiquitination leads to PGAM5 degradation that is inhibited by conditions of oxidative stress.

A number of studies have argued disparate functions for PGAM5 in controlling cell survival, apoptosis, mitophagy, and necroptosis [215-220]. These activities might be reconciled by the physical and functional associations of PGAM5 with AIF and XIAP, all of which can mediate atypical forms of cell death and may comprise a novel regulatory axis determining cell fate. The functional significance of the AIF-PGAM5 interaction remains unclear, and points of regulation within the PGAM5 death pathway have not been identified. Moreover, how XIAP and PGAM5 are associated through ubiquitination and consequences upon cell death and survival may explain different outcomes of PGAM5 activity.

We have identified PGAM5 as a trigger for cell death when overexpressed. PGAM5-induced cell death is associated with mitophagy [53], a mitochondria-specific form of autophagy that normally serves to remove damaged mitochondria, modify mitochondrial abundance in response to metabolic needs, regulate steady-state mitochondrial turnover, and mediate erythrocyte differentiation [221]. Mitophagy is initiated by the stabilization of PINK1, which recruits the E3 ligase Parkin to the mitochondria [222, 223]. Parkin then ubiquitinates mitochondrial proteins leading to the engulfment of mitochondria into isolation membranes that fuse with lysosomes [221]. PGAM5-induced cell death is accompanied by hallmark features of mitophagy including severe structural abnormalities of the mitochondria, loss of mitochondrial membrane potential ($\Delta\Psi_m$), and elevated PINK1 protein levels [53].

In this study we identify a functional role for PGAM5 in protecting AIF from XIAP-mediated inhibition. Further, PGAM5 and XIAP regulate each other with different outcomes depending on cell type and context, likely due to differences in levels and types of non-canonical ubiquitination. Altogether this study identifies a novel PGAM5-XIAP axis and highlights significant roles for PGAM5 and XIAP in control of atypical cell death mechanisms.

Materials and methods

Materials, plasmids and antibodies

DMEM, GlutaMAX, 4–12 % bis-tris polyacrylamide gels, nitrocellulose membranes, fetal bovine serum (FBS), phosphate buffered saline (PBS), Ni-NTA agarose, glutathione agarose, and Pierce ECL 2 Western Blotting Substrate were from Thermo Fisher Scientific; immunoglobulin G-Sepharose was from Amersham; all other materials were from Sigma.

Antibodies were obtained as follows: anti-AIF (Santa Cruz Biotechnology, sc-13116), anti-PINK1 (Cell Signaling, 6946), anti-cleaved caspase-3 (Cell Signaling, 9661), anti-HA (Covance, MMS-101P), anti-Myc (Cell Signaling, 2276), anti-XIAP (Enzo, AAM-050), anti-PGAM5 (Abcam, ab126534), HRP-conjugated anti-HA (Sigma, H6533), HRP-conjugated anti-FLAG (Sigma, F3165), anti-β-actin (Sigma, A5316), HRP-conjugated anti-mouse (Amersham, NA931V), and HRP-conjugated anti-rabbit (Amersham, NA934V).

Plasmids encoding $PGAM5_L$ mutants (pEBB-$PGAM5_L$-K285A-HA, pEBB-$PGAM5_L$-K285R-HA, pEBB-$PGAM5_L$-L135E/G139E-HA, pEBB-$PGAM5_L$-E79A/S80A-HA) were generated by site-directed mutagenesis (Stratagene) using pEBB-$PGAM5_L$-HA as a template. To generate the lentiviral plasmid pSL4-$PGAM5_L$-puro, $PGAM5_L$ cDNA was subcloned from pEBB-$PGAM5_L$ into the pSL4-puro backbone [224]. Additional plasmids were obtained as follows: pLKO.1-shPINK1-puro from Sigma (TRCN0000007101). pLKO.1-puro-scramble [149]

from Dr. David Sabatini (Addgene plasmid #1864); and psPAX2 and pMD2.G-vsv-G from Dr. Didier Trono (Addgene plasmids #12260 and 12259). All remaining plasmids (pEBB-PGAM5$_L$-HA, pEBB-PGAM5$_S$-HA, pEBB-PGAM5$_L$-H105A-HA, pEBG-XIAP, pEBB-FLAG-XIAP, pEBB-FLAG-XIAP-H467A, pCW7 His$_6$-Myc-Ubiquitin WT, K6R, K11R, K27R, K29R, K48R, K63R, pEBB-AIF, pEBB-AIF-FLAG, pEBB-AIF-GST, pcDNA3-Bax, pHCMV-G, pRRE, and pRSV-rev) have been described previously [49, 50, 53, 123].

Cell culture, transfections, and plasmids

HEK293T cells were cultured in DMEM supplemented with 10% FBS supplemented with 2 mM GlutaMAX at 37 °C in an atmosphere of 95% air and 5% CO_2. Wild-type and XIAP-null MEFs are as described [225]. HEK293T cells were transfected using the calcium phosphate precipitation method [53]. Cells were harvested by trypsinization, washed, plated at equal densities, and allowed to attach overnight prior to all assays.

Lentiviral production and stable infection of cell lines

For establishment of cell lines stably suppressing PINK1, pLKO.1-based lentiviruses were generated by transfecting HEK293T cells with pMD.2, psPAX2, and pLKO-shRNA using the calcium phosphate method. Viral supernatant was collected at 48 h and 72 h post-transfection and then filtered using 0.45 μm-pore size Millex HV PVDF filter units. Target cells were then incubated with viral supernatant and 8 μg/mL polybrene for 24 h. Stably infected cells were selected using 1 μg/mL puromycin.

To establish cell lines stably overexpressing PGAM5$_L$, lentiviral particles were produced by transfecting equal amounts of pHCMV-G, pRRE, pRSV-rev, and FG12- or pSL4-derived plasmids into HEK293T cells using the calcium phosphate method. Following incubation at 37 °C for 48 h, supernatants were collected, filtered using 0.45 μm-pore size Millex HV PVDF filter

units (Millipore) and concentrated by centrifugation at 20,000 x g. Viral pellets were then resuspended in PBS at 4 °C overnight. Resuspended virus was added to cells in the presence of 4 μg/mL polybrene for 4 h at 37 °C in an environment of 93% air and 7% CO_2. Stably infected cells were selected using 1 μg/mL puromycin.

Cell lysis, immunoprecipitation, and affinity precipitations

Cell lysates were prepared in radioimmune precipitation assay (RIPA) lysis buffer (PBS containing 1% NP-40, 0.5% sodium deoxycholate, 0.1% SDS, 1 mM dithiothreitol, 1 mM PMSF, 1 mM sodium fluoride, 1 mM sodium orthovanadate, and 1 protease inhibitor mixture tablet per 10 mL) or urea lysis buffer (8 M urea, 300 mM NaCl, 0.5% NP-40, 50 mM Na2HPO4, 50 mM Tris pH 8.0, 1 mM PMSF, 1 ng/mL aprotinin, and 10 ng/mL leupeptin).

For immunoprecipitation experiments, RIPA cell lysates were normalized for protein content and then incubated with indicated antibodies for 2 h at 4 °C. Protein G-coupled agarose beads were then added and incubated for 1 h. Agarose beads were then recovered by centrifugation and washed in RIPA buffer. Precipitated protein was eluted by adding lithium dodecyl sulfate sample buffer followed by heating samples at 95 °C for 5 min. Samples were then analyzed by immunoblot as described below.

For glutathione affinity precipitation experiments, RIPA lysates were normalized for protein content and then incubated with glutathione agarose for 2 h at 4 °C. Agarose beads were then recovered by centrifugation and washed in RIPA buffer. Precipitated protein was eluted by adding lithium dodecyl sulfate sample buffer followed by heating samples at 95 °C for 5 min. Samples were then analyzed by immunoblot as described below.

For nickel affinity precipitation experiments, urea lysates were normalized for protein content and then incubated with Ni-NTA agarose for 2 h at room temperature. Agarose beads

were then recovered by centrifugation and washed in RIPA buffer. Precipitated protein was eluted by adding lithium dodecyl sulfate sample buffer followed by heating samples at 95 °C for 5 min. Samples were then analyzed by immunoblot as described below.

Immunoblot analysis

For immunoblot experiments, protein samples were separated by SDS-PAGE using 4-12% gradient SDS-polyacrylamide gels followed by electrotransfer to nitrocellulose membranes. Membranes were blocked with 5% milk or bovine serum albumin in tris-buffered saline containing 0.02 to 0.2% Tween-20 and then incubated with the indicated primary antibodies. Membranes were then washed three times and incubated with HRP-conjugated anti-mouse or anti-rabbit followed by visualization using enhanced chemiluminescence.

Measurements of mitochondrial $\Delta\Psi_m$

Staining for mitochondrial membrane potential was carried out as described previously [104] by resuspending harvested cells in PBS containing 200 nM TMRM followed by flow cytometry. Cells were then harvested and resuspended in PBS, followed by assessment of stain intensity using an Accuri C6 flow cytometer.

Cell viability

For protein toxicity assays, cells were transfected with either control vectors or the indicated plasmids. For ATO sensitivity experiments, cells were untreated or treated with ATO at 1 μg/mL for 24. Cells were then harvested, washed, and resuspended in PBS containing 2 μg/mL propidium iodide. Cell viability was then determined by flow cytometry using an Accuri C6 flow cytometer.

Results

Association of PGAM5 with AIF protects AIF from XIAP binding and ubiquitination

We have previously identified PGAM5 as an AIF-associated factor involved in cell death [53]. The PGAM5 gene can be transcribed into one of two different mRNA transcripts encoding either a long ($PGAM5_L$) or short ($PGAM5_S$) isoform. $PGAM5_L$ and $PGAM5_S$ proteins are identical from amino acids 1-239, with $PGAM5_L$ containing an additional 50 amino acids and $PGAM5_S$ containing an additional 16 amino acids [212, 214]. Both isoforms of PGAM5 bind AIF and trigger cell death when overexpressed in HEK293T cells. However, $PGAM5_S$ exhibits reduced phosphatase activity and multimerization due to differences between C-terminal amino acid residues [53]. Because functional differences between $PGAM5_L$ and $PGAM5_S$ are unclear, both isoforms were assessed as described below.

Since PGAM5 and XIAP can both bind AIF [49, 53], we questioned if these associations can impact one another or occur independently. To determine how PGAM5 and XIAP affect AIF interactions with the other protein, a binding assay was performed using GST-tagged AIF. AIF-GST was transfected into HEK293T cells with XIAP-FLAG and/or PGAM5-HA. Cell lysates were then subjected to incubation with glutathione-conjugated agarose, which precipitates GST-fused proteins. XIAP and PGAM5 expectedly precipitated with AIF (Figure 8.1), demonstrating physical associations with AIF. Notably, when both XIAP and PGAM5 were co-expressed, only PGAM5 precipitated with AIF regardless of isoform (Figure 8.1). This indicates that PGAM5 is a stronger binding partner for AIF, and that the interaction of PGAM5 with AIF blocks XIAP from binding AIF.

When ubiquitinated by XIAP, AIF fails to induce chromatin degradation during cell death [50]. Since XIAP cannot associate with PGAM5-bound AIF, PGAM5 is likely to prevent

XIAP from ubiquitinating AIF. Therefore to assess the ability of PGAM5 to inhibit XIAP-mediated ubiquitination of AIF, a nickel affinity precipitation assay was used. This assay employs ubiquitin tagged with polyhistidine (polyHis), which exhibits high affinity for nickel. Therefore polyHis-tagged ubiquitin can be precipitated using nickel-conjugated agarose. If polyHis-tagged ubiquitin conjugates with a target protein, then the protein can subsequently be identified in precipitated material, and detection of protein laddering indicates polyubiquitination. When ubiquitinated proteins were precipitated, we observed an increase in AIF ubiquitination with XIAP overexpression (Figure 8.2). Notably, overexpression of either isoform of PGAM5 suppressed XIAP-mediated ubiquitination of AIF. This indicates that binding of either $PGAM5_L$ or $PGAM5_S$ with AIF prevents XIAP from AIF access/inhibition. Therefore through AIF binding, PGAM5 is likely to promote AIF-mediated chromatin degradation [50].

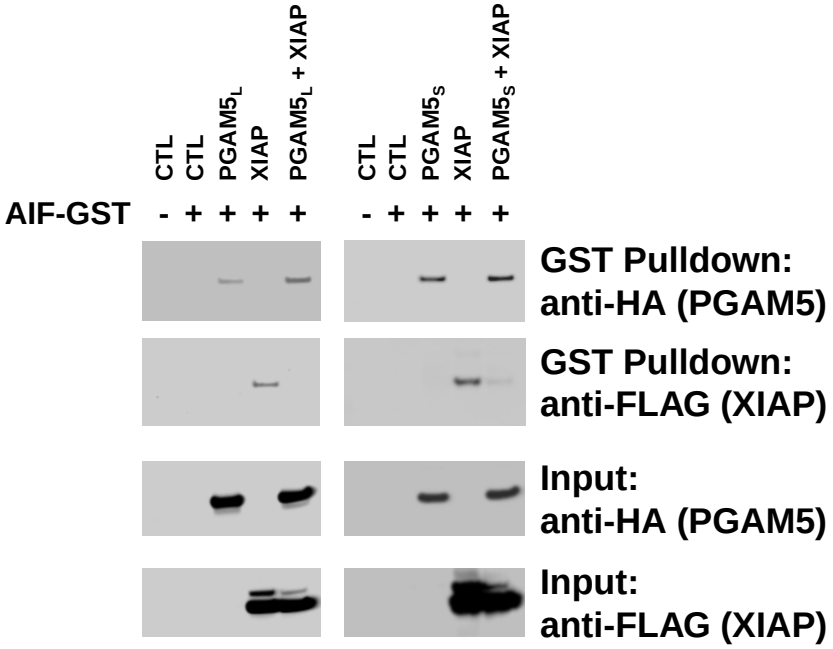

Figure 8.1. Association of PGAM5 with AIF prevents the AIF-XIAP interaction.
HEK293T cells were transfected with the indicated plasmids, lysed, and subjected to GST pulldown and subsequent immunoblots detecting the indicated protein epitope tags.

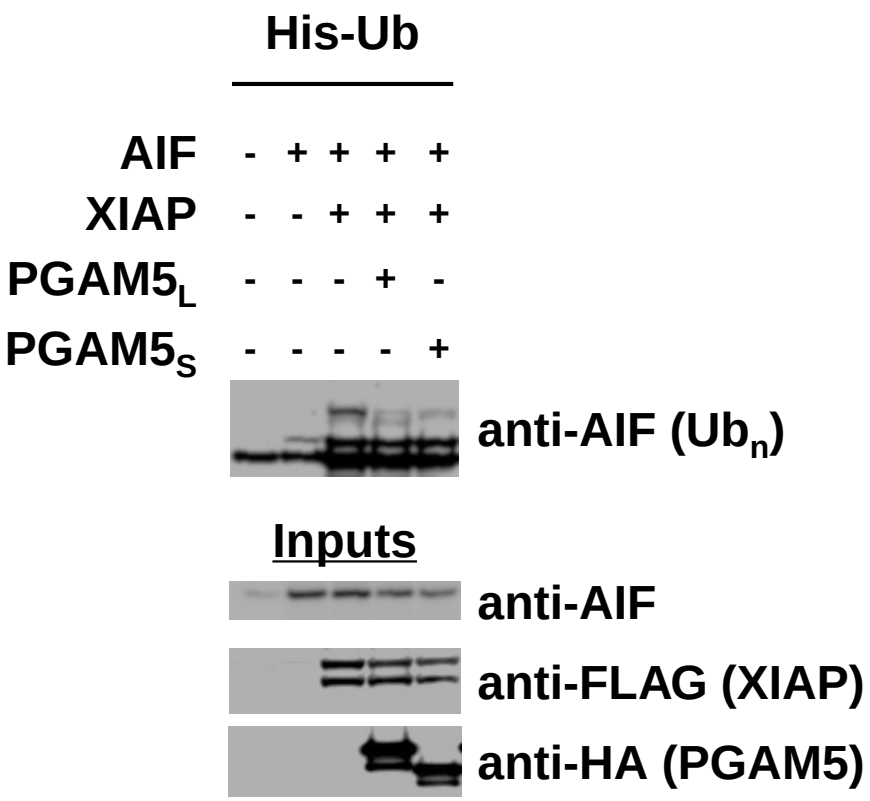

Figure 8.2. PGAM5 prevents XIAP from ubiquitinating AIF.
HEK293T cells were transfected with His-ubiquitin (Ub) and the indicated plasmids. Cells were then lysed, and ubiquitinated proteins were precipitated with Ni-NTA agarose followed by immunoblot.

XIAP prevents $PGAM5_L$ from activating PINK1 and the mitophagic death pathway

The data above show that PGAM5 can protect AIF from XIAP-mediated ubiquitination. Similar to AIF, XIAP is capable of inhibiting PGAM5 through a ubiquitination-dependent mechanism. PGAM5 can also induce cell death independently of AIF [50, 53]. We have shown previously that $PGAM5_L$ toxicity is inhibited by the ubiquitin ligase activity of XIAP, but the mechanism(s) through which XIAP inhibits PGAM5 and the stages of the death pathway involved remain undefined. PGAM5 induces mitochondrial outer membrane permeabilization (MOMP), severe mitochondrial structural abnormalities, PINK1 stabilization, and caspase

activation. In an effort to define the sequence of events within this mitophagic death pathway and to determine the points of regulation controlled by XIAP [53], HEK293T cells were transfected with PGAM5 isoforms in the absence or presence of XIAP followed by assessment of biochemical cell death signals. Cells were first assessed for mitochondrial membrane potential ($\Delta\Psi_m$), a negative indicator of MOMP, by staining with tetramethylrhodamine ester (TMRM). When TMRM stain intensities were measured by flow cytometry, substantial decreases in cell populations with high $\Delta\Psi_m$ were observed following PGAM5 overexpression that were comparable to those associated with elevated Bax levels (Figure 8.3A). Decreased $\Delta\Psi_m$ induced by $PGAM5_L$ was reversed by the introduction of XIAP, whereas $\Delta\Psi_m$ loss triggered by $PGAM5_S$ was unaffected (Figure 8.3B). This agrees with previous data [53] showing that XIAP ubiquitinates and inhibits only the long isoform of PGAM5, indicating that XIAP prevents $PGAM5_L$ from depolarizing mitochondria.

Mitochondrial dysfunction often leads to MOMP and subsequent induction of PINK1, which is also an effect of PGAM5 overexpression. To determine if XIAP affects PGAM5-mediated PINK1 signaling, lysates of cells transfected with HA-tagged PGAM5 and FLAG-tagged XIAP were subjected to immunoblot for PINK1. Similar to observations that XIAP inhibits $PGAM5_L$-mediated MOMP and cell death, XIAP suppressed PINK1 induced by $PGAM5_L$, and $PGAM5_S$-induced PINK1 was unaffected (Figure 8.3C).

Induction of PINK1 is required for PGAM5 to kill cells

Since XIAP prevents $PGAM5_L$ from stabilizing PINK1, we then questioned if suppression of PINK1 is a mechanism by which XIAP protects cells. Under normal cellular conditions PINK1 is perpetually degraded but is stabilized under stress stimuli (*e.g.*, $\Delta\Psi_m$ loss),

leading to the phosphorylation of Parkin and subsequent recruitment of mitophagic machinery that induce mitochondrial degradation via autolysosomes [221]. PGAM5 is a significant stimulus

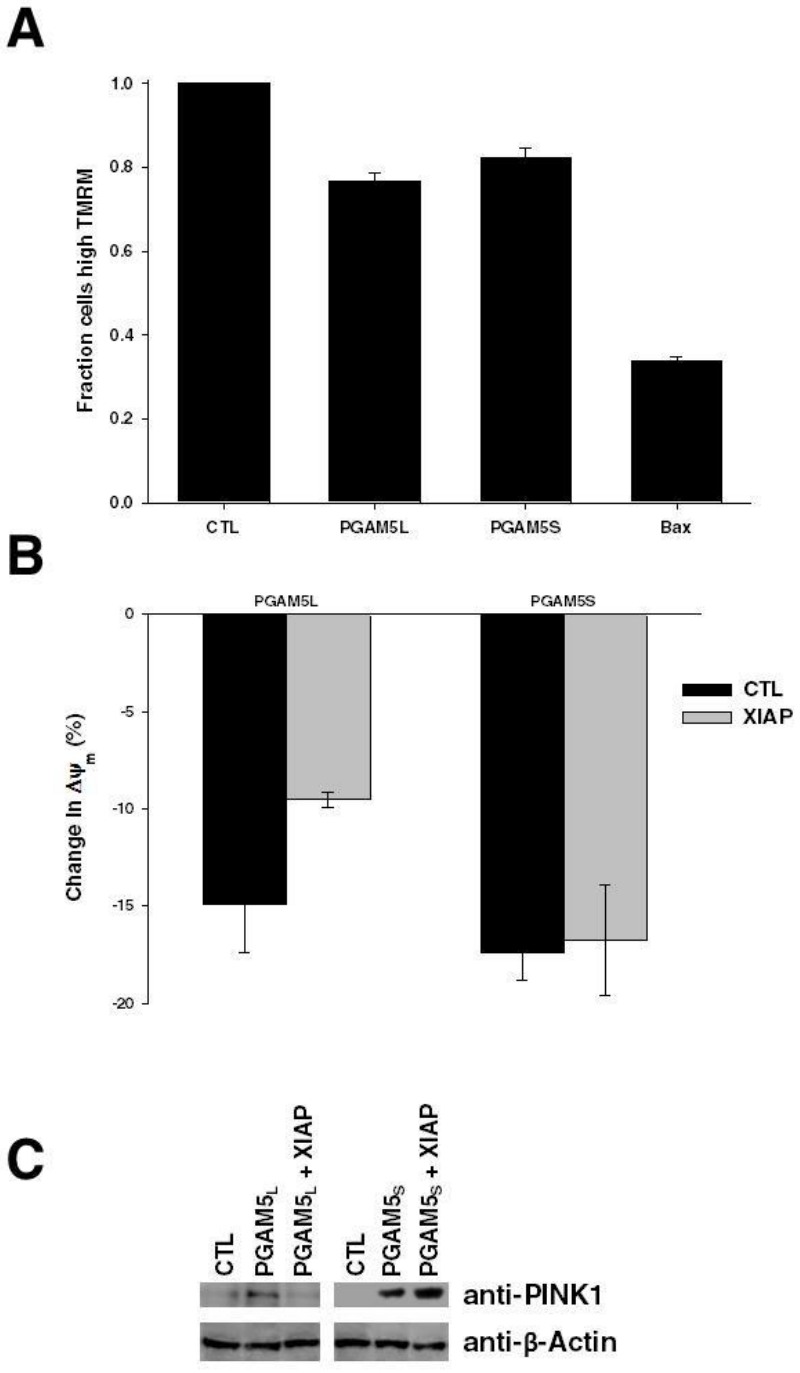

Figure 8.3. XIAP prevents $PGAM_L$ from inducing MOMP and PINK1.
A, B) HEK293T cells were transfected with the indicated plasmids, stained with TMRM, and then assessed by flow cytometry. Data are presented as average ± standard deviation. C) PINK1 levels were assessed by immunoblot in HEK293T cells transfected with the indicated plasmids.

for mitophagic cell death, and the observation that PGAM5 induces PINK1 [53] leads to a significant open question: in the context of PGAM5 does mitophagy accompany cell death, or does PGAM5-induced mitophagy directly cause cell death? To address this question, we sought to suppress PINK1 and impair the cell's ability to trigger the series of molecular events signaling for mitophagy.

Lentiviruses harboring either control nonspecific shRNA (shCTL) or shRNA targeting PINK1 (shPINK1) were generated and then used to stably infect HEK293T cells. Following selection with puromycin, cells were transfected with either $PGAM5_L$ or $PGAM5_S$. Stable knockdown of PINK1 was then verified by immunoblot analysis, which demonstrated PINK1 induction 48 h following PGAM5 transfection in control cells but not shPINK1 cells (Figure 8.4A).

To test the hypothesis that PINK1 functions within the PGAM5 death pathway, lysates were probed for caspase-3, an executioner protease activated by cleavage and functioning at the end of cell death signal cascades. Cleavage of caspase-3 was observed when either PGAM5 isoform was introduced to control cells but not PINK1-deficient cells (Figure 8.4A). This suggests that when PGAM5 is overexpressed, PINK1 induction is required for caspase activation, therefore implicating PINK1 as a potential death molecule.

In order to determine if PINK1 is required for PGAM5-mediated cell death, shCTL and shPINK1 cells were transfected with PGAM5, and after 48 h harvested and stained with propidium iodide followed by viability measurements using flow cytometry. While both $PGAM5_L$ and $PGAM5_S$ exhibited substantial toxicity in control cells, PINK1-deficient cells were resistant to PGAM5 toxicity, showing viability levels essentially unchanged relative to control (empty) transfected cells (Figure 8.4B). This confirms that PINK1 is required for death when

induced by PGAM5, suggesting mitophagy is the cause of PGAM5 toxicity and demonstrating a mechanism by which PGAM5 triggers cell death.

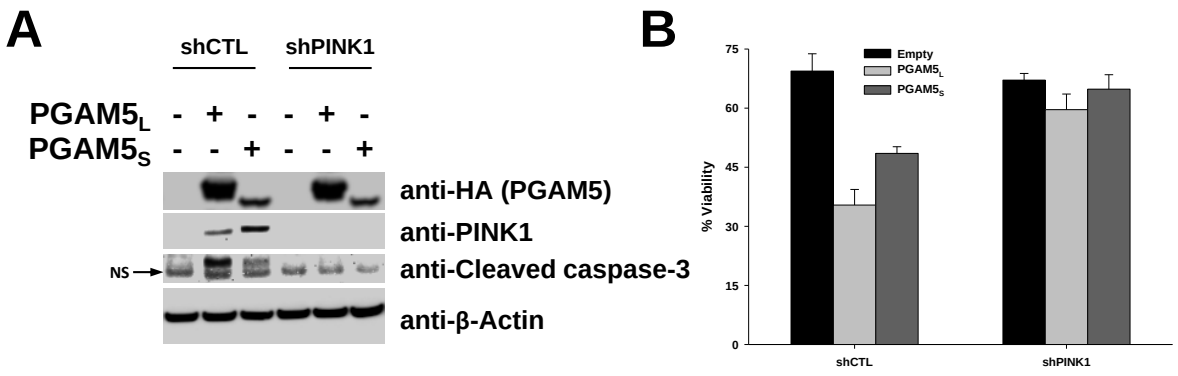

Figure 8.4. Both isoforms of PGAM5 trigger cell death by activating PINK1.
A) HEK293T cells stably infected with either control shCTL sequences or shPINK1 were transfected with the indicated plasmids followed by immunoblot with the indicated antibodies. NS, nonspecific signal. B) Cells were stained with PI and then assessed for viability levels by flow cytometry. Data are presented as average ± standard deviation.

XIAP interacts with PGAM5 and triggers non-productive hetero-oligomerization

The data above demonstrate that XIAP prevents $PGAM5_L$ from activating cell death signals (Figure 8.3) and inducing cellular toxicity. This XIAP-mediated inhibition of $PGAM5_L$ occurs via XIAP E3 ligase activity that ubiquitinates $PGAM5_L$ [53]. If XIAP directly ubiquitinates PGAM5, an association between the two would be required for XIAP to access the ubiquitination target residue(s) of PGAM5. Notably, XIAP has not been demonstrated to affect the short isoform in any assays assessed here or previously [53]. This suggests that only the long isoform is a target for ubiquitination by XIAP and may explain why XIAP inhibits only $PGAM5_L$.

To determine if XIAP can bind either PGAM5 isoform, cells were transfected with PGAM5 isoforms and/or XIAP, followed by coimmunoprecipitation using an anti-HA (PGAM5) antibody and subsequent evaluation of FLAG epitope (XIAP) levels. $PGAM5_L$ precipitated with

XIAP (Fig 8.5A), suggesting a physical association between the two proteins and further supporting a role for XIAP as an E3 ligase for $PGAM5_L$. Following precipitation of $PGAM5_S$, XIAP was not detected. However, due to the nature of this assay the possibility of a $PGAM5_S$-XIAP interaction cannot be ruled out. The hydrophobic character of the C-terminal tail of $PGAM5_S$ reduces extraction levels (Figure 8.5A) from the mitochondrial membrane [53], and use of stronger lysis buffers is likely to disrupt protein interactions with $PGAM5_S$. Since XIAP neither causes ubiquitination of $PGAM5_S$ nor inhibits $PGAM5_S$-mediated toxicity, either XIAP does not bind $PGAM5_S$, or binding does not affect $PGAM5_S$ signaling capacity.

XIAP appears to inhibit the long but not short isoform of PGAM5. Interestingly, we and others have previously reported that only the long isoform forms homodimers and/or higher order oligomers, corresponding to phosphatase activity levels present in $PGAM5_L$ but deficient in $PGAM5_S$ [53, 226] and demonstrating further isoform-specific differences that may be differentially regulated by XIAP. Recent biophysical studies have defined multimeric assembly mechanisms for $PGAM5_L$ [227, 228], which explain the absence of oligomer formation and phosphatase activity in the short isoform of PGAM5. Within $PGAM5_L$, the C-terminal tail (different in $PGAM5_S$) stabilizes dimer formation, and six PGAM5 dimers subsequently multimerize into a dodecameric ring. Dodecamerization then allosterically activates the phosphatase by promoting an ordering of the catalytic loop [227]. PGAM5 dodecameric rings can polymerize into filamentous structures within cells [228], similar other death effectors including DISCs [229] and necrosomes [230]. PGAM5 polymerization does not affect phosphatase activity but appears to play a structural role on mitochondrial membranes [228].

Based on the exclusivity of $PGAM5_L$ oligomerization and inhibition by XIAP, we hypothesized that XIAP might impact the multimeric state of $PGAM5_L$. To test this hypothesis

cells were transfected with PGAM5 plasmids containing separate epitope tags as follows: $PGAM5_L$-FLAG + $PGAM5_S$-HA, $PGAM5_L$-FLAG + $PGAM5_L$-HA, and $PGAM5_S$-FLAG + $PGAM5_S$-HA, with all pairs in the absence or presence of untagged XIAP. Coimmunoprecipitation with a FLAG antibody followed by immunoblot for the HA epitope can therefore be used to determine if PGAM5 interacts with other PGAM5 molecules. As shown in Figure 8.5B, $PGAM5_L$ exhibited robust oligomerization, whereas $PGAM5_S$ showed no self-interaction, in agreement with previous work [53]. Overexpression of XIAP did not influence homo-oligomerization of either isoform (Figure 8.5B). However, XIAP strongly enhanced hetero-oligomerization of $PGAM5_L$ with $PGAM5_S$ (Fig 8.5B). Since $PGAM5_S$ lacks the capacity for self-association, it is possible that XIAP-mediated ubiquitination of $PGAM5_L$ could increase $PGAM5_S$ affinity, leading to the formation of a nonproductive hetero-oligomer and therefore inhibiting $PGAM5_L$.

Because the significance of $PGAM_L$-$PGAM5_S$ binding is unknown, we assessed mitophagy and cell death as markers of PGAM5 activity following co-transfection with both PGAM5 isoforms. Interestingly, while both isoforms trigger PINK1 stabilization, PINK1 was not induced when $PGAM5_L$ and $PGAM5_S$ were overexpressed together (Figure 8.5C). Since PINK1 triggers cell death when PGAM5 is overexpressed, cells were then assessed for death levels. In agreement with an inability of PGAM5 to induce PINK1 when both isoforms were co-expressed, cells did not exhibit toxicity in the presence of both isoforms despite the ability of each isoform to kill on its own (Figure 8.5D). Altogether these data suggest that hetero-oligomerization of $PGAM5_L$ with $PGAM5_S$ causes neutralization of both isoforms. Since XIAP promotes this interaction, this could provide further insight into how XIAP can inhibit PGAM5-mediated cell death.

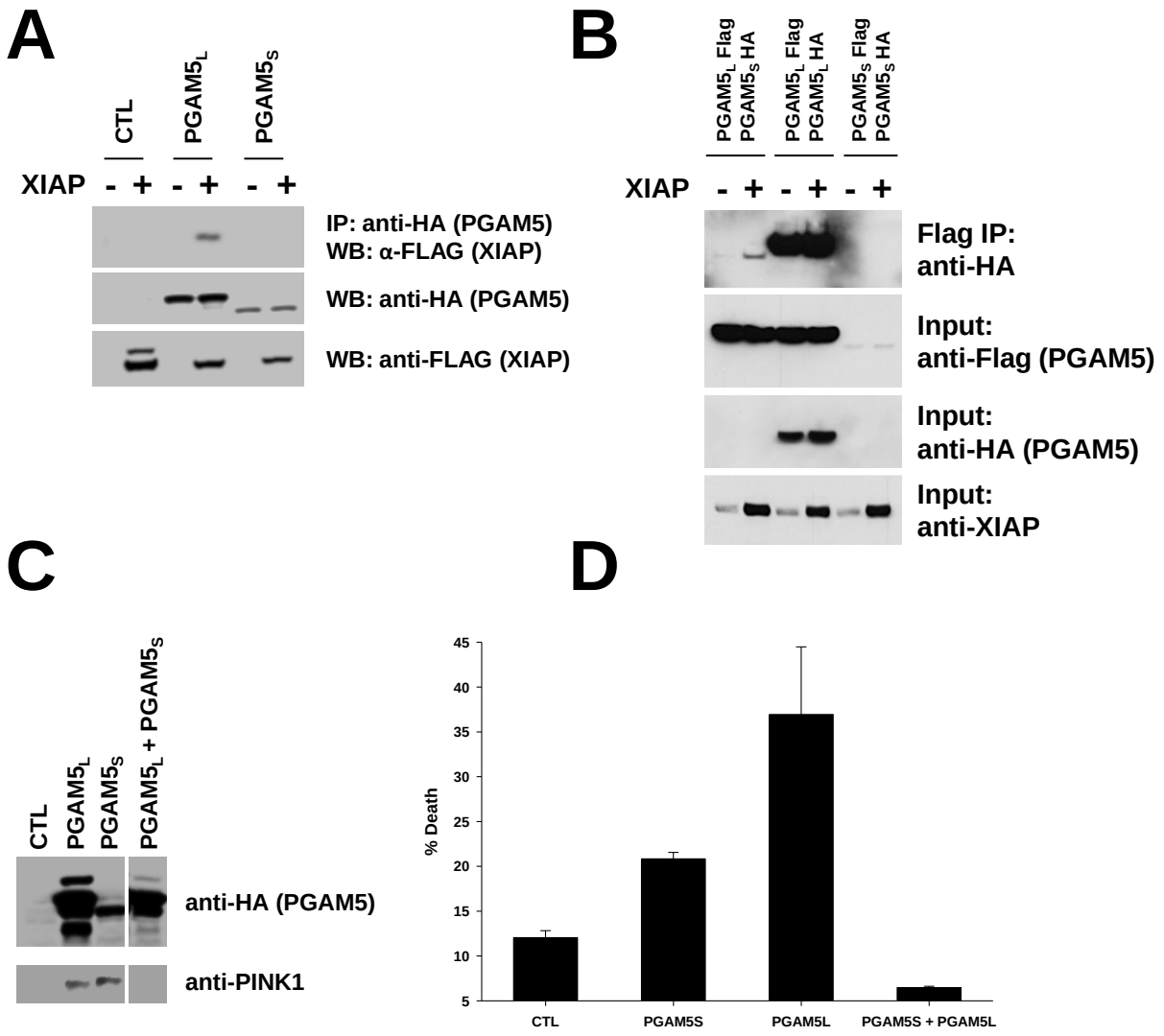

Figure 8.5. XIAP binds $PGAM5_L$ and promotes non-productive hetero-oligomerization with $PGAM5_S$.

A, B) HEK293T cells were transfected with the indicated plasmids, lysed, and subjected to co-immunoprecipitation assay and immunoblot with the indicated antibodies. Data for panel b were acquired by A.S. Wilkinson. C) PINK1 levels were assessed by immunoblot of HEK293T cells transfected with the indicated plasmids. D) HEK293T cells were transfected with indicated plasmids followed by PI staining and flow cytometry. Data are presented as average ± standard deviation.

XIAP ubiquitinates $PGAM5_L$ at lysine residue 285 via a noncanonical linkage

Collectively the data so far have shown that XIAP suppresses the long isoform of PGAM5 through ubiquitin modification. Ubiquitin is a 76-amino acid protein highly conserved across species and used by cells to post-translationally modify proteins. Proteins can be either mono- or polyubiquitinated, with polyubiquitination occurring through the attachment of additional ubiquitin molecules at different lysine residues. Ubiquitin contains 7 lysines (K6, K11, K27, K29, K33, K48, K63), all capable of forming covalent bonds with other ubiquitin units, and methionine residue 1 (M1) can additionally be used for ubiquitin modification.

The well-studied canonical ubiquitination mechanism involves covalent attachment of ubiquitin resides to lysine units of target proteins, and extension of polyubiquitin chains occurring via linkages at lysine 48 (K48) of ubiquitin residues. K48-linked ubiquitination is a common signal for proteasomal recognition and subsequent degradation. However, a variety of alternative linkages and functions have been identified [231]. A notable example is the case of XIAP-mediated ubiquitination of AIF. XIAP binds and ubiquitinates AIF at residue K255, which is required for DNA binding. Notably, this ubiquitin modification is not K48-linked and does not target AIF to the proteasome. Rather, XIAP-mediated ubiquitination of AIF occurs through a non-canonical linkage (probably K27, K33, or M1), and ubiquitination of AIF at K255 prevents DNA binding. As a result of this modification, AIF is inhibited from inducing chromatin degradation when involved in cell death [50].

$PGAM5_L$ toxicity is suppressed by the ubiquitin ligase activity of XIAP, and XIAP-mediated ubiquitination of $PGAM5_L$ occurs via a non-degradative mechanism [53]. The ability of XIAP to modify activity of the PGAM5 binding partner AIF through non-canonical ubiquitination led us to question how XIAP modifies PGAM5. In order to identify ubiquitin

residues important for XIAP-mediated ubiquitination of PGAM5, cells were transfected with $PGAM5_L$, XIAP, and either wild-type (WT) ubiquitin or one of six different ubiquitin point mutants (K6R, K11R, K27R, K29R, K48R, K63R) tagged with polyHis. The indicated lysine to arginine point mutations retain a positive charge are but incapable of conjugation with other ubiquitin molecules. Transfected cells were lysed and subjected to nickel affinity precipitation, followed by assessment of $PGAM5_L$ ubiquitination by immunoblot. When compared to WT-ubiquitin, $PGAM5_L$ was modified by XIAP to similar levels when K48R-ubiquitin was used (Figure 8.6). This suggests that $PGAM5_L$ is not significantly modified by canonical K48-linked ubiquitination. Similar levels of ubiquitination were also observed with K6R-, K11R-, and K63R-ubiquitin (Figure 8.6). Interestingly, XIAP failed to modify $PGAM5_L$ with K27R-ubiquitin or K29R-ubiquitin (Figure 8.6). While K27R-ubiquitin failed to conjugate with $PGAM5_L$, it is possible this occurs as a result of structural destabilization of ubiquitin [50]. However, data here suggest that XIAP ubiquitinates $PGAM5_L$ via alternative linkage(s) that may include K27 and/or K29. Altogether these data narrow the range of possible XIAP-mediated ubiquitination mechanisms for $PGAM5_L$ and add to the list of non-canonical XIAP activities.

Having shown that XIAP ubiquitinates $PGAM5_L$ via an alternative linkage, we next questioned the site of ubiquitination within $PGAM5_L$. Both the long and short PGAM5 isoforms exhibit high basal levels of ubiquitination, but only $PGAM5_L$ is ubiquitinated by XIAP [53]. The observation that XIAP does not ubiquitinate $PGAM5_S$ prompted us to hypothesize that XIAP ubiquitinates $PGAM5_L$ at a long isoform-specific position. $PGAM5_L$ and $PGAM5_S$ are identical in sequence from residues 1-239, with $PGAM5_L$ containing an additional 50 C-terminal residues and $PGAM5_S$ containing an additional 16 C-terminal residues. Assessment of PGAM5 primary structures revealed 10 lysine residues shared by both isoforms, and 1 lysine residue (K285)

unique to $PGAM5_L$ located within the C-terminal tail (Figure 8.7). To test the hypothesis that XIAP ubiquitinates $PGAM5_L$ at K285, nickel pulldown assays were performed using $PGAM5_L$ K285 mutants. Residue K285 of $PGAM5_L$ was mutated either to alanine (A) or arginine (R), with the K285A abolishing potential ubiquitin modifications and K285R retaining positive charge, allowing us to determine if either ubiquitination or electrostatic properties are involved with PGAM5 activity. Nickel pulldown assay revealed that XIAP increases ubiquitination of WT-$PGAM5_L$, but does not affect ubiquitination of either $PGAM5_L$ K285 mutant (Figure 8.8A). Notably, extensive ubiquitination of PGAM5 occurs for both WT and K285 mutants of $PGAM5_L$, suggesting other ubiquitination sites exist within PGAM5 that may not be XIAP targets. Altogether these data indicate that XIAP ubiquitinates $PGAM5_L$ at residue K285.

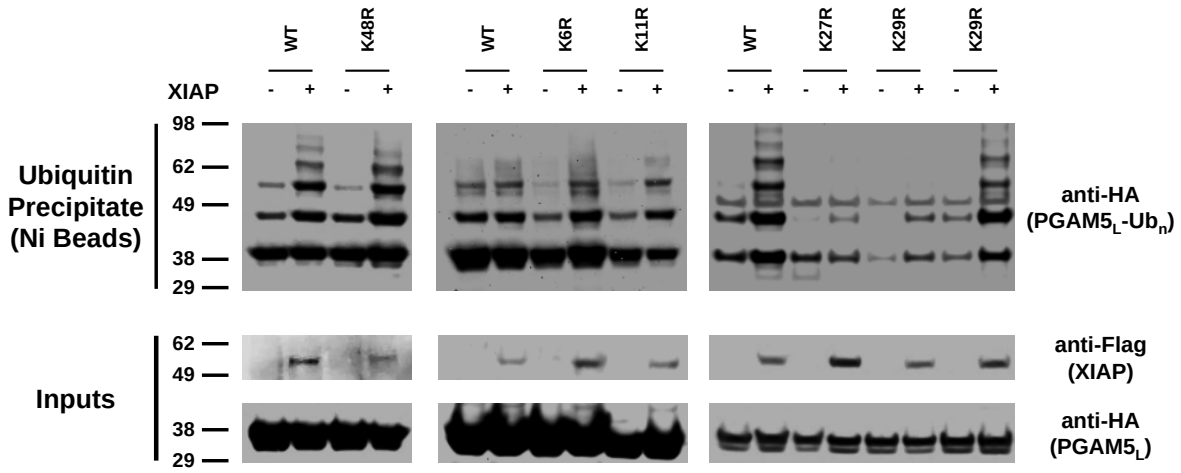

Figure 8.6. XIAP ubiquitinates $PGAM5_L$ via non-canonical linkage(s).
HEK293T cells were transfected with $PGAM5_L$-HA and polyHis-Ub variants in the absence or presence of XIAP and then subjected to precipitation with Ni-NTA agarose followed by immunoblot.

XIAP ubiquitinates $PGAM5_L$ and inhibits $PGAM5_L$-mediated cell death via its ubiquitin ligase activity. Since this modification occurs at residue K285, we then questioned if XIAP would fail to prevent $PGAM5_L$ toxicity induced by $PGAM5_L$ K285 mutants. Cells were therefore

transfected with either WT-PGAM5$_L$, K285A-PGAM5$_L$, or K285R-PGAM5$_L$ in the absence or presence of exogenous XIAP, followed by assessment cell death using propidium iodide staining. Both PGAM5$_L$ mutants exhibited toxicity levels comparable to WT-PGAM5$_L$ (Figure 8.8B). Interestingly, both PGAM5$_L$ K285A and K285R retained capacity to be inhibited by XIAP, suggesting XIAP is capable of suppressing PGAM5$_L$ through other mechanisms, and/or additional factors are involved.

```
                  10         20         30         40         50
PGAM5_L    MAFRQALQLA ACGLAGGSAA VLFSAVAVGK PRAGGDAEPR PAEPPAWAGG
PGAM5_S    MAFRQALQLA ACGLAGGSAA VLFSAVAVGK PRAGGDAEPR PAEPPAWAGG

                  60         70         80         90         100
PGAM5_L    ARPGPGVWDP NWDRREPLSL INVRKRNVES GEEELASKLD HYKAKATRHI
PGAM5_S    ARPGPGVWDP NWDRREPLSL INVRKRNVES GEEELASKLD HYKAKATRHI

                  110        120        130        140        150
PGAM5_L    FLIRHSQYHV DGSLEKDRTL TPLGREQAEL TGLRLASLGL KFNKIVHSSM
PGAM5_S    FLIRHSQYHV DGSLEKDRTL TPLGREQAEL TGLRLASLGL KFNKIVHSSM

                  160        170        180        190        200
PGAM5_L    TRAIETTDII SRHLPGVCKV STDLLREGAP IEPDPPVSHW KPEAVQYYED
PGAM5_S    TRAIETTDII SRHLPGVCKV STDLLREGAP IEPDPPVSHW KPEAVQYYED

                  210        220        230        240        250
PGAM5_L    GARIEAAFRN YIHRADARQE EDSYEIFICH ANVIRYIVCR ALQFPPEGWL
PGAM5_S    GARIEAAFRN YIHRADARQE EDSYEIFICH ANVIRYIVCS IPPLLSAGDF

                  260        270        280
                                        ↓
PGAM5_L    RLSLNNGSIT HLVIRPNGRV ALRTLGDTGF MPPDKITRS
PGAM5_S    VLLGS
```

Figure 8.7. Sequences of PGAM5$_L$ and PGAM5$_S$.
Primary structures of PGAM5 isoforms are shown with lysine residues underlined. Residues unique to PGAM5$_S$ are italicized. Arrow denotes the lysine residue unique to PGAM5$_L$.

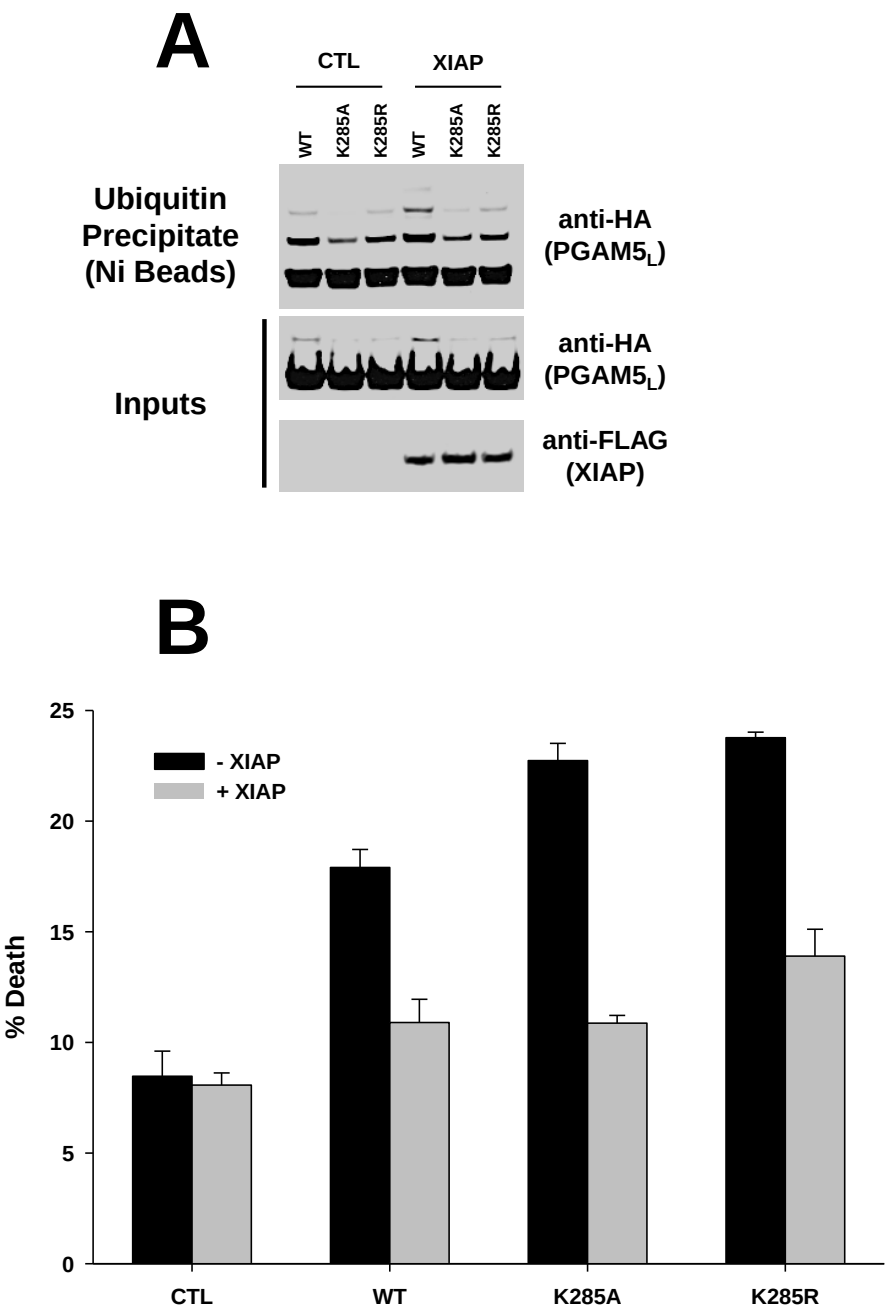

Figure 8.8. XIAP ubiquitinates PGAM5$_L$ at residue K285.
A) HEK293T cells were transfected with polyHis-Ub and PGAM5$_L$ variants in the absence or presence of XIAP, lysed, and incubated with Ni-NTA agarose followed by immunoblot analysis. B) HEK293T cells transfected with PGAM5$_L$ variants in the absence or presence of XIAP were stained with PI and assessed by flow cytometry. Data are presented as average ± standard deviation.

XIAP-mediated ubiquitination and inhibition of PGAM5 is facilitated through binding of PGAM5 to Keap1 and Bcl-X_L

In an effort to understand why blocking XIAP-mediated ubiquitination does not affect the ability of XIAP to rescue cells from PGAM5 toxicity, we then questioned the involvement of other factors that may regulate PGAM5 activity. Since the abilities of PGAM5 to bind Keap1 and Bcl-X_L are known to regulate ubiquitination and cell death [212, 213, 232], the roles of Keap1 and Bcl-X_L in XIAP-dependent suppression of PGAM5 were assessed. Therefore $PGAM5_L$ binding mutants were generated: mutation of residues E79 and S80 to alanine (E79A/S80A) within the Keap1 binding motif impairs Keap1 binding, and mutation of residues L135 and G139 to glutamate (L135E/G139E) within a BH3-like motif impairs Bcl-X_L binding [213].

To determine if Keap1 and/or Bcl-X_L binding affect the affinity of $PGAM5_L$ for XIAP, $PGAM5_L$ mutants were transfected into HEK293T cells in the absence or presence of GST-tagged XIAP followed by precipitation with glutathione-conjugated agarose beads. XIAP precipitated $PGAM5_L$ L135E/G139E, but not $PGAM5_L$ E79A/S80A (Figure 8.9A), suggesting that $PGAM5_L$ must bind Bcl-X_L in order to become physically accessible to XIAP. This observation agrees with the well-established pro-survival role for Bcl-X_L and indicates Bcl-X_L might promote survival by facilitating XIAP-dependent inhibition of PGAM5.

In order to evaluate the significance of Bcl-X_L and Keap1 binding to XIAP-mediated ubiquitination of $PGAM5_L$, $PGAM5_L$ mutants were then transfected into cells in the absence or presence of XIAP with polyHis-ubiquitin followed by nickel pulldown assay. Since Bcl-X_L binding is required for XIAP to bind $PGAM5_L$, the L135E/G139E $PGAM5_L$ mutant expectedly exhibited low ubiquitination levels despite XIAP overexpression (Figure 8.9B). Strikingly,

impairment of $PGAM5_L$ binding with Keap1 additionally suppressed the ability of XIAP to ubiquitinate $PGAM5_L$ (Figure 8.9B). This indicates that association of PGAM5 with Bcl-X_L and Keap1 is required for XIAP to ubiquitinate PGAM5. It is likely that Bcl-X_L stabilizes the XIAP-$PGAM5_L$ interaction, and binding of $PGAM5_L$ with Keap1 (notably an adaptor for protein ubiquitination) is required for XIAP to ubiquitinate $PGAM5_L$.

Having found that $PGAM5_L$ interactions with Keap1 and Bcl-X_L are required for XIAP to ubiquitinate $PGAM5_L$, we then tested the ability of XIAP to inhibit $PGAM5_L$-dependent cell death when Keap1 and Bcl-x_L binding to $PGAM5_L$ are impaired. Cells were transfected with PGAM5 mutants and/or XIAP, followed by viability measurements. In agreement with the observations that XIAP does not ubiquitinate PGAM5L E79A/S80A or $PGAM5_L$ G135E/L139E, XIAP similarly failed to prevent these mutants from inducing toxicity (Figure 8.9C). Overall these data suggest that endogenous Keap1 and Bcl-x_L inhibit $PGAM5_L$ through binding and facilitating ubiquitination by XIAP. Additionally, since mutating the ubiquitation target lysine 285 of $PGAM5_L$ does not affect the ability of XIAP to suppress cell death, it appears that $PGAM5_L$ associations with Keap1 and Bcl-X_L, as well as $PGAM5_L$ ubiquitination by XIAP, are simultaneous requirements for XIAP to block $PGAM5_L$ death induction.

PGAM5 phosphatase activity confers resistance to XIAP

The above data indicate that binding of PGAM5 with Keap1 and Bcl-X_L do not affect the ability of PGAM5 to kill, but are required for XIAP-mediated inhibition of $PGAM5_L$. Since we have also observed that the phosphatase activity of PGAM5 is not essential for toxicity, we questioned if $PGAM5_L$ phosphatase activity exhibits an involvement with XIAP, similar to Keap1/Bcl-X_L binding.

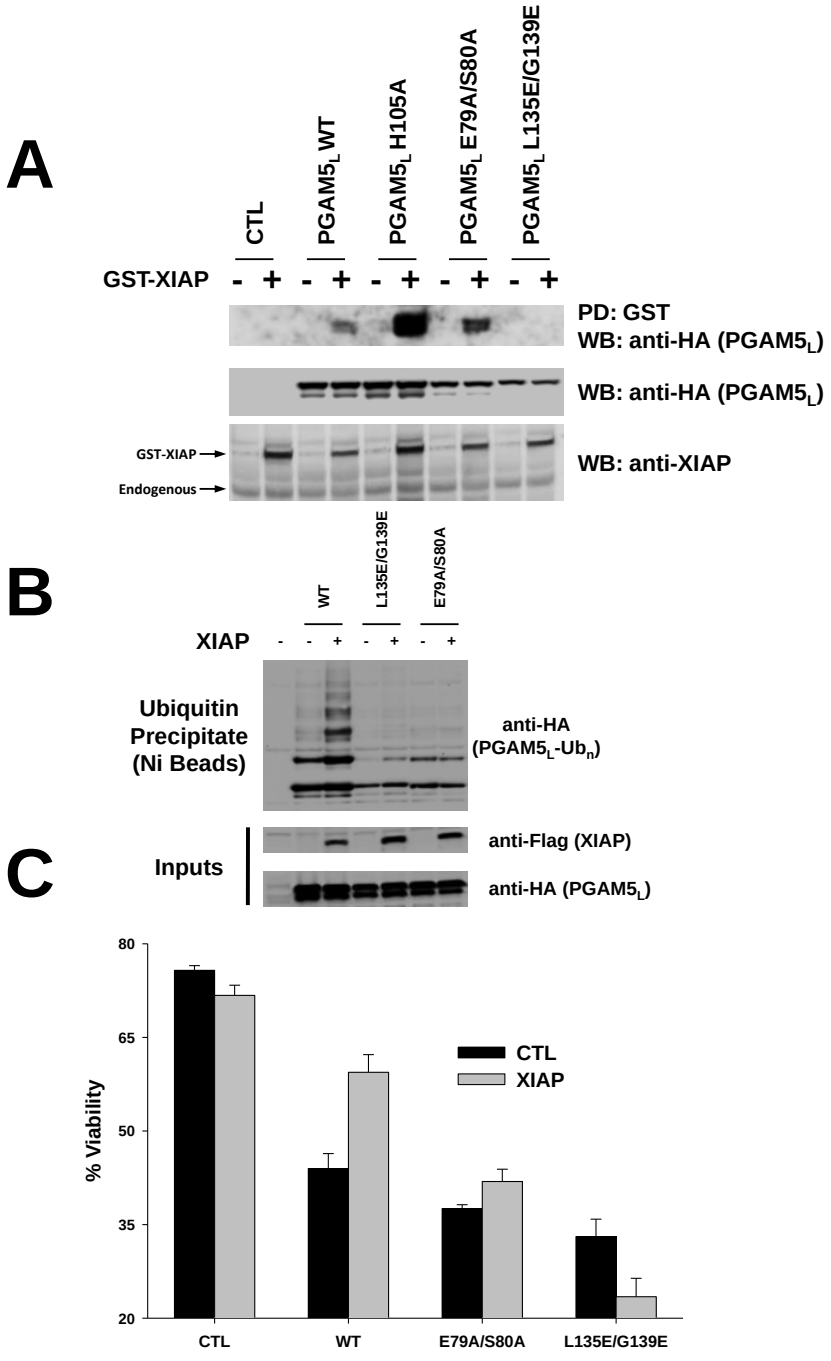

Figure 8.9. XIAP-mediated inhibition of $PGAM5_L$ requires $PGAM5_L$ binding with Keap1 and Bcl-X_L .

A) HEK293T cells were transfected with the indicated plasmids , lysed, and incubated with glutathione-agarose followed by immunoblot. B) HEK293T cells were transfected with polyHis-Ub and $PGAM5_L$ variants in the absence or presence of XIAP and subjected to affinity precipitation using Ni-NTA agarose followed by immunoblot. C) HEK293T cells transfected with $PGAM5_L$ variants in the absence or presence of XIAP were stained with PI and assessed by flow cytometry. Data are presented as average ± standard deviation.

Mutation of H105 to alanine within the PGAM domain of PGAM5 renders the protein catalytically inactive [211], and the PGAM5 H105A mutant can therefore be used to assess the role of PGAM5 phosphatase activity upon XIAP-regulated cell death. Interestingly, co-precipitation of $PGAM5_L$ with XIAP revealed substantially increased XIAP binding when PGAM5 phosphatase activity was abolished (Figure 8.9A), suggesting that the phosphatase activity of PGAM5 inhibits association with XIAP. Based on this observation, we then questioned if $PGAM5_L$ H105A exhibits altered XIAP-dependent ubiquitination due to increased binding. To test this hypothesis polyHis-tagged ubiquitin was precipitated with Ni-NTA agarose following co-transfection with $PGAM5_L$ H105A and XIAP. When compared with WT-$PGAM5_L$, the $PGAM5_L$ phosphatase mutant displayed strongly increased levels of ubiquitination both under basal conditions and following overexpression of XIAP (Figure 8.10A). Altogether these data suggest that the phosphatase activity of PGAM5 blocks interaction with XIAP, conferring resistance to XIAP-mediated ubiquitination.

$PGAM5_L$ H105A is more susceptible to XIAP binding and ubiquitination that WT-$PGAM5_L$, prompting the hypothesis that $PGAM5_L$ phosphatase activity regulates the ability of XIAP to block cell death. Cells transfected with $PGAM5_L$ variants and/or XIAP were subjected to propidium iodide staining and flow cytometry, followed by evaluation of extents of XIAP-mediated rescue from cell death. In agreement with an increased ability of XIAP to bind and ubiquitinate $PGAM5_L$ H105A, XIAP protected cells at magnitudes of >1.5x more than WT-$PGAM5_L$ (Figure 8.10B) despite equivalent levels of protein overexpression (data not shown). Collectively these data suggest that PGAM5 can trigger cell death in part through phosphatase-mediated neutralization of XIAP.

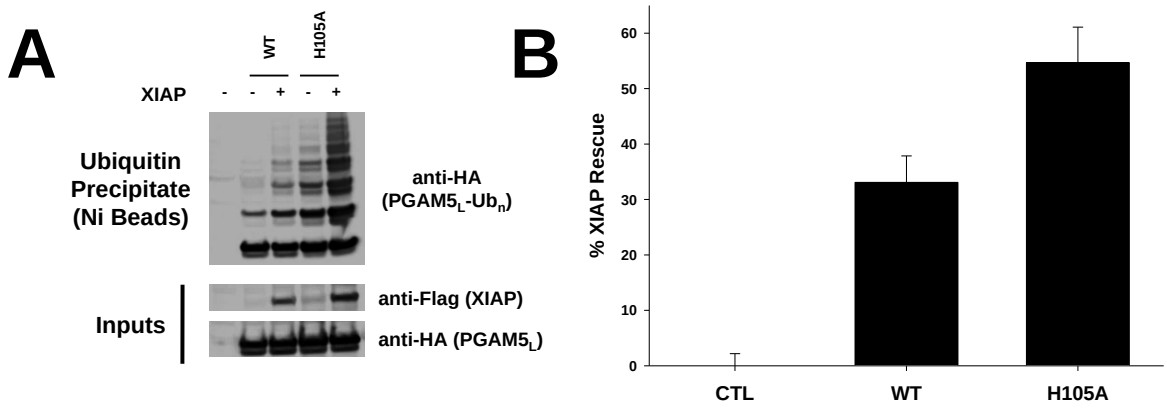

Figure 8.10. The phosphatase activity of PGAM5$_L$ protects against XIAP ubiquitination and inhibition.
A) HEK293T cells were transfected with polyHis-Ub and PGAM5$_L$ variants in the absence or presence of XIAP, lysed, and subjected to Ni affinity precipitation followed by immunoblot. B) HEK293T cells were transfected with PGAM5$_L$ variants in the absence or presence of XIAP followed by PI staining and flow cytometry. Percent rescue is defined by the percent difference in viability between PGAM5+XIAP and PGAM5 only. Data are presented as average ± standard deviation.

XIAP autoubiquitinates via non-canonical mixed linkages

PGAM5 prevents XIAP from protecting cells, but how XIAP activity is suppressed by PGAM5 remains unclear. One possibility is that PGAM5 inhibits XIAP auto-ubiquitination, a self-regulatory mechanism leading to degradation [48, 206]. XIAP self-ubiquitination has been studied *in vitro* [206], but has not been assessed within cells. Therefore cells transfected with polyHis-tagged ubiquitin and either WT-XIAP or an E3 ligase mutant (H467A) were subjected to nickel pulldown assay. In contrast to pitfalls of co-immunoprecipitation assays, the strongly denaturing conditions of urea lysis buffer used make post-lysis ubiquitination artifacts unlikely. Immunoblot analysis of nickel precipitate revealed extensive ubiquitination of WT-XIAP, but not XIAP H467A (Figure 8.11A). This suggests that the E3 ligase activity of XIAP is required for its own ubiquitination, indicative of a potential target for PGAM5 (explored below).

Although XIAP induces its own ubiquitination and degradation, it is unknown if XIAP can self-ubiquitinate using ubiquitin linkages that do not signal for degradation. Because XIAP can ubiquitinate PGAM5 and AIF through non-K48 linkages, it is possible XIAP could also mediate its own activity through alternative signaling-related ubiquitination mechanisms. Cells were transfected with XIAP and polyHis-tagged ubiquitin variants K6R, K11R, K27R, K29R, K48R, and K63R and then assessed for XIAP ubiquitination. Interestingly, all ubiquitin variants conjugated to XIAP except for the K27R variant (Figure 8.11B), which may be structurally unstable [50]. This indicates that XIAP exhibits flexibility in ubiquitin linkage mechanisms and can be polyubiquitinated potentially through mixed linkages. Since these linkages do not induce protein degradation, it is possible XIAP may control its own activity levels through such a mechanism. This non-canonical ubiquitination is similar to AIF and PGAM5, which are targets of XIAP [50, 53].

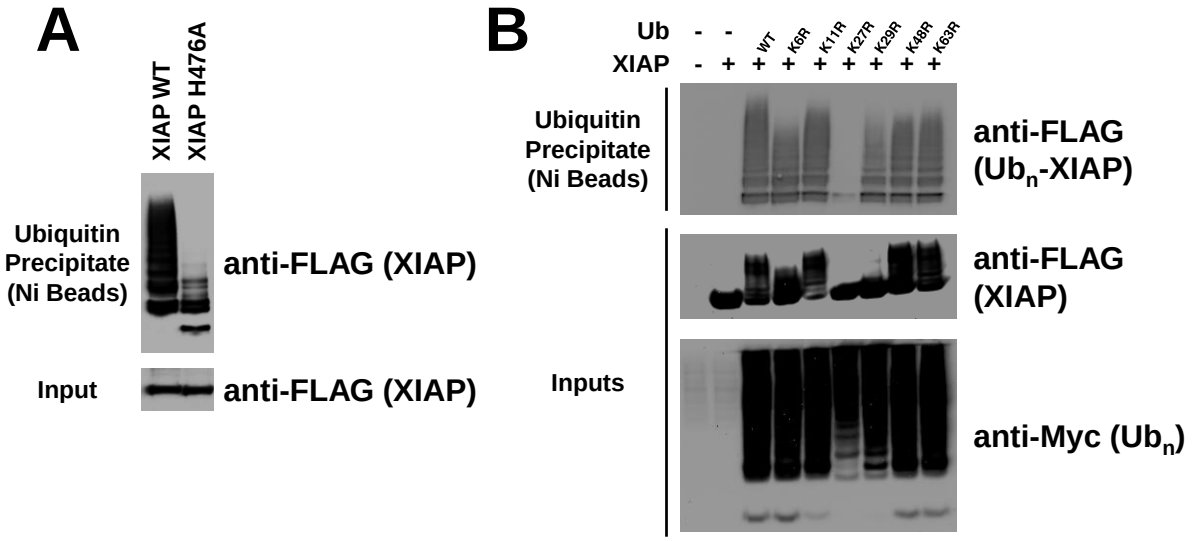

Figure 8.11. XIAP auto-ubiquitinates via mixed non-canonical linkages.
A) The indicated plasmids were transfected into HEK293T cells with polyHis-Ub followed by lysis and nickel affinity precipitation assay. Samples were then assessed by immunoblot. B) XIAP-FLAG was transfected into HEK293T cells in the absence or presence of the indicated polyHis-Ub variants followed by lysis, nickel affinity precipitation assay and immunoblot.

PGAM5 phosphatase activity inhibits XIAP dimerization and ubiquitination

Data presented so far indicate that XIAP regulates PGAM5 through ubiquitination, and that the phosphatase activity of PGAM5 can neutralize this inhibition by preventing XIAP binding. Based on this ability of PGAM5 to resist XIAP, we wondered if PGAM5 is capable of regulating XIAP. Since XIAP regulates $PGAM5_L$ through binding and non-canonical ubiquitination, this raised the question of whether PGAM5 can act upon XIAP in a similar manner. Specifically, can PGAM5 control non-canonical XIAP autoubiquitination?

To explore this possibility, cells were transfected with GST-tagged XIAP and FLAG-tagged XIAP in the absence and presence of PGAM5 isoforms. Transfection with two differently tagged XIAP plasmids allows co-precipitation assays that can assess self-association of XIAP molecules. Following precipitation with glutathione beads, FLAG epitope was present in precipitated material (Figure 8.12A), suggesting dimerization that is consistent with previous reports [48, 206]. This dimerization was impaired when either isoform of PGAM5 was overexpressed (Figure 8.12A), indicating that both PGAM5 isoforms can block dimerization of XIAP.

Since PGAM5 blocks XIAP dimerization, this loss of self-association may lead to a decrease in ubiquitination. Moreover, since $PGAM5_L$ phosphatase activity protects against XIAP-mediated inhibition (Figure 8.10), we hypothesized that the phosphatase activity of PGAM5 serves to regulate XIAP activity. Nickel affinity pulldown with polyHis-tagged ubiquitin was used to determine the extent of XIAP ubiquitination following the introduction of PGAM5 variants. Introduction of either PGAM5 isoform abolished XIAP ubiquitination almost completely (Figure 8.12B). Interestingly, $PGAM5_L$ H105A fully restored ubiquitination (Figure 8.12C), strongly suggesting that the phosphatase activity of $PGAM5_L$ inhibits ubiquitination of

XIAP. Since $PGAM5_S$ exhibits very low catalytic activity relative to $PGAM5_L$ [53], it is particularly notable that $PGAM5_S$ H105A partially restored XIAP ubiquitination (Figure 8.12C). Given the reduced phosphatase activity of $PGAM5_S$, the observation of any laddering with $PGAM5_S$ H105A overexpression suggests a high potency of PGAM5 phosphatase activity towards XIAP. However, since restoration of ubiquitination by $PGAM5_S$ H105A was incomplete (Figure 8.12C), $PGAM5_S$ is likely to inhibit ubiquitination through other mechanisms and indicates that $PGAM5_L$ and $PGAM5_S$ can function differently within cells. Altogether these data show that PGAM5 blocks dimerization and non-canonical autoubiquitination of XIAP, suggesting a possible mechanism through which PGAM5 can kill cells.

The PGAM5-XIAP axis controls cell fate in embryonic fibroblasts

Experiments so far have shown that PGAM5 and XIAP control cell death through mutual antagonism when overexpressed in HEK293T cells. However, the significance of the PGAM5-XIAP axis to death induction in other cell types and its physiological relevance remain unknown. Therefore the roles of PGAM5 and XIAP in cell death control were assessed in mouse embryonic fibroblasts (MEFs).

To test the PGAM5-XIAP axis in MEFs, PGAM5 was overexpressed in the context of XIAP loss in order to determine if PGAM5 toxicity is associated with endogenous levels of XIAP. While $PGAM5_S$ has been identified as an alternative splice variant of the PGAM5 gene, it has not been identified at the protein level in cells; whether endogenous $PGAM5_S$ protein exists remains an open question. Therefore the long isoform of PGAM5 was assessed. MEFs derived from wild-type and XIAP knockout mice have been reported previously [225]. Lentiviral vectors were generated and then used to deliver $PGAM5_L$ into XIAP-proficient and deficient cells (Figure 8.13A). Consistent with experiments in HEK293T cells, overexpression of $PGAM5_L$ in

MEFs induced substantial quantities of cell death (Figure 8.13B). Moreover, XIAP-deficient cells exhibited greater sensitivity to $PGAM5_L$ (Figure 8.13B), demonstrating that XIAP inhibits $PGAM5_L$ in MEFs.

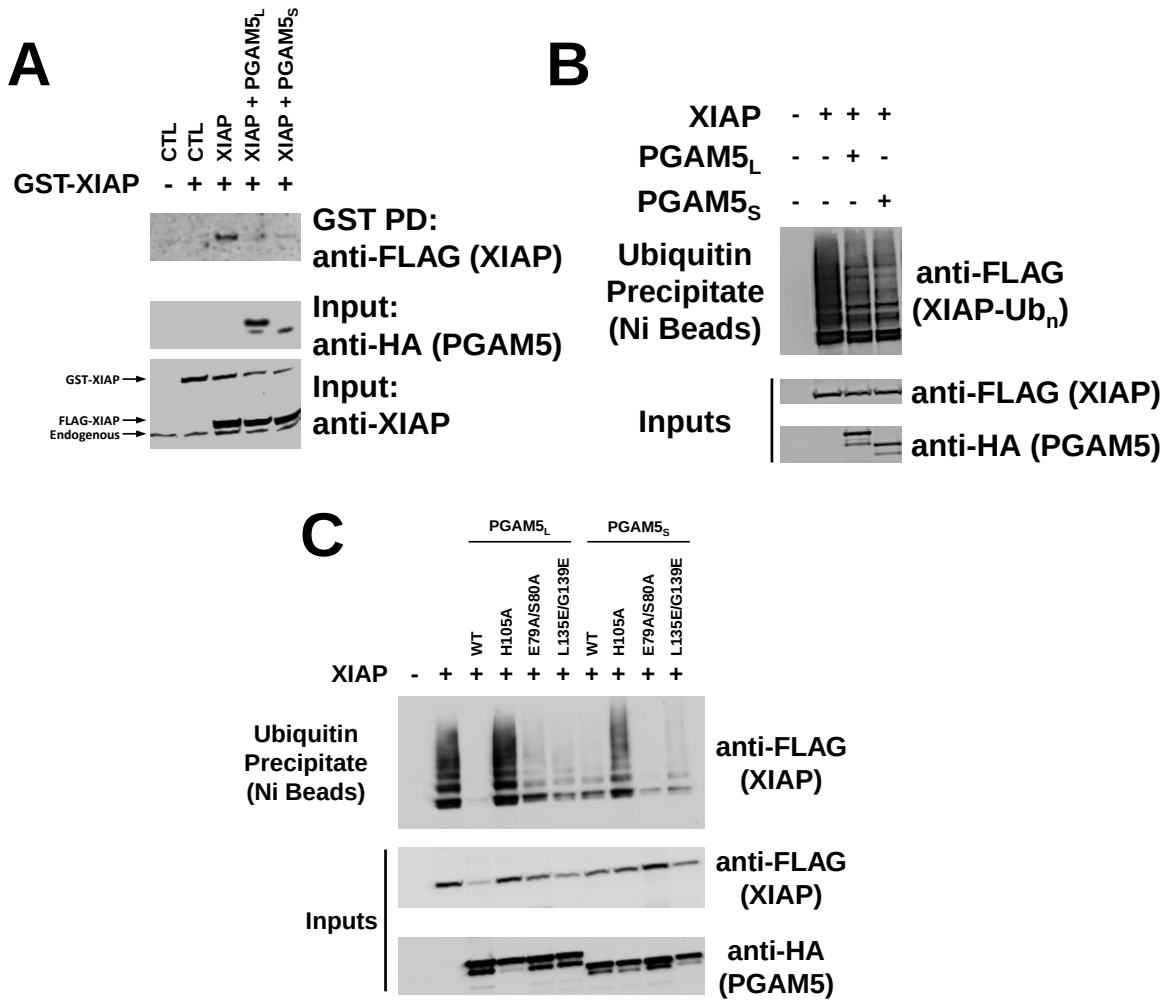

Figure 8.12. PGAM5 phosphatase activity inhibits XIAP dimerization and ubiquitination. A) HEK293T cells were transfected with the indicated plasmids, lysed, and incubated with glutathione beads followed by immunoblot with the indicated antibodies. B, C) HEK293T cells were transfected with polyHis-Ub and the indicated plasmids, lysed, and subjected to nickel affinity precipitation followed by immunoblot.

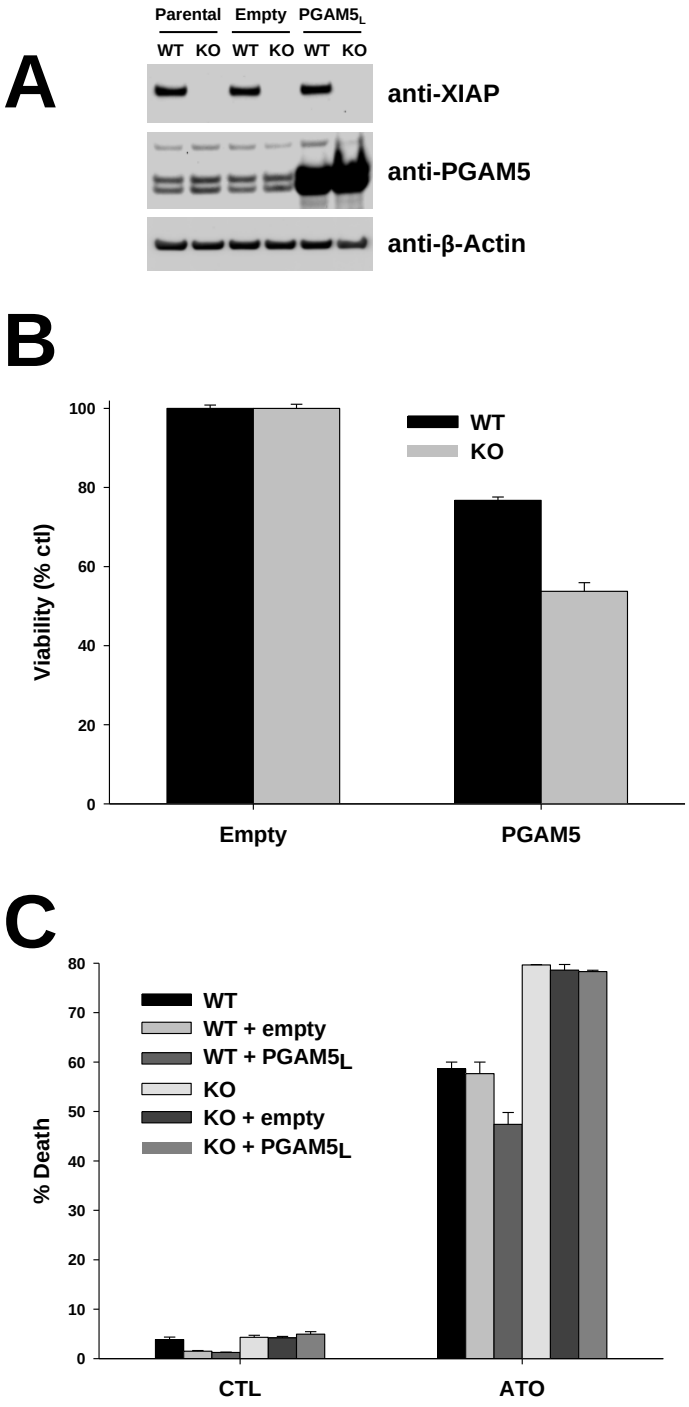

Figure 8.13. The PGAM5-XIAP axis controls cell fate in MEFs.
A) Immortalized wild-type (WT) and XIAP-null (KO) MEFs [225] were infected with lentiviruses harboring either an empty cassette or $PGAM5_L$, lysed, and assessed for the indicated proteins by immunoblot. B) WT and KO MEFs were infected with either an empty lentivirus or lentivirus harboring $PGAM5_L$, stained with PI and assessed for viability by flow cytometry. C) Surviving WT and KO MEFs that stably express either empty vector or $PGAM5_L$ were left untreated or treated with arsenic trioxide (ATO) followed by PI staining and flow cytometry.

PGAM5 has been linked to control of apoptosis, necroptosis, and mitophagy, leading to both death and survival outcomes [215-220]. Since a variety of death and pro-survival roles for PGAM5 have been reported, we questioned how PGAM5 and XIAP influence cell fate in cells that are resistant to PGAM5 toxicity. Therefore XIAP-proficient and deficient cells were stably infected with lentiviruses harboring $PGAM5_L$. As expected $PGAM5_L$ induced substantial toxicity that was exacerbated by loss of XIAP, but cells that survived were further cultured to derive cell lines stably expressing $PGAM5_L$.

Following the derivation of cells stably overexpressing $PGAM5_L$, cell death was induced by arsenic trioxide (ATO), an oxidative stress agent that triggers apoptosis but can also prompt necrosis and mitophagy [233-235]. When cells were treated with ATO, PGAM5 protected cells in the presence of XIAP, but not in XIAP-deficient cells (Figure 8.13C). Interestingly, this suggests that in this context PGAM5 promotes survival by acting upon XIAP. Altogether, these data demonstrate alternative activities for PGAM5 that depend on cell context/stimulus and XIAP, highlighting the multifunctional nature of PGAM5.

Discussion

PGAM5 and XIAP regulate PINK1-dependent mitophagic cell death

Altogether this study outlines mechanisms through which both isoforms of PGAM5 induce cellular toxicity and their inhibition by XIAP. PGAM5 and XIAP exhibit an antagonistic relationship involving non-canonical ubiquitination. The inhibitory nature of PGAM5 and XIAP extends to MEFs and appears to control decisions of cell fate depending on stimulus and intrinsic sensitivity to PGAM5 activity.

While both PGAM5 isoforms induce cell death via PINK1 stabilization, XIAP is capable of suppressing the long but not short isoform of PGAM5. This is likely because $PGAM5_S$ lacks a

key lysine residue within the $PGAM5_L$ C-terminal tail that is targeted by XIAP when PGAM5 binds Keap1 and Bcl-X_L.

The PGAM5-XIAP axis defines cell death and survival mechanisms

Both isoforms of PGAM5 suppress XIAP dimerization and non-canonical ubiquitination, suggesting that $PGAM5_L$ and $PGAM5_S$ can regulate XIAP activity. PGAM5-mediated suppression of XIAP is dependent upon the phosphatase activity of $PGAM5_L$, but likely involves other factors when suppressed by $PGAM5_S$ activity. The PGAM5-XIAP axis is confirmed with $PGAM5_L$ overexpression in MEFs: acute upregulation of PGAM5 induces cell death that is inhibited by XIAP, whereas long-term overexpression of PGAM5 protects cells from ATO through an XIAP-dependent mechanism. Interestingly, other studies have indicated roles for PGAM5 in both cell death and survival through mechanisms involving mitophagy and necroptosis [215-220]. These disparate findings may be explained by experiments presented here, which show that XIAP and PGAM5 serve to balance cell death and survival, inducing different cell fate outcomes in response to different stimuli.

XIAP can autoubiquitinate through a variety of non-canonical linkage types that may regulate its own different activities. Similarly, XIAP ubiquitinates PGAM5 through a non-degradative mechanism, raising the possibility that XIAP may regulate PGAM5 activity, binding partners, localization, etc. Since XIAP and PGAM5 regulate each other, these potential mechanisms may explain how the XIAP-PGAM5 axis mediates different cellular functions. It is notable that XIAP is often upregulated in cancer as a pro-survival protein, contributing to aggressiveness and therapeutic resistance. Small molecules targeting XIAP in cancer have shown some therapeutic potential and are used as a unique tool for studying the death pathway known as necroptosis (Appendix C). The involvement of the XIAP-PGAM5 axis in cancer cell death

and survival and their intersection with molecular targeting techniques represent significant future directions.

Summary

Overall this study shows that the interaction of AIF with PGAM5 serves to protect AIF from XIAP-mediated ubiquitination, and defines additional routes through which PGAM5 and XIAP further regulate one another in cell death associated with PINK1-dependent mitophagy. Therefore these studies add to the growing list of cell death signaling pathways and reveals novel mechanisms by which cells control death vs. survival through the XIAP-PGAM5 axis.

IX. SUMMARY AND CONCLUDING REMARKS

AIF survival activity benefits tumorigenesis

AIF was initially characterized for its role in caspase-independent cell death and once thought to function primarily as a death signaling molecule [24]. However, accumulating evidence indicates that an essential role for AIF in cell death is cell type and context-specific [55-58]. Independent of a role in cell death, AIF possesses an intrinsic NADH-oxidase activity [60]. The mechanisms through which AIF enzymatic activity operates in cells are largely enigmatic, but demonstrated to play an essential role in cellular metabolism and redox control. AIF exhibits a predominant role in promoting survival and homeostasis in healthy cells through the regulation of mitochondrial metabolism and redox balance, with loss or mutation of AIF leading to a variety of mitochondrial disorders observed in mice and humans [26, 62-68]. AIF exerts control of mitochondrial activity through the regulation of ETC protein subunits, metabolic flux, and cellular redox state [73].

AIF is required for normal mitochondrial function and homeostasis in healthy cells, and this role is poised to benefit cancer cell growth and survival. The rapid proliferation and aggressiveness exhibited by tumor cells demands a significant rewiring of both metabolism and oxidative stress signaling. These tumorigenic processes may be supported by the pro-survival activities of AIF in metabolism and redox balance. Indeed, AIF is upregulated at the RNA and protein levels in a variety of cancers relative to normal cells [51, 52, 83-88], indicating a potentially tumorigenic function. The work of Urbano *et al*. [54] was the first to demonstrate a pro-tumor role for AIF in colorectal cancer, showing that the enzymatic activity of AIF protects cancer cells from chemotherapeutic agents and is required for tumorigenic growth.

The work of our laboratory then demonstrated a contributory role for the enzymatic activity of AIF to prostate tumorigenesis [51]. Transcript levels of AIF are elevated in PCa relative to normal prostatic tissues, indicating a potential role in PCa pathogenesis. AIF protein levels increase with progression of PCa, and knockdown of AIF suppresses tumorigenesis both *in vitro* and *in vivo* in advanced but not early-stage PCa cells. This indicates that AIF is a significant factor for the progression of PCa to advanced stage and is required for the growth and aggressiveness of advanced PCa cells. Moreover, changes in cell growth and survival following AIF ablation are accompanied by metabolic changes that are indicative of a metabolic switching event from OXPHOS to glycolysis as a predominant source of ATP production. Importantly, aggressiveness and metabolism of PCa cells are restored by WT-AIF, but not the enzymatically deficient TVA-AIF mutant. Altogether these findings strongly suggest that the enzymatic activity of AIF mediates mitochondrial metabolism supporting the growth and survival of advanced PCa cells.

With a tumorigenic role for AIF established, several questions surrounding the mechanisms of AIF activity in cancer arose, and the breadth of AIF pro-tumor activity across cancer types remained to be determined. Why and how does AIF promote mitochondrial metabolism in some cell types but not others? With a metabolic role for AIF demonstrated in PCa, the redox role of AIF in cancer cells (and normal cells) was unaddressed. Therefore the work presented in Chapters 3-7 sought to determine both the metabolic and redox impacts of AIF and their integration across cell types.

A spectrum of AIF-dependent metabolic effects in PDAC

Exploration of the intersection of abnormal metabolism and tumorigenesis (Chapter 2) led to the striking finding that MIA PaCa-2 PDAC cells are capable of being metabolically

reconditioned from a glycolytic to OXPHOS-dependent phenotype. Rather than exhibiting mitochondrial impairment as Warburg hypothesized [74], cells appear to intentionally downregulate mitochondrial activity. Notably, under conditions of altered metabolic requirements cells can adapt by increasing mitochondrial metabolism. Remarkably, this metabolic adaptation is reversible but triggers persistent therapeutic resistance, demonstrating the paramount importance of metabolism to tumorigenesis.

Assessment of AIF metabolic activity in the context of PDAC (Chapter 3) revealed an important role for AIF-dependent metabolism in pancreatic tumorigenesis. PDAC cell types (PANC-1, BxPC-3, HPAC, HPAF-II, MIA PaCa-2) were selected for their diversity of metabolic requirements [100]. Stable knockdown of AIF in PDAC cells induced the loss of complex I and an increase in glucose uptake, similar to the effects of AIF ablation in PCa cells. Loss of AIF in PDAC cells additionally impaired cell growth both *in vitro* and in Matrigel™ substrate, which correlated to metabolic changes observed (complex I levels, glucose consumption, sensitivity to 2-deoxyglucose).

Similar to the observations of AIF ablation in PCa, not all PDAC cell types exhibited metabolic changes. Interestingly, there appears to be a continuum of metabolic sensitivities to AIF ablation that was not identified in PCa. PANC-1 and BxPC-3 cells exhibit changes in both growth and metabolism when AIF is suppressed. HPAC cells show changes in metabolism and growth, but retain enough metabolic flexibility to survive glycolytic inhibition. HPAF-II cells do not exhibit substantial metabolic changes until introduced to Matrigel™ substrate. MIA PaCa-2 cells show no change in either metabolism or growth following AIF ablation. The spectrum of sensitivities to AIF ablation is distinct from observations in PCa, in which cells exhibited A) changes in both metabolism and growth, or B) no changes in either metabolism or growth.

One explanation for the differences between AIF ablation sensitivity in PCa and PDAC may simply be the evaluation of only 3 cells types in PCa vs. 5 cell types in PDAC. A more likely explanation is the greater metabolic addiction in PDAC cells vs. PCa cells. Relative to other cancers, PDACs often encounter more demanding *in vivo* metabolic constraints that stem from hypovascular and fibrotic microenvironments leading to hypoxia and limited nutrient availability [76, 102]. Moreover, PDACs exhibit increased crosstalk with whole-body metabolic conditions that lead to additional metabolic signals within tumors. PDAC development is influenced by pathological environments such as type II diabetes and obesity, and can also trigger further metabolic dysregulation leading to cachexia and diabetes [102]. As a result of this more metabolically elaborate setting, AIF is likely to function differently in PDAC when compared with PCa. Moreover, AIF may be more important to growth and survival of PDAC than PCa. This idea is supported by greater metabolic changes in PDAC and the observation that growth is impaired *in vitro* when AIF is suppressed; in PCa growth rates following AIF ablation are unaffected until introduction to growth stress in Matrigel™ or *in vivo*.

The stringent metabolic requirements for the survival and growth of PDAC cells makes the setting of PDAC an ideal system for studying the role of AIF in different metabolic environments and evaluating phenotypes when AIF-dependent metabolic requirements are not met (*e.g.*, glucose consumption, growth). PDAC cell types have recently been categorized into metabolic subtypes [100] including OXPHOS-dependent and glycolytic subtypes. It is notable that complex I is dependent upon AIF only in OXPHOS-dependent cells, suggesting that AIF responds to metabolic cues in order to promote ETC stability. The types of signals (*e.g.*, NAD^+/NADH ratios, oxygen availability, $\Delta\Psi_m$) that could influence AIF-mediated complex I control remain to be determined.

While much work remains in establishing how AIF controls the ETC, Chapter 4 identifies a significant role for AIF in mediating translation of mitochondria-encoded genes. AIF interacts with both the mitochondrial translation factor TUFM and the MRPL18 subunit of the mitoribosome, facilitating their essential interactions with each other. Further, ablation of either AIF or TUFM triggers the loss of both mitochondria- and nuclear-encoded ETC protein subunits, demonstrating a possible mechanism by which AIF controls the respiratory chain and links the extra-mitochondrial environment with mitochondrial activity.

Altogether experiments of AIF activity in PDAC cells demonstrate an important role for AIF in promoting pancreatic tumorigenesis. Importantly, the range of AIF-dependent growth changes corresponds to the magnitudes of metabolic sensitivities to AIF ablation. The correlation of AIF-mediated metabolic control with cellular energy preferences indicates a possible responsiveness of AIF to metabolic requirements, thus expanding our understanding of AIF activity in control of mitochondrial metabolism and disease.

AIF enzymatic activity exhibits control of cellular ROS and redox signals

The enzymatic activity of AIF promotes homeostasis in normal cells [73] and can be used by a variety of cancer cell types to promote a tumor permissive metabolic state supporting aggressive phenotypes [51, 52, 54]. The enzymatic activity of AIF has additionally been shown to produce ROS *in vitro* [60], but the *in vivo* significance of AIF-mediated ROS control has remained poorly understood. Chapter 5 of this work assesses the ability of AIF to regulate ROS levels in PC3 and HeLa cells, showing for the first time that AIF enzymatic activity is required for cells to increase ROS levels in response to oxidative stress triggers. Interestingly, AIF appears to control different ROS types depending on cell type, but in both cases AIF ablation protects cells from oxidative stress-induced cell death. Given the selective nature of AIF-

mediated cell death, it is interesting that AIF is required for cell death under heightened oxidative stress levels. Since AIF enzymatic activity increases ROS levels in cells, it is likely that AIF-mediated cell death is actually due to AIF-dependent increases in cellular ROS and not nuclear translocation of AIF.

We additionally show for the first time that through control of redox signaling, AIF is capable of regulating nuclear gene expression. Nuclear accumulation of the antioxidant transcription factor Nrf2 is dependent upon AIF in HeLa cells but not PC3 cells, which may be due to different types and/or levels of AIF-mediated ROS between cell types. In both cell types AIF ablation leads decreased levels of a variety of antioxidant transcript levels under both basal conditions and oxidative stress stimulation, with several transcripts showing increases that are confirmed at the protein level. Altogether these data suggest that AIF-mediated ROS induce nuclear responses.

AIF redox signaling promotes a JNK1-mediated cadherin switch that determines decisions of cell fate

Following the findings that AIF enzymatic activity promotes cellular redox signaling, we then questioned the ability of AIF to influence other redox sensitive pathways, focusing on the MAPK family of proteins. AIF suppresses DUSP4, an endogenous inhibitor of MAPKs, leading to MAPK phosphorylation and activation. The ability of AIF to control JNK-mediated signaling events in a variety of cell types was then explored. In Chapter 6 we show that via an oxidative stress mechanism, AIF signals JNK1 to induce the cadherin switch and promote cell survival. We additionally report the finding of other AIF-dependent EMT genes that are independent of JNK activation. These findings reveal a novel function for AIF and confirm its role as a pivotal redox signaling molecule (Figure 9.1).

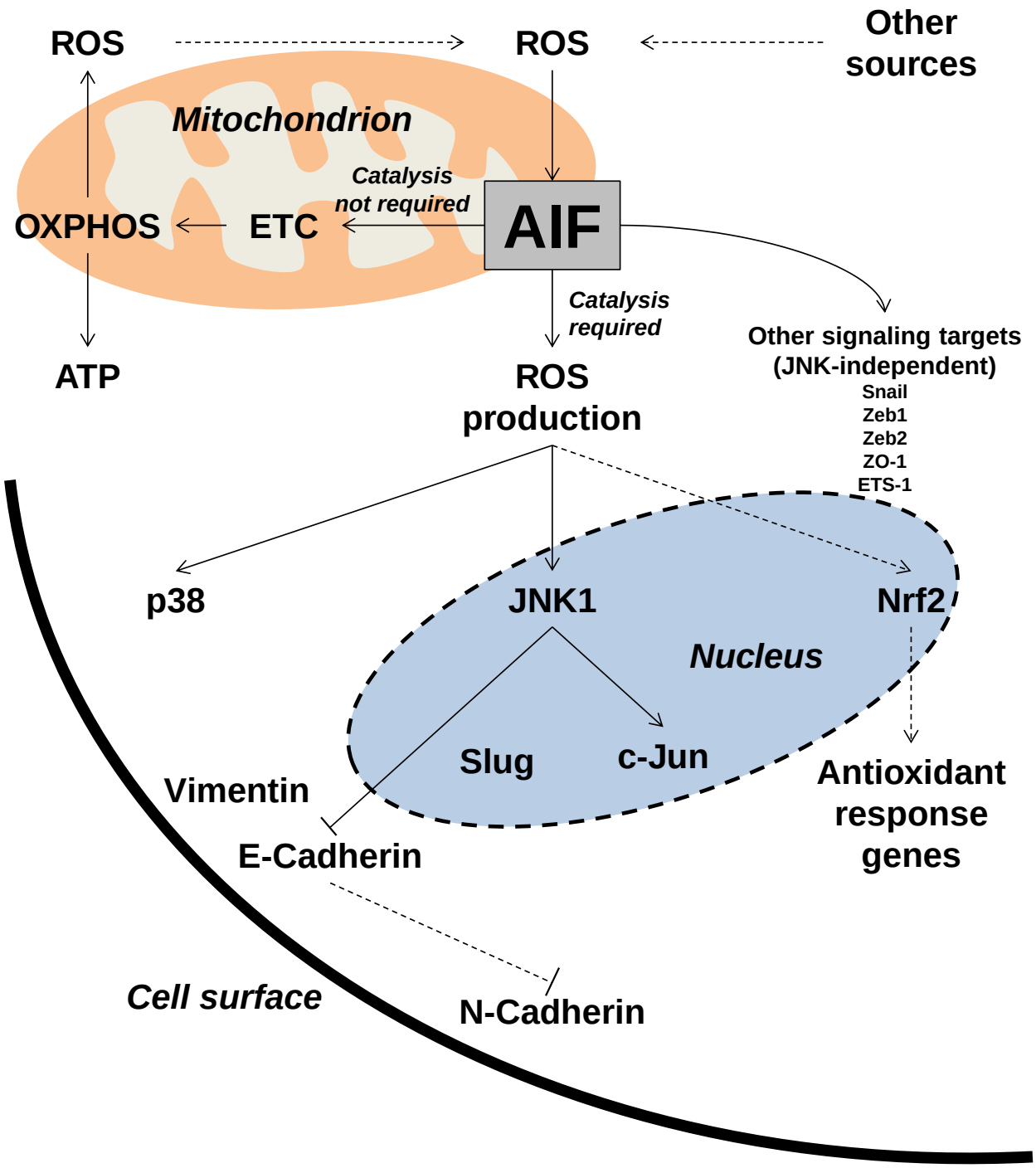

Figure 9.1. AIF-mediated control of metabolism and redox signaling in tumorigenesis. AIF mediates control metabolism in part by regulating ETC/OXPHOS within the mitochondria. Distinct from this metabolic function, AIF enzymatic activity promotes extra-mitochondrial redox signals regulating a variety of pathways.

Interestingly, loss of AIF induces apoptosis in Matrigel™ substrate, and levels of apoptosis significantly increase when E-cadherin levels are reversed (Figure 9.2). This shows that AIF suppresses apoptosis, which sharply contrasts its initial characterization and namesake. Although less rigorously assessed, we also find that AIF mediates metabolic signaling (Chapters 4, 6). Specifically, AIF ablation leads to increased levels of the oncogenic regulator of metabolism c-Myc and upregulation of a variety of glycolysis enzymes. AIF ablation additionally impairs phosphorylation of the metabolic signaling molecule AMPK, and knockdown of E-cadherin further inhibits AMPK phosphorylation. An established function of AMPK is the regulation of cellular glucose uptake levels, which increase following AIF knockdown but do not further change with knockdown of E-cadherin (Chapter 6). This suggests that increased apoptosis with dual AIF/E-cadherin knockdown is due to an imbalance of metabolism and pro-tumor signaling.

Functional dissociation of AIF-mediated metabolism and redox signaling

Chapter 7 assesses the relationship of AIF-mediated metabolism with redox signaling. Remarkably, the abilities of AIF to promote mitochondrial metabolism and oxidative stress signaling are functionally uncoupled (Figure 9.1), and AIF-mediated control of JNK and E-cadherin are not due to AIF-dependent complex I activity. While AIF-mediated regulation of complex I is cell type specific, AIF-dependent promotion of JNK signaling is widespread and occurs independently of complex I levels. JNK phosphorylation, but not complex I, is dependent upon the enzymatic activity of AIF in all cell types assessed. Additionally, replacement of impaired complex I with yeast NDI1 restores metabolism, but not JNK phosphorylation or E-cadherin levels in AIF-deficient cells.

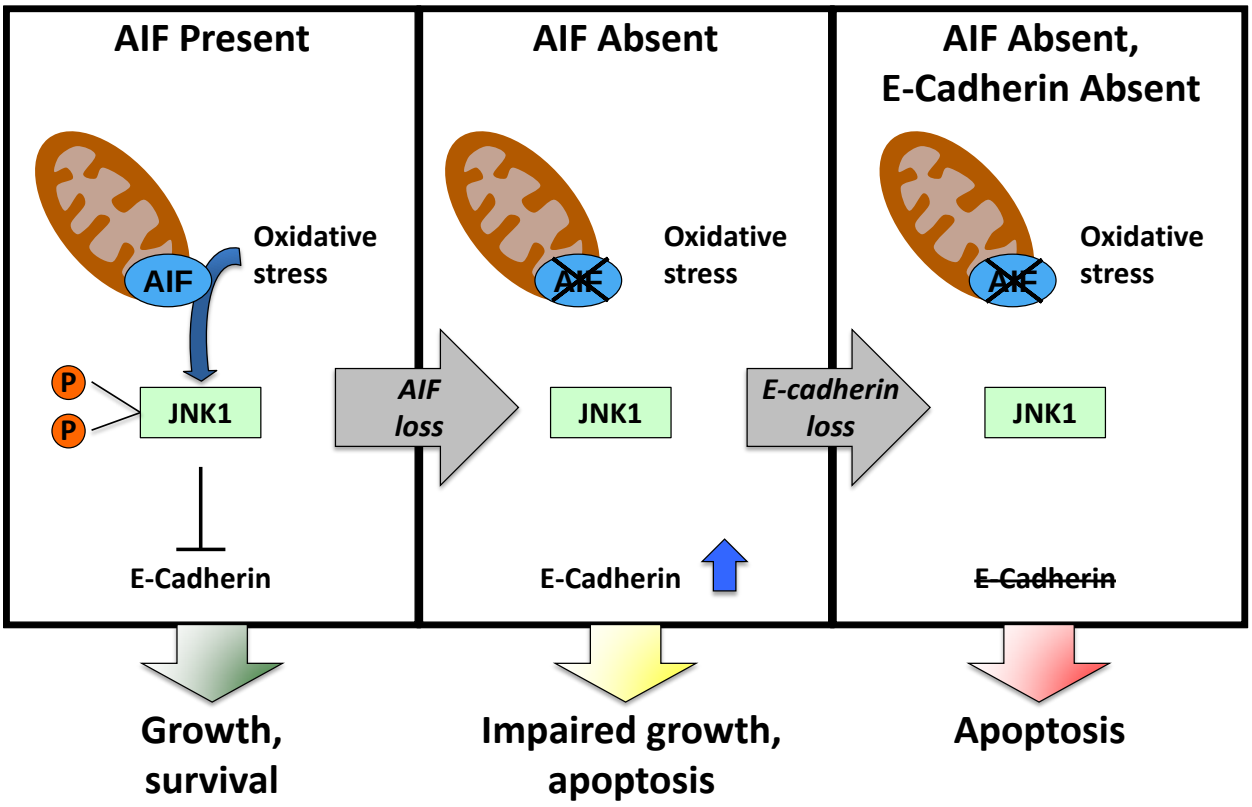

Figure 9.2. Effects of AIF and E-cadherin on signaling and decisions of cell fate.
AIF promotes JNK1 activity by transmitting extra-mitochondrial redox cues leading to the suppression of E-cadherin and promotion of the cadherin switch. When AIF is suppressed, JNK1 activity is decreased and E-cadherin levels subsequently increase, leading to impaired growth and apoptosis. When E-cadherin is suppressed, AIF-deficient cells undergo apoptosis due to unrestrained growth with metabolic demands that cannot be met without AIF.

AIF association with cell death regulators XIAP and PGAM5

AIF pro-survival activity is dissociable from its roles in cell death. In addition to determining how AIF promotes tumorigenesis through control of cellular metabolism and oxidative stress signaling, we also assessed the involvement of AIF with atypical cell death pathways through interactions with XIAP and PGAM5. While AIF is not typically pivotal for the cell to die (Chapter 3), under certain circumstances alternative death pathways are necessary, and through XIAP and PGAM5 activities AIF may regulate these cell death signaling events.

AIF is protected from XIAP-mediated ubiquitination by interaction with PGAM5, suggesting roles for PGAM5 in mediating alternative cell death mechanisms. Indeed, experiments in Chapter 8 demonstrate that PGAM5 induces toxic mitophagy that requires PINK1 and can be suppressed by noncanonical XIAP-mediated ubiquitination. Further, PGAM5 can promote cell death by neutralizing the prosurvival activities of XIAP. Collectively these data demonstrate the existence of a novel AIF-XIAP-PGAM5 axis that regulates decisions of cell fate.

Conclusion

Overall, experiments presented here underscore the role of AIF in mediating the balance of cell death and survival and its dysregulation in cancer. We and others have demonstrated that in addition to its nuclear activity in cell death, AIF controls mitochondrial energy production by regulating respiratory chain protein levels while its NADH-oxidase activity functions as a redox conduit that senses and responds to the metabolic and oxidative environment. The unification of metabolism, oxidative stress, MAPK signaling, and the cadherin switch by AIF activity raises numerous possibilities that include roles in normal physiology, development, redox balance, and disease. Altogether we demonstrate a cellular role for AIF-mediated catalysis and the existence of AIF-dependent redox pathways (Figure 9.1) that can be uncoupled from ETC control, implicating AIF as a fundamental control point for cell signaling and homeostatic regulation.

REFERENCES

1. Nunnari, J. and A. Suomalainen, *Mitochondria: in sickness and in health.* Cell, 2012. **148**(6): p. 1145-1159.
2. Shadel, G.S. and T.L. Horvath, *Mitochondrial ROS signaling in organismal homeostasis.* Cell, 2015. **163**(3): p. 560-569.
3. Murphy, M.P., *How mitochondria produce reactive oxygen species.* Biochem J, 2009. **417**(1): p. 1-13.
4. Tretter, L., I. Sipos, and V. Adam-Vizi, *Initiation of neuronal damage by complex I deficiency and oxidative stress in Parkinson's disease.* Neurochem Res, 2004. **29**(3): p. 569-577.
5. Li, N., et al., *Mitochondrial complex I inhibitor rotenone induces apoptosis through enhancing mitochondrial reactive oxygen species production.* J Biol Chem, 2003. **278**(10): p. 8516-8525.
6. Phaniendra, A., D.B. Jestadi, and L. Periyasamy, *Free radicals: properties, sources, targets, and their implication in various diseases.* Indian J Clin Biochem, 2015. **30**(1): p. 11-26.
7. Thannickal, V.J. and B.L. Fanburg, *Reactive oxygen species in cell signaling.* Am J Physiol Lung Cell Mol Physiol, 2000. **279**(6): p. L1005-L1028.
8. Brieger, K., et al., *Reactive oxygen species: from health to disease.* Swiss Med Wkly, 2012. **142**: p. w13659.
9. Finkel, T., *Signal transduction by reactive oxygen species.* J Cell Biol, 2011. **194**(1): p. 7-15.

10. Valko, M., et al., *Free radicals and antioxidants in normal physiological functions and human disease.* Int J Biochem Cell Biol, 2007. **39**(1): p. 44-84.

11. Nikoletopoulou, V., et al., *Crosstalk between apoptosis, necrosis and autophagy.* Biochim Biophys Acta, 2013. **1833**(12): p. 3448-3459.

12. Kerr, J.F., A.H. Wyllie, and A.R. Currie, *Apoptosis: a basic biological phenomenon with wide-ranging implications in tissue kinetics.* Br. J. Cancer, 1972. **26**: p. 239-257.

13. Duprez, L., et al., *Major cell death pathways at a glance.* Microbes Infect, 2009. **11**(13): p. 1050-1062.

14. Kroemer, G., et al., *Classification of cell death: recommendations of the Nomenclature Committee on Cell Death 2009.* Cell Death Differ, 2009. **16**(1): p. 3-11.

15. Brill, A., et al., *The role of apoptosis in normal and abnormal embryonic development.* J Assist Reprod Genet, 1999. **16**(10): p. 512-519.

16. Rathmell, J.C. and C.B. Thompson, *Pathways of apoptosis in lymphocyte development, homeostasis, and disease.* Cell, 2002. **109 Suppl**: p. S97-S107.

17. Elmore, S., *Apoptosis: a review of programmed cell death.* Toxicol Pathol, 2007. **35**(4): p. 495-516.

18. Cory, S., D.C. Huang, and J.M. Adams, *The Bcl-2 family: roles in cell survival and oncogenesis.* Oncogene, 2003. **22**(53): p. 8590-8607.

19. Vaseva, A.V. and U.M. Moll, *The mitochondrial p53 pathway.* Biochim Biophys Acta, 2009. **1787**(5): p. 414-420.

20. Kroemer, G., L. Galluzzi, and C. Brenner, *Mitochondrial membrane permeabilization in cell death.* Physiol Rev, 2007. **87**(1): p. 99-163.

21. Bernardi, P. and G.F. Azzone, *Cytochrome c as an electron shuttle between the outer and inner mitochondrial membranes.* J Biol Chem, 1981. **256**(14): p. 7187-7192.

22. Cain, K., S.B. Bratton, and G.M. Cohen, *The Apaf-1 apoptosome: a large caspase-activating complex.* Biochimie, 2002. **84**(2-3): p. 203-214.

23. Fischer, U., R.U. Janicke, and K. Schulze-Osthoff, *Many cuts to ruin: a comprehensive update of caspase substrates.* Cell Death Differ, 2003. **10**(1): p. 76-100.

24. Susin, S.A., et al., *Molecular characterization of mitochondrial apoptosis-inducing factor.* Nature, 1999. **397**(6718): p. 441-446.

25. Vahsen, N., et al., *AIF deficiency compromises oxidative phosphorylation.* Embo J, 2004. **23**(23): p. 4679-4689.

26. Klein, J.A., et al., *The harlequin mouse mutation downregulates apoptosis-inducing factor.* Nature, 2002. **419**(6905): p. 367-374.

27. Daugas, E., et al., *Apoptosis-inducing factor (AIF): a ubiquitous mitochondrial oxidoreductase involved in apoptosis.* FEBS Lett, 2000. **476**(3): p. 118-23.

28. Lorenzo, H.K., et al., *Apoptosis inducing factor (AIF): a phylogenetically old, caspase-independent effector of cell death.* Cell Death Differ, 1999. **6**(6): p. 516-524.

29. Cande, C., et al., *Apoptosis-inducing factor (AIF): key to the conserved caspase-independent pathways of cell death?* J Cell Sci, 2002. **115**(Pt 24): p. 4727-4734.

30. Koonin, E.V. and L. Aravind, *Origin and evolution of eukaryotic apoptosis: the bacterial connection.* Cell Death Differ, 2002. **9**(4): p. 394-404.

31. Otera, H., et al., *Export of mitochondrial AIF in response to proapoptotic stimuli depends on processing at the intermembrane space.* Embo J, 2005. **24**(7): p. 1375-1386.

32. Polster, B.M., et al., *Calpain I induces cleavage and release of apoptosis-inducing factor from isolated mitochondria.* J Biol Chem, 2005. **280**(8): p. 6447-6454.

33. Susin, S.A., et al., *Two distinct pathways leading to nuclear apoptosis.* J Exp Med, 2000. **192**(4): p. 571-580.

34. Ye, H., et al., *DNA binding is required for the apoptogenic action of apoptosis inducing factor.* Nat Struct Biol, 2002. **9**(9): p. 680-684.

35. Susin, S.A., et al., *Bcl-2 inhibits the mitochondrial release of an apoptogenic protease.* J. Exp. Med., 1996. **184**: p. 1331-1341.

36. Yuste, V.J., et al., *Cysteine protease inhibition prevents mitochondrial apoptosis-inducing factor (AIF) release.* Cell Death Differ, 2005. **12**(11): p. 1445-1448.

37. Bidere, N., et al., *Cathepsin D triggers Bax activation, resulting in selective apoptosis-inducing factor (AIF) relocation in T lymphocytes entering the early commitment phase to apoptosis.* J Biol Chem, 2003. **278**(33): p. 31401-31411.

38. Cao, G., et al., *Critical role of calpain I in mitochondrial release of apoptosis-inducing factor in ischemic neuronal injury.* J Neurosci, 2007. **27**(35): p. 9278-9293.

39. Loeffler, M., et al., *Dominant cell death induction by extramitochondrially targeted apoptosis-inducing factor.* Faseb J, 2001. **15**(3): p. 758-767.

40. Cande, C., et al., *AIF and cyclophilin A cooperate in apoptosis-associated chromatinolysis.* Oncogene, 2004. **23**(8): p. 1514-1521.

41. Wang, X., et al., *Mechanisms of AIF-mediated apoptotic DNA degradation in Caenorhabditis elegans.* Science, 2002. **298**(5598): p. 1587-1592.

42. Zhu, C., et al., *Cyclophilin A participates in the nuclear translocation of apoptosis-inducing factor in neurons after cerebral hypoxia-ischemia.* J Exp Med, 2007. **204**(8): p. 1741-1748.

43. Artus, C., et al., *AIF promotes chromatinolysis and caspase-independent programmed necrosis by interacting with histone H2AX.* Embo J, 2010. **29**(9): p. 1585-1599.

44. Saleh, A., et al., *Negative regulation of the Apaf-1 apoptosome by Hsp70.* Nat Cell Biol, 2000. **2**(8): p. 476-483.

45. Beere, H.M., et al., *Heat-shock protein 70 inhibits apoptosis by preventing recruitment of procaspase-9 to the Apaf-1 apoptosome.* Nat Cell Biol, 2000. **2**(8): p. 469-475.

46. Ravagnan, L., et al., *Heat-shock protein 70 antagonizes apoptosis-inducing factor.* Nat Cell Biol, 2001. **3**(9): p. 839-843.

47. Gurbuxani, S., et al., *Heat shock protein 70 binding inhibits the nuclear import of apoptosis-inducing factor.* Oncogene, 2003. **22**(43): p. 6669-6678.

48. Galban, S. and C.S. Duckett, *XIAP as a ubiquitin ligase in cellular signaling.* Cell Death Differ, 2010. **17**(1): p. 54-60.

49. Wilkinson, J.C., et al., *Apoptosis-inducing factor is a target for ubiquitination through interaction with XIAP.* Mol Cell Biol, 2008. **28**(1): p. 237-247.

50. Lewis, E.M., et al., *Nondegradative ubiquitination of apoptosis inducing factor (AIF) by X-linked inhibitor of apoptosis at a residue critical for AIF-mediated chromatin degradation.* Biochemistry, 2011. **50**(51): p. 11084-11096.

51. Lewis, E.M., et al., *The Enzymatic Activity of Apoptosis Inducing Factor Supports Energy Metabolism Benefitting the Growth and Invasiveness of Advanced Prostate Cancer Cells.* J Biol Chem, 2012. **287**(52): p. 43862-43875.

52. Scott, A.J., A.S. Wilkinson, and J.C. Wilkinson, *Basal metabolic state governs AIF-dependent growth support in pancreatic cancer cells.* BMC cancer, 2016. **16**(1): p. 286.

53. Lenhausen, A.M., et al., *Apoptosis Inducing Factor Binding Protein PGAM5 Triggers Mitophagic Cell Death That Is Inhibited by the Ubiquitin Ligase Activity of X-Linked Inhibitor of Apoptosis.* Biochemistry, 2016. **55**(23): p. 3285-3302.

54. Urbano, A., et al., *AIF suppresses chemical stress-induced apoptosis and maintains the transformed state of tumor cells.* Embo J, 2005. **24**(15): p. 2815-2826.

55. Cregan, S.P., et al., *Apoptosis-inducing factor is involved in the regulation of caspase-independent neuronal cell death.* J Cell Biol, 2002. **158**(3): p. 507-517.

56. van Empel, V.P., et al., *Downregulation of apoptosis-inducing factor in harlequin mutant mice sensitizes the myocardium to oxidative stress-related cell death and pressure overload-induced decompensation.* Circ Res, 2005. **96**(12): p. e92-e101.

57. Wang, H., et al., *Apoptosis-inducing factor substitutes for caspase executioners in NMDA-triggered excitotoxic neuronal death.* J Neurosci, 2004. **24**(48): p. 10963-10973.

58. Zhu, C., et al., *Apoptosis-inducing factor is a major contributor to neuronal loss induced by neonatal cerebral hypoxia-ischemia.* Cell Death Differ, 2007. **14**(4): p. 775-784.

59. Ferreira, P., et al., *Structural insights into the coenzyme mediated monomer-dimer transition of the pro-apoptotic apoptosis inducing factor.* Biochemistry, 2014. **53**(25): p. 4204-15.

60. Miramar, M.D., et al., *NADH oxidase activity of mitochondrial apoptosis-inducing factor.* J Biol Chem, 2001. **276**(19): p. 16391-16398.

61. Churbanova, I.Y. and I.F. Sevrioukova, *Redox-dependent changes in molecular properties of mitochondrial apoptosis-inducing factor.* J Biol Chem, 2008. **283**(9): p. 5622-5631.

62. Brown, D., et al., *Loss of Aif function causes cell death in the mouse embryo, but the temporal progression of patterning is normal.* Proc Natl Acad Sci U S A, 2006. **103**(26): p. 9918-9923.

63. Cheung, E.C., et al., *Dissociating the dual roles of apoptosis-inducing factor in maintaining mitochondrial structure and apoptosis.* Embo J, 2006. **25**(17): p. 4061-4073.

64. Joza, N., et al., *Muscle-specific loss of apoptosis-inducing factor leads to mitochondrial dysfunction, skeletal muscle atrophy, and dilated cardiomyopathy.* Mol Cell Biol, 2005. **25**(23): p. 10261-10272.

65. Ghezzi, D., et al., *Severe X-linked mitochondrial encephalomyopathy associated with a mutation in apoptosis-inducing factor.* Am J Hum Genet, 2010. **86**(4): p. 639-649.

66. Berger, I., et al., *Early prenatal ventriculomegaly due to an AIFM1 mutation identified by linkage analysis and whole exome sequencing.* Mol Genet Metab, 2011. **104**(4): p. 517-520.

67. Sancho, P., et al., *A newly distal hereditary motor neuropathy caused by a rare AIFM1 mutation.* Neurogenetics, 2017. **18**(4): p. 245-250.

68. Rinaldi, C., et al., *Cowchock syndrome is associated with a mutation in apoptosis-inducing factor.* Am J Hum Genet, 2012. **91**(6): p. 1095-1102.

69. Joza, N., et al., *Essential role of the mitochondrial apoptosis-inducing factor in programmed cell death.* Nature, 2001. **410**(6828): p. 549-554.

70. Elguindy, M.M. and E. Nakamaru-Ogiso, *Apoptosis Inducing Factor (AIF) and its Family Member, AMID, are Rotenone-Sensitive NADH:ubiquinone Oxidoreductases (NDH-2).* J Biol Chem, 2015.

71. Hangen, E., et al., *Interaction between AIF and CHCHD4 Regulates Respiratory Chain Biogenesis.* Mol Cell, 2015. **58**(6): p. 1001-1014.

72. Meyer, K., et al., *Loss of apoptosis-inducing factor critically affects MIA40 function.* Cell Death Dis, 2015. **6**: p. e1814.

73. Sevrioukova, I.F., *Apoptosis-inducing factor: structure, function, and redox regulation.* Antioxid Redox Signal, 2011. **14**(12): p. 2545-2579.

74. Warburg, O., *On the origin of cancer cells.* Science, 1956. **123**(3191): p. 309-314.

75. Deberardinis, R.J. and C.B. Thompson, *Cellular metabolism and disease: what do metabolic outliers teach us?* Cell, 2012. **148**(6): p. 1132-1144.

76. Blum, R. and Y. Kloog, *Metabolism addiction in pancreatic cancer.* Cell Death Dis, 2014. **5**: p. e1065.

77. Trachootham, D., et al., *Redox regulation of cell survival.* Antioxid Redox Signal, 2008. **10**(8): p. 1343-74.

78. Williams, K.J., R.L. Cowen, and I.J. Stratford, *Hypoxia and oxidative stress. Tumour hypoxia--therapeutic considerations.* Breast Cancer Res, 2001. **3**(5): p. 328-331.

79. Schieber, M. and N.S. Chandel, *ROS function in redox signaling and oxidative stress.* Curr Biol, 2014. **24**(10): p. R453-R462.

80. Son, Y., et al., *Reactive oxygen species in the activation of MAP kinases.* Methods Enzymol, 2013. **528**: p. 27-48.

81. Redza-Dutordoir, M. and D.A. Averill-Bates, *Activation of apoptosis signalling pathways by reactive oxygen species.* Biochim Biophys Acta, 2016. **1863**(12): p. 2977-2992.

82. Liou, G.Y. and P. Storz, *Reactive oxygen species in cancer.* Free Radic Res, 2010. **44**(5): p. 479-496.

83. Fan, T., et al., *Implications of Bit1 and AIF overexpressions in esophageal squamous cell carcinoma.* Tumour Biol, 2014. **35**(1): p. 519-527.

84. Skyrlas, A., et al., *Expression of apoptosis-inducing factor (AIF) in keratoacanthomas and squamous cell carcinomas of the skin.* Exp Dermatol, 2011. **20**(8): p. 674-676.

85. Jeong, E.G., et al., *Immunohistochemical and mutational analysis of apoptosis-inducing factor (AIF) in colorectal carcinomas.* APMIS, 2006. **114**(12): p. 867-873.

86. Millan, A. and S. Huerta, *Apoptosis-inducing factor and colon cancer.* J Surg Res, 2009. **151**(1): p. 163-70.

87. Lee, J.W., et al., *Immunohistochemical analysis of apoptosis-inducing factor (AIF) expression in gastric carcinomas.* Pathol Res Pract, 2006. **202**(7): p. 497-501.

88. Li, S., et al., *Expression of AIF and HtrA2/Omi in small lymphocytic lymphoma and diffuse large B-cell lymphoma.* Arch Pathol Lab Med, 2011. **135**(7): p. 903-908.

89. Varambally, S., et al., *Integrative genomic and proteomic analysis of prostate cancer reveals signatures of metastatic progression.* Cancer Cell, 2005. **8**(5): p. 393-406.

90. Devi, G.R., *XIAP as target for therapeutic apoptosis in prostate cancer.* Drug News Perspect, 2004. **17**(2): p. 127-134.

91. Murphy, M.E., *The HSP70 family and cancer.* Carcinogenesis, 2013. **34**(6): p. 1181-1188.

92. Frenzel, A., et al., *Bcl2 family proteins in carcinogenesis and the treatment of cancer.* Apoptosis, 2009. **14**(4): p. 584-596.

93. Solaini, G., G. Sgarbi, and A. Baracca, *Oxidative phosphorylation in cancer cells.* Biochim Biophys Acta, 2011. **1807**(6): p. 534-542.

94. Viale, A., et al., *Oncogene ablation-resistant pancreatic cancer cells depend on mitochondrial function.* Nature, 2014. **514**(7524): p. 628-632.

95. Tan, A.S., et al., *Mitochondrial Genome Acquisition Restores Respiratory Function and Tumorigenic Potential of Cancer Cells without Mitochondrial DNA.* Cell Metab, 2015. **21**(1): p. 81-94.

96. LeBleu, V.S., et al., *PGC-1alpha mediates mitochondrial biogenesis and oxidative phosphorylation in cancer cells to promote metastasis.* Nat Cell Biol, 2014. **16**(10): p. 992-1003, 1-15.

97. Wang, S., et al., *Prostate-specific deletion of the murine Pten tumor suppressor gene leads to metastatic prostate cancer.* Cancer Cell, 2003. **4**(3): p. 209-221.

98. Cleary, S.P., et al., *Prognostic factors in resected pancreatic adenocarcinoma: analysis of actual 5-year survivors.* J Am Coll Surg, 2004. **198**(5): p. 722-31.

99. Collisson, E.A., et al., *Subtypes of pancreatic ductal adenocarcinoma and their differing responses to therapy.* Nat Med, 2011. **17**(4): p. 500-503.

100. Daemen, A., et al., *Metabolite profiling stratifies pancreatic ductal adenocarcinomas into subtypes with distinct sensitivities to metabolic inhibitors.* Proc Natl Acad Sci U S A, 2015. **112**(32): p. E4410-4417.

101. Siegel, R., et al., *Cancer statistics, 2014.* CA Cancer J Clin, 2014. **64**(1): p. 9-29.

102. Perera, R.M. and N. Bardeesy, *Pancreatic Cancer Metabolism: Breaking It Down to Build It Back Up.* Cancer Discov, 2015. **5**(12): p. 1247-1261.

103. Panieri, E. and M.M. Santoro, *ROS homeostasis and metabolism: a dangerous liason in cancer cells.* Cell Death Dis, 2016. **7**(6): p. e2253.

104. Wilkinson, J.C., et al., *Upstream Regulatory Role for XIAP in Receptor-Mediated Apoptosis.* Mol Cell Biol, 2004. **24**(16): p. 7003-7014.

105. Liang, C.C., A.Y. Park, and J.L. Guan, *In vitro scratch assay: a convenient and inexpensive method for analysis of cell migration in vitro.* Nat Protoc, 2007. **2**(2): p. 329-333.

106. Biancur, D.E. and A.C. Kimmelman, *The plasticity of pancreatic cancer metabolism in tumor progression and therapeutic resistance.* Biochim Biophys Acta Rev Cancer, 2018. **1870**(1): p. 67-75.

107. Burris, H.A., 3rd, et al., *Improvements in survival and clinical benefit with gemcitabine as first-line therapy for patients with advanced pancreas cancer: a randomized trial.* J Clin Oncol, 1997. **15**(6): p. 2403-2413.

108. Cheng, G., et al., *Mitochondria-targeted drugs synergize with 2-deoxyglucose to trigger breast cancer cell death.* Cancer Res, 2012. **72**(10): p. 2634-2644.

109. Zafarullah, M., et al., *Molecular mechanisms of N-acetylcysteine actions.* Cell Mol Life Sci, 2003. **60**(1): p. 6-20.

110. Kumari, S., et al., *Reactive Oxygen Species: A Key Constituent in Cancer Survival.* Biomark Insights, 2018. **13**: p. 1-9.

111. Verweij, J., M. Clavel, and B. Chevalier, *Paclitaxel (Taxol) and docetaxel (Taxotere): not simply two of a kind.* Ann Oncol, 1994. **5**(6): p. 495-505.

112. Meresse, P., et al., *Etoposide: discovery and medicinal chemistry.* Curr Med Chem, 2004. **11**(18): p. 2443-2466.

113. Grutzmann, R., et al., *Gene expression profiling of microdissected pancreatic ductal carcinomas using high-density DNA microarrays.* Neoplasia, 2004. **6**(5): p. 611-622.

114. Buchholz, M., et al., *Transcriptome analysis of microdissected pancreatic intraepithelial neoplastic lesions.* Oncogene, 2005. **24**(44): p. 6626-6636.

115. Iacobuzio-Donahue, C.A., et al., *Exploration of global gene expression patterns in pancreatic adenocarcinoma using cDNA microarrays.* Am J Pathol, 2003. **162**(4): p. 1151-1162.

116. Segara, D., et al., *Expression of HOXB2, a retinoic acid signaling target in pancreatic cancer and pancreatic intraepithelial neoplasia.* Clin Cancer Res, 2005. **11**(9): p. 3587-3596.

117. Ishikawa, M., et al., *Experimental trial for diagnosis of pancreatic ductal carcinoma based on gene expression profiles of pancreatic ductal cells.* Cancer Sci, 2005. **96**(7): p. 387-393.

118. Badea, L., et al., *Combined gene expression analysis of whole-tissue and microdissected pancreatic ductal adenocarcinoma identifies genes specifically overexpressed in tumor epithelia.* Hepatogastroenterology, 2008. **55**(88): p. 2016-2027.

119. Pei, H., et al., *FKBP51 affects cancer cell response to chemotherapy by negatively regulating Akt.* Cancer Cell, 2009. **16**(3): p. 259-266.

120. Rhodes, D.R., et al., *Oncomine 3.0: genes, pathways, and networks in a collection of 18,000 cancer gene expression profiles.* Neoplasia, 2007. **9**(2): p. 166-180.

121. Turner, R.L., J.C. Wilkinson, and D.A. Ornelles, *E1B and E4 oncoproteins of adenovirus antagonize the effect of apoptosis inducing factor.* Virology, 2014. **456-457**: p. 205-219.

122. Yu, J., et al., *SMAC/Diablo mediates the proapoptotic function of PUMA by regulating PUMA-induced mitochondrial events.* Oncogene, 2007. **26**(29): p. 4189-98.

123. Qin, X.F., et al., *Inhibiting HIV-1 infection in human T cells by lentiviral-mediated delivery of small interfering RNA against CCR5.* Proc Natl Acad Sci U S A, 2003. **100**(1): p. 183-188.

124. Galban, S., et al., *Cytoprotective effects of IAPs revealed by a small molecule antagonist.* Biochem J, 2009. **417**(3): p. 765-71.

125. Lieber, M., et al., *Establishment of a continuous tumor-cell line (panc-1) from a human carcinoma of the exocrine pancreas.* Int J Cancer, 1975. **15**(5): p. 741-747.

126. Tan, M.H., et al., *Characterization of a new primary human pancreatic tumor line.* Cancer Invest, 1986. **4**(1): p. 15-23.

127. Gower, W.R., Jr., et al., *HPAC, a new human glucocorticoid-sensitive pancreatic ductal adenocarcinoma cell line.* In Vitro Cell Dev Biol Anim, 1994. **30A**(3): p. 151-161.

128. Yunis, A.A., G.K. Arimura, and D.J. Russin, *Human pancreatic carcinoma (MIA PaCa-2) in continuous culture: sensitivity to asparaginase.* Int J Cancer, 1977. **19**(1): p. 128-135.

129. Metzgar, R.S., et al., *Antigens of human pancreatic adenocarcinoma cells defined by murine monoclonal antibodies.* Cancer Res, 1982. **42**(2): p. 601-608.

130. Deer, E.L., et al., *Phenotype and genotype of pancreatic cancer cell lines.* Pancreas, 2010. **39**(4): p. 425-435.

131. Moore, P.S., et al., *Genetic profile of 22 pancreatic carcinoma cell lines. Analysis of K-ras, p53, p16 and DPC4/Smad4.* Virchows Arch, 2001. **439**(6): p. 798-802.

132. Sobell, H.M., *Actinomycin and DNA transcription.* Proc Natl Acad Sci U S A, 1985. **82**(16): p. 5328-5331.

133. Palorini, R., et al., *Oncogenic K-ras expression is associated with derangement of the cAMP/PKA pathway and forskolin-reversible alterations of mitochondrial dynamics and respiration.* Oncogene, 2013. **32**(3): p. 352-362.

134. Maher, J.C., et al., *Differential sensitivity to 2-deoxy-D-glucose between two pancreatic cell lines correlates with GLUT-1 expression.* Pancreas, 2005. **30**(2): p. e34-9.

135. Kim, G.T., et al., *Role of apoptosis-inducing factor in myocardial cell death by ischemia-reperfusion.* Biochem Biophys Res Commun, 2003. **309**(3): p. 619-624.

136. Zhang, X., et al., *Intranuclear localization of apoptosis-inducing factor (AIF) and large scale DNA fragmentation after traumatic brain injury in rats and in neuronal cultures exposed to peroxynitrite.* J Neurochem, 2002. **82**(1): p. 181-191.

137. Granville, D.J., et al., *Mitochondrial release of apoptosis-inducing factor and cytochrome c during smooth muscle cell apoptosis.* Am J Pathol, 2001. **159**(1): p. 305-311.

138. Cao, G., et al., *Translocation of apoptosis-inducing factor in vulnerable neurons after transient cerebral ischemia and in neuronal cultures after oxygen-glucose deprivation.* J Cereb Blood Flow Metab, 2003. **23**(10): p. 1137-1150.

139. Zhu, C., et al., *Involvement of apoptosis-inducing factor in neuronal death after hypoxia-ischemia in the neonatal rat brain.* J Neurochem, 2003. **86**(2): p. 306-317.

140. Zhang, W., et al., *Nuclear translocation of apoptosis inducing factor is associated with cisplatin induced apoptosis in LNCaP prostate cancer cells.* Cancer Lett, 2007. **255**(1): p. 127-134.

141. Kang, Y.H., et al., *Caspase-independent cell death by arsenic trioxide in human cervical cancer cells: reactive oxygen species-mediated poly(ADP-ribose) polymerase-1 activation signals apoptosis-inducing factor release from mitochondria.* Cancer Res, 2004. **64**(24): p. 8960-8967.

142. Aguilar, R.C. and B. Wendland, *Ubiquitin: not just for proteasomes anymore.* Curr Opin Cell Biol, 2003. **15**(2): p. 184-90.

143. Kim, K.H. and M.S. Lee, *Autophagy--a key player in cellular and body metabolism.* Nat Rev Endocrinol, 2014. **10**(6): p. 322-337.

144. Pearce, S.F., et al., *Regulation of Mammalian Mitochondrial Gene Expression: Recent Advances.* Trends Biochem Sci, 2017. **42**(8): p. 625-639.

145. Amunts, A., et al., *Ribosome. The structure of the human mitochondrial ribosome.* Science, 2015. **348**(6230): p. 95-98.

146. Ramakrishnan, V., *Ribosome structure and the mechanism of translation.* Cell, 2002. **108**(4): p. 557-572.

147. Brady, G.F., et al., *Regulation of the copper chaperone CCS by XIAP-mediated ubiquitination.* Mol Cell Biol, 2010. **30**(8): p. 1923-1936.

148. Zhang, X., et al., *Translational control of the cytosolic stress response by mitochondrial ribosomal protein L18.* Nat Struct Mol Biol, 2015. **22**(5): p. 404-410.

149. Sarbassov, D.D., et al., *Phosphorylation and regulation of Akt/PKB by the rictor-mTOR complex.* Science, 2005. **307**(5712): p. 1098-1101.

150. Chae, S., et al., *A systems approach for decoding mitochondrial retrograde signaling pathways.* Sci Signal, 2013. **6**(264): p. rs4.

151. Palmieri, D., et al., *Analyses of resected human brain metastases of breast cancer reveal the association between up-regulation of hexokinase 2 and poor prognosis.* Mol Cancer Res, 2009. **7**(9): p. 1438-1445.

152. Gjesing, A.P., et al., *Studies of a genetic variant in HK1 in relation to quantitative metabolic traits and to the prevalence of type 2 diabetes.* BMC Med Genet, 2011. **12**: p. 99.

153. Mor, I., E.C. Cheung, and K.H. Vousden, *Control of glycolysis through regulation of PFK1: old friends and recent additions.* Cold Spring Harb Symp Quant Biol, 2011. **76**: p. 211-216.

154. Vora, S., *Isozymes of human phosphofructokinase: biochemical and genetic aspects.* Isozymes Curr Top Biol Med Res, 1983. **11**: p. 3-23.

155. Kim, S.G., et al., *Crystal structure of the hypoxia-inducible form of 6-phosphofructo-2-kinase/fructose-2,6-bisphosphatase (PFKFB3): a possible new target for cancer therapy.* J Biol Chem, 2006. **281**(5): p. 2939-2344.

156. Sakakibara, R., et al., *Characterization of a human placental fructose-6-phosphate, 2-kinase/fructose-2,6-bisphosphatase.* J Biochem, 1997. **122**(1): p. 122-128.

157. Loiseau, A.M., et al., *Rat hepatoma (HTC) cell 6-phosphofructo-2-kinase differs from that in liver and can be separated from fructose-2,6-bisphosphatase.* Eur J Biochem, 1988. **175**(1): p. 27-32.

158. Capello, M., et al., *Targeting the Warburg effect in cancer cells through ENO1 knockdown rescues oxidative phosphorylation and induces growth arrest.* Oncotarget, 2016. **7**(5): p. 5598-5612.

159. Liu, C.C., et al., *ENO2 Promotes Cell Proliferation, Glycolysis, and Glucocorticoid-Resistance in Acute Lymphoblastic Leukemia.* Cell Physiol Biochem, 2018. **46**(4): p. 1525-1535.

160. Hitosugi, T., et al., *Phosphoglycerate mutase 1 coordinates glycolysis and biosynthesis to promote tumor growth.* Cancer Cell, 2012. **22**(5): p. 585-600.

161. Miller, D.M., et al., *c-Myc and cancer metabolism.* Clin Cancer Res, 2012. **18**(20): p. 5546-5553.

162. Englmeier, R., S. Pfeffer, and F. Forster, *Structure of the Human Mitochondrial Ribosome Studied In Situ by Cryoelectron Tomography.* Structure, 2017. **25**(10): p. 1574-1581 e2.

163. Liu, M. and L. Spremulli, *Interaction of mammalian mitochondrial ribosomes with the inner membrane.* J Biol Chem, 2000. **275**(38): p. 29400-29406.

164. Stewart, S.A., et al., *Lentivirus-delivered stable gene silencing by RNAi in primary cells.* RNA, 2003. **9**(4): p. 493-501.

165. Ichijo, H., et al., *Induction of apoptosis by ASK1, a mammalian MAPKKK that activates SAPK/JNK and p38 signaling pathways.* Science, 1997. **275**: p. 90-94.

166. Lei, K., et al., *The Bax subfamily of Bcl2-related proteins is essential for apoptotic signal transduction by c-Jun NH(2)-terminal kinase.* Mol Cell Biol, 2002. **22**(13): p. 4929-4942.

167. Wang, W., et al., *Excess capacity of the iron regulatory protein system.* J Biol Chem, 2007. **282**(34): p. 24650-24659.

168. Wiraswati, H.L., et al., *Apoptosis inducing factor (AIF) mediates lethal redox stress induced by menadione.* Oncotarget, 2016. **7**(47): p. 76496-76507.

169. Nguyen, T., P. Nioi, and C.B. Pickett, *The Nrf2-antioxidant response element signaling pathway and its activation by oxidative stress.* J Biol Chem, 2009. **284**(20): p. 13291-13295.

170. Sobel, R.E. and M.D. Sadar, *Cell lines used in prostate cancer research: a compendium of old and new lines--part 1.* J Urol, 2005. **173**(2): p. 342-359.

171. Dougherty, J.A., et al., *Dual-Specificity Phosphatase 4 Overexpression in Cells Prevents Hypoxia/Reoxygenation-Induced Apoptosis via the Upregulation of eNOS.* Front Cardiovasc Med, 2017. **4**: p. 22.

172. Hazzalin, C.A., et al., *Anisomycin selectively desensitizes signalling components involved in stress kinase activation and fos and jun induction.* Mol Cell Biol, 1998. **18**(4): p. 1844-1854.

173. Tobiume, K., et al., *ASK1 is required for sustained activations of JNK/p38 MAP kinases and apoptosis.* EMBO Rep, 2001. **2**(3): p. 222-228.

174. Bode, A.M. and Z. Dong, *The functional contrariety of JNK.* Mol Carcinog, 2007. **46**(8): p. 591-598.

175. Krasnik, V., et al., *Prognostic value of apoptosis inducing factor in uveal melanoma.* Neoplasma, 2017. **64**(2).

176. Lamouille, S., J. Xu, and R. Derynck, *Molecular mechanisms of epithelial-mesenchymal transition.* Nat Rev Mol Cell Biol, 2014. **15**(3): p. 178-196.

177. Burger, G.A., E.H.J. Danen, and J.B. Beltman, *Deciphering Epithelial-Mesenchymal Transition Regulatory Networks in Cancer through Computational Approaches.* Front Oncol, 2017. **7**: p. 162.

178. Aroeira, L.S., et al., *Epithelial to mesenchymal transition and peritoneal membrane failure in peritoneal dialysis patients: pathologic significance and potential therapeutic interventions.* J Am Soc Nephrol, 2007. **18**(7): p. 2004-2013.

179. Onder, T.T., et al., *Loss of E-cadherin promotes metastasis via multiple downstream transcriptional pathways.* Cancer Res, 2008. **68**(10): p. 3645-3654.

180. Hui, L., et al., *Proliferation of human HCC cells and chemically induced mouse liver cancers requires JNK1-dependent p21 downregulation.* J Clin Invest, 2008. **118**(12): p. 3943-3953.

181. Goel, H.L., et al., *beta1 integrins mediate resistance to ionizing radiation in vivo by inhibiting c-Jun amino terminal kinase 1.* J Cell Physiol, 2013. **228**(7): p. 1601-1609.

182. Rouget, R., et al., *A sensitive flow cytometry-based nucleotide excision repair assay unexpectedly reveals that mitogen-activated protein kinase signaling does not regulate the removal of UV-induced DNA damage in human cells.* J Biol Chem, 2008. **283**(9): p. 5533-5541.

183. Su, K.H., et al., *HSF1 critically attunes proteotoxic stress sensing by mTORC1 to combat stress and promote growth.* Nat Cell Biol, 2016. **18**(5): p. 527-539.

184. Davis, R.J., *Signal transduction by the JNK group of MAP kinases.* Cell, 2000. **103**(2): p. 239-252.

185. Hazan, R.B., et al., *Cadherin switch in tumor progression.* Ann N Y Acad Sci, 2004. **1014**: p. 155-163.

186. Horoszewicz, J.S., et al., *LNCaP model of human prostatic carcinoma.* Cancer Res, 1983. **43**(4): p. 1809-1818.

187. Bennett, B.L., et al., *SP600125, an anthrapyrazolone inhibitor of Jun N-terminal kinase.* Proc Natl Acad Sci U S A, 2001. **98**(24): p. 13681-13686.

188. Goldman, R.D., et al., *The function of intermediate filaments in cell shape and cytoskeletal integrity.* J Cell Biol, 1996. **134**(4): p. 971-983.

189. Schmalhofer, O., S. Brabletz, and T. Brabletz, *E-cadherin, beta-catenin, and ZEB1 in malignant progression of cancer.* Cancer Metastasis Rev, 2009. **28**(1-2): p. 151-166.

190. Bays, J.L., et al., *Linking E-cadherin mechanotransduction to cell metabolism through force-mediated activation of AMPK.* Nat Cell Biol, 2017. **19**(6): p. 724-731.

191. Faubert, B., et al., *AMPK is a negative regulator of the Warburg effect and suppresses tumor growth in vivo.* Cell Metab, 2013. **17**(1): p. 113-124.

192. Hawley, S.A., et al., *Characterization of the AMP-activated protein kinase kinase from rat liver and identification of threonine 172 as the major site at which it phosphorylates AMP-activated protein kinase.* J Biol Chem, 1996. **271**(44): p. 27879-27887.

193. Lizcano, J.M., et al., *LKB1 is a master kinase that activates 13 kinases of the AMPK subfamily, including MARK/PAR-1.* EMBO J, 2004. **23**(4): p. 833-843.

194. Shaw, R.J., et al., *The tumor suppressor LKB1 kinase directly activates AMP-activated kinase and regulates apoptosis in response to energy stress.* Proc Natl Acad Sci U S A, 2004. **101**(10): p. 3329-3335.

195. Warden, S.M., et al., *Post-translational modifications of the beta-1 subunit of AMP-activated protein kinase affect enzyme activity and cellular localization.* Biochem J, 2001. **354**(Pt 2): p. 275-283.

196. Vander Heiden, M.G. and R.J. DeBerardinis, *Understanding the Intersections between Metabolism and Cancer Biology.* Cell, 2017. **168**(4): p. 657-669.

197. Modjtahedi, N., et al., *Apoptosis-inducing factor: vital and lethal.* Trends Cell Biol, 2006. **16**(5): p. 264-272.

198. Tournier, C., *The 2 Faces of JNK Signaling in Cancer.* Genes Cancer, 2013. **4**(9-10): p. 397-400.

199. Rodriguez, F.J., L.J. Lewis-Tuffin, and P.Z. Anastasiadis, *E-cadherin's dark side: possible role in tumor progression.* Biochim Biophys Acta, 2012. **1826**(1): p. 23-31.

200. Birsoy, K., et al., *Metabolic determinants of cancer cell sensitivity to glucose limitation and biguanides.* Nature, 2014. **508**(7494): p. 108-112.

201. Wilkinson, J.C., et al., *VIAF, a conserved inhibitor of apoptosis (IAP)-interacting factor that modulates caspase activation.* J Biol Chem, 2004. **279**(49): p. 51091-51099.

202. Seo, B.B., A. Matsuno-Yagi, and T. Yagi, *Modulation of oxidative phosphorylation of human kidney 293 cells by transfection with the internal rotenone-insensitive NADH-quinone oxidoreductase (NDI1) gene of Saccharomyces cerevisiae.* Biochim Biophys Acta, 1999. **1412**(1): p. 56-65.

203. Wheaton, W.W., et al., *Metformin inhibits mitochondrial complex I of cancer cells to reduce tumorigenesis.* Elife, 2014. **3**: p. e02242.

204. Milasta, S., et al., *Apoptosis-Inducing-Factor-Dependent Mitochondrial Function Is Required for T Cell but Not B Cell Function.* Immunity, 2016. **44**(1): p. 88-102.

205. Scott, A.J., et al., *AIF promotes a JNK1-mediated cadherin switch independently of respiratory chain stabilization.* J Biol Chem, 2018.

206. Yang, Y., et al., *Ubiquitin protein ligase activity of IAPs and their degradation in proteasomes in response to apoptotic stimuli.* Science, 2000. **288**: p. 874-877.

207. MacFarlane, M., et al., *Proteasome-mediated degradation of Smac during apoptosis: XIAP promotes Smac ubiquitination in vitro.* J Biol Chem, 2002. **277**(39): p. 36611-36616.

208. Jedrzejas, M.J., *Structure, function, and evolution of phosphoglycerate mutases: comparison with fructose-2,6-bisphosphatase, acid phosphatase, and alkaline phosphatase.* Prog Biophys Mol Biol, 2000. **73**(2-4): p. 263-287.

209. Carpino, N., et al., *Regulation of ZAP-70 activation and TCR signaling by two related proteins, Sts-1 and Sts-2.* Immunity, 2004. **20**(1): p. 37-46.

210. Kowanetz, K., et al., *Suppressors of T-cell receptor signaling Sts-1 and Sts-2 bind to Cbl and inhibit endocytosis of receptor tyrosine kinases.* J Biol Chem, 2004. **279**(31): p. 32786-32795.

211. Takeda, K., et al., *Mitochondrial phosphoglycerate mutase 5 uses alternate catalytic activity as a protein serine/threonine phosphatase to activate ASK1.* Proceedings of the National Academy of Sciences of the United States of America, 2009. **106**(30): p. 12301-12305.

212. Lo, S.C. and M. Hannink, *PGAM5, a Bcl-XL-interacting protein, is a novel substrate for the redox-regulated Keap1-dependent ubiquitin ligase complex.* J Biol Chem, 2006. **281**(49): p. 37893-37903.

213. Lo, S.C. and M. Hannink, *PGAM5 tethers a ternary complex containing Keap1 and Nrf2 to mitochondria.* Exp Cell Res, 2008. **314**(8): p. 1789-1803.

214. Hammond, P.W., et al., *In vitro selection and characterization of Bcl-X(L)-binding proteins from a mix of tissue-specific mRNA display libraries.* J Biol Chem, 2001. **276**(24): p. 20898-20906.

215. Wang, Z., et al., *The mitochondrial phosphatase PGAM5 functions at the convergence point of multiple necrotic death pathways.* Cell, 2012. **148**(1-2): p. 228-243.

216. Ishida, Y., et al., *Prevention of apoptosis by mitochondrial phosphatase PGAM5 in the mushroom body is crucial for heat shock resistance in Drosophila melanogaster.* PLoS One, 2012. **7**(2): p. e30265.

217. Chen, G., et al., *A regulatory signaling loop comprising the PGAM5 phosphatase and CK2 controls receptor-mediated mitophagy.* Mol Cell, 2014. **54**(3): p. 362-377.

218. Lu, W., et al., *Genetic deficiency of the mitochondrial protein PGAM5 causes a Parkinson's-like movement disorder.* Nat Commun, 2014. **5**: p. 4930.

219. Xu, W., et al., *Bax-PGAM5L-Drp1 complex is required for intrinsic apoptosis execution.* Oncotarget, 2015. **6**(30): p. 30017-30034.

220. Lu, W., et al., *Mitochondrial Protein PGAM5 Regulates Mitophagic Protection against Cell Necroptosis.* PLoS One, 2016. **11**(1): p. e0147792.

221. Youle, R.J. and D.P. Narendra, *Mechanisms of mitophagy.* Nat Rev Mol Cell Biol, 2011. **12**(1): p. 9-14.

222. Narendra, D.P., et al., *PINK1 is selectively stabilized on impaired mitochondria to activate Parkin.* PLoS biology, 2010. **8**(1): p. e1000298.

223. Narendra, D., et al., *Parkin is recruited selectively to impaired mitochondria and promotes their autophagy.* The Journal of cell biology, 2008. **183**(5): p. 795-803.

224. Cao, P., et al., *MicroRNA-101 negatively regulates Ezh2 and its expression is modulated by androgen receptor and HIF-1alpha/HIF-1beta.* Mol Cancer, 2010. **9**: p. 108.

225. Rumble, J.M., et al., *Apoptotic sensitivity of murine IAP-deficient cells.* Biochem J, 2008. **415**(1): p. 21-5.

226. Wilkins, J.M., et al., *A conserved motif mediates both multimer formation and allosteric activation of phosphoglycerate mutase 5.* J Biol Chem, 2014. **289**(36): p. 25137-25148.

227. Chaikuad, A., et al., *Structures of PGAM5 Provide Insight into Active Site Plasticity and Multimeric Assembly.* Structure, 2017. **25**(7): p. 1089-1099 e3.

228. Ruiz, K., et al., *Functional role of PGAM5 multimeric assemblies and their polymerization into filaments.* Nat Commun, 2019. **10**(1): p. 531.

229. Fu, T.M., et al., *Cryo-EM Structure of Caspase-8 Tandem DED Filament Reveals Assembly and Regulation Mechanisms of the Death-Inducing Signaling Complex.* Mol Cell, 2016. **64**(2): p. 236-250.

230. Li, J., et al., *The RIP1/RIP3 necrosome forms a functional amyloid signaling complex required for programmed necrosis.* Cell, 2012. **150**(2): p. 339-350.

231. Swatek, K.N. and D. Komander, *Ubiquitin modifications.* Cell Res, 2016. **26**(4): p. 399-422.

232. Yang, C., et al., *Mitochondrial phosphatase PGAM5 regulates Keap1-mediated Bcl-xL degradation and controls cardiomyocyte apoptosis driven by myocardial ischemia/reperfusion injury.* In Vitro Cell Dev Biol Anim, 2017. **53**(3): p. 248-257.

233. Miller, W.H., Jr., et al., *Mechanisms of action of arsenic trioxide.* Cancer Res, 2002. **62**(14): p. 3893-3903.

234. Lew, Y.S., et al., *Arsenic trioxide causes selective necrosis in solid murine tumors by vascular shutdown.* Cancer Res, 1999. **59**(24): p. 6033-6037.

235. Niu, Z., et al., *Mitophagy inhibits proliferation by decreasing cyclooxygenase-2 (COX-2) in arsenic trioxide-treated HepG2 cells.* Environ Toxicol Pharmacol, 2016. **45**: p. 212-221.

236. Tsujimoto, Y. and S. Shimizu, *Another way to die: autophagic programmed cell death.* Cell Death Differ, 2005. **12 Suppl 2**: p. 1528-1534.

237. Levine, B. and D.J. Klionsky, *Development by self-digestion: molecular mechanisms and biological functions of autophagy.* Dev Cell, 2004. **6**(4): p. 463-477.

238. Ohsumi, Y., *Molecular dissection of autophagy: two ubiquitin-like systems.* Nat Rev Mol Cell Biol, 2001. **2**(3): p. 211-216.

239. Huang, W.P. and D.J. Klionsky, *Autophagy in yeast: a review of the molecular machinery.* Cell Struct Funct, 2002. **27**(6): p. 409-420.

240. Mizushima, N., Y. Ohsumi, and T. Yoshimori, *Autophagosome formation in mammalian cells.* Cell Struct Funct, 2002. **27**(6): p. 421-429.

241. Yang, Z. and D.J. Klionsky, *Eaten alive: a history of macroautophagy.* Nat Cell Biol, 2010. **12**(9): p. 814-822.

242. Shintani, T. and D.J. Klionsky, *Autophagy in health and disease: a double-edged sword.* Science, 2004. **306**(5698): p. 990-995.

243. Vandenabeele, P., et al., *Molecular mechanisms of necroptosis: an ordered cellular explosion.* Nat Rev Mol Cell Biol, 2010. **11**(10): p. 700-714.

244. Kaczmarek, A., P. Vandenabeele, and D.V. Krysko, *Necroptosis: the release of damage-associated molecular patterns and its physiological relevance.* Immunity, 2013. **38**(2): p. 209-223.

245. Upton, J.W., W.J. Kaiser, and E.S. Mocarski, *Virus inhibition of RIP3-dependent necrosis.* Cell Host Microbe, 2010. **7**(4): p. 302-313.

246. Liu, P., et al., *Dysregulation of TNFalpha-induced necroptotic signaling in chronic lymphocytic leukemia: suppression of CYLD gene by LEF1.* Leukemia, 2012. **26**(6): p. 1293-1300.

247. Cerhan, J.R., et al., *Genetic variation in 1253 immune and inflammation genes and risk of non-Hodgkin lymphoma.* Blood, 2007. **110**(13): p. 4455-4463.

248. Fulda, S., *The mechanism of necroptosis in normal and cancer cells.* Cancer Biol Ther, 2013. **14**(11): p. 999-1004.

249. Lu, H., W. Ouyang, and C. Huang, *Inflammation, a key event in cancer development.* Mol Cancer Res, 2006. **4**(4): p. 221-33.

250. Eckhart, L., et al., *Cell death by cornification.* Biochim Biophys Acta, 2013. **1833**(12): p. 3471-3480.

251. David, K.K., et al., *Parthanatos, a messenger of death.* Front Biosci (Landmark Ed), 2009. **14**: p. 1116-1128.

252. Boatright, K.M. and G.S. Salvesen, *Mechanisms of caspase activation.* Curr Opin Cell Biol, 2003. **15**(6): p. 725-731.

253. Aggarwal, B.B., *Signalling pathways of the TNF superfamily: a double-edged sword.* Nat Rev Immunol, 2003. **3**(9): p. 745-756.

254. Debatin, K.M. and P.H. Krammer, *Death receptors in chemotherapy and cancer.* Oncogene, 2004. **23**(16): p. 2950-2966.

255. Cory, S. and J.M. Adams, *The Bcl2 family: regulators of the cellular life-or-death switch.* Nat Rev Cancer, 2002. **2**(9): p. 647-656.

256. Cote, J. and A. Ruiz-Carrillo, *Primers for mitochondrial DNA replication generated by endonuclease G.* Science, 1993. **261**(5122): p. 765-769.

257. Li, L.Y., X. Luo, and X. Wang, *Endonuclease G is an apoptotic DNase when released from mitochondria.* Nature, 2001. **412**(6842): p. 95-99.

258. Porter, A.G. and A.G. Urbano, *Does apoptosis-inducing factor (AIF) have both life and death functions in cells?* Bioessays, 2006. **28**(8): p. 834-843.

259. Chipuk, J.E. and D.R. Green, *Do inducers of apoptosis trigger caspase-independent cell death?* Nat Rev Mol Cell Biol, 2005. **6**(3): p. 268-275.

260. Kroemer, G. and S.J. Martin, *Caspase-independent cell death.* Nat Med, 2005. **11**(7): p. 725-730.

261. Gunther, C., et al., *Caspase-8 regulates TNF-alpha-induced epithelial necroptosis and terminal ileitis.* Nature, 2011. **477**(7364): p. 335-339.

262. Wrighton, K.H., *Cell death: A killer puts a stop on necroptosis.* Nat Rev Mol Cell Biol, 2011. **12**(5): p. 279.

263. Christofferson, D.E. and J. Yuan, *Necroptosis as an alternative form of programmed cell death.* Curr Opin Cell Biol, 2010. **22**(2): p. 263-268.

264. Cho, Y.S., et al., *Phosphorylation-driven assembly of the RIP1-RIP3 complex regulates programmed necrosis and virus-induced inflammation.* Cell, 2009. **137**(6): p. 1112-1123.

265. He, S., et al., *Receptor interacting protein kinase-3 determines cellular necrotic response to TNF-alpha.* Cell, 2009. **137**(6): p. 1100-1111.

266. Zhang, D.W., et al., *RIP3, an energy metabolism regulator that switches TNF-induced cell death from apoptosis to necrosis.* Science, 2009. **325**(5938): p. 332-336.

267. Imai, Y., et al., *The loss of PGAM5 suppresses the mitochondrial degeneration caused by inactivation of PINK1 in Drosophila.* PLoS Genet, 2010. **6**(12): p. e1001229.

268. Maeda, A. and B. Fadeel, *Mitochondria released by cells undergoing TNF-alpha-induced necroptosis act as danger signals.* Cell Death Dis, 2014. **5**: p. e1312.

269. Kelly, C.M. and A.U. Buzdar, *Using multiple targeted therapies in oncology: considerations for use, and progress to date in breast cancer.* Drugs, 2013. **73**(6): p. 505-515.

270. Cid-Arregui, A. and V. Juarez, *Perspectives in the treatment of pancreatic adenocarcinoma.* World J Gastroenterol, 2015. **21**(31): p. 9297-9316.

271. Moffitt, R.A., et al., *Virtual microdissection identifies distinct tumor- and stroma-specific subtypes of pancreatic ductal adenocarcinoma.* Nat Genet, 2015. **47**(10): p. 1168-1178.

272. Noll, E.M., et al., *CYP3A5 mediates basal and acquired therapy resistance in different subtypes of pancreatic ductal adenocarcinoma.* Nat Med, 2016. **22**(3): p. 278-287.

273. Biankin, A.V. and A. Maitra, *Subtyping Pancreatic Cancer.* Cancer Cell, 2015. **28**(4): p. 411-413.

274. Carr, R.M. and M.E. Fernandez-Zapico, *Pancreatic cancer microenvironment, to target or not to target?* EMBO Mol Med, 2016. **8**(2): p. 80-82.

275. Bailey, P., et al., *Genomic analyses identify molecular subtypes of pancreatic cancer.* Nature, 2016. **531**(7592): p. 47-52.

276. Wrighton, S.A., et al., *Studies on the expression and metabolic capabilities of human liver cytochrome P450IIIA5 (HLp3).* Mol Pharmacol, 1990. **38**(2): p. 207-213.

277. MacPhee, I.A., *Pharmacogenetic biomarkers: cytochrome P450 3A5.* Clin Chim Acta, 2012. **413**(17-18): p. 1312-1317.

278. Kuehl, P., et al., *Sequence diversity in CYP3A promoters and characterization of the genetic basis of polymorphic CYP3A5 expression.* Nat Genet, 2001. **27**(4): p. 383-391.

279. Walsky, R.L., et al., *Selective mechanism-based inactivation of CYP3A4 by CYP3cide (PF-04981517) and its utility as an in vitro tool for delineating the relative roles of CYP3A4 versus CYP3A5 in the metabolism of drugs.* Drug Metab Dispos, 2012. **40**(9): p. 1686-1697.

280. Crook, N.E., R.J. Clem, and L.K. Miller, *An apoptosis-inhibiting baculovirus gene with a zinc finger-like motif.* J. Virol., 1993. **67**(4): p. 2168-2174.

281. Birnbaum, M.J., R.J. Clem, and L.K. Miller, *An apoptosis-inhibiting gene from a nuclear polyhedrosis virus encoding a polypeptide with Cys/His sequence motifs.* J Virol, 1994. **68**(4): p. 2521-2528.

282. Verhagen, A.M., E.J. Coulson, and D.L. Vaux, *Inhibitor of apoptosis proteins and their relatives: IAPs and other BIRPs.* Genome Biol, 2001. **2**(7): p. REVIEWS3009.

283. LaCasse, E.C., et al., *IAP-targeted therapies for cancer.* Oncogene, 2008. **27**(48): p. 6252-6275.

284. Mahoney, D.J., et al., *Both cIAP1 and cIAP2 regulate TNFalpha-mediated NF-kappaB activation.* Proc Natl Acad Sci U S A, 2008. **105**(33): p. 11778-11783.

285. Dolcet, X., et al., *NF-kB in development and progression of human cancer.* Virchows Arch, 2005. **446**(5): p. 475-482.

286. Bertrand, M.J., et al., *cIAP1 and cIAP2 facilitate cancer cell survival by functioning as E3 ligases that promote RIP1 ubiquitination.* Mol Cell, 2008. **30**(6): p. 689-700.

287. Van der Heiden, K., et al., *Role of nuclear factor kappaB in cardiovascular health and disease.* Clin Sci (Lond), 2010. **118**(10): p. 593-605.

288. Dong, C., R.J. Davis, and R.A. Flavell, *MAP kinases in the immune response.* Annu Rev Immunol, 2002. **20**: p. 55-72.

289. Oeckinghaus, A., M.S. Hayden, and S. Ghosh, *Crosstalk in NF-kappaB signaling pathways.* Nat Immunol, 2011. **12**(8): p. 695-708.

290. Piva, R., G. Belardo, and M.G. Santoro, *NF-kappaB: a stress-regulated switch for cell survival.* Antioxid Redox Signal, 2006. **8**(3-4): p. 478-486.

291. O'Donnell, M.A. and A.T. Ting, *Chronicles of a death foretold: dual sequential cell death checkpoints in TNF signaling.* Cell Cycle, 2010. **9**(6): p. 1065-1071.

292. Duckett, C.S., et al., *Human IAP-like protein regulates programmed cell death downstream of Bcl-x_L and cytochrome c.* Mol. Cell. Biol., 1998. **18**: p. 608-615.

293. Birkey Reffey, S., et al., *X-linked inhibitor of apoptosis protein functions as a cofactor in transforming growth factor-β signaling.* J Biol.Chem, 2001. **276**(28): p. 26542-26549.

294. Hofer-Warbinek, R., et al., *Activation of NF-kappa B by XIAP, the X chromosome-linked inhibitor of apoptosis, in endothelial cells involves TAK1.* J Biol Chem, 2000. **275**(29): p. 22064-22068.

295. Levkau, B., et al., *XIAP induces cell-cycle arrest and activates nuclear factor-κB : new survival pathways disabled by caspase-mediated cleavage during apoptosis of human endothelial cells.* Circ Res, 2001. **88**(3): p. 282-290.

296. Srinivasula, S.M. and J.D. Ashwell, *IAPs: what's in a name?* Mol Cell, 2008. **30**(2): p. 123-135.

297. Burstein, E., et al., *A novel role for XIAP in copper homeostasis through regulation of MURR1.* EMBO J, 2004. **23**(1): p. 244-254.

298. Deveraux, Q.L., et al., *X-linked IAP is a direct inhibitor of cell-death proteases.* Nature, 1997. **388**: p. 300-304.

299. Takahashi, R., et al., *A single BIR domain of XIAP sufficient for inhibiting caspases.* J. Biol. Chem., 1998. **273**: p. 7787-7790.

300. Deveraux, Q.L., et al., *Cleavage of human inhibitor of apoptosis protein XIAP results in fragments with distinct specificities for caspases.* EMBO J., 1999. **18**(19): p. 5242-5251.

301. Srinivasula, S.M., et al., *A conserved XIAP-interaction motif in caspase-9 and Smac/DIABLO regulates caspase activity and apoptosis.* Nature, 2001. **410**(6824): p. 112-116.

302. Suzuki, Y., et al., *A serine protease, HtrA2, is released from the mitochondria and interacts with XIAP, inducing cell death.* Mol Cell, 2001. **8**(3): p. 613-621.

303. Verhagen, A.M., et al., *HtrA2 promotes cell death through its serine protease activity and its ability to antagonise inhibitor of apoptosis proteins.* J Biol Chem, 2001. **277**(1): p. 445-454.

304. Hegde, R., et al., *Identification of Omi/HtrA2 as a mitochondrial apoptotic serine protease that disrupts IAP-caspase interaction.* J Biol Chem, 2001. **277**(1): p. 432-438.

305. Martins, L.M., et al., *The serine protease Omi/HtrA2 regulates apoptosis by binding XIAP through a Reaper-like motif.* J Biol Chem, 2001. **277**(1): p. 439-444.

306. van Loo, G., et al., *The serine protease Omi/HtrA2 is released from mitochondria during apoptosis. Omi interacts with caspase-inhibitor XIAP and induces enhanced caspase activity.* Cell Death Differ, 2002. **9**(1): p. 20-26.

307. Du, C., et al., *Smac, a mitochondrial protein that promotes cytochrome c-dependent caspase activation by eliminating IAP inhibition.* Cell, 2000. **102**(1): p. 33-42.

308. Verhagen, A.M., et al., *Identification of DIABLO, a mammalian protein that promotes apoptosis by binding to and antagonizing IAP proteins.* Cell, 2000. **102**(1): p. 43-53.

309. Chai, J., et al., *Structural and biochemical basis of apoptotic activation by Smac/DIABLO.* Nature, 2000. **406**(6798): p. 855-862.

310. Sun, C., et al., *NMR structure and mutagenesis of the third Bir domain of the inhibitor of apoptosis protein XIAP.* J Biol Chem, 2000. **275**(43): p. 33777-33781.

311. Ekert, P.G., et al., *DIABLO promotes apoptosis by removing MIHA/XIAP from processed caspase 9.* J Cell Biol, 2001. **152**(3): p. 483-90.

312. Scott, F.L., et al., *XIAP inhibits caspase-3 and -7 using two binding sites: evolutionarily conserved mechanism of IAPs.* Embo J, 2005. **24**(3): p. 645-55.

313. Wu, G., et al., *Structural basis of IAP recognition by Smac/DIABLO.* Nature, 2000. **408**(6815): p. 1008-1012.

314. Martinez-Ruiz, G., et al., *Role of Smac/DIABLO in cancer progression.* J Exp Clin Cancer Res, 2008. **27**: p. 48.

315. Liu, Z., et al., *Structural basis for binding of Smac/DIABLO to the XIAP BIR3 domain.* Nature, 2000. **408**(6815): p. 1004-1008.

316. Kipp, R.A., et al., *Molecular targeting of inhibitor of apoptosis proteins based on small molecule mimics of natural binding partners.* Biochemistry, 2002. **41**(23): p. 7344-9.

317. Sun, H., et al., *Design of small-molecule peptidic and nonpeptidic Smac mimetics.* Acc Chem Res, 2008. **41**(10): p. 1264-1277.

318. Schmidt, N., et al., *Arginine-rich cell-penetrating peptides.* FEBS Lett, 2010. **584**(9): p. 1806-1813.

319. Yang, L., et al., *Predominant suppression of apoptosome by inhibitor of apoptosis protein in non-small cell lung cancer H460 cells: therapeutic effect of a novel polyarginine-conjugated Smac peptide.* Cancer Res, 2003. **63**(4): p. 831-837.

320. Arnt, C.R., et al., *Synthetic Smac/DIABLO peptides enhance the effects of chemotherapeutic agents by binding XIAP and cIAP1 in situ.* J Biol Chem, 2002. **277**(46): p. 44236-44243.

321. Prochiantz, A., *Getting hydrophilic compounds into cells: lessons from homeopeptides.* Curr Opin Neurobiol, 1996. **6**(5): p. 629-634.

322. Derossi, D., G. Chassaing, and A. Prochiantz, *Trojan peptides: the penetratin system for intracellular delivery.* Trends Cell Biol, 1998. **8**(2): p. 84-87.

323. Thoren, P.E., et al., *The antennapedia peptide penetratin translocates across lipid bilayers - the first direct observation.* FEBS Lett, 2000. **482**(3): p. 265-268.

324. Zeng, C., et al., *Sigma-2 receptor ligand as a novel method for delivering a SMAC mimetic drug for treating ovarian cancer.* Br J Cancer, 2013. **109**(9): p. 2368-2377.

325. Garg, G., et al., *Conjugation to a SMAC mimetic potentiates sigma-2 ligand induced tumor cell death in ovarian cancer.* Mol Cancer, 2014. **13**: p. 50.

326. Li, L., et al., *A small molecule Smac mimic potentiates TRAIL- and TNFalpha-mediated cell death.* Science, 2004. **305**(5689): p. 1471-1474.

327. Sun, H., et al., *Design, synthesis, and characterization of a potent, nonpeptide, cell-permeable, bivalent Smac mimetic that concurrently targets both the BIR2 and BIR3 domains in XIAP.* J Am Chem Soc, 2007. **129**(49): p. 15279-15294.

328. Sun, H., et al., *Potent bivalent Smac mimetics: effect of the linker on binding to inhibitor of apoptosis proteins (IAPs) and anticancer activity.* J Med Chem, 2011. **54**(9): p. 3306-3318.

329. Petersen, S.L., et al., *Autocrine TNFalpha signaling renders human cancer cells susceptible to Smac-mimetic-induced apoptosis.* Cancer Cell, 2007. **12**(5): p. 445-456.

330. Vince, J.E., et al., *IAP antagonists target cIAP1 to induce TNFalpha-dependent apoptosis.* Cell, 2007. **131**(4): p. 682-693.

331. Varfolomeev, E., et al., *IAP antagonists induce autoubiquitination of c-IAPs, NF-kappaB activation, and TNFalpha-dependent apoptosis.* Cell, 2007. **131**(4): p. 669-681.

332. Wu, H., J. Tschopp, and S.C. Lin, *Smac mimetics and TNFalpha: a dangerous liaison?* Cell, 2007. **131**(4): p. 655-658.

333. Fulda, S., et al., *Smac agonists sensitize for Apo2L/TRAIL- or anticancer drug-induced apoptosis and induce regression of malignant glioma in vivo.* Nat Med, 2002. **8**(8): p. 808-815.

334. Laukens, B., et al., *Smac mimetic bypasses apoptosis resistance in FADD- or caspase-8-deficient cells by priming for tumor necrosis factor alpha-induced necroptosis.* Neoplasia, 2011. **13**(10): p. 971-979.

335. Christofferson, D.E., et al., *A novel role for RIP1 kinase in mediating TNFalpha production.* Cell Death Dis, 2012. **3**: p. e320.

336. Chromik, J., et al., *Smac mimetic primes apoptosis-resistant acute myeloid leukaemia cells for cytarabine-induced cell death by triggering necroptosis.* Cancer Lett, 2014. **344**(1): p. 101-109.

337. Steinhart, L., K. Belz, and S. Fulda, *Smac mimetic and demethylating agents synergistically trigger cell death in acute myeloid leukemia cells and overcome apoptosis resistance by inducing necroptosis.* Cell Death Dis, 2013. **4**: p. e802.

338. Philchenkov, A., et al., *Caspases and cancer: mechanisms of inactivation and new treatment modalities.* Exp Oncol, 2004. **26**(2): p. 82-97.

339. Tourneur, L. and G. Chiocchia, *FADD: a regulator of life and death.* Trends Immunol, 2010. **31**(7): p. 260-269.

340. Flygare, J.A., et al., *Discovery of a potent small-molecule antagonist of inhibitor of apoptosis (IAP) proteins and clinical candidate for the treatment of cancer (GDC-0152).* J Med Chem, 2012. **55**(9): p. 4101-4113.

341. Tolcher, A.W., et al., *Phase I study of safety and pharmacokinetics (PK) of GDC-0917, an antagonist of inhibitor of apoptosis (IAP) proteins in patients (Pts) with refractory solid tumors or lymphoma.* J Clin Oncol, 2013. **31**: p. (suppl; abstr 2503).

342. Bai, L., D.C. Smith, and S. Wang, *Small-molecule SMAC mimetics as new cancer therapeutics.* Pharmacol Ther, 2014. **144**(1): p. 82-95.

343. Hurwitz, H., et al., *Preliminary report of a first-in-human, open-label, multicenter, phase I study of AT-406 (Debio 1143), an oral small molecule multi-IAP inhibitor, in solid tumors and lymphomas.* Eur J Cancer, 2012. **48**: p. 25 (Suppl. 6).

344. Infante, J.R., et al., *Phase I dose-escalation study of LCL161, an oral inhibitor of apoptosis proteins inhibitor, in patients with advanced solid tumors.* J Clin Oncol, 2014. **32**(28): p. 3103-3110.

345. Houghton, P.J., et al., *Initial testing (stage 1) of LCL161, a SMAC mimetic, by the Pediatric Preclinical Testing Program.* Pediatr Blood Cancer, 2012. **58**(4): p. 636-639.

346. Sikic, B.I., et al., *Safety, pharmacokinetics (PK), and pharmacodynamics (PD) of HGS1029, an inhibitor of apoptosis protein (IAP) inhibitor, in patients (Pts) with advanced solid tumors: Results of a phase I study.* J Clin Oncol, 2011. **29**: p. (suppl; abstr 3008).

347. Amaravadi, R.K., et al., *Phase 1 study of the Smac mimetic TL32711 in adult subjects with advanced solid tumors and lymphoma to evaluate safety, pharmacokinetics, pharmacodynamics, and antitumor activity.* Cancer Res, 2011. **71**: p. (8 Suppl):Abstract nr LB-406.

348. Amaravadi, R.K., et al., *A phase I study of birinapant (TL32711) combined with multiple chemotherapies evaluating tolerability and clinical activity for solid tumor patients.* J Clin Oncol, 2013. **31**: p. (suppl; abstr 2504).

349. Senzer, N.N., et al., *Phase II clinical activity and tolerability of the SMAC-mimetic birinapant (TL32711) plus irinotecan in irinotecan-relapsed/refractory metastatic colorectal cancer.* J Clin Oncol, 2013. **31**: p. (suppl; abstr 3621).

APPENDIX A. CELL DEATH MECHANISMS: AN OVERVIEW

Cell death and cancer

Cancer is one of the leading causes of death in the world, arising when cells accumulate genomic mutations that render them incapable of controlling their own proliferation. The inability of cancer cells to properly regulate their division cycles and their capabilities of therapeutic resistance are often due to impairment of cell death, a critical process in multicellular organisms.

As a fundamental requirement for biological homeostasis, cellular death systems serve to remove cells that are old, unwanted, damaged, and/or defective. Although many distinct death pathways have been defined in various cell types and contexts, cell death is traditionally classified into three broad categories: apoptosis (type I or heterophagy), autophagy (type II), and necrosis (type III) [11]. Cell death promotes proper organismal development and the prevention of disease through a wide variety of biochemical mechanisms and contexts.

In cancer, the dysregulation of these processes leads to invasiveness and resistance to treatment. Therefore developing methods to reactivate death pathways in tumor cells is an attractive pharmacological goal, both as a primary method of eliminating cancer cells as well as sensitizing them to other therapeutics.

Cell death types

Apoptosis

Type I cell death, the most common and well-studied type of cell death known as apoptosis (Greek, "*falling away*"), was named for the characteristic morphology of cells condensing and breaking into smaller apoptotic bodies that are phagocytosed by neighboring cells [12]. In contrast to premature or accidental cell death (necrosis), the quiet incorporation of

apoptotic bodies into phagocytes allows immune evasion without inducing inflammation [13]. Biochemical hallmarks of apoptosis include the activation of pro-apoptotic Bcl-2 protein family members and caspases, permeabilization of the mitochondrial membrane, flipping of phosphatidylserine membrane lipids, high ROS levels, DNA fragmentation and degradation, and rupture of the cell membrane [14]. Apoptosis is a routine event in multicellular organisms (>1 million cells per second in humans), promoting normal development (*e.g.*, organ morphogenesis and lymphocyte maturation) and eliminating diseased cells, *e.g.*, those infected with pathogens or that have accumulated irreparable and potentially tumorigenic mutations [15, 16]. However, many cancer cells contain defects or deletions of pro-apoptotic genes and/or upregulated or mutationally activated anti-apoptotic genes, leading to therapeutic resistance.

Autophagic cell death

Type II cell death, or autophagic death, is defined by characteristic autophagic vacuoles in dying cells [236]. Similar to apoptosis, autophagic death does not induce an immune response [237]. Autophagy is normally a survival mechanism in response to starvation, stress, or the invasion of pathogens. In this tightly regulated catabolic process, eukaryotic cells recycle their internal components by degrading macromolecular structures. When autophagy occurs, components of the cytoplasm (damaged or excess organelles, macromolecular structures, or pathogens) are isolated and sequestered into membrane-bound vacuoles called autophagosomes. Autophagosomes then fuse with lysosomes to form autolysosomes, which degrade their contents using lysosomal hydrolases [238-240]. While autophagy is an important pathway for cellular homeostasis and survival, uncontrolled autophagy can result in death. Unlike apoptosis, cells undergoing autophagic death exhibit an abundance of autophagic vacuoles and die independently of caspase activation. Currently it is unknown whether autophagy is the cause of death in these

cells or an attempt to survive [241]. In cancer, autophagy is considered a double-edged sword; while the altered metabolic state and associated signaling pathways are tumor-suppressive by nature, some advanced tumors may rely on autophagy to survive [242].

Necroptosis

Distinct from apoptosis and autophagy, necrosis is a premature, accidental, and most often detrimental form of cell death. Unlike apoptosis but similar to autophagy, necrosis is caspase-independent. Characterized by organelle swelling, membrane rupture, and spillage of cellular contents into the extracellular space, necrosis results in inflammation [243]. While necrosis has long been viewed as a chaotic type of death that is not genetically programmed in the cell, a substantial body of research has begun to show that necrosis can be a structured process in some situations [244]. Programmed necrosis, or "necroptosis," can occur as a backup form of death when the execution of apoptosis is not possible. Necroptosis is thought to function as an anti-viral response system that is carried out when caspases are inhibited or inadequate for cell death [245]. By triggering necroptosis, infected cells can call on the immune system for assistance in clearing the infection [244]. As a failsafe form of cell death, necroptosis has anticancer potential, and defective necroptosis signaling pathways have been observed in a number of tumor specimens [246-248]. However, like autophagy, necroptosis also has the potential to support cancer. In contrast to the altered metabolic state associated with autophagy, necroptosis may play a supportive role in tumorigenesis by inducing inflammation, a process known to promote cancer development [249].

While cell death is classically viewed as manifesting in one of three different forms, it is becoming clear that there are not only three types; rather, cell death involves a highly elaborate signaling network whose class and phenotype is defined by the activation and repression of

specific sets of signaling molecules. Apoptosis, necroptosis, and autophagy pathways overlap with one another with significant crosstalk in response to different stimuli [11]. Furthermore, many more related but distinct forms of cell death have been shown including anoikis, mitotic catastrophe, pyroptosis, paraptosis, pyronecrosis, cornification, entosis, and parthanatos [14, 250, 251]. In cancer, cells evade normal death processes due to malfunction of this signaling regime, mainly apoptosis, autophagy, and necroptosis. Thus, targeting proteins that play important pro-survival roles at the crossroads of multiple death pathways is a plausible method for cancer therapy. One such family of proteins is the inhibitor of apoptosis (IAP) family, which mediates cellular functions crucial to survival, apoptosis, and necroptosis. In recent years a class of molecules known as Smac mimetics has shown promise in reactivating caspases by suppression of IAP activity (Appendix C). Several of these synthetic peptides are currently in clinical development for the treatment of cancer.

Caspase control of apoptosis and necroptosis

When cell death is a physiological necessity or cells become potentially tumorigenic, apoptosis is the most frequent biological outcome. Depending on stimulus and context, apoptosis can be activated through either an extrinsic or intrinsic pathway. Extrinsic apoptosis involves the binding of an external signaling ligand with its cognate receptor, in turn inducing toxic pathways within the cell. Intrinsic apoptosis is activated by cellular stresses such as radiation or chemical damage that are detected by the mitochondria, which respond by releasing apoptotic molecules that activate death pathways in the cytosol. Both extrinsic and intrinsic pathways are mediated by cascades of cysteine-aspartate proteases called caspases. Caspases activated by proteolytic cleavage serve as the executioners of apoptosis [17].

Extrinsic apoptosis

In the extrinsic pathway, cells respond to external signaling molecules that bind membrane-bound tumor necrosis factor (TNF) receptors (TNFRs). Binding of TNF family members, such as Fas, TNFα, and TNF-related apoptosis-inducing ligand (TRAIL), to TNFRs from outside the cell permits the recruitment of the adaptor Fas-associated protein with death domain (FADD) on the interior side of the membrane. This death-inducing signaling complex (DISC) can associate with other proteins that also influence cell fate (*i.e.*, survival or necroptosis, discussed later) [252, 253]. To trigger apoptosis, DISC recruits the zymogen procaspase-8 and induces its cleavage to form the active initiator caspase-8 [254]. Caspase-8 then cleaves and activates caspase-3 and caspase-7 (caspase-7 can also be activated by cleaved caspase-3) [255]. Subsequently the effector caspases-3 and 7 cleave many target substrates including nuclear lamins and poly-ADP ribose polymerase (PARP) to disassemble the cell at the end of the apoptotic pathway [23].

Intrinsic apoptosis

In contrast to extrinsic apoptosis, the intrinsic pathway is activated by nonspecific internal stresses that directly or indirectly lead to changes in mitochondrial membrane permeability. Under nonstress conditions, the pro-survival proteins Bcl-2 and Bcl-xL maintain mitochondrial membrane integrity by inhibiting their pro-apoptotic family members Bax, Bak, and Bid [18]. When the cell death pathway is induced, apoptotic proteins are activated through a variety of mechanisms relieving these inhibitory interactions. An example of this mitochondrial death protein activation can occur via the tumor suppressor p53. Following lethal signals, p53 is stabilized and can induce apoptotic genes as a nuclear transcription factor but also promote cell death proteins through direct interactions with Bcl-2 family members at the mitochondria [19].

Following apoptotic insult, Bax and Bak oligomerize, causing the formation of pores in the OMM that increase its permeability [20].

Once the mitochondrial membrane has permeabilized, various death factors are released into the cytosol including Smac (second mitochondria-derived activator of caspases) and the ETC molecule cytochrome c [21]. Upon release from the mitochondria, Smac binds X-linked inhibitor of apoptosis (XIAP), neutralizing its ability to inhibit caspases, while cytosolic cytochrome c binds Apaf-1 and induces its oligomerization, forming the death complex known as the apoptosome [22]. The apoptosome recruits procaspase-9 and induces its cleavage into active caspase-9, which subsequently activates caspases-3 and 7 to mediate cellular disassembly [23].

Caspase-independent death

Independent of caspase activation, additional mitochondrial proteins can induce cell death when released into the cytosol. These include endonuclease G and the flavoprotein known as apoptosis-inducing factor (AIF). In healthy mitochondria, endonuclease G generates RNA primers for mitochondrial DNA replication. When cells undergo mitochondria-mediated cell death, endonuclease G migrates to the nucleus and cleaves genomic DNA [256, 257]. Like cytochrome c, AIF is involved in mitochondrial redox function with a separate role in death induction. AIF is an oxidoreductase that is critical for metabolism and redox balance in healthy conditions [25, 26, 258]. Prior to release from the mitochondria, AIF is linked to the inner membrane by a hydrophobic tether that is cleaved by calpains and/or cathepsins upon specific stimuli [32, 36]. Once released into the cytosol, AIF translocates to the nucleus and recruits proteins such as endonuclease G to cause chromatin condensation and DNA degradation characteristic of programmed cell death [24]. Despite AIF's role in cell death, however, it is

worth noting that many cancer cells can exploit AIF's NADH oxidase activity to the benefit of their own survival [51, 54]. Because only a change in mitochondrial membrane permeability (which does not absolutely require caspases) is necessary for death mediated by AIF and endonuclease G, these distinct pathways are considered caspase-independent [259, 260].

Caspase-8 and necroptosis

Caspases play a defining role in apoptosis but also control necroptosis. Specifically, caspase-8 inhibits necroptosis, preventing activation of the chaotic failsafe death pathway [261, 262]. Active caspase-8 prevents this form of death by cleaving cylindromatosis (CYLD) and receptor-interacting protein kinases 1 and 3 (RIP1/RIP3), which normally activate TNF-mediated necroptosis; only when cell death is required and caspase-8 is unable to induce apoptosis does necroptosis occur [262, 263]. Necroptosis begins with the activating phosphorylation of RIP1 and RIP3, which form a complex known as the necrosome [264-266]. Events downstream of necrosome formation are currently not well understood, but a known necroptosis-inducing substrate of RIP3 is the protein phosphoglycerate mutase family member 5 (PGAM5), a mitochondrial phosphatase capable of promoting survival by regulation of antioxidant pathways as well as mediating mitochondrial autophagy (mitophagy) [211-213, 218, 267]. When phosphorylated by RIP3, PGAM5 dephosphorylates and activates dynamin-related protein 1 (Drp1). Activated Drp1 subsequently causes mitochondrial fragmentation that leads to cell death by necroptosis [215]. How mitochondrial fragmentation executes necroptosis remains unknown, although it has been reported that mitochondria released from cells undergoing necroptosis can act as a signal for immune intervention [268]. Thus, caspase-8 is able to divert specific signals away from promotion of survival or immunogenic necroptosis and towards the activation of the quiet apoptotic death pathway. Because of this esssential role in cell death, reactivation of

caspases in cancer is an area of research under investigation, specifically with small molecules that promote caspase activation by mimicking the caspase activator Smac (Appendix C).

APPENDIX B. TARGETING SUBTYPES OF PANCREATIC CANCER

Clinical advantage of subtyping

In this post-genomic era of cancer research, our ability to molecularly define various subtypes of cancer raises tremendous promise for the concepts of patient targeted therapies and precision medicine. A particular bright spot in the utility of cancer subtyping is the example of breast cancer, which has been well defined at the molecular level: tumor subtypes are currently classified based upon the expression of estrogen receptor, progesterone receptor, and human epidermal growth factor receptor 2, and current targeted treatment strategies based on subtype assessment have increased clinical responses in the last decade [269]. In stark contrast to the subtype success achieved in breast cancer analysis is the present state of pancreatic ductal adenocarcinoma (PDAC). PDAC is one of the most lethal malignancies and the fourth leading cause of cancer deaths, associated with a dismal 5-year survival rate of only ~5%. This poor outlook results from late-stage diagnosis of disease, as non-invasive early detection methods remain elusive in the clinic, and current treatment modalities extend patient lifespan by only several weeks to months [270].

Typically PDAC has been treated as a single aggressive form of cancer, because disease is detected almost universally at advanced stages. The identification of common druggable molecular targets, especially those representing specific subgroups of PDACs, will allow therapy to be optimized to increase patient survival. In recent years genomic expression profiling has begun to define separate PDAC subtypes [99, 271], a promising discovery for our efforts in treating PDAC. The next major step will therefore be to determine how these subtypes differ in clinically relevant ways and use these findings to target PDACs in a more focused and accurate approach. Recently Noll *et al.* reported studies identifying new diagnostic markers for PDAC

subtypes and demonstrating the first putative subtype-specific drug resistance mechanism [272]. These findings highlight molecular differences among PDAC subtypes and cumulatively represent a substantial step forward in understanding the pathogenesis of pancreatic cancer. This work is an important starting point for translating molecular studies to the clinic and the development of new therapeutics with the potential to achieve a significant improvement in patient outcome.

Subtypes of pancreatic cancer

Historically subtyping PDAC has been difficult, in large part due to the complex tumor microenvironment. In 2011 Collisson *et al*. [99] reported the existence of three separate subtypes—"classical," "quasimesenchymal," (QM-PDA), and "exocrine-like"—defined by differences in gene expression signatures, KRAS addiction, and drug response. Due to the absence of exocrine-like cell lines *in vitro*, this study only evaluated features of the classical and QM-PDA subtypes; the nature of the exocrine-like subtype, and whether this population is a true subgroup, has therefore remained an open question. In another study, Moffitt *et al*. [271] employed an approach that subtracted mRNA transcripts associated with normal pancreatic tissue that defined only two PDAC subtypes, "classical" and "basal," the latter subtype showing some overlap with the previously defined QM-PDA group [273]. In the recent work of Noll *et al*. [272], patient tumor specimens were implanted into mice used to derive pancreatic adenocarcinoma (PACO) cell lines representative of each of Collisson's subtypes, accompanied by histological and RNA profile verification, which confirms the existence of all three subtypes defined by Collisson *et al*. The establishment of cell lines of each subtype is an important accomplishment, as the absence of exocrine-like cells *in vitro* has in the past posed an unidentified challenge to accurate assessment of disease representative of all PDAC patients.

Identifying molecular and functional differences among these cell types, such as metabolism [100], tumor microenvironment [274], drug resistance [99, 272], and immune evasion and immunotherapy [275], in future studies will be highly valuable.

Markers of pancreatic cancer subtypes

To extend molecular characteristics of each subtype into clinical utility, an important step is to determine diagnostic markers for patient stratification. Noll *et al.* [272] presented surrogate protein markers for the PDAC subtypes, showing that hepatocyte nuclear factor 1, alpha (HNF1A) and cytokeratin 81 (KRT81) are enriched almost exclusively to exocrine-like and QM-PDA subtypes, respectively (Table B1). Levels of HNF1A and KRT81 are inversely correlated in PDAC, and neither protein is frequently found in the classical subtype. Therefore using standard clinical immunohistochemical methods, the classical PDAC subtype can be determined by double negative ($KRT81^-HNF1A^-$, DN) status, $KRT81^+HNF1A^-$ for QM-PDA, and $KRT81^-HNF1A^+$ for the exocrine-like group in patients. HNF1A and KRT81 are associated with survival and grade: the $KRT81^+$ subtype correlates with low mean survival and poor differentiation, whereas $HNF1A^+$ tumors show the greatest mean survival and cell differentiation, with DN tumors lying in between for both survival and differentiation (Table B1). Although subtype appears to predict patient prognosis, overall average survival is very low (<5 years), underscoring the need to develop improved approaches to targeting PDACs, likely by identifying and targeting cellular processes unique to each group.

CYP3A5 mediates PDAC drug resistance

While classical and QM-PDA tumors are sensitive to cell death by small molecule chemotherapeutics, the exocrine-like subtype is resistant to these agents. Noll *et al.* go on to show that this drug resistance mechanism stems from elevated expression of cytochrome P450

3A5 (CYP3A5), a heme-thiolate monooxygenase normally expressed in the liver that mediates xenobiotic metabolism to detoxify drugs in the body [276, 277]. Expression of CYP3A5 correlates positively with HNF1A and inversely with KRT81 in PDAC, and within the exocrine-like subtype CYP3A5 expression is both elevated and drug-inducible relative to normal tissues, QM-PDA, and classical PDAC cells. CYP3A5 mediates resistance against tyrosine kinase inhibitors including erlotinib (EGFR inhibitor) and dasatinib (SRC and ABL1 inhibitor), as well as the CYP3A5 substrate paclitaxel, a cytoskeletal drug that disrupts microtubule breakdown during cell division. Both the pan-CYP inhibitor ketoconazole and shRNA-mediated knockdown of CYP3A5 sensitize exocrine-like cells to treatment, while expression of CYP3A4 or CYP3A7 appear to be neither elevated nor important to PDAC drug resistance, suggesting that CYP3A5 is the lone culprit within the CYP family of enzymes. Furthermore, tumors cannot adapt to the loss of CYP3A5 following sustained treatment, which suggests that CYP3A5 makes an important candidate therapeutic target in exocrine-like tumors. Basal CYP3A5 expression in exocrine-like tumors is mediated by the transcription factor HNF4A, while drug-induced CYP3A5 is controlled by NR1I2, also known as PXR, and the presence of both CYP3A5-regulating proteins appears to have an additive effect in PDAC drug resistance. Therefore targeting these upstream regulators of CYP3A5 may also be therapeutically valuable.

Though CYP3A5 appears to play a predominant role in facilitating cancer cell protection against chemotherapy only in exocrine-like tumors, CYP3A5-mediated drug resistance is not limited solely to exocrine-like PDACs. Indeed, when classical and QM-PDA tumors acquire resistance against therapy, CYPA5 expression and activity are elevated as an adaptation to sustained treatment, and ectopic expression of CYP3A5 confers protection to non-exocrine-like cells. Tissue microarray analyses suggest that CYP3A5-mediated drug resistance is not only a

feature of PDAC but other cancers as well, and these observations were confirmed using cancer cells of non-pancreatic origin. This suggests that CYP3A5 is a potential general target in cancer, and it will be important to determine its pro-tumor activities in other cancer types.

Table B1. Characteristics of pancreatic cancer subtypes.

	KRT81	HNF1A	CYP3A5	Percentage of tumors	Grade	Mean survival
Classical	-	-	-	45%	41.5% grade 3	26.3 months
QM-PDA	+	-	-	35%	50.6% grade 3	16.5 months
Exocrine-like	-	+	+	20%	24% grade 3	43.5 months

Clinical potential of pancreatic cancer markers

The pre-clinical characterization of all three PDAC subtypes *in vivo* is an important step forward in pancreatic cancer treatment. The establishment of PACO cell lines will be useful in determining further differences among subtypes, and the application of the finding that CYP3A5 is a protector of exocrine-like cells will be valuable clinically. Given the known physiological roles of the CYPs, it is not surprising that CYP3A5 protects cancer cells from treatment, but its now confirmed role as a mediator of exocrine-like tumor drug resistance and its regulatory mechanisms in PDAC highlight its value as a potential target. We now have a mechanistic basis for differences in drug resistance among the PDAC subtypes (Figure B1), and in light of these *in vivo* studies, development of CYP3A5 drugs is warranted. CYP3A5 is dispensable to normal tissues [278, 279], but central to chemoresistance in PDAC. Despite high levels of CYP3A5 in tumors relative to healthy tissues, inhibiting the drug clearance activities of CYPs in noncancerous tissues presents the possible clinical pitfall of elevating the systemic toxicity of other chemotherapies. Therefore the significance of achieving high chemical specificity for

CYP3A5, but not other CYPs, is worth noting. An alternative approach to CYP3A5 inhibition might instead be to seek out anti-tumor agents that are *not* metabolized by CYPs and therefore circumvent CYP3A5-mediated resistance. Another possibility is the development of small molecules that serve as substrates for CYP3A5 (such as a modified form of paclitaxel), with the oxidation product functioning as an active form of the drug, thus turning the tumor's resistance mechanism against itself.

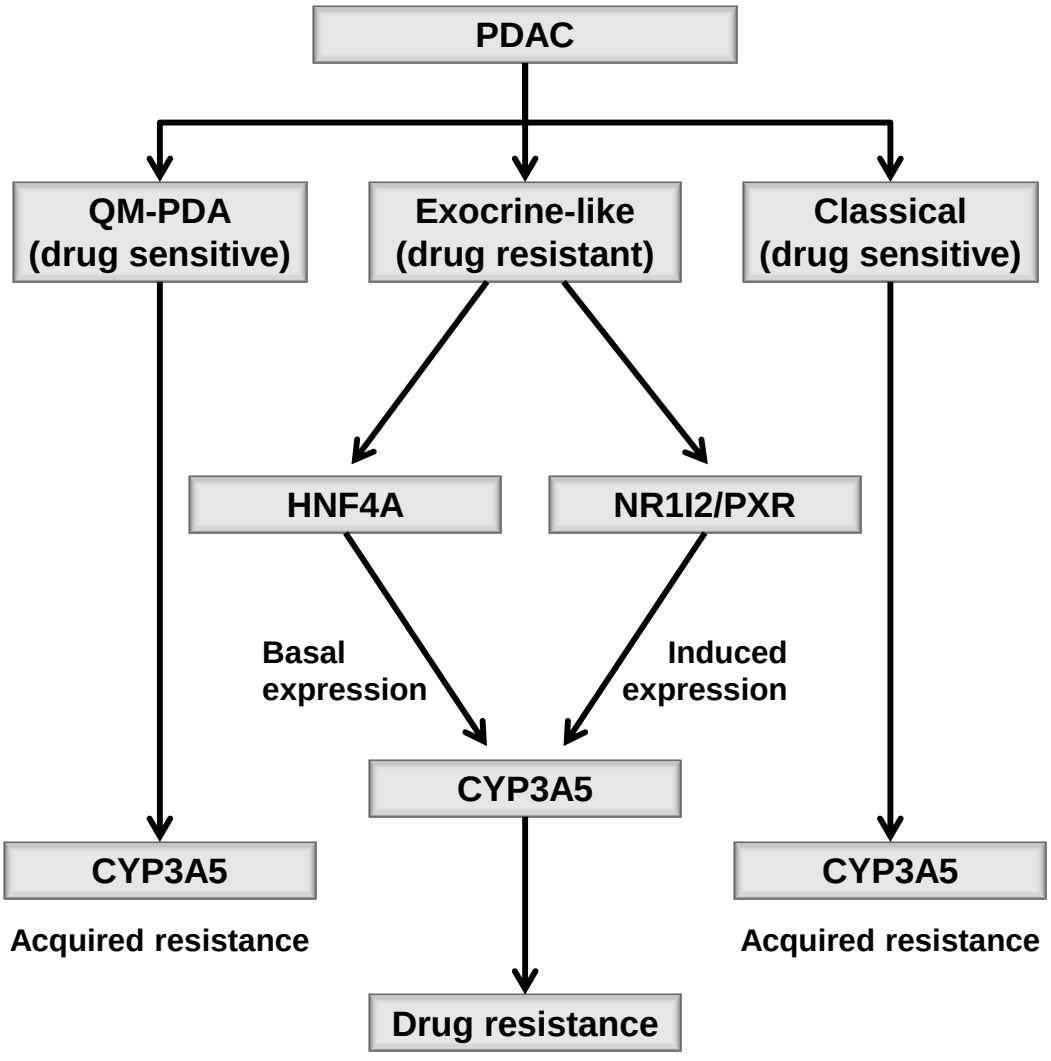

Figure B1. Mechanism of CYP3A5-mediated basal and acquired therapy resistance among PDAC subtypes.
In exocrine-like tumors, basal expression of CYP3A5 is regulated by HNF4A while drug-induced expression is mediated by NR1I2/PXR. Classical and QM-PDA tumors may acquire drug resistance via upregulation of CYP3A5 following sustained treatment.

Immunohistological detection of HNF1A and KRT81 may prove important to revealing which patients are likely to benefit from such therapy. Evaluating the subtype and context specificity of CYP3A5 in other cancer types will also be an important goal for therapeutic development, as well as determining if the correlation of HNF1A and KRT81 with CYP3A5 extends to other cancers. Altogether the work of Noll *et al*. demonstrated a substantial body of clinically useful findings, yet the "smoking gun" for PDAC treatment remains elusive. We can only hope that these targets represent three additional straws on the back of PDAC treatment, and may one day bring us that much closer to improved therapeutic intervention.

APPENDIX C. SMAC MIMETICS AND CELL DEATH

Competition of inhibitors of apoptosis (IAPs) and caspases

IAP proteins

Since caspases can trigger cell death through rapid signal amplification, their apoptosis-inducing capabilities must be tightly regulated under healthy conditions. The inhibitor of apoptosis (IAP) family of proteins prevents caspase-mediated cell death through a broad range of mechanisms, both directly and indirectly. IAPs, also known as baculoviral IAP repeat (BIR)-containing (BIRC) proteins, are defined by characteristic zing finger domains originally discovered in baculoviruses that prevent apoptosis from occurring [280, 281]. To date, 8 IAPs have been identified, each exerting unique effects on cellular signaling pathways: neuronal apoptosis inhibitory protein (NAIP/BIRC1), cellular IAP 1 (cIAP1/BIRC2), cellular IAP 2 (cIAP2/BIRC3), X-linked IAP (XIAP/BIRC4), survivin (BIRC5), BIRC ubiquitin-conjugating enzyme (BRUCE/apollon/BIRC6), melanoma IAP (ML-IAP/BIRC7), and IAP-like protein 2 (BIRC8) [282]. As promoters of cell survival, it comes with little surprise that IAPs are often elevated in cancer, directly contributing to invasiveness and resistance to treatment. Current strategies to reactivate caspases in tumor cells focus on cIAP1, cIAP2, and XIAP, which utilize really interesting new gene (RING) domains to carry out their respective cellular functions [283]. The RING domain of XIAP participates in a range of signaling functions, while in cIAPs these domains are linked to BIR function and can inhibit cell death through multiple mechanisms. By targeting the BIR domains of IAPs, caspase inhibition can be quickly relieved and allow the cell to properly respond to death signals such as chemotherapy.

Cellular IAPs 1 and 2

The survival proteins cIAP1 and cIAP2 promote survival and proliferation through ubiquitin mechanisms activating the canonical nuclear factor κB (NF-κB) pathway, which downstream results in the transcription of genes involved in inflammation, and many of these can be used by cancer cells to their own benefit [284, 285]. Upon binding of TNFα to TNFR1 on the cell surface, multiple proteins are recruited on the cytosolic side to form a protein supercomplex that includes cIAPs and RIP1. When this complex forms, cIAPs polyubiquitinate RIP1 via lysine 63 linkages in a non-degradative manner that results in activation of NF-κB and mitogen-activated protein kinase (MAPK) pathways [286-289]. NF-κB and MAPK signaling cascades lead to the activation of target genes that promote survival, proliferation, migration, and invasion [290]. TNFα can also trigger cell death, but only when cIAPs are inhibited or RIP1 is deubiquitinated [291]. Thus, while cIAP-regulated gene expression programs are crucial in cells such as lymphocytes during the immune response, cancer cells can often use the pro-survival capabilities of cIAPs to promote invasive behavior. By upregulating the activities of cIAPs, cancer cells not only prevent apoptosis from occurring but also directly promote growth and invasiveness through NF-κB and MAPK cascades, converting a death signal to a survival signal.

X-linked IAP

The most notorious of the IAPs in cancer is XIAP, which allows cells to resist many death stimuli including TNFα, Fas, ultraviolet radiation, and genotoxic agents [292]. Under normal cell conditions, XIAP ubiquitinates protein substrates through its E3 ligase activity to modulate signaling cascades of TGF-β, NF-κB, and c-Jun N-terminal kinase, as well as maintain copper homeostasis [48, 293-297]. In contrast to the cIAPs, which indirectly prevent caspase activation by ubiquitinating RIP1, XIAP is the only known IAP to suppress caspase activity

through direct binding, which is accomplished via its BIR domains [298]. The BIR2 domain of XIAP binds the active site groove of caspases-3 and 7 [299], while the BIR3 domain recognizes and binds the N-terminal Ala-Trp-Pro-Phe of caspase-9 to inhibit caspase action and promote cell survival [300, 301]. As a potent suppressor of death pathways, XIAP can also prevent caspase-independent cell death. By ubiquitinating AIF at lysine 255 via a non-canonical ubiquitin linkage, XIAP is able to prevent AIF from inducing chromatin degradation and subsequent cell death [49, 50].

HtrA2

When cells undergo apoptosis, IAP neutralization is necessary for caspases to freely activate cell death. Thus, when mitochondrial membrane permeabilization occurs upon death stimuli, IAP-neutralizing proteins are released into the cytosol alongside cytochrome c and AIF. One of these proteins is the serine protease known as HtrA2 (also known as Omi). The four amino acid resides at the N-terminus (AVPS) of HtrA2 are structurally similar to the caspase regions necessary for recruitment to cIAP1 and XIAP. Unlike caspase binding, however, association of HtrA2 with XIAP both inhibits XIAP and results in its proteolytic cleavage by HtrA2, thereby preventing the apoptotic suppression [302-306].

Smac/DIABLO

Another IAP repressor released into the cytosol is the second mitochondria-derived activator of caspases, or Smac, also known as direct IAP binding protein with low pI (DIABLO) [307, 308]. Smac exists as an elongated homodimer whose quaternary structure is stabilized by extensive hydrophobic interactions between its two subunits, an association critical for caspase activation [309]. Upon import into the mitochondrial membrane, the mitochondrial import peptide at the N-terminus is cleaved from Smac, forming the mature pro-apoptotic form [307,

308]. When released into the cytosol, the new N-terminus of Smac, which structurally resembles that of caspases, inhibits XIAP. The death-inducing N-terminus consists of four critical amino acid residues: Ala1, Val2, Pro3, and Ile4. Similar the XIAP-binding region of caspases and HtrA2, the Ala-Val-Pro-Ile (AVPI) motif of Smac recognizes and binds a distinct groove of XIAP's BIR3 domain with high affinity. Binding of Smac's AVPI peptide to XIAP's BIR3 domain is stabilized both by hydrogen bonds and hydrophobic interactions [310]. This binding event competes with binding of caspase-9 to XIAP, thereby preventing XIAP inhibition of caspase-9 [301, 311]. Additionally, binding of the AVPI motif of one Smac subunit to BIR3 also stabilizes the interaction of Smac's second subunit's interaction with the BIR2 domain of XIAP (also using the AVPI motif) [283]. Binding of Smac to XIAP's BIR2 domain prevents XIAP from inhibiting caspases-3 and 7 [312]. Monomeric Smac is rare, if present at all, in biological settings, and the binding affinity to XIAP and efficiency of neutralization by dimeric Smac far exceed that of its monomeric form [309, 313]. The discovery of Smac's ability to suppress XIAP activity and subsequently promote caspase activation and apoptosis, specifically via its AVPI tetrapeptide, has gained significant attention as a potential pharmaceutical tool to promote apoptosis in cancer cells.

Design of XIAP inhibitors to promote caspase activation and cell death

Exploiting the AVPI peptide for clinical benefit

A universal characteristic of cancer is an inability of tumor cells to properly undergo apoptosis. While many therapeutic strategies aim to induce cell death in tumors through chemical stress or death signaling ligands, cancer cells often resist treatment through elevation of anti-apoptotic molecules. XIAP is often a major culprit in therapy resistance, and Smac levels become insufficient to permit proper caspase activation, either due to XIAP upregulation, Smac

downregulation, or a combination of the two, all of which directly correlate with cancer progression [314]. Thus, peptides that mimic the AVPI motif of Smac, or "Smac mimetics," have been proposed to compensate for insufficient Smac levels and inhibit XIAP to aid the cell in undergoing apoptosis.

Smac mimetics

Because of its widespread capabilities of cell death inhibition and its activity at the convergence of multiple death pathways, XIAP theoretically makes an excellent therapeutic target. Additionally, the AVPI peptide of Smac, which binds and alters XIAP activity, makes an ideal natural template for the design of drugs targeting XIAP. The design of most small molecules that can mimic Smac-IAP interactions are based on the crystal structure of Smac, specifically the AVPI peptide that binds the BIR3 domain of XIAP. To reproduce Smac-mediated XIAP inhibition efficiently, Smac mimetics must maintain chemical properties similar to those most important for the binding of AVPI to BIR3. When the N-terminus of mature Smac recognizes XIAP's BIR3 domain, the amino group at Smac's N-terminus associates via hydrogen bonds with the Glu314 and Gln19 residues of XIAP, while the indole group of XIAP's BIR3 Trp323 forms a weaker hydrogen bond with Smac's Ala1 carbonyl group. To further stabilize binding, the methyl side chain of Smac's Ala1 fits into a hydrophobic pocket of XIAP. While the solvent-exposed side chain of Smac's Val2 residue does not interact with XIAP, its amino and carbonyl groups hydrogen bond with the carbonyl and amino groups XIAP's Thr308 residue. The hydrophobic ring of Smac Pro3 forms stabilizing interactions with XIAP's adjacent Trp323 and Tyr324 side chains. The amino group of Smac's Ile4 and XIAP's Gly306 form a hydrogen bond, while the side chain of Ile4 inserts into another hydrophobic pocket within XIAP consisting of the hydrophobic portions of Leu292, Val298, Lys297 and Lys299 [313, 315]. Overall the AVPI

peptide binds XIAP with a K_d of 480 nM [316], and many synthetic peptides that mimic AVPI are capable of eliciting potent biological responses. To date numerous small molecules have been developed to mimic Smac's N-terminal AVPI peptide. Depending on their precise chemical structure, Smac mimetics exert their biological effects through XIAP binding with a range of affinities, efficacies, and potencies. While some alterations to the AVPI template are acceptable, for example an ethyl group rather than a methyl group in Ala1 (although this does decrease affinity), other regions of the peptide are critical for effective binding and IAP neutralization, particularly the amine groups. Some modifications have even been found to improve binding affinity, notably the alteration of Ala1 to 2-aminobutyric acid or Ile4 to large hydrophobic substituents [316, 317].

Synthetic peptides based on AVPI bind IAPs with high affinity and effectively induce apoptotic pathways. However, these molecules are generally unable to cross cell membranes on their own. To promote the internalization of Smac mimetics into cells, several different chemical strategies have been used. One method frequently employed uses the cationic poly-arginine. Although the mechanism of delivery into cells by this method is not well understood, it is thought to involve electrostatic interactions between poly-arginine's positively charged side chains and the negatively charged membrane lipid head groups [318]. Indeed, conjugation of Smac mimetic peptides with 6-8 arginine units has been demonstrated to permit cellular incorporation [319]. In another technique for peptide delivery, Smac mimetic compounds are fused with penetratin, a peptide derived from the *Drosophila* transcription factor antennapedia [320]. Penetratin is an established peptide carrier that can effectively deliver molecules into cells due to its amphipathic nature [321-323]. Other Smac mimetic delivery methods have been demonstrated as well, such as exploiting validated tumor biomarkers like the σ2 receptor.

Delivery of Smac mimetics conjugated with the σ2 ligand causes tumor cells to internalize the peptides by endocytosis upon ligand-receptor binding [324, 325].

Smac mimetics are constructed as one of two forms, monovalent or bivalent, each with its own advantages and drawbacks. Monovalent Smac mimetics chemically mimic one AVPI peptide and are consequently comparable in size with AVPI. The low molecular weights of monovalent Smac mimetics provide desirable pharmacological properties, most notably high bioavailability. The primary disadvantage of monovalent Smac mimetic compounds, however, is the low potency compared to their bivalent counterparts [326, 327]. The Smac protein inhibits XIAP far more effectively as a dimer than a monomer, and for this reason bivalent Smac mimetics were developed to more accurately reproduce biological inhibition of XIAP. In contrast to monovalent compounds, bivalent Smac mimetics consist of two AVPI analogs tethered by a flexible linker [317, 328]. The linkage of two monovalent Smac mimetics to synthesize a bivalent compound can be achieved with little difficulty through the use of click chemistry techniques [317]. For effective XIAP inhibition by bivalent Smac mimetics, the tether compound must attach to each AVPI analog at a site that is solvent-exposed in the Smac protein template so not to interfere with XIAP binding. Because bivalent Smac mimetics act like a Smac dimer in cells, the efficiency of IAP neutralization by bivalent compounds exceeds that of monovalent peptides by 100-1000-fold [327]. Despite the drastic increase in potency compared to monovalent Smac mimetics, bivalent Smac mimetics have significantly greater molecular weights that result in much lower bioavailability. As a consequence bivalent Smac mimetics cannot be administered orally, and alternative routes such as intravenous administration must be used in patients [317], an option particularly unfavorable when frequent dosing is required. Although no studies have yet found routes to reconcile the advantages and setbacks of the two

Smac mimetic classes, it seems feasible that the high bioavailability of monovalent compounds and the superior potency of bivalent compounds may be combined. A potential method to achieve maximal therapeutic benefit could lie in the administration of a monovalent Smac mimetic followed by dimerization within the cell, perhaps via photooxidation methods. To date both Smac mimetic forms are in clinical trials.

Smac mimetic mechanisms of action: beyond XIAP inhibition

Effect on cIAPs

Smac mimetic design was originally based on the interaction between the AVPI motif of Smac and the BIR3 domain of XIAP [313, 315, 316]. It was first conceived that Smac mimetics would promote apoptosis by inhibiting XIAP and assisting caspase activation. Yet fortuitously, Smac mimetics were also found bind the BIR domains of cIAP1, cIAP2, and ML-IAP. In cancer cells cIAPs use their ubiquitin ligase activity to ensure that TNFR ligand binding results in survival rather than death signaling pathways. However, binding of Smac mimetics to cIAPs causes the cIAPs to ubiquitinate themselves, leading to rapid proteasomal degradation. The loss of cIAPs promotes the activation of NF-κB and subsequent production and secretion of TNFα [329-331]. Since cIAPs are known to promote NF-κB activity, the exact mechanism by which cIAP degradation induces NF-κB-activated TNFα production remains controversial. NF-κB activates both anti-apoptotic and pro-apoptotic genes, but in most cases the activation of survival genes outweighs that of NF-κB's death targets. However, it is suspected that when cIAPs are lost, the cell becomes sensitized to the death capabilities of NF-κB. Whatever the actual mechanism is, the autocrine signaling that follows TNFα secretion induces apoptosis in cancer cells. When autocrine TNFα binds TNFR1 without cIAPs present, RIP1 is no longer ubiquitinated and instead forms the DISC with FADD and caspase-8. Caspase-8 then becomes activated, and with

XIAP neutralized by Smac mimetic treatment, the caspase cascade can destroy the tumor cell free from suppression by IAPs [332]. Originally designed only to neutralize direct XIAP-mediated caspase inhibition, the actual mechanism is far more elegant: Smac mimetic compounds trick cancer cells into secreting the survival factor TNFα, while at the same time tackling its IAP defenses to convert TNFα-induced signaling into a death pathway.

Smac mimetics and necroptosis

Smac mimetics are powerful activators of apoptosis as single agents in TNFα-sensitive cancer cells but can also sensitize resistant cells to chemotherapeutic agents including paclitaxel, etoposide, SN-38, doxorubicin, and cisplatin [319, 320, 329-331, 333]. Furthermore, Smac mimetic compounds can prime apoptosis-resistant cells for necroptosis [334-337]. Although rather infrequent, caspase deficiency has been reported for some cancers [338]. The loss of FADD, an important DISC protein, can also promote resistance to apoptosis in some tumors [339]. By preventing TNFα-stimulated survival pathways, Smac mimetic compounds can force apoptosis-resistant cancer cells to undergo necroptosis as an alternative death pathway. Although this pathway is incompletely understood, the induction of necroptosis may be an effective strategy in treating particularly aggressive forms of cancer, but the ramifications of necroptotic stimulation in clinical settings save not been defined. However, because Smac mimetic compounds can sensitize cells to necroptosis, they have become a powerful research tool for elucidating the inner workings of this newly identified process in addition to their clinical potential.

Smac mimetics in clinical trials

Currently 6 Smac mimetics, both monovalent and bivalent, have reached clinical trials: GDC-0152 (Genentech), GDC-0917/CUDC427 (Genentech/Curis), SM-406/AT-406/Debio1143

(University of Michigan, Ascenta Therapeutics, and Debiopharm), LCL161 (Novartis), TL32711/Birinapant (TetraLogic Pharmaceuticals), and AEG40826/HGS1029 (Aegera and Human Sciences).

GDC-0152 and GDC-0917

Genentech has developed two monovalent Smac mimetics that are currently in clinical trials for solid tumors and lymphomas. The first, GDC-0152, binds XIAP, cIAPs, and ML-IAP with affinities at the nanomolar level and was administered intravenously. Linear pharmacokinetics dosed from 0.049 to 1.48 mg/kg were reported [340]. GDC-0917, also monovalent, reached clinical phase I and was administered orally in 42 patients. Tumor biopsies showed decreased cIAP1 levels, increased caspase-3 levels, and PARP cleavage; 2 patients had unconfirmed complete responses and 4 had stable disease lasting greater than 3 months. Adverse effects included diarrhea, nausea, fatigue, vomiting, and constipation [341, 342].

SM-406

SM-406, an orally bioavailable monovalent Smac mimetic, reached clinical phase I trials in combination with daunorubicin, cytarabine, carboplatin, paclitaxel, and chemo-radiation therapy in advanced solid tumors, lymphomas, acute myelogenous leukemias, and head and neck squamous cell carcinomas. Adverse effects were similar to GDC-0152 and GDC-0917, and a fraction of patients had stable disease at first evaluation [343]. LCL161, also monovalent and administered orally, has shown little toxicity and caused reduction in cIAP levels in biopsy samples. LCL161 has been tested in phases I and II trials as a single agent and in combination with paclitaxel, gemcitabine, and cyclophosphamide in solid cancers, metastatic pancreatic cancer, triple negative breast cancer, multiple myeloma, and leukemia. Partial responses were observed in some patients [342, 344, 345].

AEG40826

AEG40826, a bivalent Smac mimetic compound administered intravenously, has undergone phase I dose escalation studies in advanced solid cancers and lymphoid malignancies. Like other Smac mimetics in clinical development, AEG40826 rapidly induces cIAP1 degradation with evidence of apoptosis in tumor specimens. Adverse effects included fever, fatigue, vomiting, diarrhea, rash, and anorexia. Of 44 patients enrolled, 2 showed stable disease for at least 6 months, while one patient showed tumor regression [342, 346].

Birinapant

Birinapant, developed by TetraLogic Pharmaceuticals, is currently the most advanced Smac mimetic compound in clinical development. Birinapant has reached phase II trials both as a single agent and in combination with other chemotherapies. Birinapant is a bivalent compound delivered via intravenous administration and has the highest claimed efficacy of Smac mimetics with more than half of enrolled patients receiving clinical benefit. Birinapant rapidly causes cIAP1 degradation and unlike other Smac mimetics does not systemically induce inflammatory cytokines, leading to improved tolerability [342, 347-349].

Conclusion

Since the discovery of Smac as a caspase activator and XIAP inhibitor, the application of its pro-apoptotic mechanisms by molecular mimicry has achieved results greater than expected through the combination of both XIAP inhibition and cIAP degradation, leading both to apoptosis induction and sensitization of tumor cells to multiple death pathways. These findings have established the use of Smac mimetics as a powerful method for cell death research and a potential therapeutic option in clinical settings. Overall Smac mimetics in clinical development potently promote cIAP degradation, are generally well tolerated, and suppress tumorigenesis

both as single agents and synergistically with other therapies. Consistent with *in vitro* and preclinical studies, Smac mimetics are effective in a subset of cancers, and further research may expand the understanding of cell death mechanisms and the optimization of Smac mimetic therapy in cancer patients.

APPENDIX D. PRIMERS

Table D1. Primer sequences.

Gene	Forward primer	Reverse primer
AIF	TACCTCAGCAACTGGACCATGGAA	TACCTTCCTGCCGTCTTTCAGCTT
E-Cadherin	ACGCATTGCCACATACA	CGTTAGCCTCGTTCTCA
GAPDH	CCCACTCCTCCACCTTTGAC	TGTTGCTGTAGCCAAATTCGT
GCLM	CTGCTGTGTGATGCCACCAGATTT	GTGCGCTTGAATGTCAGGAATGCT
GGT1	TTCTGCCGGGATAGAAAGGTGCTT	TCAGCTCAGCACGGTAGTTGTTC
GSR	ACGAGTGATCCCAAGCCCACAATA	TGTAACCTGCACCAACAATGACGC
GSTM1	AACGCCATCTTGTGCTACATTGCC	TAGCAGATCATGCCCAGCTGCATA
HMOX1	ATTGCCAGTGCCACCAAGTTCAAG	ACGCAGTCTTGGCCTCTTCTATCA
HMOX2	AATGAGAATGGCTGACCTCTCGGA	GATGGTCCTTGTTGCGCTCCATTT
Met	GGTCAATTCAGCGAAGTCCT	CCAGTGTGTAGCCATTTTGG
N-Cadherin	GAAAGACCCATCCACG	CCTGCTCACCACCACTA
NQO1	TGCAGCGGCTTTGAAGAAGAAAGG	TTCGCAGGGTCCTTCAGTTTACCT
Serpine	ATTCAAGCAGCTATGGGATTCAA	CTGGACGAAGATCGCGTCTG
Snail	AATCGGAAGCCTAACTACAGCG	GTCCCAGATGAGCATTGGCA
Twist1	GGAGTCCGCAGTCTTACGAG	TCTGGAGGACCTGGTAGAGG
Vimentin	ACCAGCTAACCAACGACAAAG	GCAGGGTGTTTTCGGCTTC
Zeb1	TGCACTGAGTGTGGAAAAGC	TGGTGATGCTGAAAGAGACG
Zeb2	CAAGAGGCGCAAACAAGC	GGTTGGCAATACCGTCATCC
β-Actin	GCGGGAAATCGTGCGTGACATT	GATGGAGTTGAAGGTAGTTTCGTG